



Thermodynamic modeling of CO2 mixtures

Bjørner, Martin Gamel; Kontogeorgis, Georgios

Publication date:
2016

Document Version
Publisher's PDF, also known as Version of record

[Link back to DTU Orbit](#)

Citation (APA):
Bjørner, M. G., & Kontogeorgis, G. (2016). Thermodynamic modeling of CO2 mixtures. Kgs. Lyngby: Technical University of Denmark (DTU).

DTU Library

Technical Information Center of Denmark

General rights

Copyright and moral rights for the publications made accessible in the public portal are retained by the authors and/or other copyright owners and it is a condition of accessing publications that users recognise and abide by the legal requirements associated with these rights.

- Users may download and print one copy of any publication from the public portal for the purpose of private study or research.
- You may not further distribute the material or use it for any profit-making activity or commercial gain
- You may freely distribute the URL identifying the publication in the public portal

If you believe that this document breaches copyright please contact us providing details, and we will remove access to the work immediately and investigate your claim.

PhD Thesis
Doctor of Philosophy

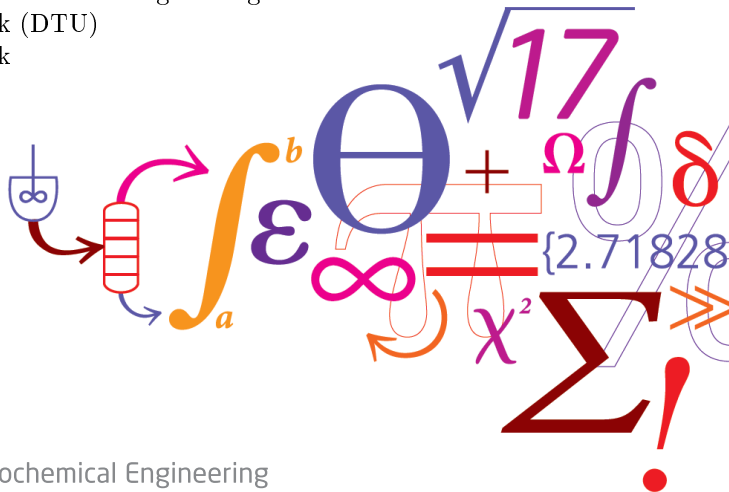


Thermodynamic modeling of CO₂ mixtures

Martin Gamél Bjørner
February 17, 2016

Supervisor:
Professor Georgios M. Kontogeorgis

Center for Energy Resources Engineering
Department of Chemical and Biochemical Engineering
Technical University of Denmark (DTU)
DK-2800 Kgs. Lyngby, Denmark



DTU Chemical Engineering
Department of Chemical and Biochemical Engineering

DTU Chemical Engineering
Department of Chemical and Biochemical Engineering
Technical University of Denmark

Søltofts Plads

Building 229

2800 Kongens Lyngby, Denmark

Phone +45 4525 2800

kt@kt.dtu.dk

www.kt.dtu.dk

Abstract

Knowledge of the thermodynamic properties and phase equilibria of mixtures containing carbon dioxide (CO_2) is important in several industrial processes such as enhanced oil recovery, carbon capture and storage, and supercritical extractions, where CO_2 is used as a solvent. Despite this importance, accurate predictions of the thermodynamic properties and phase equilibria of mixtures containing CO_2 are challenging with classical models such as the Soave-Redlich-Kwong (SRK) equation of state (EoS). This is believed to be due to the fact, that CO_2 has a large quadrupole moment which the classical models do not explicitly account for.

In this thesis, in an attempt to obtain a physically more consistent model, the cubic plus association (CPA) EoS is extended to include quadrupolar interactions. The new quadrupolar CPA (qCPA) can be used with the experimental value of the quadrupole moment and with or without introducing an additional pure compound parameter. In the absence of quadrupolar compounds qCPA reduces to CPA, which itself reduces to SRK in the absence of association.

As the number of adjustable parameters in thermodynamic models increase, the parameter estimation problem becomes increasingly complicated due to parameter identifiability issues. In an attempt to quantify and illustrate these issues, the uncertainties in the pure compound parameters of CO_2 were investigated using qCPA as well as different CPA approaches. The approaches employ between three and five parameters. The uncertainties in the parameters were propagated to physical properties, vapor liquid equilibria (VLE), and liquid-liquid equilibria (LLE) using Monte Carlo simulations.

The uncertainties in the pure compound parameters were found to be negligible for modeling approaches which employed three adjustable parameters. For modeling approaches with more than three adjustable parameters, however, the uncertainties in the pure compound parameters were significant. As a result the propagated errors were substantial for certain output properties. The uncertainties in VLE were for instance much larger when qCPA was employed with four parameters rather than three. The uncertainty analysis indicated that the parametrization of multi-parameter models is at least as important as the specific model term.

The new qCPA and several CPA approaches were extensively evaluated for their ability to predict the thermodynamic properties of pure CO_2 . The predictions of these pure compound properties were satisfactory with qCPA, although similar predictions were achieved with the other CPA approaches. The model was subsequently evaluated for its ability to predict and correlate the binary VLE and LLE of mixtures containing CO_2 and *n*-alkanes, water, alcohols, or quadrupolar compounds. For these binary mixtures qCPA appeared to offer systematically improved predictions and correlations as compared to the cases where quadrupolar interactions were ignored. The improvements were particularly pronounced for mixtures of CO_2 and hydrocarbons where the model is almost fully predictive.

Finally qCPA was evaluated for its ability to predict the phase equilibria of multi-component mixtures containing CO₂ and *n*-alkanes, water, and/or alcohols. A single binary interaction parameter was employed in qCPA for most binary combinations. Both qCPA and the best CPA approaches typically performed satisfactorily and predicted the general behavior of the systems, but qCPA used fewer adjustable parameters to achieve similar predictions.

It has been demonstrated that qCPA is a promising model which, compared to CPA, systematically improves the predictions of the experimentally determined phase equilibria between binary and ternary mixtures containing CO₂ and other non-quadrupolar compounds. However, for mixtures containing two quadrupolar compounds, or a quadrupolar and polar compound, considerable uncertainty remains as to whether these mixtures are handled in the best possible way. When binary interaction parameters were employed to correlate experimental phase equilibria data, both qCPA and CPA yielded similar correlations - and predictions in the multicomponent case.

Resumé

Kendskab til de termodynamiske egenskaber og fase­lige­væg­te, for blandinger som indeholder carbondioxid (CO_2), er vigtigt indenfor flere industrielle processer så som forbedrede olieindvindingsmetoder, indfangning og lagring af CO_2 eller superkritisk ekstraktion, hvor CO_2 benyttes som et opløsningsmiddel. På trods af dette er klassiske modeller, så som Soave-Redlich-Kwong (SRK) tilstandsligningen, stærkt begrænsede når det kommer til at forudsige faseopførselen for sådanne blandinger. Grunden til dette formodes at være, at CO_2 har et stort kvadrupolmoment, som de klassiske modeller ikke tager eksplicit højde for.

I denne afhandling, i et forsøg på at opnå en mere fysisk korrekt model, er kubisk plus association (CPA) tilstandsligningen blevet udvidet til at inkludere kvadrupole interaktioner. Den nye kvadrupolære CPA (qCPA) kan benyttes med den eksperimentelle værdi af det kvadrupolære moment og med eller uden endnu en renkomponentsparameter. I blandinger, som ikke indeholder kvadrupolære komponenter, reducerer qCPA til CPA, ligesom CPA selv reducerer til SRK, i blandinger uden komponenter der danner hydrogenbindinger.

Når antallet af justerbare parametre i termodynamiske modeller stiger, bliver det mere og mere kompliceret at estimere og identificere modelparametrene, da parametrene ikke længere kan betragtes som unikke. I et forsøg på at kvantificere og illustrere disse problemer undersøges usikkerhederne i carbondioxids renkomponentsparametre både med qCPA og med forskellige modelleringsstrategier for CPA. Modelleringsmetoderne benytter mellem tre og fem renkomponentsparametre. Ved brug af Monte Carlo simuleringer videreføres usikkerhederne i renkomponentsparametre til fysiske egenskaber, gas-væske ligevægte og væske-væske ligevægte.

For modelleringsmetoder med tre renkomponentsparametre viste usikkerhederne sig at være ubetydelige. For modelleringsmetoder med mere end tre parametre viste usikkerhederne sig derimod at være signifikante. Som et resultat heraf var de videreførte usikkerheder betydelige for visse egenskaber. Usikkerhederne i gas-væske ligevægte var for eksempel meget større når qCPA blev benyttet med fire renkomponentsparametre end med tre renkomponentsparametre. Usikkerhedsanalysen indikerede, at parametriseringen af modeller med mere end tre renkomponentsparametre er mindst lige så vigtig som selve modellen.

Den nye qCPA tilstandsligning, og indtil flere CPA modelleringsmetoder, blev først brugt til at forudsige de termodynamiske egenskaber for ren CO_2 . Forudsigelserne af disse renkomponentsegenskaber var tilfredsstillende med qCPA, skønt lignende forudsigelser blev opnået med de andre CPA modelleringsmetoder. Modellen blev efterfølgende evalueret for dens evne til at forudsige og korrelere binære gas-væske ligevægte samt væske-væske ligevægte for CO_2 -blandinger indeholdende n -alkaner, vand, alkoholer eller forskellige kvadrupolære komponenter. Sammenlignet med når kvadrupolære interaktioner blev ignoreret opnåede qCPA systematisk forbedrede forudsigelser og korrelationer. Disse forbedringer var særdeles udtalte for blandinger, som indeholdt CO_2 og kulbrinter, hvor modellen næsten var fuldstændig forudsigende.

Til sidst blev qCPA evalueret for dens evne til at forudsige fase­lige­væg­te for multi­kom­po­nent­sam­le­b­lan­dinger, som indeholdt CO_2 samt n -alkaner, vand eller alkoholer. En binær interaktionsparameter blev benyttet i qCPA for de fleste binære undersystemer. Både qCPA og de bedste CPA modelleringsmetoder forudsagde den generelle opførsel af multikomponentsblandingerne og gav typisk tilfredsstillende forudsigelser for lige­væg­ten mellem komponenterne, men qCPA skulle bruge færre binære parametre for at opnå de samme forudsigelser.

Det er blevet vist, at qCPA er en lovende model, som i forhold til CPA, systematisk forbedrer forudsigelserne af de eksperimentelt observerede fase­lige­væg­te mellem forskellige binære eller ternære blandinger, som indeholder CO_2 og andre komponenter, der ikke selv er kvadrupolære. Der er dog betydelige usikkerheder for hvorvidt blandinger som indeholder to kvadrupolære komponenter, eller en kvadrupol og en polær komponent, bliver behandlet optimalt. Når den binære interaktionsparameter blev korreleret til eksperimentelt lige­væg­ts­data, gav qCPA og CPA dog næsten ens korrelationer - og næsten ens forudsigelser for multikomponentblandinger.

Preface

This thesis is submitted in partial fulfilment of the requirements for the degree of PhD from the Technical University of Denmark (DTU). The work has been carried out at the Center for Energy Resources Engineering (CERE), Department of Chemical and Biochemical Engineering, DTU, in the period from July 2012 to February 2016 (excluding a short period of leave) under the supervision of Professor Georgios M. Kontogeorgis.

The present work, *Thermodynamic modeling of CO₂ mixtures*, was funded by the Danish Council for Independent Research | Technology and Production Sciences (Det Frie Forskningsråd | Teknologi og Produktion (FTP)) as part of the project *CO₂ Hydrates – Challenges and Possibilities*. The overall FTP project is in collaboration with Ecole de Mines in France. Experimental work was originally supposed to have been carried out during an external research stay at Ecole de Mines. However, the research stay was regrettably cancelled.

The objectives of the present work has been to develop and evaluate a thermodynamic equation of state for CO₂ and CO₂ mixtures, which includes the effect of the quadrupole moment (of CO₂) and is based on the Cubic Plus Association (CPA) equation of state.

Lyngby, 17-February-2016

Martin Gamél Bjørner

Acknowledgements

The work contained in this manuscript could not have been possible without the help and moral support of several people, to whom I will be eternally grateful.

First of all I would like to thank my supervisor, Professor Georgios M. Kontogeorgis, for ensuring the funding without which this project would not have been possible, for always supporting and encouraging me to go my own way, and giving me the freedom to do so. Your constant enthusiasm and ability to keep calm and always look on the other side of the coin has been invaluable.

I am grateful to the FTP for funding this project as part of the *CO₂ Hydrates - Challenges and Possibilities* project.

I would like to thank both my former and present colleagues at CERE for making the days more enjoyable. I would particularly like to thank some of my fellow colleagues in the CHIGP project; Bjørn, Xiadong and Michael for many fruitful discussions during the meetings and co-participation in international conferences. Thanks to Anders Schlaikjer and Andreas Frisch for their useful comments on parts of the manuscript. Thanks to Louise and Patricia for all their assistance on practical matters, your help has been invaluable.

I owe a special thanks to Dr. Bjørn Maribo-Mogensen for his guidance and help on computational aspects, especially in understanding the MEX interface which really helped the project 'fly'.

Joachim Bachmann, thank you for your friendship and our many 'coffee breaks' they certainly made the time at DTU more enjoyable.

I also wish to thank Associate Professors Philip L. Fosbøl and Kaj Thomson for giving me the opportunity to work on the 'Wet Gas' project together with EMCO Controls. It was a refreshing and rewarding experience.

Last, but certainly not least, I wish to thank my girlfriend Nina Andrea Langseth, for all her love and understanding, and for listening patiently to my ramblings on a daily basis, which cannot always have been easy.

Contents

Abstract	i
Resumé	iii
Preface	v
Acknowledgements	vi
1 Introduction	1
1.1 Thermodynamic Modeling of Mixtures Containing CO ₂	3
2 Aim and Scope of this Work	5
2.1 Specific Objectives	5
2.2 Thesis Structure	7
3 The Cubic Plus Association Equation of State	8
3.1 The Cubic Plus Association Equation of State	9
3.1.1 The SRK contribution	10
3.1.2 Association contribution	11
3.2 Modeling CO ₂ Mixtures with the CPA EoS	14
3.2.1 Applications of CPA for mixtures containing CO ₂	16
3.2.2 Summary of applications	20
4 SAFT-based Models with a Quadrupole Term	22
4.1 Applied Quadrupolar Theory	23
4.2 Quadrupolar Contributions to the SAFT	25
4.2.1 The PCP-SAFT EoS	25
4.2.2 The PC-PSAFT and the tPC-PSAFT	26
4.2.3 The polar GC-SAFT	28
4.2.4 Summary of applications	29
4.3 Similarities and Differences	29

5	The Quadrupolar CPA Equation of State	32
5.1	The Quadrupole CPA Term	33
5.1.1	Model variants	35
5.2	Model Implementation	36
5.2.1	Evaluation of derivatives	37
6	Parameter Estimation & Propagation of Uncertainty	38
6.1	Uncertainty Analysis and Uncertainty Propagation	41
6.2	Parameter Estimation - Uncertainty and Correlation	42
6.2.1	On the least squares method	43
6.2.2	Results with the least squares method	44
6.3	Bootstrapping	48
6.3.1	Bootstrap technique for uncertainty of parameter estimators	48
6.3.2	Parameters from the Bootstrap technique	48
6.4	Propagation of Parameter Uncertainty to Model Predictions	55
6.4.1	A Monte Carlo uncertainty analysis	55
6.4.2	Propagation of parameter estimation errors	56
6.4.3	The effect of adding additional output properties	64
6.5	Summary and Discussion	67
7	Pure Compound Properties of CO₂	70
7.1	Calculation of Derivative Properties	71
7.2	Pure Compound Parameters and Modeling Approaches	73
7.3	Derivative Properties and Density	75
7.3.1	Saturation region	75
7.3.2	Compressed liquid region	77
7.3.3	Critical region	82
7.3.4	Summary of derivative property results	84
7.4	Critical Points	85
7.5	The Second Virial Coefficient	87
7.6	Summary	89
8	Phase Equilibria of Binary Mixtures Containing CO₂	91
8.1	Pure Compound Parameters	91
8.2	CO ₂ + <i>n</i> -alkanes	94
8.2.1	VLE of CO ₂ + <i>n</i> -alkanes	94
8.2.2	LLE of CO ₂ + heavy <i>n</i> -alkanes	99
8.2.3	Correlations for the binary interaction parameter	106
8.3	CO ₂ + Self-associating Compounds	108
8.3.1	CO ₂ + alcohols	109
8.3.2	CO ₂ + water	111
8.4	CO ₂ + Quadrupolar Compounds	116
8.4.1	CO ₂ + benzene	118
8.4.2	CO ₂ + methylbenzene (toluene)	118
8.4.3	CO ₂ + nitrogen	120
8.4.4	CO ₂ + acetylene	123
8.5	CO ₂ + Polar Molecules	127
8.5.1	CO ₂ + acetone	127

8.6	Excess Properties	127
8.7	Summary	130
9	Multicomponent Mixtures Containing CO₂	132
9.1	Modeling approaches	133
9.2	Vapor Liquid Equilibrium	135
9.2.1	Mixtures containing CO ₂ and <i>n</i> -alkanes	137
9.2.2	Mixtures containing CO ₂ and associating compounds	141
9.3	Dew Point Pressure	148
9.4	Vapor Liquid Liquid Equilibrium	151
9.5	Concluding Remarks	153
10	Conclusion and Future Work	157
10.1	Conclusion	157
10.2	Future Investigations	160
10.2.1	Future applications	160
10.2.2	Parameter estimation and uncertainty	162
10.2.3	Improvements to qCPA	162
A	PhD Activities	164
A.1	List of Publications	164
A.2	Contributions at Conferences	165
A.2.1	International conferences	165
A.2.2	Internal conferences	165
A.3	Attended Courses	166
A.4	Teaching and Organization	166
B	Derivatives of the Reduced Residual Helmholtz Energy	167
B.1	Partial Derivatives	167
B.2	Derivatives of the Padé approximation	169
B.3	Relevant Derivatives of qCPA	170
C	Numerical Derivatives	175
C.1	First Derivative Approximations	175
C.2	Numerical Examples	176
C.2.1	Simple equations	176
C.2.2	The SRK and the quadrupolar term	178
	List of Abbreviations	179
	List of Symbols	182
	List of Figures	186
	List of Tables	197
	Bibliography	202

Introduction

Carbon dioxide (CO_2), as a solvent or refrigerant is considered an environmentally harmless chemical. Nevertheless, CO_2 has received a significant amount of negative attention in recent years due to its status as a greenhouse gas, and the fact that the amount of CO_2 in the atmosphere continues to rise. Between 1850 and 2015 the concentration of CO_2 in the atmosphere has increased from approximately 280 ppm to an annual mean of about 400 ppm [1–3]. The atmospheric concentration of CO_2 has been rising with increased rapidity since the 1950's [1]. Its increase is believed to be largely due to anthropogenic emissions, resulting primarily from a world-wide increased energy consumption since the industrial revolution.

The International Energy Agency (IEA) have estimated the total worldwide emission of CO_2 from the combustion of fossil fuels to be about 32.2 Gigatonnes in 2013 [2]. According to the IEA, the largest share comes from electricity and heat generation, which accounts for about 42% of the total CO_2 emission. Transport accounts for about 23% and industrial processes account for about 19% of the total CO_2 emission [2]. Alone in Denmark, more than 40 million tonnes of CO_2 is emitted per year, about 45% of the emitted CO_2 originates from the energy industry [4]. Renewable energy sources, such as solar and wind, may be more sustainable than fossil fuels in the long term, however, these technologies are not yet widespread nor developed enough to fully replace fossil fuels. As a result of this, there will be a long transition period during which both renewable and hydrocarbon-based energy sources must coexist. Moreover, a considerable amount of the emitted CO_2 comes as a by-product from industrial processes, particularly cement production, and cannot readily be avoided.

Transition technologies are thus needed, which can limit the emission of CO_2 to the atmosphere, at least until such a time when renewable energy sources can

replace fossil fuels. One such potential technology is carbon capture and storage (CCS). The reduction of the CO_2 emission by effective CCS is considered one of the '14 Grand Challenges for Engineering in the 21st century' [5]. In the CCS process a CO_2 rich mixture is captured from an emission source, such as a power or cement plant, transported to a storage point and ultimately stored in an underground geological formation. These steps should prevent the emission of CO_2 to the atmosphere. Proper CCS requires accurate knowledge of various thermodynamic properties as well as the phase behavior of mixtures containing CO_2 and hydrocarbons, water and/or other fluids such as alcohols and glycols [6].

Various techniques exist for capturing CO_2 from flue gas. Chemical absorption of CO_2 , using alkanolamines such as monoethanolamine as a solvent, are probably the most mature technique for CO_2 capture from flue gas. The technique, however, is still very expensive, primarily due to a high energy consumption.

Gas hydrates (or clathrate hydrates) are ice-like crystalline compounds formed by hydrogen bonded water and stabilized by the encapsulation of small guest molecules, such as CO_2 and small hydrocarbons, within the water lattice [7]. Hydrates are known to be a nuisance in the petroleum industry, as they can cause blockage in natural gas and oil pipelines. Hydrate formation is prevented industrially by the addition of inhibitors such as methanol or mono-ethylene glycol (MEG) [8]. On the other hand CO_2 hydrates also constitute a possible new method for CO_2 capture; For instance a new technique for CO_2 capture from flue gases, which exploits the formation of gas hydrates, has recently been patented [9–11]. The operating pressure of the technique, however, is currently too high to be economically profitable. The technique could be improved by using specific thermodynamic hydrate promoters, such as tetrahydrofuran and cyclopentane [12], to reduce the operating pressure. Screening for the optimal promoters, however, is expensive and time consuming. Rigorous models for CO_2 and CO_2 mixtures, which are accurate over a wide range of conditions and chemicals (i.e. hydrate formers or inhibitors) would greatly facilitate this process.

Modeling the thermodynamic properties and phase equilibria of CO_2 , both as a pure fluid and in mixtures containing CO_2 is also of high importance in several other industrial applications; In the chemical industry, for instance, CO_2 is considered an excellent solvent for supercritical extraction. Mixtures of CO_2 + hydrocarbons and CO_2 + alcohols have received particular attention, as they behave as co-solvent pairs, e.g. for the extraction of organic compounds from aqueous solutions [13, 14]. The phase equilibria of mixtures containing CO_2 , hydrocarbons, water, and glycols are also of particular importance in the petroleum and chemical industry [13, 14], where CO_2 is injected into reservoirs to enhance oil recovery.

1.1 Thermodynamic Modeling of Mixtures Containing CO₂

Pseudo-empirical equations of state for pure fluids, such as the Span and Wagner Equation of State (EoS) for CO₂ [15], are typically accurate down to experimental error, at least in the temperature and pressure range for which they have been developed. Unfortunately such equations of state are difficult to extend to multicomponent systems.

Despite the importance of mixtures containing CO₂, accurate thermodynamic modeling of such mixtures is a challenge for most classical equations of state. The reason for this is believed to be that CO₂ has a large quadrupole moment, i.e. a concentration of charges at four separate points in the molecule, which result in some directional interactions (see chapter 4). The large quadrupole moment of CO₂ is for instance believed to be the reason for the the low temperature azeotrope observed for the vapor liquid equilibrium (VLE) between mixtures of CO₂ and ethane and the reason, along with size asymmetry, for the liquid liquid equilibrium (LLE) between CO₂ and heavy hydrocarbons.

Cubic equations of state such as the Soave-Redlich-Kwong (SRK) EoS [16] does, however, not take quadrupolar interactions explicitly into account and effectively treat CO₂ as an inert compound. Even in a modern equation of state such as the Statistical Association Fluid Theory (SAFT) [17–19] only dispersive forces are usually considered for CO₂. The continued use of these models may be attributed to the fact that several binary mixtures, such as CO₂ + hydrocarbons, are described quite well when a single, relatively large (and often temperature dependent), binary interaction parameter is correlated to the experimental data. However, the predictive nature of the models (for binary mixtures) is lost. Moreover, it is uncertain whether these large binary interaction parameters can be used to accurately predict e.g. excess properties or the equilibria of multicomponent mixtures.

Modeling the phase behavior of mixtures containing CO₂ and associating mixtures can be a challenge with traditional equations of state. For instance, the SRK EoS cannot correlate the minimum in the water concentration of the CO₂-rich vapor phase for the binary CO₂ + water mixture, even when a large binary interaction parameter is employed. The minimum can be modeled by advanced association models such as the cubic plus association (CPA) EoS (developed by Kontogeorgis et al. [20]) or SAFT [17–19], but only if CO₂ is assumed to be self-associating or solvating (i.e. a molecule with either electron donor or electron acceptor sites, see chapter 3).

To model mixtures containing CO₂ more accurately with models that can account for association, a pragmatic approach is thus to treat CO₂ either as a self-associating or solvating molecule. Especially the latter approach is not en-

tirely without justification as there is some evidence for strong Lewis acid-Lewis base interactions between mixtures of CO_2 and water or alcohols, and it may be reasonable to model these interactions by assuming CO_2 to be solvating. Unfortunately the solvation approach does not improve the predictions for mixtures of CO_2 and hydrocarbons. The theoretically less justified assumption, where CO_2 is assumed to be self-associating, does improve these predictions. These pragmatic procedures often work well resulting in good correlations with small interaction parameters [14, 21–23]. The improvement, however, is often obtained at the cost of additional pure component parameters and, in some cases, an extra adjustable parameter is employed to correlate the binary mixtures.

Alternatively, to explicitly account for the quadrupolar interactions several quadrupolar terms have been proposed within the SAFT framework. These terms are typically based on a perturbation theory developed from statistical mechanics by Stell and co-workers [24–27]. Gross [28], for instance, developed a quadrupolar expression, which was included in the Perturbed-Chain SAFT (PC-SAFT) framework. The quadrupolar term employed the experimental quadrupolar moment and did not introduce additional adjustable parameters. Economou and co-workers [29–31] also extended PC-SAFT with two quadrupolar expressions; a simplified and a non-simplified term. The simplified term, which seems to be the one used most often, employs an additional adjustable parameter (as compared to PC-SAFT). Finally NguyenHuynh et al. [32] introduced a quadrupolar term to a group contribution SAFT version. More detail about the quadrupolar approaches may be found in Chapter 4.

Although the quadrupolar models are not without their limitations (see chapter 4), compared to the base SAFT variant the addition of a quadrupolar term appears to result in improved predictions and correlations (smaller interaction parameters) for phase equilibrium calculations of binary VLE. Inspired by the recent advances within the SAFT-family, and in an effort to obtain a physically more correct and predictive model, a quadrupolar term is proposed in this thesis and combined with the well-known CPA EoS. The performance of the new equation of state (herein known as quadrupolar CPA (qCPA)) is thoroughly evaluated in this work, especially for equilibrium calculations of both pure CO_2 and mixtures containing CO_2 .

CHAPTER 2

Aim and Scope of this Work

This thesis is part of a grant funded by the Danish Council for Independent Research | Technology and Production Sciences (FTP) under the project *CO₂ Hydrates - Challenges and Possibilities*. The objectives of the overall FTP project is to acquire a solid experimental and theoretical basis for understanding and addressing the problems of CO₂, CO₂ mixtures and CO₂ hydrates, for the possible utilization of hydrate formation as a CO₂ capture technology.

2.1 Specific Objectives

To understand and address the challenges and potential opportunities of CO₂ containing mixtures, accurate models, valid over a wide range of conditions and chemicals, are necessary. The present PhD project thus focuses on the thermodynamic modeling of CO₂ and CO₂ mixtures. The base model to be employed for this task is chosen to be the CPA EoS. In an extensive study Kontogeorgis and co-workers have previously systematically investigated the applicability of CPA for modeling mixtures containing CO₂ [14, 33–36] (see Chapter 3). Based on this study a number of pragmatic approaches for CO₂ mixtures was suggested. Some of the approaches lead to excellent phase equilibrium results, at the same time, however, the approaches typically lead to an increase in the number of adjustable parameters, possibly due to the fact, that quadrupolar forces was not explicitly taken into account.

CPA in its current form does not account for quadrupolar (or polar) forces. To obtain and evaluate such a physically more consistent and, hopefully, more predictive model, the CPA needs to be modified so that it can account for

quadrupolar interactions. This led to a set of specific objectives for this PhD project, which we will attempt to provide solutions for throughout the thesis.

The following objectives should be addressed:

- Within the framework of the CPA, develop a thermodynamic model which extends the CPA to also include quadrupolar interactions (qCPA).
- While the model should, in principle, be applicable to any mixture containing quadrupolar molecules, particular emphasis should be on mixtures containing CO₂.
- Compared to the base CPA the model should improve the prediction of mixtures containing CO₂ and/or other quadrupolar compounds.
- In the absence of quadrupolar compounds the model should reduce to CPA.
- The model should focus on simplicity and should employ as few adjustable parameters as possible.
- If possible the pure compound parameters should be estimated based on pure compound properties.
- The model should be thoroughly evaluated for its ability to:
 - Predict pure fluid properties of CO₂.
 - Predict and correlate the VLE and LLE of binary mixtures related to CO₂ hydrates, such as mixtures containing CO₂ and *n*-alkanes, water or alcohols.
 - Predict the VLE and vapor liquid liquid equilibrium (VLLE) of multicomponent mixtures containing CO₂, water, *n*-alkanes or alcohols.
- The model should furthermore be evaluated for its ability to describe the equilibrium between mixtures of several quadrupolar molecules.
- The results of the new model should preferably be compared to the unmodified CPA. So that the best CPA approaches can be compared with the new model, both in terms of performance, but also the number of adjustable parameters.

The work has been carried out at the Center for Energy Resources Engineering (CERE), Department of Chemical and Biochemical Engineering, Technical University of Denmark (DTU) under the supervision of Professor Georgios M. Kontogeorgis. Throughout the project the results have continuously been presented and discussed both internally at the center, with external industrial collaborators, and with researchers at international conferences. The main results have been published in two peer-reviewed journals. Furthermore an additional manuscript have been submitted for publication in Molecular Physics and is

currently under review. The manuscripts are referenced in this thesis as Refs. [37–39]. An overview of attended conferences and publications, along with other PhD activities, are presented in appendix A.

2.2 Thesis Structure

The bulk of the thesis is based on the three aforementioned manuscripts. Note that two typos have been found in Eqs. (15) and (16) in Bjørner and Kontogeorgis [37]. A corrigendum have been submitted to address these typos [40]. A few of the binary interaction parameters for $\text{CO}_2 + n$ -alkane mixtures in Ref. [37] have furthermore been refined since publication. The correct equations and the most recent results for the binary mixtures are presented in this thesis. The corrected equations correspond to Eqs. (5.5) and (5.6) in this work. Several chapters and appendices include additional material, which have not been presented as journal papers.

Chapters 1 and 2 are introductory chapters which introduce the problems and possibilities associated with CO_2 . The approaches taken to model CO_2 thus far are outlined, and the motivation and structure for the present work is presented.

Chapter 4 contains a brief introduction to quadrupoles and a small literature overview of the quadrupolar models employed within the SAFT framework, including their results for CO_2 mixtures. Chapters 3 and 5 presents the CPA and the new quadrupolar model extension (qCPA) respectively. Chapter 3 also include a literature survey over how CO_2 containing mixtures have been handled previously with CPA. Appendix B-C complements certain parts of chapter 5.

The first part of chapter 6 deals with the estimation of pure compound parameters for the developed qCPA as well as for certain CPA modeling approaches. In the second part of the chapter the uncertainties are utilized to quantify the effect of the parameter uncertainty, by propagating the uncertainties to both pure compound properties and binary VLEs. Most results contained in chapter 6 have been published in *Fluid Phase Equilib.* (2016), 414, 29-47 [38].

Based on the results and conclusions from chapter 6 pure compound parameters for CO_2 are selected and presented in chapter 7.

Chapters 7-9 evaluate the selected CPA and qCPA parameters and approaches for their ability to predict thermodynamic pure compound properties of CO_2 , as well as their ability to correlate and predict the phase equilibria of binary and multicomponent mixtures containing CO_2 . Chapters 7 and 8 are based on work published in *Fluid Phase Equilib.* (2016), 408, 151-169 [37]. Chapter 9 is based on results submitted to *Molecular Physics (Thermodynamics 2015 Special Issue)* [39]. Additional results have been included in all three chapters.

CHAPTER 3

The Cubic Plus Association Equation of State

Classical cubic equations of state derived from the van der Waals EoS, such as the industrially popular Peng-Robinson (PR) [41] or SRK EoS [16], usually represent the phase equilibria of hydrocarbon mixtures quite well. Their simplicity makes these models the first choice for many hydrocarbon phase equilibrium calculations used in the petroleum industry [42]. It is well-known, however, that cubic equations of state typically fail for mixtures which contain polar or associating (hydrogen bonding) compounds such as water, alcohols or glycols. The phase equilibria of associating systems are important in many practical cases e.g. when calculating the amount of inhibitor need to prevent gas hydrate formation.

To take the hydrogen bonding between associating species into account, at the high pressures often needed industrially, the attractive energy parameter in the cubic equations of state may be combined with an excess Gibbs energy mixing rule (a modified activity coefficient model). These EoS/ G^E models can, in certain cases, perform satisfactorily, however they are also known to have problems representing VLLEs [43]. Furthermore, the performance of the EoS/ G^E models depend on the success of the underlying activity coefficient model.

During the past two or three decades substantial improvements have been achieved concerning the development of advanced thermodynamic models, which can describe mixtures containing associating compounds. These improvements are primarily due to a perturbation theory for hydrogen bonding compounds originally developed by Wertheim [44–47].

Based on the work of Chapman and co-workers [17–19, 48] the SAFT EoS was the first equation of state to directly incorporate Wertheim’s association term. Since development of the first SAFT EoS the model have become very popular due to the excellent results obtained for complex mixtures. Several different modifications and extensions of the original model have been suggested, and there is now a whole family of different SAFT variants in the available literature [8].

The CPA EoS, first presented in the open literature in 1996 by Kontogeorgis et al. [20], is another popular choice amongst the equations of state, which takes association into account. The CPA EoS has been developed in collaboration with the industry,¹ and is an engineering equation of state which combines a classic cubic EoS with Wertheim’s association theory. The model has been employed to calculate the equilibrium of several complex associating mixtures, particularly those relevant to the petroleum industry, and is largely successful in the description of these mixtures.

The CPA has been extensively studied in the literature and a large number of publications concerning different aspects of the CPA EoS has become available since the first appearances of the model in the open literature (see Refs. [20, 50–52]). An excellent review of important results can be found in chapter 9-12 of the recent book by Kontogeorgis and Folas [8] as well as in Refs. [49, 53].

This chapter presents equations for the CPA EoS and describe the approaches employed with CPA to model mixtures containing CO₂.

3.1 The Cubic Plus Association Equation of State

The CPA EoS combines the SRK EoS with the association term from Wertheim’s theory [44–47], which is also employed in SAFT [17–19, 48]. The SRK term accounts for the physical interactions between molecules, while the association term takes hydrogen bonding interactions into account. Polar and quadrupolar interactions are not explicitly taken into account in the original formulation of CPA (see chapter 5).

The CPA EoS is typically presented as a pressure explicit EoS in the literature. It is often much more convenient, however, to express an EoS in terms of the (reduced) residual Helmholtz energy, ($A^r(T, V, \mathbf{n})$), since all other residual properties can be obtained as partial derivatives of the Helmholtz energy function with respect to the state variables T , V and \mathbf{n} (where T is the temperature, V the volume and \mathbf{n} is the molar composition vector). The reduced residual Helmholtz free energy for CPA can be expressed as the addition of the physical

¹Shell from 1995-1999 and since 1999 various other companies amongst these BP, TOTAL and Statoil Norway [49].

SRK term and Wertheim's association term as shown in Eq. (3.1)

$$\frac{A_{CPA}^r(T, V, \mathbf{n})}{RT} = \frac{A_{SRK}^r(T, V, \mathbf{n})}{RT} + \frac{A_{Assoc}^r(T, V, \mathbf{n})}{RT} \quad (3.1)$$

where R is the ideal gas constant. In the absence of association, Eq. (3.1) reduces to the SRK EoS.

3.1.1 The SRK contribution

Consider a mixture of total composition n , with total volume V and temperature T . The reduced residual Helmholtz energy of the SRK EoS for n moles of a mixture is expressed as [54]:

$$\frac{A_{SRK}^r(T, V, \mathbf{n})}{RT} = -n \ln \left(1 - \frac{B}{V} \right) - \frac{D(T)}{RTB} \ln \left(1 + \frac{B}{V} \right) \quad (3.2)$$

If the conventional van der Waals one-fluid (vdW1f) mixing rules are employed then $D(T)$ and B are given by quadratic sums of their pure component values:

$$D(T) = \sum_i n_i \sum_j n_j a_{ij}(T) \quad (3.3a)$$

$$nB = \sum_i n_i \sum_j n_j b_{ij} \quad (3.3b)$$

where the cross co-volume is calculated as the arithmetic mean

$$b_{ij} = b_{ji} = \left(\frac{b_{ii} + b_{jj}}{2} \right) (1 - l_{ij}) \quad (3.4)$$

It is often assumed that $l_{ij} = 0$ in which case Eq. (3.3b) reduces to

$$B = \sum_i n_i b_{ii} \quad (3.5)$$

where b_{ii} is the pure compound co-volume parameter for component i , also denoted b_0 . In this work l_{ij} is always assumed to be zero and Eq. (3.5) is effectively employed. The cross energetic parameter, a_{ij} , is calculated using the classical geometric mean rule

$$a_{ij} = \sqrt{a_{ii}(T)a_{jj}(T)}(1 - k_{ij}) \quad (3.6)$$

The temperature dependent attractive energetic parameter of component i , $a_{ii}(T)$, is typically calculated from Eq. (3.7)

$$a_{ii}(T) = a_{0,i} \left(1 + c_{1,i} \left(1 - \sqrt{T_{r,i}} \right) \right)^2 \quad (3.7)$$

where $a_{0,i}$ and $c_{1,i}$ are pure compound parameters of component i and $T_{r,i}$ is the reduced temperature ($T_{r,i} = T/T_{c,i}$) of component i , where $T_{C,i}$ is the critical temperature.

The k_{ij} , is a binary interaction parameter, which can be used to adjust the cross-interactions between two compounds. For the perfect model where all interactions were dealt with correctly it would be equal to zero. Often, however, it is necessary correlated it to binary VLE or LLE data, in which case part of the predictive capability of the EoS is lost.

The k_{ij} is typically assumed to be a constant, specific for each binary pair. However, to correlate binary mixtures over a wide temperature range it is sometimes necessary to make the k_{ij} temperature dependent. The temperature dependence is typically assumed to be directly proportional with either the temperature or the inverse temperature. The temperature dependence is generalized in Eq. (3.8) [55]

$$k_{ij} = a_{kij} + b_{kij}T + c_{kij}T^{-1} \quad (3.8)$$

The inverse relation is preferred from a theoretical point of view [56] (i.e. $b_{kij} = 0$).

It is straight-forward to calculate the derivatives required for the calculation of thermodynamic properties, see [54]. In the absence of association CPA has the three pure compound parameters, b_0 , c_1 and a_0 . To avoid ambiguity with the units it is common practice to express the energetic parameter, a_0 , on reduced from, i.e. $\Gamma = a_0/(Rb_0)$.

3.1.2 Association contribution

The contribution to the reduced residual Helmholtz free energy from the association term is given by [17, 19, 48, 54]:

$$\frac{A_{Assoc}^r(T, V, \mathbf{n})}{RT} = \sum_i n_i \sum_{A_i} (\ln X_{A_i} - \frac{1}{2}X_{A_i} + \frac{1}{2}) \quad (3.9)$$

where A_i indicates bonding sites on molecule i and X_{A_i} denotes the fraction of A-sites on molecule i *not* bonded to another association site. These fractions are found by solving the system of non-linear equations given by

$$X_{A_i} = \frac{1}{1 + \frac{1}{V} \sum_j n_j \sum_{B_j} X_{B_j} \Delta^{A_i B_j}} \quad (3.10)$$

where the association strength, $\Delta^{A_i B_j}$, between site A on molecule i and site B on molecule j depends on both T , V and n according to

$$\Delta^{A_i B_j} = g(n, V) \left(\exp \left(\frac{\varepsilon^{A_i B_j}}{RT} \right) - 1 \right) b_{ij} \beta^{A_i B_j} \quad (3.11)$$

where $\varepsilon^{A_i B_j}$ and $\beta^{A_i B_j}$ are the association energy and volume between site A of molecule i and site B of molecule j respectively. b_{ij} is the cross-covolume calculated from Eq. (3.4) and g is the Radial distribution function (RDF). Originally the RDF was approximated with the expression for the Carnahan-Starling (CS) hard-sphere RDF [20], Eq. (3.12).

$$g(n, V) = \frac{2 - \eta}{2(1 - \eta)^3} \quad (3.12)$$

where the reduced fluid density, η , is given by $\eta = B/4V$. Use of Eq. (3.12) in CPA is an approximation, however, since CPA uses the van der Waals repulsive term rather than the CS hard-sphere term employed in SAFT. Kontogeorgis et al. [52] proposed a simpler expression for g give by

$$g(n, V) = \frac{1}{1 - 1.9\eta} \quad (3.13)$$

It can be shown that Eq. (3.13) is, under certain assumptions, essentially the RDF of CPA [8]. In this work the simplified form of the RDF is employed for all calculations.

No mixing rules are required in the association term, but combining rules are required to obtain the cross-association parameters $\varepsilon^{A_i B_j}$ and $\beta^{A_i B_j}$ if more than one associating compound is present. Different combining rules have been investigated in the literature [57, 58], but only the so-called CR-1 combining rule (Eqs. (3.14) and (3.15)), Elliott's combining rule (Eq. (3.16)) and the near-Elliott combining rule² (Eqs. (3.14) and (3.17)) are used today, possibly due to the fact that they perform well and can be justified theoretically.

$$\varepsilon^{A_i B_j} = \frac{1}{2} (\varepsilon^{A_i B_i} + \varepsilon^{A_j B_j}) \quad (3.14)$$

$$\beta^{A_i B_j} = \sqrt{\beta^{A_i B_i} \beta^{A_j B_j}} \quad (3.15)$$

$$\Delta^{A_i B_j} = \sqrt{\Delta^{A_i B_i} \Delta^{A_j B_j}} \quad (3.16)$$

$$\beta^{A_i B_j} = \sqrt{\beta^{A_i B_i} \beta^{A_j B_j}} \frac{\sqrt{b_i b_j}}{b_{ij}} \quad (3.17)$$

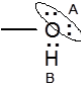
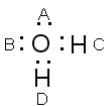
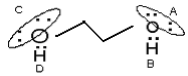
Certain compounds, which do not self-associate, may act as an electron donor (Lewis base) or electron acceptor (Lewis acid) and form hydrogen bonds with a self-associating compound. Such interactions are typically called induced association or solvation. These interactions are difficult to treat with current models since the association parameters, $\varepsilon^{A_i B_i}$ and $\beta^{A_i B_i}$, are available only for

²The near-Elliott combining rule can be obtained from Elliott's combining rule by assuming, that $\exp(\varepsilon^{AB}/(RT) - 1) \approx \exp(\varepsilon^{AB}/RT)$ and $g \approx 1$.

the self-associating compound and Eq. (3.15) and Eq. (3.17) cannot be used to calculate $\beta^{A_i B_j}$. For such mixtures $\beta^{A_i B_j}$ is typically fitted to binary data and $\varepsilon^{A_i B_j}$ is determined from equation (3.14), i.e. $\varepsilon^{A_i B_j} = \varepsilon^{A_i B_i} / 2$ since the association energy of the solvating compound is zero. This is often referred to as the modified CR-1 (mCR-1) combining rule [59]. This approach typically works well, however, the improved correlations may, at least partially, be attributed to an increased flexibility due to a higher number of adjustable parameters. The approach is, however, useful in many situations, in which one component is self-associating but interacts with a solvating compound. In this work we typically employ the CR-1 combining rule or the modified CR-1 combining rule for solvating mixtures. Alternatively an approach to induced solvation suggested by Kleiner and Sadowski [60] is employed, see chapter 8 for more details.

It can be seen from Eq. (3.10) that the association term is dependent on the association scheme, i.e. the number and type of association sites for the associating compound. In this work the notation for the different association schemes is either presented as *Xed-Yea*,³ or with the simpler notation proposed by Huang and Radosz [61]. Table 3.1 illustrate the notation of Huang and Radosz [61], as well as the corresponding number of electron donor and acceptor sites.

Table 3.1: Examples of association schemes using the notation of Huang and Radosz [61] as well as the corresponding number of negative and positive association sites.

Species	Formula	Scheme	Association sites
Alcohol		2B	1ed-1ea
Water		4C	2ed-2ea
Glycol		4C	2ed-2ea

The two additional pure compound parameters in the association term, $\varepsilon^{A_i B_i}$ and $\beta^{A_i B_i}$ implies that the model has five pure compound parameters for self-associating compounds.

The calculation of derivative properties in the association term can be rather involved but is significantly simplified if the procedure suggested by Michelsen and Hendriks is employed [62, 63].

³Where *X* and *Y* are the number of sites, and *ed* and *ad* are abbreviations for electron donor and electron acceptor sites respectively.

3.2 Modeling CO₂ Mixtures with the CPA EoS

As described in chapter 1 modeling the phase equilibrium of mixtures containing CO₂ is of high importance in the petroleum and chemical industry. A number of modeling attempts with the CPA EoS have been published for CO₂-containing mixtures. While recent work have given clear guidelines there is no general consensus on how mixtures of CO₂ (and other molecules with a high quadrupolar moment) should be modeled in the framework of CPA.

Rigorously, since CPA does not contain an explicit quadrupolar term, CO₂ should be treated as an 'inert' (i.e. non-associating, non-solvating) or possibly as a solvating molecule for mixtures containing CO₂ and self-associating compounds. In the non-associating (n.a.) case the model essentially reduces to the SRK for mixtures of CO₂ and non-associating mixtures. Modeling the phase equilibrium of mixtures containing CO₂, however, is not as simple as e.g. modeling the phase equilibrium of mixtures containing only hydrocarbons, where the k_{ij} 's are typically close to zero.

In general the predictive performance of CPA when CO₂ is treated as an inert (referred to as inert CPA or CPA n.a.) is quite poor for binary CO₂ + *n*-alkane mixtures containing CO₂. It is possible to accurately correlate the phase equilibria of CO₂ + *n*-alkane mixtures to experimental data when CO₂ is modeled as an inert compound, but relatively large binary interaction parameters of around 0.12-0.15 are needed. Figure 3.1 illustrates this with the prediction ($k_{ij} = 0$) and correlation ($k_{ij} \neq 0$) of the CO₂ + ethane VLE using CPA with CO₂ modeled as an inert. The azeotropic behaviour of the CO₂ + ethane VLE cannot be predicted with CPA if CO₂ is modeled as an inert compound, but it can be accurately correlated with a binary interaction parameter of about $k_{ij} = 0.13$.

That the azeotrope is not predicted *a priori* is believed to be due to the large quadrupolar moment of CO₂, which inert CPA does not account for; when quadrupolar interactions are ignored their interactions are effectively included in the attractive energetic CPA parameter, a_{ii} , leading to artificially large attractive energies in the SRK term for the quadrupolar compound. This leads to poor predictions for mixtures of quadrupolar and inert fluids, as $\sqrt{a_{ii}a_{jj}}$ in Eq. (3.6) becomes too large. Resultantly the k_{ij} must be large to compensate for the lack of quadrupolar interactions (as explained for polar molecules by Jog and co-workers [64, 65]). Satisfactory predictions of multicomponent VLEs containing CO₂ and hydrocarbons are typically obtained with the SRK, and most likely also with inert CPA, when a single k_{ij} per binary subsystem is employed [8].

The oxygen atoms in CO₂ are electron rich and have two lone pairs each whereas the carbon atom is electron poor. CO₂ may thus act as either a Lewis acid (electron acceptor) or base (electron donor) depending on the surrounding molecules. Due to resonance stabilization of the carbon-oxygen double bonds, however, it

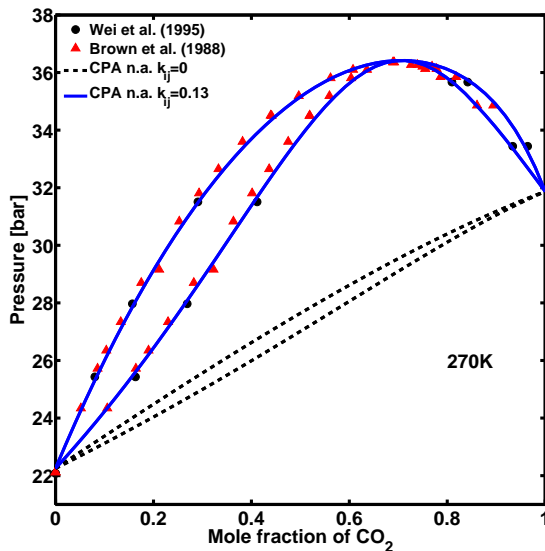


Figure 3.1: Prediction ($k_{ij} = 0$) and correlation ($k_{ij} = 0.13$) of the CO₂ + ethane VLE at T=270 K using the CPA EoS with CO₂ modeled as an inert. Experimental data from [66, 67].

primarily acts as a Lewis acid in solution with an electron donor. In mixtures containing CO₂ and e.g. alcohols or water the Lewis acid-Lewis base interaction thus occurs between the electron poor carbon atom in CO₂ and the electron rich oxygen atoms in alcohols or water, although some cooperative effect is expected [68]. Several studies indicate that the Lewis acid-Lewis base type interactions are the primary interaction (excluding dispersion) for CO₂ with associating molecules such as water, methanol and ethanol [68–71]. Results from molecular dynamics for the CO₂ + ethanol mixture suggests that the strongest interactions between the molecules are of the Lewis acid-Lewis base type [72].

From an engineering perspective these Lewis acid-Lewis base interactions may be viewed as an induced cross-association (similarly to what is typically done with e.g. benzene). For mixtures of CO₂ + self-associating compounds, such as alcohols and water, it is thus worth considering whether CO₂ should be modeled as an inert, or a solvating compound. When CO₂ is modeled as a solvating compound in CPA, quadrupolar interactions are effectively ignored and the electron donor-acceptor interactions are assumed to be the primary interaction between CO₂ and a self-associating compound. Unfortunately this approach does not affect the phase equilibrium predictions for mixtures containing CO₂ and non-associating compounds such as hydrocarbons. In an attempt to simultaneously improve the predictions for such mixtures a more pragmatic approach, which have been employed by several researchers, is to assume CO₂ to be a self-associating compound (which it is not). It is hoped, that the contribution from the association term may account, at least partially, for the lack

of an explicit quadrupolar term in the model, if nothing else then by lowering the attractive a_{ii} parameter, and thus obtain a more realistic cross-interaction.

These procedures often work well resulting in good phase equilibrium correlations with small interaction parameters [14, 21–23]. Unfortunately the improvement is obtained at the cost of additional pure component parameters and, in some cases, an extra adjustable parameter is employed to correlate the binary mixtures of CO_2 + a self-associating compound.

3.2.1 Applications of CPA for mixtures containing CO_2

Pfohl et al. [73] studied binary mixtures containing CO_2 and o-cresol, p-cresol, m-cresol, phenol, toluene, water or ethanol and ternary mixtures of CO_2 + o-cresol + p-cresol and ethanol using a PR-CPA variant where CO_2 was assumed to be an inert. The authors used a 2-parameter mixing rule for the energy parameter instead of the vdW1f mixing rule. Moreover they used a more advanced expressions for the radial distribution function. The results, however, were not very convincing.

Assuming CO_2 to be inert Folas et al. [59] modeled the solubility of CO_2 in the water-rich liquid phase and demonstrated that excellent correlations can be obtained with 'inert' CPA using $k_{ij} = -0.066$. Unfortunately the solubility of water in the CO_2 -rich phase, particularly the observed minimum, cannot be represented if CO_2 is assumed to be inert. The minimum in the solubility of water in the CO_2 -rich phase is related to a phase transition from vapor to liquid phase. Initially the solubility of water in the CO_2 -rich vapor phase decreases, but as the pressure increases CO_2 condenses to a liquid. Water is more soluble in liquid CO_2 and the solubility begins to increase again.

Kontogeorgis et al. [53, 74] showed that the minimum can be modeled, using a $k_{ij} = 0$, if the Lewis acid-Lewis base interactions are taken into account by assuming CO_2 to solvate with water, where the 4C association scheme is employed for water. Kontogeorgis et al. [53] also found that, somewhat surprisingly, it is possible to predict the minimum without accounting for solvation if the (erroneous) 2B or 3B association scheme is employed for water. This effect is attributed to a cancellation of errors. To model both phases simultaneously, however, a non-zero binary interaction parameter is needed.

Figure 3.2 show the modeling results for the solubility of water in the CO_2 -rich phase when CO_2 is modeled as an inert or solvating compound respectively. It is clear that not accounting for solvation yields poor results, as the minimum in the water solubility and thus the phase transition is not captured.

Kontogeorgis et al. [74] demonstrated that satisfactory modeling results are obtained with CPA for binary CO_2 containing mixtures with water, methanol or

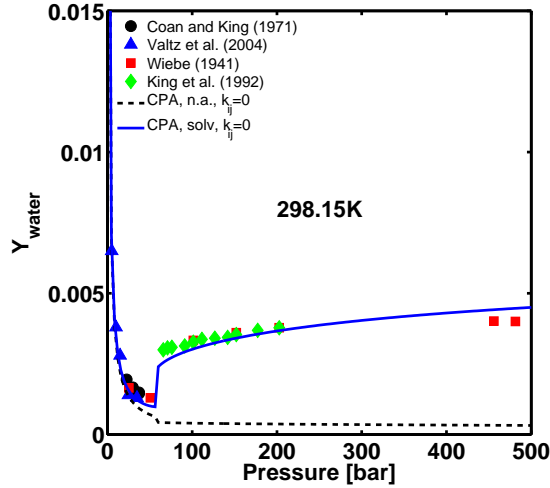


Figure 3.2: Calculation of the solubility of water in the CO₂-rich phase at 298.15 K assuming CO₂ to be either inert (black dashed line) or solvating (blue full line). In both cases $k_{ij} = 0$, additionally in the solvating case $\beta_{crs} = 0.06$ after Kontogeorgis et al. [74]. Pure compound parameters from [74]. Experimental data from [75–78].

glycols when solvation is accounted for. In the case of CO₂ + water and CO₂ + glycols only one phase is considered.

Voutsas and co-workers [21, 22, 79, 80] employed a PR-CPA on various systems containing CO₂. The PR-CPA employed in these works is similar to the CPA presented in this chapter except that it uses; i) the PR EoS as the physical term rather than the SRK, ii) the original hard sphere RDF (Eq. (3.12)) and iii) a geometric combining rule for both the cross-association energy and cross-association volume. In addition to the geometric combining rule, Perakis et al. [21] also employs the CR-1 mixing rule. For solvating mixtures, instead of using the mCR-1 combining rule, Perakis et al. [21] calculate the degree of cross-association with an adjustable "solvation factor", s_{ij} , (i.e. $\Delta^{A_i B_j} = \Delta^{A_i} s_{ij}$).

Assuming CO₂ to be either an inert, a solvating or a self-associating compound, Perakis et al. [21] modeled the binary CO₂ + water and CO₂ + ethanol mixture as well as the ternary CO₂ + ethanol + water system. The authors conclude that the best results are obtained when CO₂ is treated as an associating molecule following the 4C scheme and using the geometric mean rule for both the cross-association energy and volume.

Following this work, Voutsas et al. [22] and Papa et al. [80] employed the 4C association scheme for CO₂ to evaluate the performance of the PR-CPA for several VLE and LLE systems containing CO₂ and both non-polar (n-dodecane, benzene), polar (diethyl ether, acetone) and hydrogen bonding compounds

(ethanol, water). The obtained results are generally quite satisfactory. When modeling the CO_2 + water + acetic acid system Perakis et al. [21] used the 3B association scheme for water, rather than the typical 4C scheme, and assumed CO_2 to be solvating. For mixtures containing CO_2 and a self-associating compound an additional adjustable parameter is typically introduced in the cross-association energy.

Oliveira et al. [23] investigated the effect of modeling CO_2 as an inert compound, a solvating compound or a self-associating compound (following the 2B or 4C association scheme) for the prediction and correlation of several binary VLE systems containing CO_2 . The authors results indicate that binary systems containing CO_2 and heavy alcohols, esters or carboxylic acids may be modeled satisfactorily by simply assuming CO_2 to be an inert. On the other hand the authors found that it was necessary to assume CO_2 to be solvating or self-associating to obtain better results for mixtures containing CO_2 and light alcohols. Assuming CO_2 to be self-associating also seemed to result in a better description for the VLEs between CO_2 + n -alkanes.

As part of a comprehensive investigation on the performance of CPA for modeling the phase equilibria of mixtures with acid gases (H_2S and CO_2), Kontogeorgis and co-workers [14, 33–36, 81] recently evaluated the performance of CPA for modeling both binary and multicomponent mixtures containing CO_2 . The overall purpose of the study was to arrive at the best approach for modeling the phase equilibria of multicomponent acid gas mixtures with CPA without introducing significant changes to the model. To this end several approaches for modeling CO_2 (and H_2S) have been evaluated for their ability to model the phase behaviour of a large number of binary and multicomponent mixtures containing CO_2 .

The first study dealt mainly with the evaluation of different modeling approaches for H_2S although CO_2 was considered to be both inert and solvating [81]. In the second part of the investigation Tsivintzelis et al. [14] modeled the phase behavior and densities of binary mixtures containing CO_2 and water, n -alkanes, alcohols or glycols. CO_2 was modeled either as an inert, a solvating species or a self-associating molecule, using both the 2B, 3B, or 4C association scheme. When mixtures with cross-association were considered, two approaches for estimating the cross-association parameters were employed and compared to each other. In the first approach the regular combining rules (Eqs. (3.14) and (3.15)) were used to calculate the cross-association parameters, and in the second approach experimental values for the interaction energy, obtained from spectroscopic or calorimetric data or *ab initio* calculations, were employed for the cross-association energy. Two adjustable parameters were used when CO_2 was assumed to be solvation or when experimental cross-association energies were used. The best results were obtained when CO_2 was considered to be a solvating compound or when experimental values were employed for the cross-association energy. Rather poor results are obtained if CO_2 is modeled as a self-associating compound using the CR-1 combining rules.

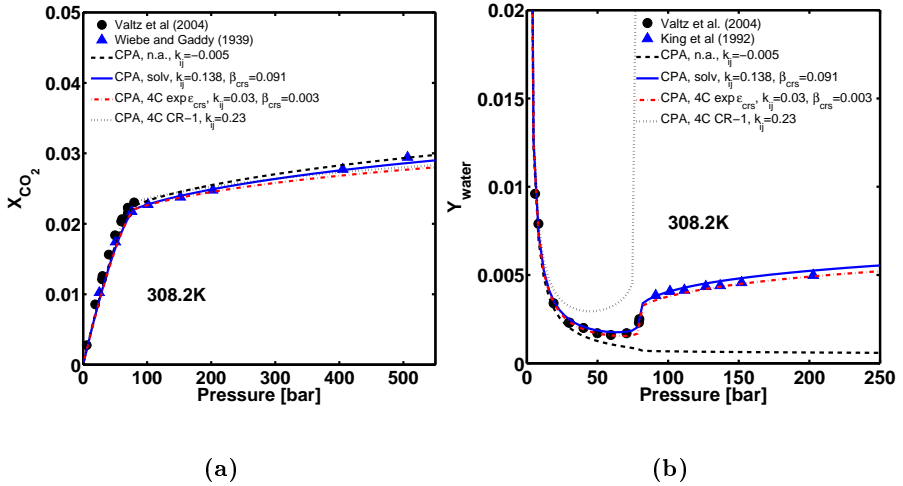


Figure 3.3: Correlation of the CO₂ solubility in the water rich liquid phase (a) and the water solubility in the CO₂ vapor/supercritical phase (b) of the CO₂ + water VLE and LLE at 308.2 K. CO₂ is assumed to be either inert (black dashed line), solvating (blue full line) (using the modified CR-1 rule), or following the 4C scheme (both with CR-1 and an experimental association energy (red dash-dotted and black dotted line respectively)). The employed parameter resemble those from [14]. Compared to experimental data from [76, 78, 82]

Figure 3.3 illustrate the correlative performance of four of the approaches evaluated by Tsivintzelis et al. [14] for calculating the phase equilibrium of the binary CO₂ + water mixture at 308.2 K. In the figure CO₂ is modeled as an inert, a solvating compound (with the modified CR-1 rule), or as a self-associating compound abiding by the 4C scheme. In the latter case both association approaches from Tsivintzelis et al. [14] are employed. It is clear from figure 3.3a that all approaches can correlate the solubility of CO₂ in the water rich phase, although some approaches employ a very large k_{ij} to do so. Figure 3.3b, however, shows that quite poor results are obtained for the water solubility in the CO₂ rich phase if CO₂ is assumed to be an inert or self-associating compound using the CR-1 rule in the latter case. Accurate results are obtained when solvation is accounted for, or when experimental values are employed for the cross-association energy. Both of these approaches use two binary parameters, whereas the other approaches use only one.

In a subsequent study Tsivintzelis et al. [33] employed a similar range of approaches for modeling CO₂, although the main focus was on the approaches which had already been found to perform well in the previous work. The work evaluated the phase equilibria of mixtures such as CO₂ + N₂ and CO₂ + O₂ and multicomponent mixtures such as CO₂ + water + methane, CO₂ + H₂S + methane, and CO₂ + water + H₂S-methane. The best approaches were again when CO₂ was considered to be solvating or self-associating (following

the 3B or 4C scheme), using two adjustable parameters and the experimental cross-association energy.

In two very recent publications Tsivintzelis and Kontogeorgis [35, 36] evaluated the performance of CPA for modeling multicomponent CO_2 mixtures containing alcohols, water, glycols, and/or n -alkanes. CO_2 was considered to be inert, solvating, or self-associating. When CO_2 is assumed to be self-associating only the approaches which use the experimental cross-association energy are considered. In all cases binary parameters were adopted from the corresponding binary systems. No adjustable parameters were fitted to the multicomponent systems. In most cases the results are similar and satisfactory with the different approaches for CO_2 .

Based on an overall assessment of their work Kontogeorgis and co-workers [14, 33–36, 81] concluded that CO_2 should be treated as a solvating or self-associating compound (with the 4C association scheme). In the latter case experimental values for the cross-association energy should be used. Chapter 8 and chapter 9 evaluates the new qCPA for several of the same mixtures studied by Kontogeorgis and co-workers in Refs. [14, 35]

3.2.2 Summary of applications

Despite the substantial work by Kontogeorgis and co-workers it is still difficult to clearly point towards a single approach which is overall superior for modeling CO_2 with CPA. It is important to consider the number of binary adjustable interaction parameters as well as the correlative and, in the multicomponent case, predicted phase equilibrium results. It is typically desired to keep the number of adjustable parameters to a minimum, to ensure physical consistency.

Treating CO_2 as a solvating compound, which may be the most appealing approach from a physical point of view, certainly works well when CO_2 is in a mixture with a self-associating compound, however it does not improve predictions for systems such as $\text{CO}_2 + n$ -alkanes where there are no cross-association interactions (but non-included quadrupolar interactions). The approach employs two adjustable parameters per binary for CO_2 plus a self-associating compound.

On the other hand, it is clear from both the investigations performed by Kontogeorgis and co-workers [14, 33–36, 81] and Voutsas and co-workers [21, 22, 79, 80] that treating CO_2 as a (pseudo) self-associating (4C) compound may greatly improve the predictive performance of the model for $\text{CO}_2 + n$ -alkane mixtures, as well as the correlative performance of the model for mixtures with self-associating compounds. It is unclear, however, how cross-association between CO_2 and the self-associating compound should be treated; Poor results are obtained if CO_2 is modeled as a self-associating compound with the normal CR-1 combing rules (one adjustable interaction parameter). If experimental

values for the cross-association energy are employed instead, the correlations are similar to those of the solvating approach (but better for CO₂ + *n*-alkanes). Unfortunately this approach also employs two adjustable parameters.

Voutsas et al. [22] employed, with good results, a single interaction parameter for CO₂ modeled as a 4C molecule, although somewhat unusual geometric combining rules are employed. In the three other works [21, 79, 80] between 2 and 8 adjustable parameters are employed per binary.

It is thus apparent that several modeling approaches gives excellent phase equilibrium results, however, the conclusions are partially clouded by the number of adjustable parameters and mixing rules employed: Rather poor results are obtained for the approaches which employ a single interaction parameter (inert CO₂ and self-associating with the CR-1 rule). Satisfactory results are typically obtained when CO₂ is modeled as either a solvating or self-associating compound when two adjustable parameters are employed. In general similar results are obtained when the same number of binary adjustable parameters are used, and it is thus difficult to say whether the improved results are due to the use of experimental cross-association energies, or if it can be attributed primarily to an increased flexibility of the model when an additional adjustable parameter is included.

CHAPTER 4

SAFT-based Models with a Quadrupole Term

The quadrupole moment is caused by the concentration of charges at four separate points in a molecule. The effect of a quadrupole is that certain molecular conformations are favoured more than others (see figure 4.1). That is, quadrupole interactions are directional, which is probably why researchers have assumed that quadrupolar interactions could be approximated, at least qualitatively, as pseudo-associating [83] (see chapter 3, section 3.2). This chapter describes three somewhat more rigorous approaches in the SAFT framework.

In the general case the quadrupole moment is a three by three symmetric tensor which in a discrete system and in terms of Cartesian tensors can be written as Eq. (4.1) [84]

$$\mathbf{Q} = \sum_i q_i \mathbf{r}_i \mathbf{r}_i \quad (4.1)$$

where \mathbf{Q} is the quadrupole moment tensor, q_i is the (partial) charge i in some molecule and \mathbf{r}_i is the position vector of charge i from some arbitrary origin chosen somewhere inside the charge distribution. The quadrupole moment tensor can be made traceless (i.e. $Q_{xx} + Q_{yy} + Q_{zz} = 0$, where x , y and z refer to the coordinate axes) in which case it is defined by Eq. (4.2) [84]

$$\mathbf{Q} = \frac{1}{2} \sum_i q_i (3\mathbf{r}_i \mathbf{r}_i - |r_i|^2 \mathbf{I}) \quad (4.2)$$

where \mathbf{I} is the identity matrix. The quadrupole moment tensor thus have five independent coordinates. In spherical coordinates \mathbf{Q} can be diagonalized, and since \mathbf{Q} is traceless it only has two independent components. The remaining three components becomes the angles which specify the orientation.

For linear (axially symmetric) molecules the quadrupole moment reduce to a scalar value [84], which is the most convenient for engineering applications. By convention the z -axis is chosen as the molecular symmetry axis (the principle axis), and the quadrupole moment becomes the z -component of the quadrupole moment tensor, and the two other directions cancel out due to symmetry i.e. $Q = Q_{zz}$. All the SAFT based quadrupolar terms are used with a scalar value for the quadrupole moment, which is also the case for almost any other quadrupolar model. For general shape molecules Gubbins et al. [85] have devised a reasonable approximation for an 'effective' scalar quadrupole moment, at least so long as the Q_{yy} and Q_{xx} components are reasonably small. In this work we will almost exclusively consider simple molecules, for which the quadrupole moment reduce to a scalar, such as CO_2 and benzene.

Figure 4.1 illustrates three types of preferred orientations for a linear point charge quadrupole. Figure 4.1a shows the ideal minimum energy "T" configuration for two quadrupoles of the same sign and figure 4.1b shows the minimum energy configuration for two quadrupoles of opposite sign. There may be additional interactions, such as shape and dispersion interactions, which can lead to different orientations being the most favored [84]. For instance, a parallel-staggered orientation as the one shown in figure 4.1c has been suggested as the most stable configuration for CO_2 [84].

The SI unit of the quadrupole moment is coulomb meters squared (C m^2), however, the quadrupole moments are often reported in Buckingham (B) or, equivalently, Debye Ångström ($\text{D}\text{\AA}$) ($1 \text{ D}\text{\AA} = 1 \text{ B} = 10^{-26} \text{ esu cm}^2 = 3.3356 \cdot 10^{-40} \text{ C m}^2$).

CO_2 has two electron rich oxygen atoms and an electron poor carbon atom (due to the higher electronegativity of the oxygen atoms relative to the carbon atom). These partial charges are the cause of the quadrupole moment of CO_2 . As CO_2 furthermore is a linear symmetric molecule its quadrupole moment reduces to a scalar. The experimental value of the quadrupolar moment of CO_2 is relatively well-defined, ranging from $-4.1 \text{ D}\text{\AA}$ to $-4.6 \text{ D}\text{\AA}$ [84, 86–91], with a typical value for the direct methods of about $-4.3 \text{ D}\text{\AA}$, which is employed in this work.

The direct experimental methods for obtaining the quadrupole moment, are expected to be accurate to within 5-10% [84]. These methods give both the sign and the magnitude of the quadrupole moment. There are also several indirect methods which are associated with considerable uncertainty [84].

4.1 Applied Quadrupolar Theory

Despite their similar theoretical background considerably less work has been done on understanding the effect of quadrupolar interactions compared to dipole-

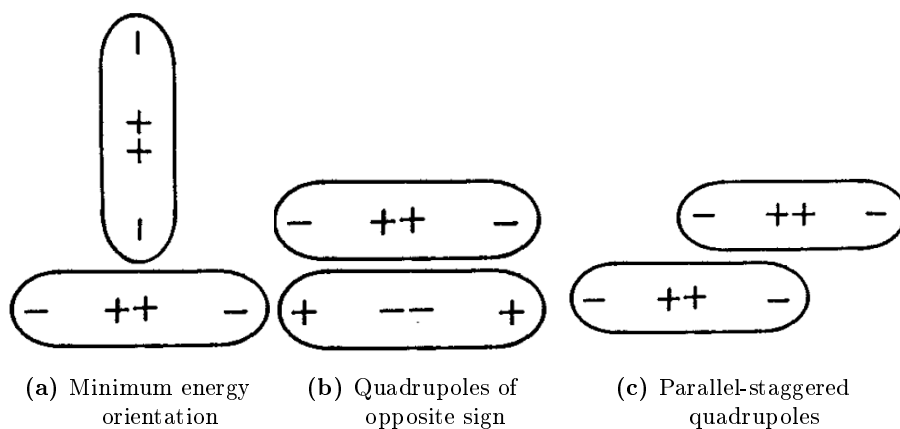


Figure 4.1: Simplified point-charge interaction schematics of (a) the minimum energy orientation for two quadrupoles (b) minimum energy orientation for two quadrupoles of opposite sign (c) two parallel-staggered quadrupoles, a stable configuration for $(\text{CO}_2)_2$ dimers). Illustrations modified from [84]

lar interactions, and the number of models which attempt to deal with polar molecules far exceeds the number of models which attempt to account for the quadrupolar forces between molecules [92]. This is most likely due to their short ranged nature. Quadrupolar forces, however, may become important for molecules with a significant quadrupole. It is generally recognized that a molecule's quadrupole moment may significantly influence its thermodynamic properties and phase behavior, especially at low temperatures. The quadrupole moment of CO_2 , for instance, is believed to be the reason for the unusual phase behavior of mixtures containing CO_2 .

To deal with polar and quadrupolar interactions a number of multipolar terms have been proposed in the literature. These terms are mainly based on modifications of a third order perturbation theory developed from statistical mechanics (the so-called u -expansion) by Stell and co-workers [24–27] and Flytzani-Stephanopoulos and Gubbins [93]. The perturbation series is expanded to include both two- and three-body interactions. Due to the slow convergence of the perturbation expansion the effect of higher order terms are approximated by a Padé approximation. The perturbation theory was originally developed for pure fluids using the Stockmayer potential (a Lennard-Jones reference potential with a point electric dipole moment) and for the hard sphere model with a central point dipole or quadrupole. Using the former potential, Gubbins and Twu [94] and Twu and Gubbins [95] (henceforth referenced simply as Gubbins and Twu [94, 95]) developed directly applicable expressions for polar and quadrupolar fluid mixtures.

4.2 Quadrupolar Contributions to the SAFT

During the last couple of decades the SAFT family have received an increasing amount of attention. To improve the predictions of the model several modifications and additions to the original EoS have been suggested, including the incorporation of several polar and quadrupolar terms. Three of the most well-known model terms, and relevant results, will be discussed in this section. The models are:

- The quadrupolar term proposed by Gross [28].
- The quadrupolar term(s) proposed by Economou and co-workers [30, 31].
- The quadrupolar term proposed by de Hemptinne and co-workers [32].

The reader is referred to the original publications for the model terms themselves.

4.2.1 The PCP-SAFT EoS

Inspired by the perturbation theory of Stell and co-workers [24–27] and Gubbins and Twu [94, 95] Gross [28] developed a new contribution for quadrupole-quadrupole interactions using a two center Lennard-Jones (2CLJ) pair potential as the reference fluid. Model constants were adjusted to molecular simulation results from Stoll et al. [96]. The proposed expression for the quadrupolar contribution was incorporated into the PC-SAFT. The resulting model is referred to as the Perturbed-Chain Polar SAFT (PCP-SAFT). The PCP-SAFT can be employed with the experimental quadrupole moment and contrary to most other equation of state contributions for polar or quadrupolar mixtures, the new EoS can be used without any additional adjustable parameters. Following this work Gross and co-workers developed expressions for dipole-dipole, quadrupole-dipole and induced dipole interactions see Refs. [97–99].

Applications of the PCP-SAFT for mixtures containing CO₂

As the experimental quadrupole moment is employed, the PCP-SAFT use the same five adjustable pure compound parameters as PC-SAFT, for non-associating compounds only three parameters are needed. The deviations in the properties which the parameters are correlated to with the PCP-SAFT are consistently similar to or smaller than when quadrupolar interactions are ignored [28]. The best correlations are obtained for the most quadrupolar molecules.

The VLE and LLE of several binary $\text{CO}_2 + n$ -alkane mixtures have been investigated with the PCP-SAFT [28, 100]. In all cases clear improvements in the form of smaller interaction parameters, are obtained relative to the regular PC-SAFT.

Issues may arise for mixtures containing more than one quadrupolar compound. For the $\text{CO}_2 + \text{benzene}$ system, for instance, correlations with the PCP-SAFT were poorer than with regular PC-SAFT. On the other hand, when the cross-quadrupolar interaction was set to zero improved predictions were obtained. This indicates that the cross-quadrupolar interactions are not adequately modeled and may indicate a fundamental problem with the proposed mixture terms. Tang and Gross [100], however, studied the same mixture, with the same experimental data and model, and obtained very good results with a very small binary interaction parameter ($k_{ij} = 0.007$).

Tang and Gross [100] furthermore employed the PCP-SAFT and PC-SAFT to model several binary mixtures containing either H_2S or CO_2 with various hydrocarbons or water. Compared to PC-SAFT the PCP-SAFT is generally in better agreement (i.e. smaller k_{ij}) with experimental phase equilibrium data for binary mixtures containing CO_2 and n -alkanes, other hydrocarbons or aromatic compounds, in particular for the solubility of CO_2 in the liquid phase. Tang and Gross [100] furthermore showed that it is necessary to use a strongly temperature dependent interaction parameter to model the $\text{CO}_2 + \text{H}_2\text{O}$ mixture over a temperature range of 323-421 K and pressures up to 70 MPa. Ramírez et al. [101] modeled the VLE of binary $\text{CO}_2 + \text{alcohol}$ systems using the PC-SAFT and different versions of the PCP-SAFT (depending on whether quadrupole, dipole and/or dipole-quadrupole interaction are considered). The authors concluded that the best model was obtained when the quadrupole moment of CO_2 was explicitly considered. Their conclusions, however, are partially clouded by the use of temperature dependent binary interaction parameters.

4.2.2 The PC-PSAFT and the tPC-PSAFT

Almost simultaneously with the development of the PCP-SAFT, Karakatsani et al. [29, 30] and Karakatsani and Economou [31] extended the SAFT and PC-SAFT framework with the quadrupolar, dipolar and induction terms derived by Larsen et al. [27]. Originally the proposed model only accounted for the dipole-dipole interactions of polar mixtures [29]. The model was later extended to explicitly account for quadrupole-quadrupole, quadrupole-dipole and dipole-induced dipole interactions [30, 31]. The perturbation terms use the hard sphere potential as the reference fluid. This leads to relatively simple correlation integrals, which are a function of the reduced density only, whereas they are a function of both density and temperature when the Lennard-Jones potential is used as the reference potential.

Two modeling approaches are suggested; In the first approach the two- and three body correlation integrals are approximated by the density polynomials of fifth- and third order employed by Larsen et al. [27]. Like the PCP-SAFT this approach does not use any additional adjustable parameters. The second approach is a simplified expression where the correlation integrals are truncated at the zeroth order term. Corresponding to the low density limit. To account for the higher order terms which are omitted in the truncation, an additional volumetric pure compound parameter is introduced.

The truncated version, which seems to be the one most used, is thus simpler at the cost of an additional adjustable parameter. The models are referred to as Perturbed-Chain Polar-SAFT (PC-PSAFT) and truncated Perturbed-Chain Polar SAFT (tPC-PSAFT) respectively.

Applications of the tPC-PSAFT for mixtures containing CO₂

The PC-PSAFT has five pure compound parameters, while tPC-PSAFT has six adjustable parameters. For non-associating compounds three or four parameters are needed. Multiple sets of parameters may provide accurate correlations to the data which the models are fitted to [29], something which is, unfortunately, not uncommon for modern equations of state (see chapter 6).

Karakatsani et al. [29] investigated (only with the dipolar contribution) several binary mixtures including CO₂ + alcohols. The alcohols were modeled with a dipole moment and as self-associating following the 2B scheme. The tPC-PSAFT has also been successfully used to correlate mixtures such as CO₂ + N₂, CO₂ + *n*-alkanes, CO₂ + cyclohexane and quadrupolar and polar mixtures such as CO₂ + acetone [102].

Focusing on the minimum in the water solubility in the CO₂-rich phase Karakatsani et al. [103] investigated the accuracy of the tPC-PSAFT for modeling the phase equilibrium of the CO₂ + water mixture. The authors considered CO₂ to be both solvating (with two association sites) and quadrupolar. Excellent correlations are obtained for the minimum in the water solubility over a wide temperature range using a temperature dependent binary interaction parameter. Recently Diamantonis and Economou [104] also evaluated the accuracy of the tPC-PSAFT and PC-SAFT for modeling the CO₂ + water mixture. Several PC-SAFT and tPC-PSAFT approaches were considered for CO₂. The best correlations were obtained with PC-SAFT, when the solvation between CO₂ and water was explicitly accounted for, although if the same number of binary adjustable parameters were employed, similar correlations could be obtained when CO₂ was considered to be self-associating. These conclusions are in agreement with conclusions for CPA (see chapter 3). Contrary to the result by Karakatsani et al. [103] correlations with the tPC-PSAFT resulted in significantly deteriorated correlations compared to PC-SAFT. The reason for this

discrepancy is probably that CO_2 was not assumed to be solvating when the tPC-PSAFT was employed by Diamantonis and Economou [104].

Kroon et al. [105] utilized the tPC-PSAFT for mixtures with CO_2 and ionic liquids. In subsequent works Karakatsani and co-workers [103, 106] re-estimated the parameters for the ionic liquids using new experimental data for the liquid density of the ionic liquids. With the new experimental data significantly lower interaction parameters are needed for to correlate the tPC-PSAFT to experimental data.

4.2.3 The polar GC-SAFT

Tamouza et al. [107] developed group contribution methods for the original SAFT, PC-SAFT and SAFT-VR respectively. NguyenHuynh et al. [32] extended these group contribution methods to quadrupolar (and polar) fluid mixtures. The quadrupolar and polar term used by the authors is based on the work by Gubbins and Twu [94, 95]. The term was extended to chain molecules using a procedure suggested by Jog et al. [65] and Jog and Chapman [64], which introduces the parameter, $x_{p,i}$, to the second and third order perturbation terms. $x_{p,i}$ is, in principle, the fraction of dipolar or quadrupolar segments in the chain molecule, but is used simply as an adjustable parameter.

Applications of the polar GC-PC-SAFT for mixtures containing CO_2

The model has primarily been evaluated for binary mixtures of numerous different polar and quadrupolar compounds, including several CO_2 containing mixtures. NguyenHuynh et al. [108] evaluated the polar Group Contribution PC-SAFT (pGC-PC-SAFT) for an extensive number of $\text{CO}_2 + n$ -alkane mixtures. To obtain unique pure compound parameters, the authors correlated the CO_2 parameters to the $\text{CO}_2 + \text{propane}$ VLE at four temperatures, in addition to the saturated liquid density and saturated vapor pressure. A method for correlating the binary interaction parameter based on segment 'pseudo-ionization energies' was also proposed [108]. NguyenHuynh et al. [109] subsequently employed the pGC-PC-SAFT to model binary mixtures containing CO_2 and either aromatic compounds, branched alkanes or H_2S . For aromatic compounds such as benzene and toluene the quadrupolar moment was considered an adjustable parameter in addition to the fraction of quadrupolar segments.

In two recent works NguyenHuynh and co-workers [110, 111] modeled the phase equilibria of mixtures containing $\text{CO}_2 + \text{alcohols}$ and $\text{CO}_2 + \text{water}$ using the polar GC-PC-SAFT. CO_2 was treated as a solvating compound with two solvation sites.

4.2.4 Summary of applications

Table 4.1 provides a partial list of binary mixtures containing CO₂, for which three of the SAFT based quadrupolar equations of state have been employed for phase equilibrium calculations. Both VLE and LLE data have been considered for alcohols and water. For alkanes both VLE and LLE data were considered with PCP-SAFT and pGC-PC-SAFT. The PC-PSAFT, which is not included in the table, have only been used to calculate the phase equilibria of mixtures containing CO₂ and ethanol or methanol. All the models have also been employed for a considerable number of non-CO₂ containing mixtures, see Refs. [8, 83] for a partial overview.

Table 4.1: Binary mixtures containing CO₂ + a compound group or compound, to which the SAFT-based quadrupolar equations of state have been employed for phase equilibrium calculations in Refs. [28, 100–106, 108–112]. Similar compounds or compound groups are horizontally aligned.

tPC-PSAFT [30, 31]	PCP-SAFT [28]	polar GC-PC-SAFT [32]
<i>n</i> -alkanes [102]	<i>n</i> -alkanes [28, 100]	<i>n</i> -alkanes [108] branched alkanes [109]
cyclohexane [102]	cyclic alkanes [100]	aromatic hydrocarbons [109]
water ^a [103, 104]	aromatic hydrocarbons [28, 100]	aromatic hydrocarbons [109]
nitrogen [102]	water ^a [100]	water [110]
acetone [102]	alcohols [28] [101] ^a	alcohols [111]
	H ₂ S [100]	H ₂ S [109] benzofuran [112] ethylphenol [112]
ionic liquids [103, 105, 106]	refrigerants [99]	

^a A temperature dependent binary interaction parameter was employed.

With the exception of tPC-PSAFT the quadrupolar SAFT models have only been employed to calculate the phase equilibrium of a limited number of multicomponent mixtures, something which is clearly reflected in table 4.2 which contains a list of CO₂ containing ternary mixtures for which the quadrupolar equations of state have been employed.

4.3 Similarities and Differences

All model terms are based on similar third order perturbation theories (the *u*-expansion), typically based on work by Stell and co-workers [24–27] and Gubbins and Twu [94, 95]. All quadrupolar (and polar) terms are approximated by a Padé approximation (see Eq. (5.2)). Finally all quadrupolar expressions ignore the first order term, A_1 , which is zero for spheres and non-zero but small for hard dumbbells [113].

Table 4.2: Ternary mixtures containing CO_2 + two other components, to which the SAFT-based quadrupolar equations of state have been applied in Refs. [29, 100, 102, 103, 111].

tPC-PSAFT [30, 31]	PCP-SAFT [28]	polar GC-PC-SAFT [32]
		methanol+ethanol [111]
N_2+n -propane [102]		
N_2+n -butane [102]		
N_2 +cyclohexane [102]		
water+[bmim ⁺][NO ₃ ⁻] [103]	methane+H ₂ S [100]	methanol+propane [111]
water+[HOPmim ⁺][NO ₃ ⁻] [103]		
acetone+[bmin ⁺][PF ₆ ⁻] [102]		

Both the PCP-SAFT developed by Gross [28] and the PC-PSAFT developed by Economou and co-workers [30, 31] employ the experimental value of the quadrupole or dipole moment. No additional pure compound parameters are introduced in either model. The tPC-PSAFT and the pGC-PC-SAFT on the other hand both employ an additional adjustable parameter in the quadrupolar term.

The two model terms developed by Economou and co-workers are, of course, very similar as they are both based on the quadrupolar term developed by Larsen et al. [27]. The difference between the two terms is solely that in the full version the two- and three-body correlation integrals are approximated by density polynomials of fifth and third order respectively, whereas these polynomials are truncated at the zeroth order term in the tPC-PSAFT, at the cost of an additional pure compound parameter.

The main difference between the different quadrupolar terms is probably whether or not they employ an additional adjustable parameter and how the two- and three-body correlation integrals are approximated in the various models. The pGC-PC-SAFT employ the expressions presented by Gubbins and Twu [94, 95], which are functions of both the temperature and the reduced density. In PCP-SAFT the three-body term is approximated by a fourth order polynomial in the reduced density, the second-order two-body term is a function of both the density and the temperature and finally the third order two-body term is set to zero. The latter approximation is clearly the most severe. As mentioned above the correlation functions for the PC-PSAFT are approximated by density polynomials. Due to the zeroth order approximation the correlation integrals are approximated simply by a constant value in the tPC-PSAFT.

Table 4.3 attempts to summarize the differences and similarities in the different SAFT-based equations of state.

Compared to the base SAFT variant it seems that improved predictions and correlations (smaller k_{ij}) are typically obtained for binary VLE when a quadrupolar term is coupled to PC-SAFT. The quadrupolar models, however, have several limitations; The models are (in principle) only applicable to linear axially sym-

Table 4.3: Summary of differences and similarities for SAFT-based equations of state for quadrupolar mixtures. $J_{i,k}$ denotes the two- and three body correlation integrals present in the theories.

Model	PC-PSAFT	tPC-PSAFT	PCP-SAFT	pGC-PC-SAFT
Reference	[30, 31]	[30, 31]	[28]	[32]
Quadrupole term	[27]	[27]	[28] ^a	[94, 95]
Base EoS	PC-SAFT	PC-SAFT	PC-SAFT	GC-PC-SAFT
Expansion	u-exp	u-exp	u-exp	u-exp
Series approx.	Padé	Padé	Padé	Padé
Ref. fluid	HS	HS	2CLJ	LJ
Corr. integrals	$J_{i,k}(\rho^*)$	$J_{i,k}(\rho^* \rightarrow 0)$	$J_{3,2} = 0^b$	$J_{i,k}(\rho^*, T)$
Mixing rules	geometric	geometric	none	none
Extra Adjustable	0	1 (v_p)	0	1 (x_p) ^c

^a Adjusted to molecular simulation data from Stoll et al. [96].

^b Additionally for the remaining correlations integrals $J_2(\rho^*, T)$ and $J_{3,3}(\rho^*)$.

^c Two adjustable parameters for benzene and esters.

metric molecules, where the quadrupole moment tensor reduces to a scalar value. It has furthermore been shown for the polar SAFT variants that false liquid-liquid splits may be predicted by the models [114]. While no such study has been made for the quadrupolar versions of SAFT, similar problems may be expected, as the models have been derived in a similar manner. Mixtures of several quadrupolar (or dipolar) molecules are challenging, and the results are sometimes better if only one component is assumed to have a quadrupole or dipole moment [28], which suggests that the way the cross-quadrupolar interaction are calculated could be improved [28]. Finally, the quadrupolar (and dipolar) terms are in principle not directly applicable with associating mixtures, due to the local structuring caused by both terms.

CHAPTER 5

The Quadrupolar CPA Equation of State

From the discussion in chapter 3 it is clear, that there are several cases where CPA works quite well for mixtures containing CO_2 , even when CO_2 is treated as an inert. Treating CO_2 as a solvating compound may result in improved correlations for mixtures containing CO_2 and one or more self-associating compounds. Unfortunately, relatively high interaction parameters are still needed for simple CO_2+n -alkane mixtures. On the other hand, if CO_2 is treated as a self-associating compound improved predictions may be obtained. Explicit inclusion of self-association for CO_2 seem to increase the intermolecular CO_2 - CO_2 interactions, while simultaneously reducing the cross-interactions in the SRK term, just like a quadrupole term would do [14]. The procedure is, however, physically inconsistent as CO_2 is not self-associating.

To address this issue it is believed that a physically more consistent and predictive model may be obtained if the effect of the quadrupole moment is taken into account by introducing an explicit quadrupolar term in CPA. From the preceding discussion in chapter 4 it seems that the structure of all terms is quite similar, which may suggest, that the choice of which term should be modified to CPA is somewhat arbitrary. As CPA does not contain segments, but effectively treat molecules as spheres, it is much more convenient to build directly upon the originally developed quadrupolar terms. The simplified quadrupolar term presented here is thus based on the explicit expressions developed by Larsen et al. [27] for hard spheres with a point quadrupole. qCPA may be employed with the experimental quadrupolar moment, and may be used with or without introducing an additional pure compound parameter.

5.1 The Quadrupole CPA Term

Chapter 3 showed how CPA could be expressed in terms of the residual Helmholtz energy, where the total Helmholtz energy is a sum of the SRK and association contributions. To include a quadrupolar term in the model an additional perturbation term due to the quadrupole is added to CPA:

$$\frac{A_{CPA}^r(T, V, \mathbf{n})}{RT} = \frac{A_{SRK}^r(T, V, \mathbf{n})}{RT} + \frac{A_{Assoc}^r(T, V, \mathbf{n})}{RT} + \frac{A_{Quad}^r(T, V, \mathbf{n})}{RT} \quad (5.1)$$

The expression for the final quadrupolar term is an adaptation of the third order perturbation theory developed by Stell and co-workers [24–27]. The quadrupolar term is, as almost any other quadrupolar or dipolar model, set in a Padé approximation as suggested by Rushbrook [25]. The reduced residual Helmholtz free energy for the quadrupolar expression is thus calculated from a Padé approximation as Eq. (5.2)

$$\frac{A_{Quad}^r(T, V, \mathbf{n})}{RT} = \frac{A_{2,Quad}^r(T, V, \mathbf{n})/RT}{1 - A_{3,Quad}^r(T, V, \mathbf{n})/A_{2,Quad}^r(T, V, \mathbf{n})} \quad (5.2)$$

Where A_2^r and A_3^r indicate the second- and third-order perturbation terms respectively. The first-order term is effectively zero [27]. The third-order term is the sum of both a two-body and a three-body contribution, since it has been shown that for multi-polar interactions three-body contributions cannot be ignored [26]. That is;

$$\frac{A_{3,Quad}^r(T, V, \mathbf{n})}{RT} = \frac{A_{3,2,Quad}^r(T, V, \mathbf{n})}{RT} + \frac{A_{3,3,Quad}^r(T, V, \mathbf{n})}{RT} \quad (5.3)$$

To develop expressions, applicable in CPA, for the quadrupole contribution the explicit expressions developed by Larsen et al. [27] for pure symmetric hard spheres with a point quadrupole at their centre are employed. The expressions are extended to mixtures, following the work of Twu and Gubbins [95] and Karakatsani et al. [30, 31] and related to the model parameters of CPA. In terms of the state variables, V , T , and \mathbf{n} the expressions become:

$$\frac{A_{2,Quad}^r}{RT} = -\frac{7}{10} \frac{N_A}{V (k_b T)^2} \sum_i^{nc} n_i \sum_j^{nc} n_j \frac{Q_{ij}^4}{\sigma_{ij}^7} I_{10}^{HS} \quad (5.4)$$

$$\frac{A_{3,2,Quad}^r}{RT} = \frac{36}{245} \frac{N_A}{V (k_b T)^3} \sum_i^{nc} n_i \sum_j^{nc} n_j \frac{Q_{ij}^6}{\sigma_{ij}^{12}} I_{15}^{HS} \quad (5.5)$$

$$\frac{A_{3,3,Quad}^r}{RT} = \frac{1}{6400} \frac{N_A^2}{V^2 (k_b T)^3} \sum_i^{nc} n_i \sum_j^{nc} n_j \sum_k^{nc} n_k \frac{Q_{ijk}^6}{\sigma_{ij}^3 \sigma_{ik}^3 \sigma_{jk}^3} I_{TQ}^{HS} \quad (5.6)$$

where N_A is the Avogadro constant, k_b is Boltzmann's constant, Q is the scalar quadrupolar moment, σ is the hard sphere diameter and I_n and I_{TQ} are correlation integrals with the hard sphere model as the reference fluid. The terms

may look familiar as Economou and co-workers [30, 31] employed the same base model in the development of the tPC-PSAFT equations of state.

In the work of Larsen et al. [27] the correlation integrals in equations (5.4)-(5.6) were approximated by analytical (reduced) density polynomials of fifth and third order respectively, that is

$$I_n^{HS} = \sum_{i=0}^5 J_{i,n}(V, n)^i \quad (5.7a)$$

$$I_{TQ}^{HS} = \sum_{i=0}^3 J_{i,TQ}(V, n)^i \quad (5.7b)$$

where the coefficients $J_{i,n}$ and $J_{i,TQ}$ can be found in the original reference [27].

To simplify the model, and in particular the volume derivatives, we assume that these correlation functions can be truncated already at the zeroth order term. The zeroth order coefficients are given analytically as [27]:

$$I_n^{HS} \approx J_{0,n} = \frac{4\pi}{n-3} \quad (5.8a)$$

$$I_{TQ}^{HS} \approx J_{0,TQ} = 54\pi^2 \quad (5.8b)$$

Thus, the correlation functions are no longer a function of the (molar) volume, but are simply three constants. Although this is clearly a major simplification the approach has been employed with success in tPC-PSAFT [29–31] as discussed in chapter 4, although an additional adjustable parameter was needed to retain a performance comparable to the non-truncated version. The assumption may be particularly suited for CPA as the van der Waals EoS (or SRK in the case of CPA) is essentially derived as a hard spheres model in the low density limit.

No mixing rules are required in the quadrupolar term (Eq. (5.4)-(5.6)). Combining rules may however be employed. If geometric-mean combining rules are employed like in the work by Economou and co-workers the the cross quadrupolar moment for two- and three-body contributions are calculated as

$$Q_{ij} = \sqrt{Q_{ii}Q_{jj}} \quad (5.9)$$

$$Q_{ijk} = \sqrt[3]{Q_{ii}Q_{jj}Q_{kk}} \quad (5.10)$$

Note, however, that more general mixing terms, which avoid the square and cubic roots may be preferred, as the combining rules presented here does not consider quadrupoles of opposite sign, which are effectively treated as two quadrupole of the same sign (to avoid complex values). This is discussed further in chapter 8 section 8.4.4.

Finally, it is advantageous to relate the molecular diameter of the hard-sphere, to a co-volume parameter similar to that used in CPA. When de Villiers et al. [115]

extended CPA with the dipolar theories of Gross [97] and Jog and Chapman [64] they assumed that the original definition of the co-volume in terms of the molecular hard-sphere diameter could be employed ($b = 4V^{mol} = (2/3) N_A \pi \sigma^3$). The quadrupolar term, however, is based on a hard sphere reference fluid, whereas CPA is based on the van der Waals repulsive term. Wong and Prausnitz [116] showed that the difference between the CS EoS and the van der Waals repulsive term can be reduced if $b^{eff} = b_0^Q \approx b/2$.¹ This is illustrated in figure 5.1 which shows, that the CS EoS and the repulsive part of the van der Waals EoS are in much better agreement if an 'effective' van der Waals volume of $b/2$ is employed.

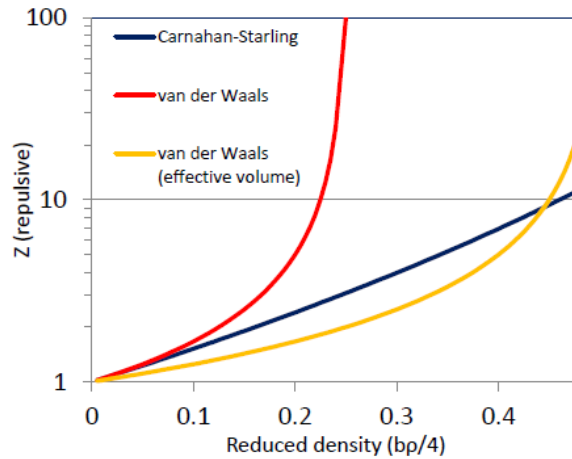


Figure 5.1: Compressibility factor for a hard-sphere fluid. Comparison of the CS EoS and the repulsive part of the van der Waals EoS as a function of reduced density. Adapted from [116].

Using the effective co-volume we get

$$b_0^Q = (1/3) N_A \pi \sigma^3 \quad (5.11)$$

where b_0^Q is the co-volume parameter in the quadrupolar term. When Eq. (5.11) is employed the value of b_0^Q should, ideally, be similar to that of b_0 .

5.1.1 Model variants

In this thesis we will mainly investigate and evaluate two variations of the qCPA; In the first version it is assumed that the co-volume from CPA can be set equal

¹It is of historical interest to note that in his Nobel lecture Van der Waals remarked that the definition of $4V^{mol}$ for the co-volume parameter only applies for infinitely diluted systems, and that empirical values of the co-volume parameter decrease to about half the theoretical value as the volume decreases (J. D. van der Waals, Nobel Lecture, **1910**) [117]. This in good agreement with the findings by Wong and Prausnitz [116].

to the effective quadrupolar hard sphere co-volume i.e. $b_0 = b_0^Q$. Equation (5.11) is then used to directly calculate σ , which is used in eq. (5.4)-(5.6). In this way no additional adjustable parameters are introduced by the quadrupolar term. In the second variant b_0^Q is employed as an additional adjustable parameter. The experimental quadrupolar moment is employed in both cases. Note, however, that, if desired, the quadrupolar moment may also be used as an adjustable parameter, in which case the model would employ an 'effective' quadrupolar moment (this is investigated briefly in chapter 8). As it is typically desired to use as few adjustable parameters as possible it cannot be recommended to use both adjustable parameters simultaneously.

It is clear that qCPA uses three or four adjustable pure compound parameters for non-associating compounds with a quadrupole moment (such as CO_2). For self-associating compounds which also has a quadrupole moment (such as water) the quadrupole is, in this work, assumed to be negligible, and thus ignored.

To justify the addition of the adjustable parameter in the second model variant, we note that due to the powers which both the co-volume and the quadrupolar moment are in (see equations (5.4)-(5.6)), the value of these variables may strongly affect the magnitude of the quadrupolar term. Economou and co-workers also used an adjustable quadrupolar volume related parameter in an attempt to compensate for the truncation of the correlation integrals (Eq. (5.8a) and Eq. (5.8b)). As the zeroth order approximation is employed in this work as well, it would make sense that an additional adjustable parameter was needed in qCPA, and as the use of equation (5.11) in this work is a further approximation it makes even more sense to use the co-volume parameter as an adjustable parameter in qCPA than it did in tPC-PSAFT. However, as described above the model will be evaluated both with and without an additional adjustable parameter.

5.2 Model Implementation

As all other residual properties can be calculated as first or second order partial derivatives of the residual Helmholtz energy function with respect to the state variables T , V and \mathbf{n} , implementation of the quadrupolar term in CPA is a relatively simple matter of adding the partial derivatives of the quadrupolar term to the corresponding derivatives of CPA. The derivatives of the quadrupolar term are comparatively simple to calculate, due to the fact that the correlation integrals are treated as constants rather than functions of V and n and sometimes even T . All necessary derivatives can be found in Appendix B.

The quadrupolar term have been implemented both in MATLAB and in Fortran. The Fortran implementation has been included in the CPA module created by Dr. Bjørn Maribo-Mogensen and subsequently linked to MATLAB though the

MEX interface. This interface allows the use of routines such as fugacity and flash calculation in MATLAB, but (almost) with the computational efficiency of FORTRAN. Essentially all calculations and visualizations are performed in MATLAB.

5.2.1 Evaluation of derivatives

Unfortunately, even the most systematic approach does not exclude the possibility of programming errors. To counteract this risk, all partial derivatives in the quadrupolar term are evaluated for errors by comparing the analytical derivatives with their numerical approximation. Both the central difference formula as well as the complex step approximation are used to estimate the numerical derivatives, see Appendix C for details.

As an example, using pure CO₂ as a sample compound, table 5.1 shows the relative difference between the analytical and the numerical derivatives with central differences at the conditions $T = 250$ K, $n = 10$ mol and $V = 1$ L.² The low relative errors in table 5.1 clearly indicate that the analytical derivatives of the quadrupolar term seem to be calculated correctly.

Table 5.1: Relative error in the numerical derivatives of the Helmholtz energy function for the quadrupole term at $T = 250$ K, $n = 10$ mol and $V = 1$ L, using CO₂ as the sample compound. The numerical derivatives are calculated with the central difference formula.

Derivative	$\frac{ f'_{centraldiff} - f'_{analytic} }{ f'_{analytic} }$
$\partial F/\partial V$	$2.0 \cdot 10^{-11}$
$\partial F/\partial T$	$3.7 \cdot 10^{-9}$
$\partial F/\partial n_i$	$7.0 \cdot 10^{-12}$
$\partial^2 F/\partial V^2$	$5.0 \cdot 10^{-11}$
$\partial^2 F/\partial T^2$	$1.3 \cdot 10^{-9}$
$\partial^2 F/\partial n_i \partial n_j$	$1.6 \cdot 10^{-10}$
$\partial^2 F/\partial V \partial T$	$1.3 \cdot 10^{-10}$
$\partial^2 F/\partial n_i \partial T$	$2.8 \cdot 10^{-11}$
$\partial^2 F/\partial n_i \partial V$	$4.4 \cdot 10^{-11}$

²The step size is $h = \mathbf{x}\epsilon^{1/3}$ for the central differences, where $\mathbf{x} \in \{T, V, \mathbf{n}\}$ and ϵ is machine accuracy ($\approx 2.2 \cdot 10^{-16}$).

CHAPTER 6

Parameter Estimation & Propagation of Uncertainty

The pure compound parameters of advanced thermodynamic models such as CPA and SAFT are typically correlated to experimental saturated vapor pressures, P^{sat} , and saturated liquid densities, ρ_{sat}^{liq} (over a specified temperature range) by minimizing a weighted Least Squares (LSQ) objective function. The objective function is typically similar to that shown in Eq. (6.1)

$$OF = \sum_i^{N_P} \left(\frac{P_{i,exp}^{sat} - P_{i,calc}^{sat}}{P_{i,exp}^{sat}} \right)^2 + \sum_i^{N_\rho} \left(\frac{\rho_{i,exp,sat}^{liq} - \rho_{i,calc,sat}^{liq}}{\rho_{i,exp,sat}^{liq}} \right)^2 \quad (6.1)$$

where N_P and N_ρ are the number of data points for the saturated pressure and liquid density respectively, and each data point i is at a different temperature. The parameters obtained from such a minimization procedure are generally assumed to be unique, and can be employed directly for phase equilibrium calculations. No parameter uncertainties are typically presented. While such an assumption may be reasonable for three parameter cubic equations of state, it is highly questionable for models such as CPA or SAFT, which contain considerable more adjustable parameters.

As the number of adjustable parameters in thermodynamic models increase, the parameter estimation problem becomes more complicated due to parameter identifiability issues. For example, often, and for the same model, different parameter sets are proposed in the literature for the same compound, even if the same objective function is employed [20, 74, 118]. This multiplicity of the parameters suggests that the parameters are *not* unique and that multiple parameter sets can reproduce the experimental data to within experimental uncertainty [8, 119]. This is particularly true for self-associating compounds

due to the high correlation between the two parameters in the association term (see sections 6.2.2 and 6.3.2).

To illustrate this difficulty figure 6.1 shows a contour plot of equation (6.1) for (a) inert CO_2 and (b) CO_2 treated as a self-associating compound following the 4C association scheme. Figure 6.1a shows that the minimum seems to be relatively well-defined when CO_2 is treated as an inert. On the other hand when CO_2 is treated as a self-associating compound (figure 6.1b) the minimum is ill-defined and elongated. Although the contour plots does not show the full complexity of the parameter estimation, as only two parameters can be varied at a time, they aptly serve to illustrate the problem.

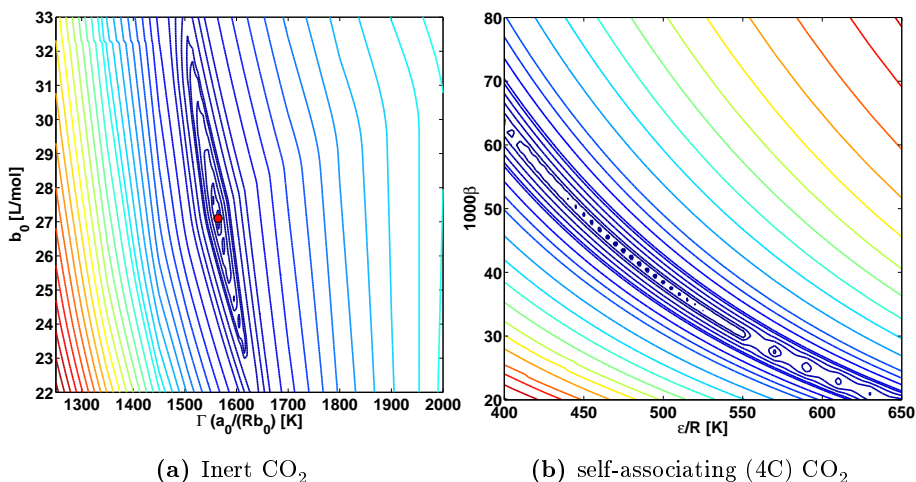


Figure 6.1: Contour plot of the objective function in Eq. (6.1) calculated for CO_2 treated as an inert compound with CPA at varying Γ and b_0 and with $c_1 = 0.73$ (a) and as a self-associating compound at varying β and ε with $c_1 = 0.73$, $b_0 = 28.4$ L/mol and $\Gamma = 1250$ K using CPA. Blue contours indicate the lowest values and red contours the highest values. The red dot in (a) represents the minimum with the chosen value of c_1 . There is no clear minimum in (b)

Sauer and Chapman [120] found that a wide range of parameters could represent the experimental pure compound data due to a very flat minimum in the objective function of a four parameter polar SAFT variant proposed by Jog and Chapman [64]. Dominik et al. [121] arrived at a similar conclusion using the same polar SAFT variant as well as one where SAFT was combined with the (mainly empirical) polar term of Saager and Fischer [122]. The authors suggested that a binary VLE should be included in the parameter estimation. Using a polar GC-SAFT NguyenHuynh et al. [32] similarly found that numerous parameter sets could be obtained, particularly due to the strong correlation between the energetic parameter ε in SAFT and the quadrupole or dipole moment. Recently Korden et al. [123] stated that it is difficult to determine meaningful

parameters for polar models, when a parameter is adjusted in the polar term in addition to the parameters in the dispersion term.

Based on a significant amount of trial and error, it appears that several parameter sets can also correlate the experimental data within experimental error for CO_2 when qCPA is employed with four adjustable parameters. Figure 6.2 for example shows the CO_2 + ethane VLE, predicted with four different parameter sets obtained with the four parameter version of qCPA using equation (6.1) as the objective function and four different initial guesses for the pure compound parameters. All parameter sets correlate the saturated liquid density and pressure satisfactorily.

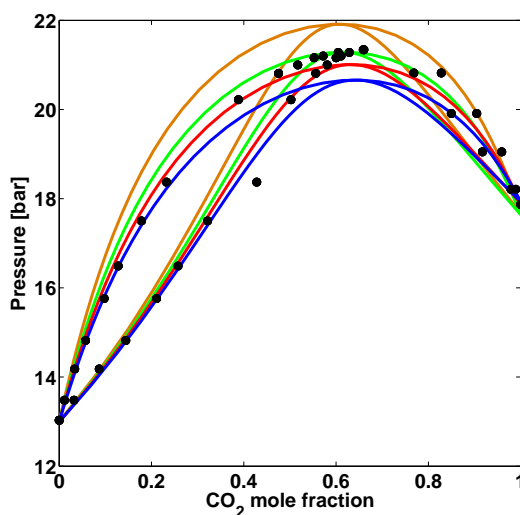


Figure 6.2: Predictions of the CO_2 + ethane VLE at 250K using four different parameter sets for qCPA with four adjustable parameters. All parameter sets correlate the saturated liquid density and pressure within experimental error and have been obtained by using different initial guesses for the parameters.

One approach for identifying the optimum parameters is to incorporate mixture data in the parameter selection [8, 32, 74, 118, 121]. LLE data of the compound in question with an inert compound (e.g. an *n*-alkane) is particularly useful and a stringent test, as LLE is typically sensitive to the parameters. The approach, however, seem to have some drawbacks; if LLE data is incorporated directly in the objective function there is a risk of putting too much weight on the LLE thus loosing pure compound accuracy, on the other hand, if LLE data is only employed to select the optimal parameters after several parameter sets have been generated there is an obvious risk that the 'right' parameter set has not yet been found. Moreover the approach implicitly assumes the model to be accurate, and not an approximation to the real system.

An often overlooked issue in this regard is the estimation of uncertainties in the pure compound parameters. Even the most accurate experiments are subject to measurement errors. Moreover the parameters may be correlated, so that a change in one parameter can be compensated by a change in another. Consequently the pure compound parameters will be associated with some degree of uncertainty, which is typically ignored or assumed insignificant in the majority of studies thus far. Even small errors in the parameters, however, may significantly affect the result of a simulation [124]. While several researchers have drawn attention to this problem [124–130] surprisingly little work has been done on analyzing and quantifying the uncertainty of parameters in thermodynamic models and their effect on physical property and equilibrium calculations.

6.1 Uncertainty Analysis and Uncertainty Propagation

The work of Whiting and co-workers [131–137] is perhaps one of the most notable contributions to uncertainty estimates of thermodynamic models. Using a Monte Carlo approach the authors analyzed the effect of uncertainties in thermodynamic data and their propagated effect on process design. More recently Mathias and co-workers [138–140] also investigated the importance of uncertainty and uncertainty propagation for processes such as CO₂ capture. Hajipour and co-workers [141–143] estimated the critical properties for a large number of hydrocarbons. The authors took both the experimental uncertainty in the data as well as the correlation between thermodynamic model parameters into account. Subsequently the uncertainties of the binary interaction parameters for 87 binary mixtures were estimated by use of the pure compound uncertainties.

Most research has focused on the propagated error from a thermodynamic model to various unit operations such as distillation columns (e.g. [125, 126, 138, 144]). Uncertainty analysis, however, can also be used for model development and comparison; by comparing the propagated uncertainties of selected physical properties and equilibria for different models, or model variants, the models can be compared more objectively. For instance when models such as CPA and SAFT are compared, they often perform almost identically and what differences are present may, in many cases, be due to statistical uncertainties in the pure compound parameters of the models, rather than due to one model being superior to the other.

In an effort to improve the performance and physical consistency of advanced thermodynamic models, additional terms are often added to the base EoS, such as qCPA in this work. Unfortunately the addition of an extra term often leads to an increase in the number of adjustable parameters. This may make it difficult to estimate unique pure compound parameters due to high correlations

between parameters as well as the possible presence of multiple local minima. One reason for this is that the data used for parameter estimation is too limited in relation to the model complexity, which must be able to predict a wide range of properties besides those its parameters are fitted to. This may be particularly relevant for a molecule such as CO₂, for which the saturation curve is very short. Both SAFT and CPA can for instance correlate the saturated vapor pressure and liquid density of CO₂ almost within experimental error, using only the three pure compound parameters commonly employed for non-associating molecules [14].

During the past decade several quadrupolar terms have been added to the SAFT framework (see chapter 4). Unfortunately the new terms are often parametrized by using an additional pure compound parameter (such as an 'effective' quadrupolar moment). Other more pragmatic approaches tend to treat CO₂ as a self-associating or solvating molecule. Tsivintzelis et al. [14], for instance, demonstrated that such an approach often works quite well, at the cost of two additional pure compound parameters (see chapter 3, section 3.2). If the uncertainties in parameters are significant, however, it may be difficult to compare the performance of various modeling approaches, as their differences may be due to the parametrization, rather than the superiority of one model over the other.

In this chapter the uncertainties in the pure compound parameters of CO₂ are systematically evaluated, when different modeling approaches are employed with CPA as the base model. The uncertainty estimates are obtained from either a linear approximation of the covariance matrix of parameters estimated from nonlinear regression (LSQ) or using the Bootstrap method [145] (section 6.2). A Monte Carlo procedure (with Latin Hypercube Sampling (LHS) and Iman-Conover correlation control) is subsequently employed to quantify the effect of the parameter uncertainty by propagating the uncertainties to various physical properties (see section 6.4). This work was published in *Fluid Phase Equilib.* (2016), 414, 29-47 [38].

6.2 Parameter Estimation - Uncertainty and Correlation

The pure compound parameters in CPA are typically fitted to saturated pressures and saturated liquid densities using a weighted LSQ objective function such as Eq. (6.1). Ideally experimental data should be used for such correlations, however, more often than not, pure compound correlations, such as the Span and Wagner EoS for CO₂ [15], as implemented in the Reference Fluid Thermodynamic and Transport Properties (REFPROP) program [146] and disseminated through the National Institute of Standards and Technology (NIST) Chemistry Webbook [147] are employed as pseudo-experimental data, since their

correlations are accurate to within experimental error for many compounds. While such pseudo-experimental data are a convenient way of quickly obtaining quite accurate data for many compounds, the measurement errors present in the experimental data is lost. Moreover as the number of model parameters is increased and the closeness of fit improves, there is a clear risk of over-fitting.

This section investigates and compares the uncertainty when CO₂ is treated as either an inert (non-associating, non-quadrupolar) molecule, an associating molecule, and as a quadrupolar molecule. In the first two cases regular CPA is employed with and without association (with focus primarily on association scheme 4C). In the latter case qCPA is employed. Two cases are evaluated when CO₂ is considered to be a quadrupolar molecule, one where no additional adjustable parameter is employed and one where an additional volumetric parameter is employed. Table 6.1 summarizes the various approaches and the adjustable parameters involved in each approach.

Table 6.1: Modeling approaches with CPA, including the number of adjustable pure compound parameters, investigated for CO₂.

Designation	Modeling approach	Association sites	no. Adj	Adj. parameters.
A	inert	no sites	3	Γ^a, b_0, c_1
B	2B ^b	1ed-1ea	5	$\Gamma, b_0, c_1, \epsilon, \beta$
C	3B	2ed-1ea	5	$\Gamma, b_0, c_1, \epsilon, \beta$
D	4C	2ed-2ed	5	$\Gamma, b_0, c_1, \epsilon, \beta$
E	Quadrupolar	no sites ^c	3	Γ, b_0, c_1
F	Quadrupolar	no sites	4	Γ, b_0, c_1, b_0^Q

^a $\Gamma = a_0/Rb_0$.

^b Terminology from Huang and Radosz [61].

^c Whether CO₂ should be solvating or not is immaterial for the purposes of this chapter.

6.2.1 On the least squares method

The LSQ method is a frequentist approach, in which the underlying model parameters are assumed to have true fixed (unique) values. However, since experimental data are subject to measurement errors these values can only be estimated by probability distributions of the measurement errors with the aid of statistical estimators [148, 149]. That is, the model parameters are not random but the estimators are, since they depend on the measurements. If it is assumed that the experimental error can be described by a normal distribution with mean equal to the experimental measurement, then the LSQ method is equivalent to minimizing the weighted sum of squares of the difference between measurements (exp) and mathematical model (m):

$$\min \chi^2(\theta) = \sum_{i=1}^N \left(\frac{y_i^{exp} - y_i^m(\theta; T_i)}{s_{exp,i}} \right)^2 \quad (6.2)$$

where N is the number of experiments, y_i^{exp} is the i th experimental value of an output property, such as the saturated density or saturated pressure, $y_i^m(\theta; T_i)$

represent the results from the model at temperature, T_i , where θ is a vector of adjustable parameters which depends on the modeling approach. The weight of the i th term is given as the inverse variance of the i th measurement, ($s_{exp,i}^2$). In principle s is the total standard deviation including both the uncertainty in dependent and independent variables. In this work it is assumed that the uncertainty in the independent variables is insignificant, which greatly simplifies the data fitting problem.

Notice that the function in equation (6.2) is similar to the weighted least squares objective function used by most researchers for parameter estimation. However rather than use the inverse of the variance as the weight factor it is typically assumed that the measurements have the same relative error. In which case it can be shown that the weight function can be approximated by the inverse of the experimental measurement, $w = 1/y_i^{exp}$.

Under a linear approximation the covariance matrix of parameter estimators can be calculated from Eq. (6.3) [150, 151]

$$Cov(\hat{\theta}) \approx \frac{\chi^2}{N-p} \left(\left(\frac{\partial \mathbf{y}}{\partial \theta} \right)^T \mathbf{V}^{-1} \left(\frac{\partial \mathbf{y}}{\partial \theta} \right) \right)^{-1} \quad (6.3)$$

where p is the number of estimators, \mathbf{y} is a vector of outputs, and \mathbf{V} is the diagonal variance matrix of measurement errors. The correlation matrix, a normalized symmetric matrix which approximates the correlation between parameters, is calculated from the covariance matrix (Eq. (6.3)) as

$$cor(\theta_i, \theta_k) = \frac{Cov(\hat{\theta})}{\sqrt{\text{diag}(Cov(\hat{\theta}))\text{diag}(Cov(\hat{\theta}))}} \quad (6.4)$$

For large N the $100(1 - \alpha)\%$ confidence interval of the parameters can be approximated by

$$\hat{\theta} \pm t_{N-p}^{\alpha/2} \sqrt{\text{diag}(Cov(\hat{\theta}))} \quad (6.5)$$

where $t_{N-p}^{\alpha/2}$ is the student's t-distribution corresponding to the $\alpha/2$ percentile and with $N-p$ degrees of freedom. In Eq. (6.5) it is implicitly assumed that the various parameters are independent of each other, in reality the parameters are correlated resulting in confidence ellipsoids, or hyper-ellipsoids.

6.2.2 Results with the least squares method

The pure compound parameters of approaches A-F were correlated to the experimental saturated liquid density and saturated vapor pressures using Eq. (6.2) as the objective function. The very accurate data from Duschek et al. [152] are used for the saturated liquid density (below 295 K the experimental uncertainty

is estimated to less than $\pm 0.015\%$). For the saturated vapor pressure data from [152–154] is employed (experimental uncertainty estimated to $\pm 0.016 - 0.012\%$, ± 100 Pa and $\pm 0.1\%$ respectively). It is assumed that the standard deviation, $s_{exp,i}$, of each experimental point can be approximated by the experimental uncertainties given in the references.

Table 6.2 summarizes the estimated parameters for each modeling approach. As expected from the work of Tsvintzelis et al. [14], excellent agreement with saturated vapor pressures and saturated liquid densities are obtained for approaches A-D. As may also be expected the quadrupolar approaches E and F results in equally good correlations. With the exception of association scheme 2B the parameters obtained with approach A-D are similar to those presented by Tsvintzelis et al. [14]. The small difference in parameters might be explained by the slightly different objective function and the use of experimental data for the correlation, rather than pseudo-experimental data. The deviations generally decrease when CO_2 is treated as either an associating or a quadrupolar compound. For approaches with four or five parameters the excellent correlations, however, may simply be due to the added flexibility of additional model terms and parameters. The good correlations which are already obtained for the approaches using only three adjustable parameters (A and E) suggest that models with more parameters may be over-parameterized, which in turn reduces the reliability of the obtained parameters (see tables 6.4 and 6.5).

Table 6.2: Correlated pure compound parameters and %AADs in saturated liquid density and saturated pressure for CO_2 with the CPA EoS (Approaches A-D) and the qCPA (Approaches E-F). The parameters are correlated in the temperature range $T_r = 0.7 - 0.9$.

Case	Approach	b_0 [mL/mol]	Γ [K]	c_1 -	$\beta \cdot 10^3$ -	ε/R [K]	b_0^Q [mL/mol]	%AAD ^a	
								P^{sat}	ρ_{sat}^{liq}
A	n.a. ^b	27.3	1550	0.77	-	-	-	0.18	0.95
B	2B	26.9	1145	0.43	42.3	1089	-	0.07	0.11
C	3B	28.1	1310	0.64	34.7	671	-	0.06	0.10
D	4C	28.4	1329	0.66	25.7	513	-	0.07	0.10
E	Quad	27.9	1284	0.68	-	-	-	0.13	0.46
F	Quad	28.5	1027	0.60	-	-	20.2	0.12	0.07

$${}^a\%AAD = \frac{100}{N^{exp}} \sum_i^{N^{exp}} \left| \frac{x_i^{calc} - x_i^{exp}}{x_i^{exp}} \right| \quad \text{where } x \text{ in this case stands for } P^{sat} \text{ or } \rho_{sat}^{liq} \text{ and}$$

N^{exp} is the number of experimental data.

^b Not associating.

Tables 6.3-6.6 show the estimated parameter uncertainty, the correlation matrix between the parameters and the mean estimate for modeling approaches B, D, E and F. The confidence intervals are presented as a percentage of its mean estimator. Only the lower triangular part of the symmetric correlation matrix is shown.

It can be seen from table 6.3 that small confidence intervals are obtained as well as low correlations between b_0 and both Γ and c_1 for approach E. A higher correlation is observed between Γ and c_1 . This is probably the reason for the slightly

Table 6.3: Estimated CO₂ parameters, uncertainty as a 95% confidence interval (CI) in percent of the parameter estimate, and parameter correlation matrix when modeling approach **E** is employed.

θ	Estimator	95% CI (%)	Correlation matrix		
			b_0	Γ	c_1
b_0	27.9	0.08	1		
Γ	1284	0.13	0.29	1	
c_1	0.68	0.77	-0.01	-0.95	1

larger confidence interval of the c_1 parameter. The correlation is unsurprising considering that these two parameters are closely related in the attractive SRK term (see Eq. (3.7)). Similar results are obtained when CO₂ is modeled as an inert (approach A).

Table 6.4: Estimated CO₂ parameters, uncertainty as a 95% confidence interval (CI) in percent of the parameter estimate, and parameter correlation matrix when modeling approach **F** is employed.

θ	Mean estimator	95% CI (%)	Correlation matrix			
			b_0	Γ	c_1	b_0^Q
b_0	28.5	0.09	1			
Γ	1027	1.19	-0.98	1		
c_1	0.60	0.63	-0.91	0.91	1	
b_0^Q	20.2	1.15	-0.98	0.99	0.92	1

The results for approach F, shown in table 6.4, indicate that when one additional adjustable parameter is added to the model, all model parameters become highly correlated. That is, a small change in one parameter can be compensated by a change in another parameter. This suggests that the model is over-parametrized making it difficult, if not impossible, to uniquely identify its parameters. The large correlations, however, have not increased the estimated confidence intervals significantly, which may suggest that the parameters are also highly sensitive. This may indicate that such model extensions are undesirable, at least when it comes to parameter estimation from classical LSQ estimation, even if they have the potential to improve model predictions.

Table 6.5: Estimated CO₂ parameters, uncertainty as a 95% confidence interval (CI) in percent of the parameter estimate, and parameter correlation matrix when modeling approach **D** is employed.

θ	Mean estimator	95% CI (%)	Correlation matrix				
			b_0	Γ	c_1	β	ϵ
b_0	28.4	0.06	1				
Γ	1329	0.79	-0.47	1			
c_1	0.66	4.96	-0.24	-0.69	1		
β	25.7	22.65	-0.10	-0.80	0.97	1	
ϵ	512.7	9.63	0.26	0.68	-0.99	0.98	1

When CO₂ is modeled as an associating species (approaches B-D) there are even more adjustable parameters. Due to the added flexibility from the parameters, one would also expect the approaches with association to be highly correlated. It turns out, however, that the degree of correlation depends very much on the chosen association scheme. Tables 6.5 and 6.6 show the confidence intervals and correlation matrices for the 4C and 2B association scheme respectively. When the 2B scheme is employed high correlations are obtained between all parameters, on the other hand, when the 4C scheme is employed only the association parameters (β and ϵ) and the c_1 parameter are highly correlated with each other. It is suspected that the correlation between these three parameters is due to the fact, that they all incorporate part of the models temperature dependence (see Eq. (3.7) and (3.11)). As a consequence of the high correlations, relatively high confidence intervals are obtained for the correlated parameter in both approaches.

The highly correlated parameters indicate that it is not possible to uniquely determine all the adjustable parameters with approaches B-D and F. That is, the parameters are not unique but depend on each other, which means that one should be careful about attaching too much physical meaning to the actual parameter values. Essentially the obtained mean estimators merely constitute a set of values, amongst many possible sets, which provide a good fit to the saturation data. This may be due to the model structure or because the data is too limited in relation to the model complexity [148, 151]. Since excellent correlations are obtained with only three adjustable parameters, one may suspect that the latter possibility is predominant. However, the model structure clearly matters a great deal, as the identifiability problems are much more significant when the 2B association scheme is employed rather than the 4C or 3B association schemes. This may indicate that the 2B scheme is less suited to model CO₂ than the 4C and 3B scheme. It is interesting to note that Kontogeorgis and co-workers [14, 33–36] arrived at the same conclusion by evaluating the phase equilibria of a large number of binary and multicomponent mixtures containing CO₂.

Table 6.6: Estimated CO₂ parameters, uncertainty as a 95% confidence interval (CI) in percent of the parameter estimate, and parameter correlation matrix when modeling approach **B** is employed.

θ	Mean estimator	95% CI (%)	Correlation matrix				
			b_0	Γ	c_1	β	ϵ
b_0	26.9	3.33	1				
Γ	1145	10.53	0.99	1			
c_1	0.43	38.27	0.99	0.99	1		
β	42.3	16.82	0.97	0.97	0.99	1	
ϵ	1089	19.53	-0.99	-0.99	0.99	0.99	1

6.3 Bootstrapping

The LSQ method is by far the most well-known approach for parameter estimation. There are, however, several alternative parameter estimation methods. One of these is the bootstrap technique [145].

6.3.1 Bootstrap technique for uncertainty of parameter estimators

The basic idea of the bootstrap method is that it relies on random sampling with replacement of the residuals, to generate a number of synthetic pseudo-experimental data sets. Since the development of the method by Efron [145] several bootstrapping schemes have been suggested. In this work one of the variants used for regression problems, namely re-sampling of residuals, is employed. This scheme consists of four main steps;

Step 1 Input parameters are correlated to the experimental data using Eq. (6.2) as the objective function.

Step 2 Residuals from the correlation are randomly sampled (with replacement) and added to the previously correlated output values.

Step 3 The parameters are refitted to the new synthetic data. Steps 2 and 3 are repeated a large number of times to simulate repeated experimental runs.

Step 4 The distribution of regressed mean estimators are evaluated to obtain confidence regions and parameter correlations.

If the underlying distribution of errors is close to the normal distribution, bootstrapping usually gives results similar to the LSQ approach. An advantage of bootstrapping, however, is that it does not make any assumption with respect to the underlying distribution of errors [155].

As measurement errors are associated with the measured property only, the residuals obtained from the correlation to saturated liquid density and the residuals obtained from correlation to saturated vapor pressures are only resampled onto the property to which they were correlated.

6.3.2 Parameters from the Bootstrap technique

The bootstrap method for parameter estimation gives a distribution of parameter sets generated by the, slightly different, synthetic data sets. Figure 6.3 shows

the obtained distribution of input parameters for approach E as a histogram, with the number of occurrences on the left y-axis, and with the estimated probability density function on the right y-axis. It can be seen from figure 6.3 that the distributions of all input parameters follow a normal distribution quite accurately, and one would expect the mean value of the input parameters to be similar to those obtained from LSQ. Indeed by comparing figure 6.3 with table 6.3 it can be seen that the mean input parameters are almost identical to those obtained from the LSQ estimation. The main difference is, that distributions from bootstrapping are somewhat wider than the confidence intervals obtained from LSQ estimation.

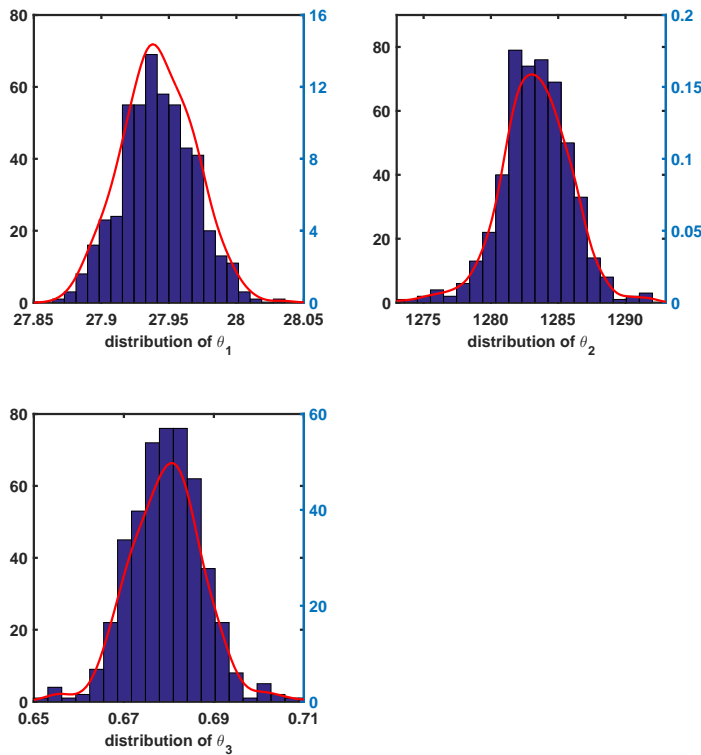


Figure 6.3: Histograms approximating the distribution of each parameter (left y-axis), obtained from 500 re-sampled bootstraps, using modeling approach E for CO_2 . The full red lines show the estimated probability density function (right y-axis).

Figure 6.4 visualizes the correlation between the parameters by plotting each input parameter as a function of another input parameter. The ellipsoids in figure 6.4 represent 95% confidence intervals. The closer an ellipsoid is to a circle the more random is the parameter pair, and thus the weaker the correlation between the two. It is clear from the figure that there is almost no correlation between Γ and b_0 and c_1 and b_0 , while the value of Γ and c_1 depend on each

other. This is consistent with the results for LSQ estimation shown in table 6.3. Almost exactly the same conclusion can be made when approach A is employed. Both modeling approaches employ only three adjustable parameters.

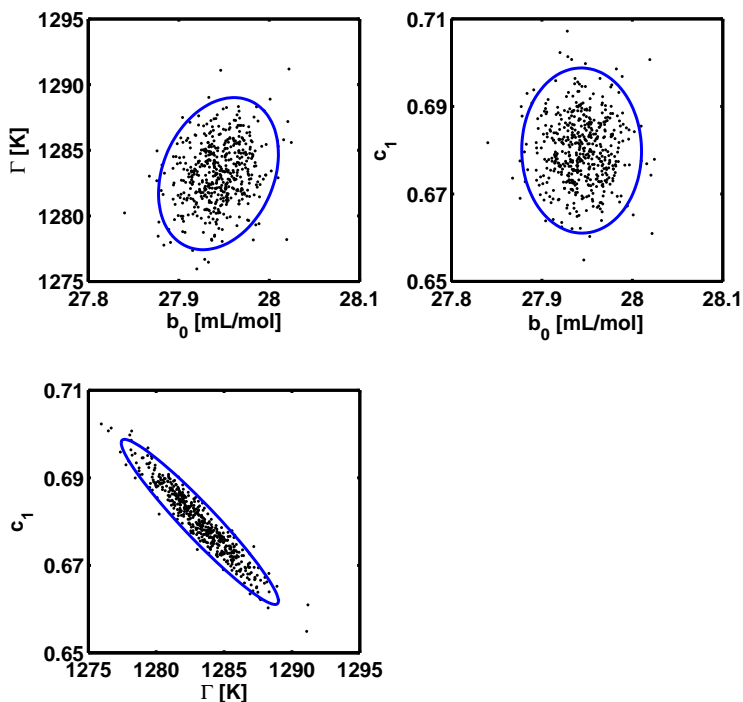


Figure 6.4: 95% confidence ellipsoids for the bootstrapped parameters of CO_2 when modeling approach E is employed. Each dot represents a realized parameter combination and each subfigures represents the dependency (if any) of one parameter on another.

Figures 6.5 and 6.6 show the parameter distributions and correlations with approach F. It is clear from figure 6.5 that the input parameter distributions are no longer found to be normal, rather it looks like the distribution of all input parameters are bimodal. That is, there are two distinct peaks, or modes, in the distributions. This may suggest that there are two different major minima in the objective function depending on the generated synthetic data. Given the highly non-linear nature of equations of state, and the fact that problems of multiple minima are not uncommon [120, 123], it does not seem unlikely that multiple modes exist. If the results are compared with table 6.4 it is obvious that the parameter set obtained with the LSQ method does not correspond with any of the modes in figure 6.5. Moreover, the confidence regions for the parameters are clearly much wider for the bootstrap than for the LSQ method. That is, a situation has arisen where both the parameters and confidence regions are different between the two estimation methods. As bootstrapping uses informa-

tion in the data, rather than an assumption about normality of the errors, it might be expected that this estimate is the most correct of the two.

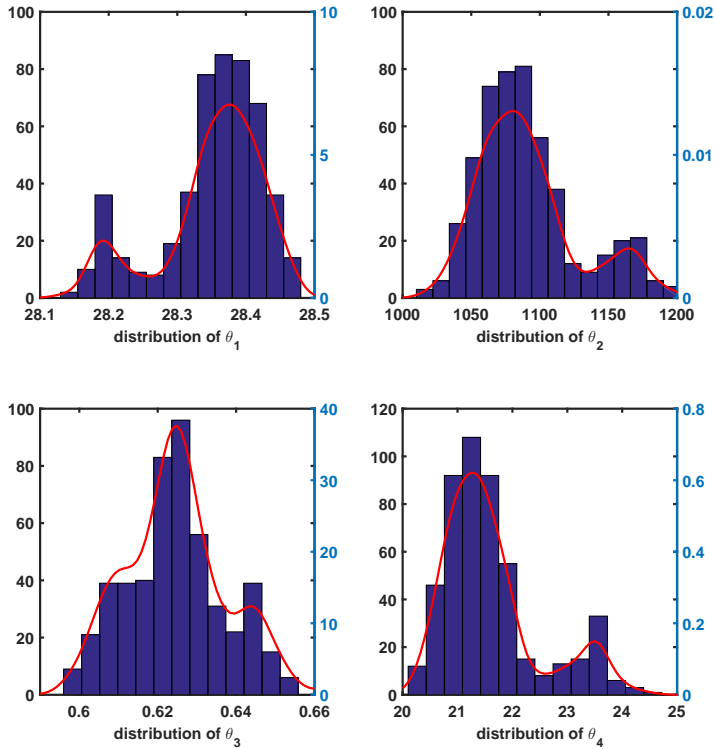


Figure 6.5: Histograms approximating the distribution of each parameter (left y-axis), obtained from 500 re-sampled bootstraps, using modeling approach **F** for CO₂. The full red lines show the estimated probability density function (right y-axis).

Figure 6.6 shows, unsurprisingly, that b_0^Q and b_0 are highly correlated. It is more surprising that the energetic parameter, Γ , is highly correlated with b_0 as well as b_0^Q . In accordance with Korden et al. [123] it is suspected that this is due to the fact that the quadrupolar term is an attractive energetic term, and since b_0^Q is the only adjustable parameter in the quadrupolar term, Γ scales with this parameter as well, to balance the two attractive terms. This in turn means that b_0 and Γ becomes intercorrelated.

Figure 6.7 shows the bootstrapping results with approach **D**. It is obvious from the figure that the distribution of b_0 and Γ appears to follow a normal distribution, with relatively narrow parameter ranges. Both parameters and confidence intervals are similar to the confidence intervals calculated with LSQ estimation. The remaining parameter distributions, however, appear to follow complex bimodal distributions. The distributions are close to a uniform distribution, and

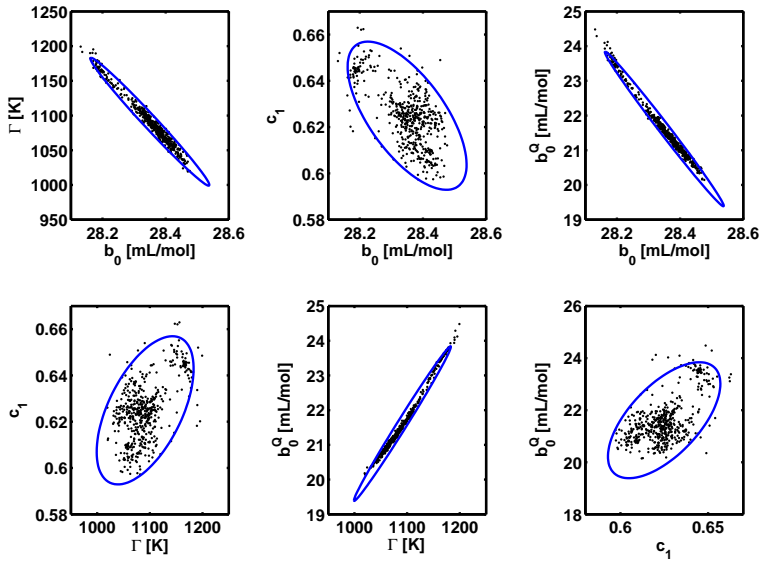


Figure 6.6: 95% confidence ellipsoids for the bootstrapped parameters of CO_2 when modeling approach **F** is employed. Each dot represents a realized parameter combination and each subfigure represents the dependency (if any) of one parameter on another.

are quite wide (the parameter $\beta^{A_i B_i}$ may for instance vary by almost 100% from its mean value), both of which suggest poor identifiability.

By comparing figure 6.8 with the correlation matrix in table 6.5 it can be seen, that although the LSQ and the bootstrap method do not agree on the size of the parameter confidence intervals, both methods tend to agree about the degree of correlation between parameters. The only strongly intercorrelated parameters are c_1 , β and ϵ .

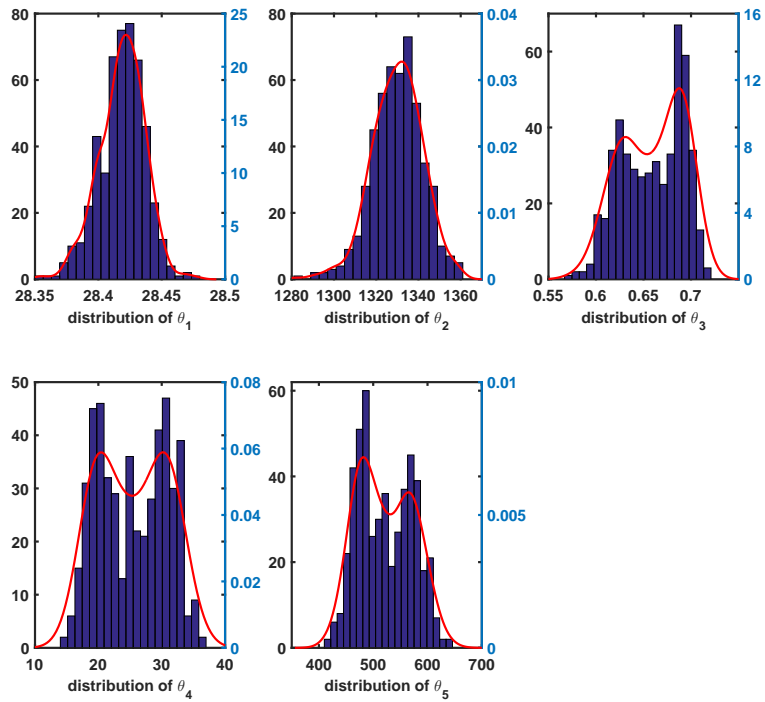


Figure 6.7: Histograms approximating the distribution of each parameter (left y-axis), obtained from 500 re-sampled bootstraps, using modeling approach **D** for CO_2 . The full red lines show the estimated probability density function (right y-axis).

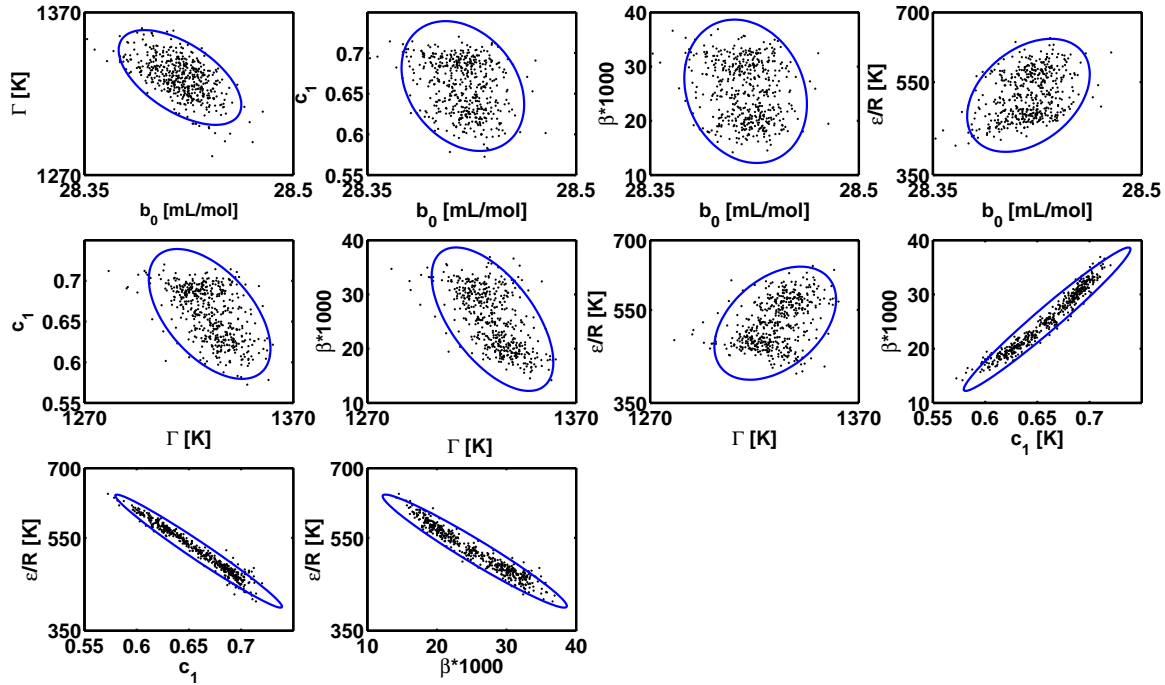


Figure 6.8: 95% confidence ellipsoids for the bootstrapped parameters of CO_2 when modeling approach **D** is employed. Each dot represents a realized parameter combination and each subfigures represents the dependency (if any) of one parameter on another.

6.4 Propagation of Parameter Uncertainty to Model Predictions

Uncertainty associated with the predictions from thermodynamic models can generally be classified as; (a) *input uncertainty* and (b) *structural uncertainty (or model error)*. The structural uncertainty deals with the mathematical form of the EoS, since all models, no matter their complexity, are only an approximation of the real physical system. The input uncertainty, on the other hand, represents the uncertainty in adjustable parameters for example due to uncertainty in the experimental data, and the method employed to find these parameters [134, 156]. The uncertainty in adjustable parameters will propagate through the model and will affect the accuracy of model outputs.

One popular method used for error propagation is Monte Carlo analysis. The Monte Carlo analysis is based on multiple model evaluations using inputs sampled from their corresponding uncertainty which is usually described by a certain distribution function (uniform, normal, etc.). The main advantage of the Monte Carlo procedure is that uncertainty results can be obtained directly from the model in question without the need for calculation of the Jacobian matrix which is required by linear error propagation. It is thus conceptually easy to implement and, perhaps most importantly for this work, it can be used to propagate uncertainties through a sequence of models without the need for modifications to the original model.

6.4.1 A Monte Carlo uncertainty analysis

For notational convenience assume that the desired output property from any of the equations of state under investigation can be represented by a function of the form

$$\mathbf{y} = \mathbf{f}(\theta, \mathbf{n}, P, T) \quad (6.6)$$

where \mathbf{y} is a vector of output model predictions, θ is a vector of model inputs and \mathbf{n} , P and T are the composition vector, pressure and temperature respectively. The expression in Eq. (6.6) may represent not only the equation of state but a sequence of linked models or expressions needed to calculate a desired output property. For instance f may represent a dew or bubble point calculation.

Monte Carlo uncertainty analysis is based on performing multiple model evaluations of a function of the form in Eq. (6.6) with inputs sampled from a probabilistic distribution. The Monte Carlo uncertainty analysis involves four steps [156]:

- Step 1** Specification of the range and underlying probability distribution of the input variables.
- Step 2** Sampling from the input range and distribution specified in the first step, to simulate parameters obtained from repeated experimental runs.
- Step 3** Evaluation of Eq. (6.6) for each input sample.
- Step 4** Representation and interpretation of results.

In this work the (kernel) probability density functions of the input variables, as estimated from the bootstrapped subsamples, are employed, although a normal distribution with mean and standard deviation from the bootstrapped results would have been sufficient for approach A and E. Commonly used methods to take samples from the input space in step 2 are; random sampling, shifted Hammersley sampling [157], equal probability sampling [134] and Latin Hypercube sampling (LHS) [158]. In this work the samples are chosen using LHS sampling. Input parameter correlation is induced by applying the Iman-Conover correlation control method [159]. Additional introductions to Monte Carlo analysis are available elsewhere e.g. [160–163] and references herein.

6.4.2 Propagation of parameter estimation errors

To estimate the effect of the input parameter uncertainty on output properties for the various modeling approaches, 500 Monte Carlo input parameter samples are generated using the LHS and Iman-Conover correlation control method [156]. Each subsample is subsequently used to calculate output properties of interest. The calculated properties are compared with pseudo-experimental data from the Span and Wagner EoS [15] as implemented in REFPROP [146].

Figure 6.9 shows the propagated uncertainty of the saturated liquid density (one of the fitted properties) for approaches A, D, E and F. Very low propagated uncertainties are predicted especially by approaches D, E and F. In fact, the largest uncertainty is observed when CO_2 is treated as an inert (Figure 6.9a). It may initially seem counter intuitive that the model with the largest uncertainty in the saturated density, is in fact the simplest of the approaches. The reason for this is, that when CO_2 is considered an inert in CPA the property fit is not quite as good, resulting in a range of realizations which favour either the high or low density region. This effect is reflected in the propagated uncertainty. That almost no propagated uncertainty is observed with approaches D, E and F for the output properties which the model parameters are correlated to, however, does not mean that the range of input parameter sets does not incur uncertainty in other outputs, which may depend on the inputs in a different way.

It is well-known that the isochoric heat capacity is a challenging property to predict even with modern equations of state [37, 115]. It is believed that this

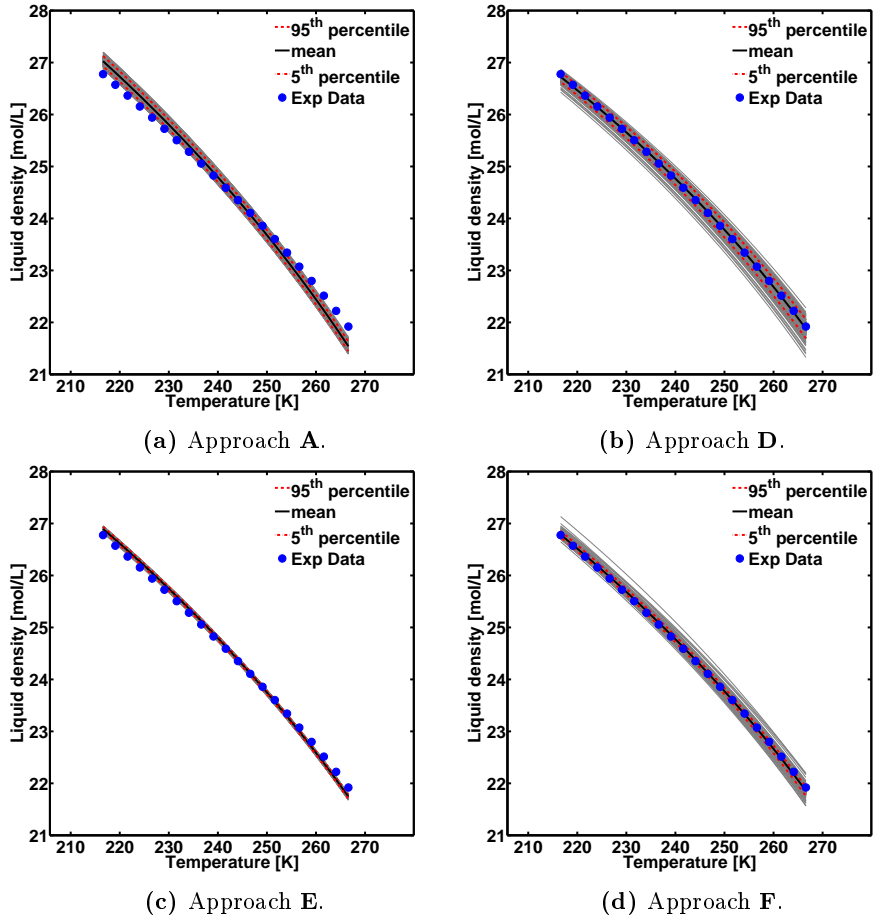


Figure 6.9: Propagated uncertainty in the model predictions for the liquid density at saturation. Approach **A** (a), **D** (b), **E** (c) and **F** (d) is employed. Grey lines represent the simulations, red dashed lines are the 5th and 95th percentile of the simulations and black full lines are the mean of the simulations. As the simulations, and their mean are almost identical the lines are difficult to see. Blue circles are pseudo-experimental data from Span and Wagner [15].

is primarily due to structural issues with the temperature dependence of the equations of state. It is possible, however, that at least part of the problem can be explained by uncertainties in the parameters. Figures 6.10 and 6.11 map the input uncertainty onto the residual isochoric and isobaric heat capacity at saturation respectively. It can be seen from both plots that the uncertainty is significant for approach D, smaller, but still present, for approaches E and F and almost non-existent for approach A. This illustrates how larger uncertainty in input parameters, e.g. for the approaches using more adjustable parameters, result in higher uncertainties in the non-fitted derivative properties. The large uncertainties for the isochoric heat capacity in figure 6.10b suggest that the uncertainty in pure compound parameters lead to significant uncertainties in the temperature derivatives of the equation of state. This should be non-surprising as the three most uncertain parameters in approach D are parameters responsible for the temperature dependence (c_1, ε, β) (Eq. (3.7) and (3.11)). This may, in part, explain why C_V^{res} is such a difficult property to calculate for many equations of state [37, 115]. However, the deviation from the pseudo-experimental data is so large, that at least part of the deviation is expected to be due to structural uncertainty rather than input uncertainty. It is somewhat surprising that CPA with CO₂ treated as an inert molecule, models C_V^{res} so well, while none of the more sophisticated equations of state yield particularly good results.

Due to the relation between C_V^{res} and C_P^{res} (see Eqs. (7.10) and (7.11) in chapter 7) uncertainties in C_V^{res} should lead to, at least, similar sized uncertainties in C_P^{res} . The uncertainty in figure 6.11 is of the same magnitude as that in figure 6.10, which suggests that the input uncertainty does not lead to significant additional uncertainties in the ratio between the $(\partial P/\partial T)^2$ and $\partial P/\partial V$ derivatives. As opposed to the results for C_V^{res} it can be seen that the more advanced approaches all estimate C_P^{res} rather well within the input uncertainty, while the calculations when CO₂ is treated as an inert compound fail to follow the trend of the pseudo-experimental data. This suggests that approach A fails in representing the right trend in either the $\partial P/\partial T$ or the $\partial P/\partial V$ derivative, possibly in both. We may note, however, that while approaches D, E and F capture the right trend of C_P^{res} as a function of temperature, the only reason that the predictions represent the pseudo-experimental data so well, is the offset caused by the poor representation of C_V^{res} , thus some cancellation of error must occur between C_V^{res} and the ratio $(\partial P/\partial T)^2/(\partial P/\partial V)$.

One of the primary objectives of most equations of state is the accurate description of phase equilibria [115, 164]. It is therefore of particular interest to investigate how the input uncertainty affects the prediction of VLE. In this work we only take the input uncertainty in the CO₂ parameters into account, and ignore the input uncertainty of the other component. The mixtures investigated are two CO₂ + hydrocarbon mixtures.

Hydrocarbons are modeled with only three parameters (approach A) and the predictions of binary hydrocarbon + hydrocarbon mixtures, are generally quite accurate. It is thus expected, that the error in their parameters are negligible,

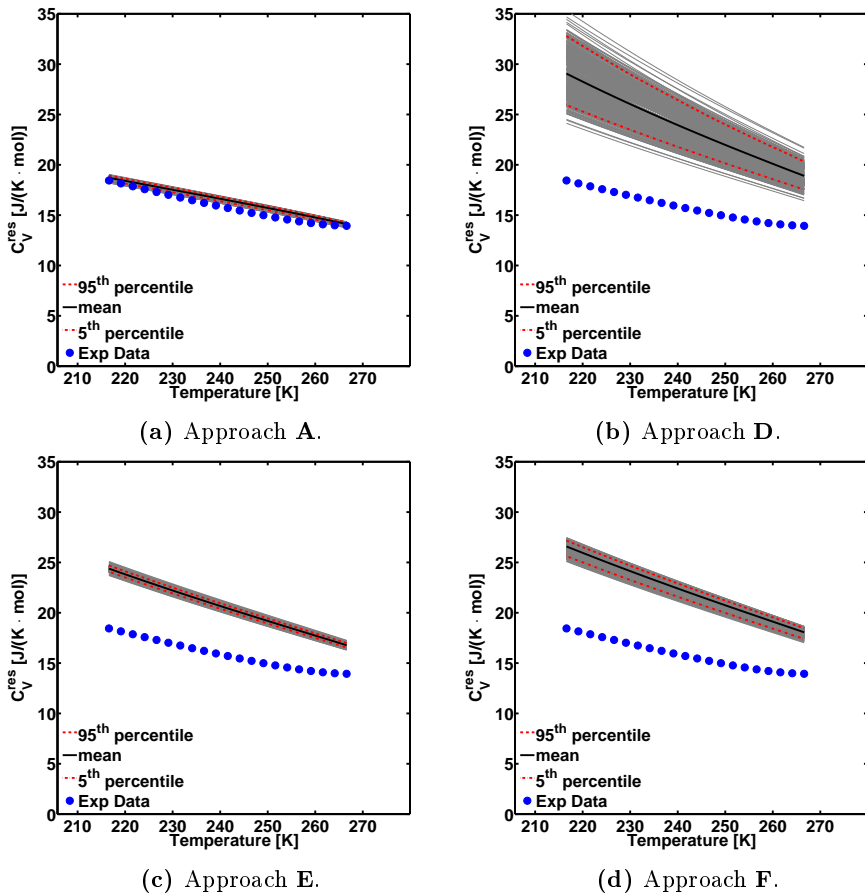
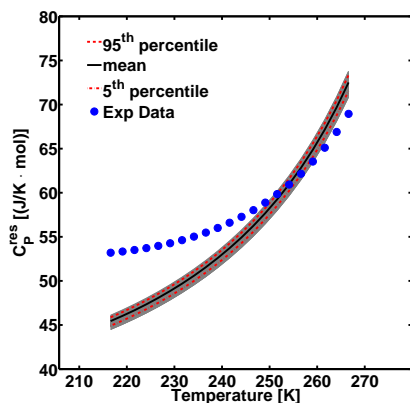
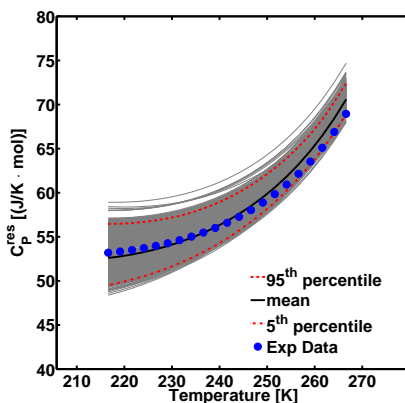


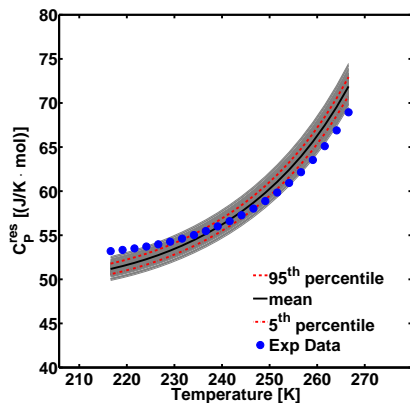
Figure 6.10: Propagated uncertainty in the model predictions for the residual isochoric heat capacity of CO_2 at saturation, employing approach **A** (a), **D** (b), **E** (c) and **F** (d). Grey lines represent the simulations, red dashed lines are the 5th and 95th percentile of the simulations and black full lines are the mean of the simulations. Pseudo-experimental data from Span and Wagner [15].



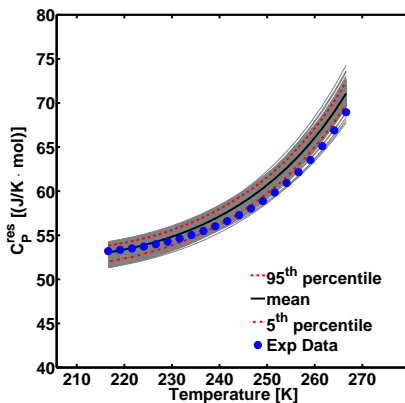
(a) Approach A.



(b) Approach D.



(c) Approach E.



(d) Approach F.

Figure 6.11: Propagated uncertainty in the model predictions for the residual isobaric heat capacity of CO_2 at saturation, employing approach **A** (a), **D** (b), **E** (c) and **F** (d). Grey lines represent the simulations, red dashed lines are the 5th and 95th percentile of the simulations and black full lines are the mean of the simulations. Pseudo-experimental data from Span and Wagner [15].

and that almost all sources of error in mixtures of CO₂ and hydrocarbons are due to the quadrupolar CO₂ molecule.

Figures 6.12-6.13 show the propagated input uncertainty of the CO₂ + ethane and CO₂ + propane VLEs at 250 K and 230 K respectively. The small quadrupole moment of ethane is ignored. All VLE plots are predictions ($k_{ij} = 0$). The uncertainty with approaches A and E, both of which have three input parameters, is negligible. The model error with approach A, however, is significant, illustrating the need for improved modeling approaches. All other model approaches qualitatively predict the azeotrope in figure 6.12 and improve the representation of the CO₂ + propane VLE.

The output uncertainty with approach D for the VLEs are quite small, which is in contrast to the uncertainties in the pure compound heat capacities. On the other hand, while uncertainties in the pure compound derivative properties were small to moderate for approach F, they are clearly significant for especially the liquid phase of the VLE systems. The uncertainty seem to depend on the mole fraction of CO₂, with the largest uncertainty in model output being around $x_{CO_2} = 0.5$. It is noteworthy that while the uncertainties in the VLE systems are significant for approach F, it is the only model which could accurately predict the VLE data within its 95% percentile, which may suggest, that the errors could be due to subjective errors rather than structural errors.

In any case, the results show that for models such as qCPA and CPA with association a simple LSQ estimation may not give the optimal parameters in terms of phase equilibrium predictions, as the input uncertainty results in significant output uncertainties. It is worth noting that it is the same parameter set which generate the best (closest to the the experimental data) predictions in figures 6.12-6.13. It is thus possible to find a parameter set, which generates excellent predictions for the VLE of CO₂ + alkanes, based only on uncertainties in the input parameters.

As already discussed the observed LLE between CO₂ and heavy hydrocarbons is believed to be caused primarily by the quadrupole moment of CO₂. Figure 6.14 shows the propagated input uncertainty on the CO₂ + n-dodecane LLE for qCPA with four parameters. The remaining modeling approaches does not predict the LLE a priori.¹ As discussed at the beginning of this chapter an often use approach for identification of good parameters is to incorporate LLE data in the parameter estimation. However, the fact that none of the modeling approaches except approach F predict the presence of the LLE suggest that including the LLE in the parameter estimation could result in a loss of accuracy in the pure compound properties beyond what can be explained by experimental errors. It is also obvious from figure 6.14 that while the LLE is predicted none of the parameter sets can accurately represent the LLE.

¹At least not with enough realizations to be statistically significant.

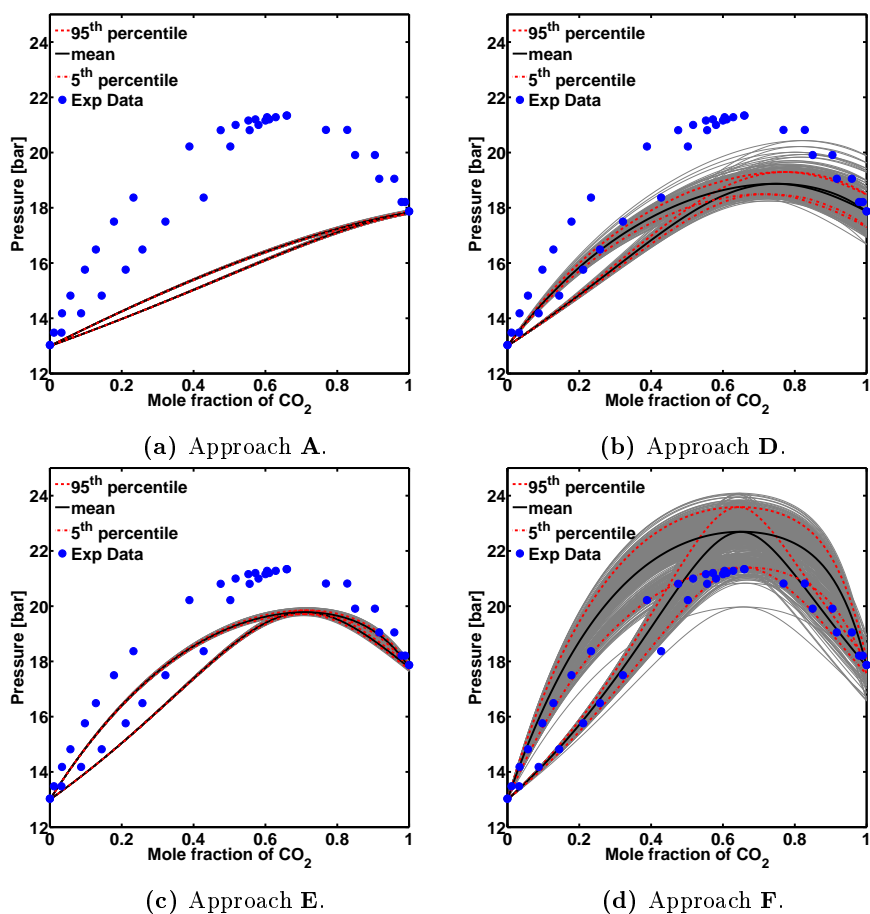


Figure 6.12: Propagated uncertainty in the model predictions for the CO_2 + ethane VLE at $T=250$ K. Employing approach **A** (a), **D** (b), **E** (c) and **F** (d). Grey lines represent the simulations, red dashed lines are the 5th and 95th percentile of the simulations and black full lines are the mean of the simulations. Experimental data from [67].

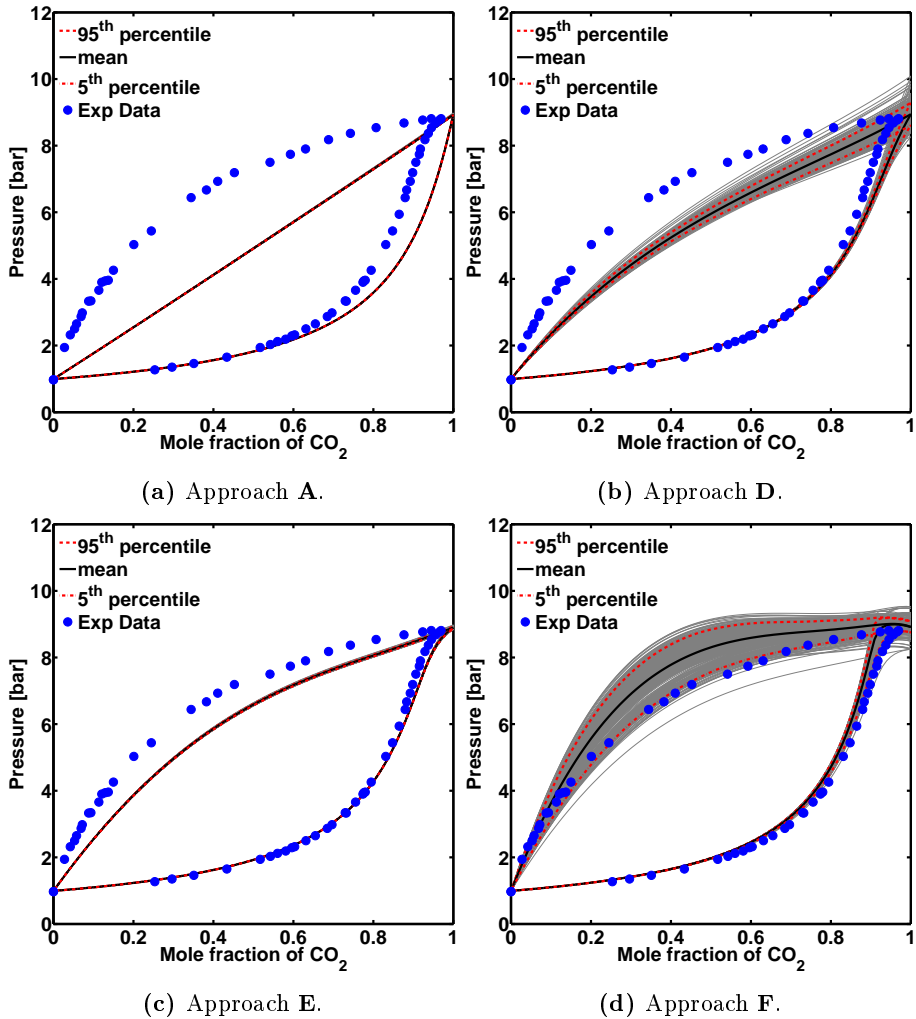


Figure 6.13: Propagated uncertainty in the model predictions for the $\text{CO}_2 + \text{propane}$ VLE at $T=230$ K. Employing approach **A** (a), **D** (b), **E** (c) and **F** (d). Grey lines represent the Monte Carlo simulations, red dashed lines are the 5th and 95th percentile of the simulations and black full lines are the mean of the simulations. Experimental data from [165].

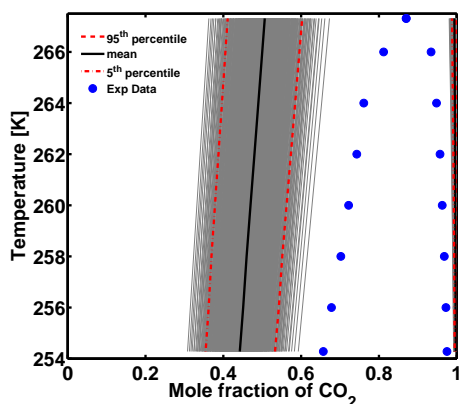


Figure 6.14: Propagated uncertainty in model predictions for the $\text{CO}_2 + n$ -dodecane LLE using qCPA with 4 adjustable parameters (Approach F). Grey lines represent the Monte Carlo simulations, red dashed lines are the 5th and 95th percentile of the simulations and black full lines are the mean of the simulations. Experimental data from [166].

6.4.3 The effect of adding additional output properties

The high degree of correlation, and the complex distributions obtained from bootstrapping may suggest that the data used for parameter estimation is too limited in relation to the model complexity.

One way to address this problem is to add more pure compound or binary data to the LSQ regression. Several authors have proposed extended fitting procedures [115, 167–169], where for instance properties such as the heat of vaporization or the speed of sound has been included in the objective function.

In order to investigate how the addition of another property in the objective function affects the parameter distribution, we re-estimate the input parameters of CO_2 to the heat of vaporization, ΔH^{vap} , in addition to the saturated vapor pressures and saturated liquid densities. Only approaches D and F are investigated, as the parameters with approaches A and E were well-defined, and any change in these parameters will probably be at the cost of the density and/or vapor pressure description.

It is clear from figure 6.15 that the distribution of the new input parameters is nearly normal, which is in clear contrast to the parameter distribution in figure 6.5 which showed evidence of bimodality. Clearly the addition of the heat of vaporization has moved the parameters towards what was the minor mode in figure 6.5, although the center of the old mode is not quite the same as the new. From figure 6.16 it can be seen that the distribution of parameter estimates also looks much smoother for approach D, especially considering the very complex distributions previously observed for especially c_1 , β , and ε . Unfortunately

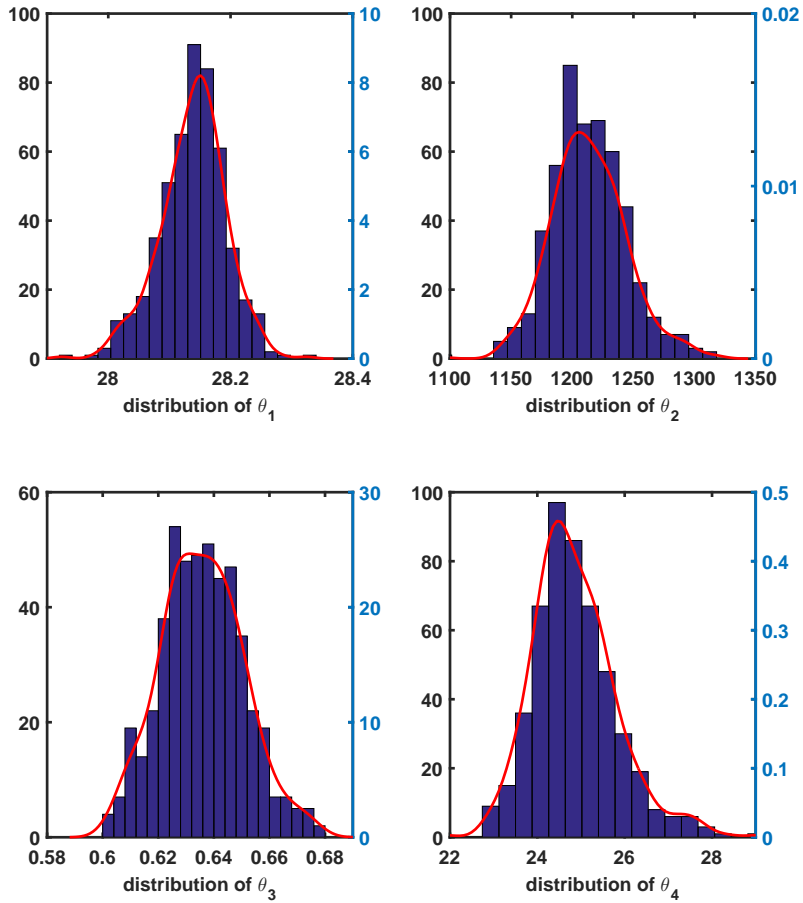


Figure 6.15: Histograms approximating the distribution of each parameter (left y-axis), obtained from 500 re-sampled bootstraps, using modeling approach \mathbf{F} for CO_2 . The parameters have been fitted to ΔH^{vap} in addition to ρ_{sat}^{liq} and P^{sat} . The full red line shows the estimated probability density function (right y-axis).

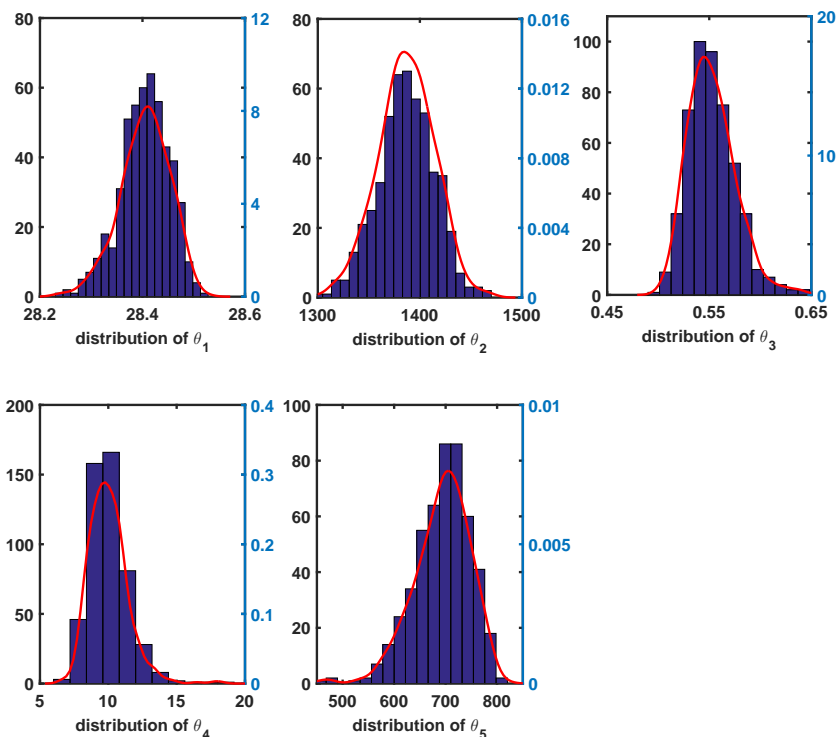


Figure 6.16: Histograms approximating the distribution of each parameter (left y-axis), obtained from 500 re-sampled bootstraps, using modeling approach **D** for CO_2 . The parameters have been fitted to ΔH^{vap} in addition to ρ_{sat}^{liq} and P^{sat} . The full red line shows the estimated probability density function (right y-axis).

the parameter distribution is quite wide (i.e. large standard deviation), and, although not shown here, the parameters are still equally correlated.

Figure 6.17b shows the uncertainty in the new input parameters propagated to the $\text{CO}_2 + \text{ethane}$ VLE, it can be seen from the figure that although the parameter distributions are close to the expected normal distribution, the uncertainty in the VLE estimation is still high for approach F. It is furthermore noteworthy that approach F is, again, the only model which can predict the data within its 95th percentile. The uncertainty range has, however, changed so that the various realizations generally under-predict the experimental VLE data, whereas they previously over-predicted the experimental data. This suggests a quite large total area of uncertainty, and a very flexible model. For approach D it is observed from figure 6.17b that the uncertainty in the VLE is larger now, than it was with the bimodal distribution, however, the VLE predictions are almost identical to those in figure 6.12b. The reason for the wide parameter

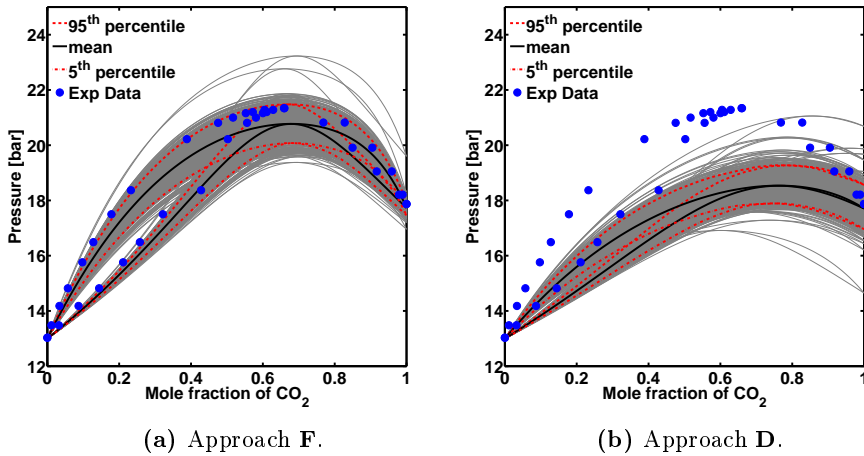


Figure 6.17: Propagated uncertainty in the model predictions for the $\text{CO}_2 + \text{ethane}$ VLE at $T=250$ K. Approach **F** (a) and **D** (b) fitted to ΔH^{vap} in addition to ρ_{sat}^{liq} and P^{sat} . Grey lines represent the simulations, red dashed lines are the 5th and 95th percentile of the simulations and black full lines are the mean of the simulations. Blue circles are experimental data from [67].

distributions may be because the obtained parameter sets constitute a compromise between correlating either of the fitted properties better than the other. Figure 6.17b, for instance, suggests that the pure compound vapor pressure is not captured very well for some parameter sets.

6.5 Summary and Discussion

This chapter investigated the uncertainty in the pure compound parameters of CO_2 with qCPA and various CPA approaches. The models and modeling approaches employ between three and five adjustable pure compound parameters. The uncertainties are estimated using either LSQ estimation or the bootstrap method. In an attempt to quantify the effect of uncertainties in the input properties (the pure compound parameters), the uncertainties in the pure compound parameters obtained from the bootstrap method is propagated to selected derivative properties and $\text{CO}_2 + \text{hydrocarbon}$ VLE systems using a Monte Carlo approach.

The results indicate that modeling approaches which use only three adjustable parameters have relatively low parameter uncertainties, and it may be reasonable to ignore this uncertainty and assume the parameters to be unique, at least insofar as the same type of correlation data is employed (here saturated pressure and saturated liquid density). Any predicted deviations from experimental

data, may be attributed either to errors or simplification in the model, rather than uncertainties in the model parameters.

When the models contained four or five parameters, however, the uncertainties and parameter correlations were significant. The association volume, β , for instance is highly correlated with the association strength, ε , and its value may vary about 100% from its mean value, without significant loss of accuracy in the properties the parameters are correlated to. The main reason for the large parameter uncertainties appears to be the high correlation between parameters, rather than the uncertainty in the experimental data, which is very small. This conclusion is in very good agreement with the observation, that several parameter sets may be found with advanced thermodynamic models such as CPA and SAFT and suggests that the primary explanation for these parameter sets may be the uncertainties and parameter correlations.

The propagated uncertainty appears to be significant for highly temperature dependent properties, such as the heat capacities, when CO_2 is treated as an associating species with five parameters. On the other hand, the propagated uncertainty is relatively small for the VLE systems. When qCPA was employed with four adjustable parameters, however, the uncertainties were relatively small in the temperature dependent properties, whereas the uncertainty in VLE was significant. Of the evaluated models qCPA (with approach F) is the only model which can predict the VLEs within the propagated uncertainty, and give reasonable results for LLE predictions. This is partly due to the larger uncertainty range of the modeling approach compared to qCPA with three parameters (approach E), but also better model predictions. This suggests that one or more parameter set(s) can be found, within the uncertainty of the adjustable parameters, which quantitatively predicts the VLE, and at least qualitatively the LLE. Alternatively qCPA with three parameters gives excellent qualitative results with low uncertainties.

Although similar parameter correlations are typically obtained, the parameter uncertainties from LSQ estimation are generally significantly smaller than those obtained from the bootstrap method. This may be because the bootstrap method accounts for the high degree of correlation between parameters, by using the experimental data itself rather than indirectly using the linear approximation of the covariance matrix for estimators. It is thus clear that one might not obtain the 'best' parameter set, e.g for modeling VLE systems, by a standard LSQ estimation procedure when dealing with advanced thermodynamic models having multiple adjustable parameters. In any case, one should be aware that an obtained parameter set may be quite uncertain, which may incur significant uncertainties in physical property predictions.

The effect of adding the heat of vaporization to the parameter estimation was also investigated. This resulted in parameter distributions, which were significantly closer to a normal distribution. Unfortunately the standard deviations for the parameters were still high and the propagated error was significant. qCPA

with four parameters is still the only model which can, within the propagated uncertainty, predict the VLEs. The propagated uncertainty, however, differs from the previously estimated one, so that the model tend to under-predict, rather than over-predict, the VLE data. The fact that the propagated uncertainty of these two correlation cases differ so much from each other, despite the fact that both cases match the correlated properties to a satisfactory degree may suggest, that the (already large) parameter uncertainty range is in fact somewhat under-predicted in both cases.

The uncertainty results for qCPA are strictly valid only for CO₂ (which has a short saturation curve) and the quadrupolar term which we have employed in this work. However, most other quadrupolar and polar terms are structurally similar, and we suspect that they may have similar uncertainty properties. Indicating that published parameters should be treated with caution. On the other hand, it is clear from the VLE examples that the quadrupolar models may offer significantly improved predictions, even if the cost of this may be a higher uncertainty in the parameters. In either case the results indicate that it is important that researchers report the parameter uncertainties when a new model is developed or parameters are estimated for a new compound. In this way better informed decisions and comparisons can be made.

Another important conclusion from this chapter is that it is inadvisable to use a simple LSQ fit (based on pure properties) for the estimation of pure compound parameters of CO₂ when advanced models with multiple parameters are employed. This conclusion should not come as a surprise to researchers dealing with uncertainties and/or thermodynamic models, however, this knowledge is often primarily experience based and rarely, if ever, systematically quantified as we have attempted in this chapter. Hopefully this may also help new researchers appreciate that a simple LSQ estimation isn't always enough. The chapter also indicate that many researches chose to add binary equilibrium data to the parameter estimation to get the right balance between the very correlated parameters. One may speculate whether the high parameter uncertainties observed, when CO₂ was treated as an associating species, are also true for a molecule such as water, for which more than 20 different parameter sets have been published with PC-SAFT [170]. If so, many of these parameter sets may simply be covered by the uncertainty range of the parameters due to the sparsity of the experimental data.

Finally we note that while we have assumed good data coverage in our analysis, it would be very informative to also analyze the effect of especially sparse or limited data on the CPA type models.

CHAPTER 7

Pure Compound Properties of CO₂

Traditionally the primary focus for the development of most equations of state has been to accurately describe the phase equilibria of mixtures. Indeed, this too is one of the main purposes of the present work (primarily for mixtures containing CO₂). An unfortunate consequence of this practise, however, is that the typical equation of state, is only evaluated to a very limited degree for other properties of interest.

An important industrial desire, however, is the simultaneous description of phase equilibria, primary physical properties and derivative properties over a wide range of temperatures and pressures [115, 171]. Moreover, thermodynamic models, once published, will often be employed for conditions or properties other than those for which they have been developed [164], for instance when used in a simulator by an engineer, who may not be familiar with the specifics of a model and its (possible) limitations. It is thus important that the predictive behaviour of an equation of state is evaluated over a wide range of conditions and properties other than those for which it has been developed.

In this regard Deiters and de Reuck [164] developed a number of criteria for how the performance of new equations of state should be evaluated for pure fluids. These criteria include, among others, the demonstration of the behaviour and physical property prediction of the model at the critical point, in the saturation region, as well as the prediction of single-phase properties.

This chapter will attempt to evaluate the performance of qCPA and CPA for the prediction of pure fluid properties of CO₂ both at the critical point, in the

saturation region, the critical region and the compressed liquid region. The predicted properties include; the density, the isobaric and isochoric heat capacity, the speed of sound, the Joule-Thomson coefficient, the critical point and finally the second virial coefficient. Most of the chapter has been published in Fluid Phase Equilib. (2016), 408, 151-169 [37].

7.1 Calculation of Derivative Properties

The enthalpy and heat capacities can be expressed as the sum of two contributions; an ideal gas contribution (ig) and a residual contribution (res):

$$C_V(T, V, \mathbf{n}) = C_V^{ig}(T, \mathbf{n}) + C_V^{res}(T, V, \mathbf{n}) \quad (7.1)$$

$$C_P(T, V, \mathbf{n}) = C_P^{ig}(T, \mathbf{n}) + C_P^{res}(T, V, \mathbf{n}) \quad (7.2)$$

$$H(T, P, \mathbf{n}) = H^{ig}(T, \mathbf{n}) + H^{res}(T, V, \mathbf{n}) \quad (7.3)$$

The (molar) ideal gas term can be calculated from Eqs. (7.4)-(7.6)

$$C_V^{ig} = \sum_i^{nc} x_i C_{V,i}^{ig}(T) \quad (7.4)$$

$$C_P^{ig} = \sum_i^{nc} x_i C_{P,i}^{ig}(T) \quad (7.5)$$

$$H^{ig} = \sum_i^{nc} x_i H_i^{ig}(T) \quad (7.6)$$

where the ideal gas enthalpy for the i pure compound is calculated from

$$H_i^{ig} = H_{i,ref}^{ig} + \int_{T_{ref}}^T C_{P,i}^{ig} dT \quad (7.7)$$

and the molar ideal isobaric heat capacity for the i th compound is calculated from the Design Institute for Physical Properties (DIPPR) correlation [172] (Eq. (7.8)), although simple power laws are also commonly used.

$$C_{P,i}^{ig} = A_i^D + B_i^D \left(\frac{C_i^D/T}{\sinh(C_i^D/T)} \right)^2 + D_i^D \left(\frac{E_i^D/T}{\cosh(E_i^D/T)} \right)^2 \quad (7.8)$$

The coefficients (A_i^D , B_i^D , C_i^D , D_i^D , and E_i^D) are adjustable parameters correlated to experimental data for each component i . The DIPPR coefficients for CO₂ are shown in table 7.1. T_{ref} in Eq. (7.7) is a reference temperature, which in this work is $T_{ref} = 298.15$ K.

The ideal isochoric heat capacity for the i th component is given simply as

$$C_{V,i}^{ig} = C_{P,i}^{ig} - R \quad (7.9)$$

Table 7.1: DIPPR coefficients for calculation of the isobaric ideal gas heat capacity of CO₂ using Eq. (7.8).

	A	B	C	D	E
	[J/(mol K)]	[J/(mol K)]	[K]	[J/(mol K)]	[K]
CO ₂	29.370	34.540	1428	26.400	588

where R is the ideal gas constant.

The residual contributions in Eqs. (7.1)-(7.3) can be obtained from the reduced residual Helmholtz energy ($F = A^{res}/RT$) of an equation of state. The residual isochoric heat capacity can be calculated from Eq. (7.10)

$$C_V^{res}(T, V, \mathbf{n}) = -RT^2 \left(\frac{\partial^2 F}{\partial T^2} \right)_{V, \mathbf{n}} - 2RT \left(\frac{\partial F}{\partial T} \right)_{V, \mathbf{n}} \quad (7.10)$$

The residual isobaric heat capacity is calculated from Eq. (7.11)

$$C_P^{res}(T, V, \mathbf{n}) = C_V^{res} - T \frac{\left(\frac{\partial P}{\partial T} \right)_{V, \mathbf{n}}^2}{\left(\frac{\partial P}{\partial V} \right)_{T, \mathbf{n}}} - nR \quad (7.11)$$

where

$$\left(\frac{\partial P}{\partial V} \right)_{T, \mathbf{n}} = -RT \left(\frac{\partial^2 F}{\partial V^2} \right)_{T, \mathbf{n}} - \frac{nRT}{V^2} \quad (7.12)$$

$$\left(\frac{\partial P}{\partial T} \right)_{V, \mathbf{n}} = -RT \left(\frac{\partial^2 F}{\partial V \partial T} \right)_{\mathbf{n}} - \frac{P}{T} \quad (7.13)$$

The residual enthalpy can be calculated from Eq. (7.14)

$$\frac{H^{res}(T, P, \mathbf{n})}{nRT} = Z - \frac{T}{n} \left(\frac{\partial F}{\partial T} \right)_{V, \mathbf{n}} - 1 \quad (7.14)$$

The Joule-Thomson coefficient is defined as the derivative of temperature with respect to pressures at constant enthalpy and can be related to C_P and the residual properties as

$$\mu_{JT} = \left(\frac{\partial T}{\partial P} \right)_{H, \mathbf{n}} = -\frac{1}{C_P} \left[V + T \left(\frac{\partial P}{\partial T} \right)_{V, \mathbf{n}} / \left(\frac{\partial P}{\partial V} \right)_{T, \mathbf{n}} \right] \quad (7.15)$$

Finally the speed of sound can be expressed as:

$$u = \sqrt{-V^2 \frac{C_P}{C_V} \frac{\left(\frac{\partial P}{\partial V} \right)_{T, \mathbf{n}}}{M_W}} \quad (7.16)$$

were M_W is the molecular weight. Note that it is the isobaric and isochoric heat capacities which are in Eqs. (7.15) and (7.16) and not only the residual part.

From the above equations it can be seen that in addition to first order properties the second order derivatives $(\partial^2 F/\partial V^2)_{\mathbf{n},T}$, $(\partial^2 F/\partial V\partial T)_{\mathbf{n}}$ and $(\partial^2 F/\partial T^2)_{\mathbf{n},V}$ are crucial in order to obtain accurate derivative property predictions. For this reason, the derivative properties are sometimes referred to as second-order properties.

As only the pure compound properties of CO_2 are evaluated in this chapter the mole fractions in Eqs. (7.4)-(7.6) are equal to one and the equations essentially reduce to the ideal properties of the pure compound. For the isochoric and isobaric heat capacities deviations and illustrations are only presented for their residual part throughout the chapter. To obtain pseudo-experimental data for the residual part of these properties the ideal contribution is subtracted the pseudo-experimental data. In this way it is implicitly assumed that the ideal contribution is accurately estimated with the DIPPR correlation.

7.2 Pure Compound Parameters and Modeling Approaches

The previous chapter illustrated that there are substantial uncertainties in the pure compound parameters of CO_2 when CO_2 is modeled as either a self-associating or quadrupolar species (with four adjustable parameters). The uncertainties in the parameters were propagated to physical properties and binary VLE and LLE using a Monte Carlo technique.

While such an analysis is a rigorous way to compare the models more objectively, it is unfortunately also impractical and time consuming to employ for an extensive investigation of the modeling approaches. It is thus desirable to obtain explicit pure compound parameters which can be compared to other modeling approaches.

Based on results from the previous chapter it was decided to select two parameter sets for qCPA, which are within the estimated uncertainty of the pure compound parameters (obtained with the bootstrap technique); one which reproduces well the VLEs of $\text{CO}_2 + \text{propane}$ at a single temperature and one which represents well the LLE of $\text{CO}_2 + \text{n-dodecane}$. While this procedure is strongly related to that where the VLE or LLE data is included in the correlation. It must be emphasized, however, that no VLE or LLE data have been used directly in the parameter estimation.

Contrary to qCPA with four parameters the parameter uncertainties for qCPA with three adjustable parameters were insignificant and had no real impact on the propagated errors. For this reason the parameters estimated from classical LSQ estimation is employed for qCPA with three parameters (see table 6.3). The performance of qCPA is compared with two other CPA approaches namely non-associating (n.a.) CPA, where CO₂ is assumed to be an inert compound, and the case when CO₂ is assumed to be (pseudo) self-associating. Based on the results in the previous chapter and following the conclusions by both Kontogeorgis and co-workers [14, 33–36, 81] and Voutsas and co-workers [21, 22, 79, 80] we choose to employ the 4C association scheme for the comparison.

The CO₂ parameters from the LSQ estimation is employed for both inert CPA and for CPA where CO₂ is assumed to be self-associating. In the latter case this may seem inconsistent, as this modeling approach also showed high parameter uncertainties. The uncertainties, however, seemed to have little effect on binary phase equilibria. Moreover no parameter set was found which would improve one property without deteriorating another.

Table 7.2 shows the CO₂ parameters and associated %AADs for the approaches which are employed in this chapter (and the next). Very good agreement with the experimental data is achieved for all approaches. It is noteworthy that the deviations from experimental data for CO₂ with qCPA are lower than CPA without association (CPA n.a.), even when the same number of adjustable parameters are employed. For qCPA with four parameters, due to the method used to obtain the parameters, it may be possible to find parameters which deviate less from the experimental data than those chosen here. Exceptionally good correlations (in terms of the closeness of fit) are found when CO₂ is assumed to be self-associating. However, as discussed in previous chapters this should probably be attributed mainly to an increased model flexibility due to the number of adjustable parameters.

Table 7.2: CPA and qCPA pure compound parameters for CO₂ together with %AADs between experimental [152–154] and calculated saturated liquid densities and saturated pressures. The quadrupolar moment of CO₂ is fixed at the (average) experimental value of -4.3 DÅ^a when qCPA is employed. Details on the parameter estimation can be found in chapter 6.

Modeling approaches	b_0 mL/mol	Γ K	c_1 -	$\beta \cdot 1000$ -	ϵ/R K	b_0^Q mL/mol	%AAD ^b	
							P^{sat}	ρ^{liq}
CPA, n.a.	27.3	1550	0.77	-	-	-	0.18	0.95
CPA, 4C	28.4	1329	0.66	25.7	513	-	0.07	0.10
qCPA, 3par	27.9	1284	0.68	-	-	= b_0	0.13	0.46
qCPA, 4par set 1 ^b	28.2	1172	0.64	-	-	23.6	0.49	0.24
qCPA, 4par set 2 ^b	28.1	1230	0.64	-	-	25.4	0.42	0.29

^a 1DÅ = 1Buckingham = 10^{-26} esu cm² = $3.3356 \cdot 10^{-40}$ Cm².

^b Parameters based on uncertainties and (indirectly) VLE or LLE data.

7.3 Derivative Properties and Density

To the best of our knowledge relatively few systematic evaluations of the performance of CPA (or SAFT) for derivative properties have been published. Lafitte et al. [167, 173] evaluated the performance of various SAFT variants, with emphasis on SAFT-VR Mie, for predicting derivative properties of alkanes and alcohols. Similarly Lundstrøm et al. [174] evaluated the performance of SRK and CPA for predicting derivative properties of water, methanol and a binary mixture of the two components. CPA is overall found to perform best of the two models. Recently, de Villiers et al. [115] compared the performance of CPA, PC-SAFT and SAFT for predicting derivative properties of various alkanes and alcohols. The authors also attempted, with some success, to improve the pure compound parameters of the models, by using heats of vaporization in the correlation in addition to the saturated liquid density and vapor pressure.

The perhaps most relevant investigation for the purposes of this work is the study performed by Diamantonis and Economou [6]. Employing SAFT and PC-SAFT the authors calculated the density and several derivative properties of various pure compounds, including CO₂, over an extensive temperature and pressure range ($T = 220 - 500$ K and $P = 0 - 200$ bar for CO₂). In general the predictions with both SAFT and PC-SAFT are in good agreement with experimental data for most properties, except in the vicinity of the critical point.

7.3.1 Saturation region

As the pure compound parameters of CO₂ for the modeling approaches investigated in this work have been correlated to the saturated liquid density and saturated vapor pressure it seems prudent to evaluate the models for their ability to predict other derivative properties at saturation. We thus compare the prediction of several derivative properties for CO₂, both in the liquid and vapor phase against pseudo-experimental data from the Span and Wagner EoS for pure CO₂ [15].

The temperature range of this investigation is $T = 216 - 300$ K, the immediate vicinity around the critical point ($T = 304.13$ K and $P = 73.8$ bar) is ignored as the uncertainty with the Span and Wagner EoS, as well as the investigated equations of state, becomes significant at these conditions. See section 7.4 for direct calculations of the critical point with CPA and qCPA.

Tables 7.3 and 7.4 compare, in terms of %AAD, the equations of state for their ability to predict the vapor density of CO₂ as well as several derivative properties (the speed of sound, the isobaric and isochoric heat capacity, the Joule-Thomson coefficient and the enthalpy of vaporization) at saturation in the

liquid and vapor phase respectively. Ideally the addition of a quadrupolar term would improve the prediction of the derivative properties due to the physically more correct model and the improved density description in the liquid phase. However, with the exception of the isobaric heat capacity in the liquid phase, $C_{P,liq}^{res,sat}$, it is observed that CPA without association often performs somewhat better for CO₂ than the more sophisticated models, especially in the vapor phase, where the EoS is superior for CO₂ both in the vapor density, isochoric heat capacity and Joule-Thomson coefficient. This is also the case for the heat of vaporization, where CPA without association again performs better, possibly due to a more accurate vapor phase enthalpy. Nevertheless the performance of the models is comparable for all properties in terms of %AAD. The prediction of most properties is satisfactory, considering that no parameters have been fitted to these properties.

Noticeable exceptions to the otherwise satisfactory performance are the predictions of the residual isochoric and isobaric heat capacities in the vapor phase as well as the isochoric heat capacity in the liquid phase (except with CPA without association).

Table 7.3: %AAD values for u_{liq}^{sat} , $C_{P,liq}^{res,sat}$, $C_{V,liq}^{res,sat}$, $\mu_{JT,liq}^{sat}$, and ΔH^{vap} of CO₂ at saturation using CPA n.a., CPA 4C and qCPA with three different parameter sets. The temperature range is $T = 216 - 300$ K. Pseudo-experimental data from the Span and Wagner EoS [15]. u represents the speed of sound, μ the Joule-Thomson coefficient and ΔH^{vap} the heat of vaporization.

Modeling approaches	% AAD				
	u_{liq}^{sat}	$C_{P,liq}^{res,sat}$	$C_{V,liq}^{res,sat}$	$\mu_{JT,liq}^{sat}$	ΔH^{vap}
CPA, n.a.	13.2	7.6	10.7	6.6	7.7
CPA, 4C	13.2	4.8	35.1	8.7	9.9
qCPA, 3par	13.0	5.2	23.8	6.2	9.6
qCPA, 4par, set 1	13.0	5.1	27.5	7.6	10.6
qCPA, 4par, set 2	13.1	5.4	24.2	7.5	10

Table 7.4: % AAD values for ρ_{vap}^{sat} , u_{vap}^{sat} , $C_{P,vap}^{res,sat}$, $C_{V,vap}^{res,sat}$ and $\mu_{JT,vap}^{sat}$ of CO₂ at saturation using CPA n.a., CPA 4C and qCPA with three different parameter sets. The temperature range is $T = 216 - 300$ K. Pseudo-experimental data from from the Span and Wagner EoS [15].

Modeling approaches	% AAD				
	ρ_{vap}^{sat}	u_{vap}^{sat}	$C_{P,vap}^{res,sat}$	$C_{V,vap}^{res,sat}$	$\mu_{JT,vap}^{sat}$
CPA, n.a.	6.9	6.2	56.7	86.4	9.1
CPA, 4C	8.1	5.7	57.1	79.1	10.5
qCPA, 3par	8.5	6.0	59.3	84.8	10.4
qCPA, 4par, set 1	9.5	6.0	60.6	84.5	11.0
qCPA, 4par, set 2	9.7	5.9	60.7	85.0	11.0

Figure 7.1 shows predictions of the liquid and vapor phase isobaric and isochoric heat capacity respectively. It is clear from figure 7.1a that using CPA with the

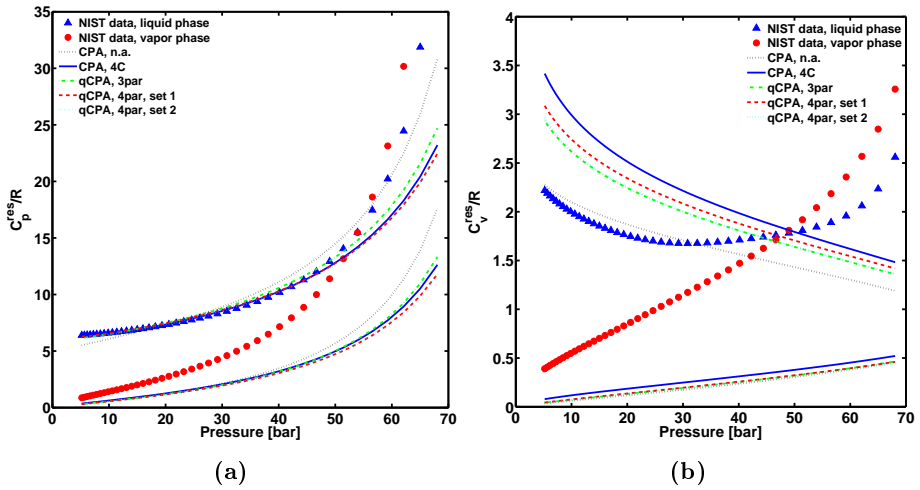


Figure 7.1: Normalized liquid and vapor residual isochoric (a) and isobaric (b) heat capacity predictions of CO_2 at saturation with CPA and qCPA. Pseudo-experimental data from the Span and Wagner EoS [15].

4C scheme and qCPA predicts the liquid isobaric heat capacity of CO_2 very well through most of the saturation region, although the predictions of all model approaches begin to deviate as the critical point is approached. On the other hand figure 7.1b shows that the trend of the liquid isochoric heat capacity is not captured by any model. The predictions in the vapor phase are quite poor for both the residual isochoric and isobaric heat capacity.

Figure 7.2 illustrates that while the speed of sound in the vapor phase and the Joule-Thomson coefficient in the liquid phase are predicted quite well, the performance begins to deteriorate close to the critical point. The liquid phase speed of sound and vapor phase Joule-Thomson coefficient predictions are quantitatively wrong and moreover the trend of the data is not fully captured.

Finally figure 7.3 shows the predicted heat of vaporization. All models predict the qualitative trend, but loose accuracy as the critical pressure is approached. Again, CPA without association actually performs slightly better than the other modeling approaches close the the critical point.

7.3.2 Compressed liquid region

Table 7.5 shows deviations for the density and the different derivative properties for CO_2 at two reduced temperatures, namely $T_r = 0.8$ and $T_r = 0.9$ and over an extensive pressure range (100 – 1000 bar, corresponding to a reduced pressure range of about 1.4-13.7) in the compressed liquid region. In most cases the predictions are similar or better when CO_2 is modeled as a self-associating or

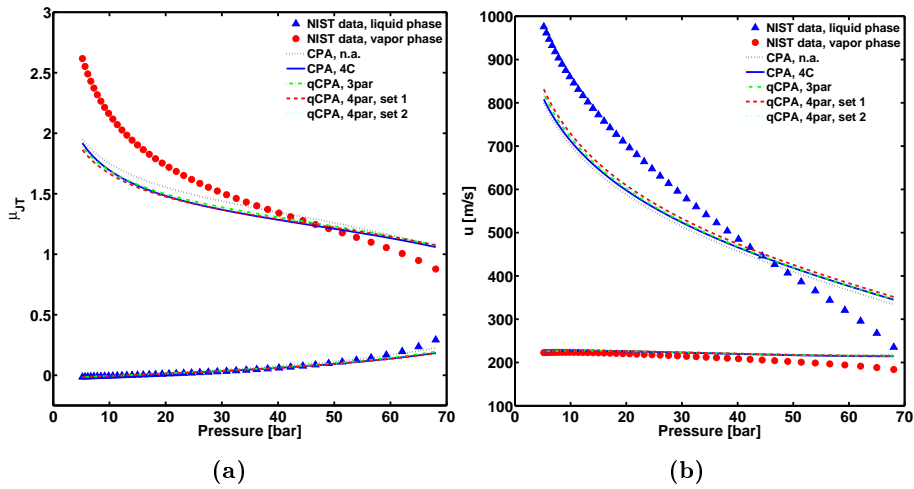


Figure 7.2: Liquid and vapor Joule-Thomson coefficient (a) and speed of sound (b) predictions of CO₂ at saturation with CPA and qCPA. Pseudo-experimental data from the Span and Wagner EoS [15].

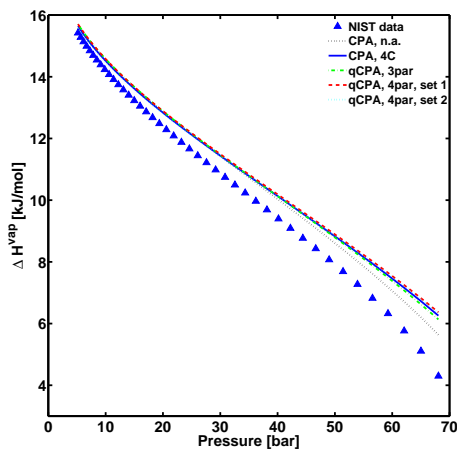


Figure 7.3: Heat of vaporization predictions of CO₂ at saturation with CPA and qCPA. Pseudo-experimental data from the Span and Wagner EoS [15].

quadrupolar compound rather than an inert species. A pronounced exception is again the prediction of the residual isochoric heat capacity of CO_2 , where both CPA with the 4C scheme and qCPA perform very poorly and CPA without association performs better, at least in terms of %AAD. A similar observation was made by de Villiers et al. [115] for n -alkanes, where the original SAFT performed better than CPA and PC-SAFT for the prediction of C_V but worse for other properties.

Diamantonis and Economou [6] calculated, using SAFT and PC-SAFT, derivative properties for several small molecules including CO_2 (modeled as an inert) over an extensive temperature range. Both models performed well far from the critical region with PC-SAFT being somewhat more accurate. With the exception of the speed of sound their results are surprisingly similar to the results for non-associating CPA, especially considering the different models and different temperature and pressure intervals considered in their work. The speed of sound predictions are significantly better with the SAFT-type models compared to the CPA-based models. This is expected as several researchers have demonstrated that SAFT can predict the trend in the speed of sound much better than CPA-based models [6, 175].

Table 7.5: %AAD values of ρ^{liq} , u , C_P^{res} , C_V^{res} , and μ_{JT} for CO_2 at two reduced temperatures in the compressed liquid region using CPA n.a., CPA 4C and qCPA with three different parameter sets. Pseudo-experimental data from the Span and Wagner EoS [15].

Modeling approaches	T_r	P range [bar]	% AAD				
			ρ^{liq}	u	C_P^{res}	C_V^{res}	μ_{JT}
CPA, n.a.	0.8	100-1000	2.6	12.2	15.2	6.5	17.0
CPA, 4C			1.1	9.8	6.2	42.5	20.1
qCPA, 3par			1.6	10.2	6.3	30.0	12.0
qCPA, 4par, set 1			1.2	9.2	4.6	35.7	13.3
qCPA, 4par, set 2			1.3	9.7	7.1	30.6	14.5
CPA, n.a.	0.9	100-1000	2.7	13.0	8.1	15.9	15.2
CPA, 4C			1.8	10.4	4.7	41.8	12.9
qCPA, 3par			2.0	11.2	3.8	33.9	4.7
qCPA, 4par, set 1			1.7	10.3	2.9	38.7	1.8
qCPA, 4par, set 2			1.7	10.7	4.6	33.8	1.7

Figure 7.4 shows (reduced) C_V^{res} and C_P^{res} predictions for CO_2 at $T_r = 0.8$ and $T_r = 0.9$. The predictions when CO_2 is modeled either with the 4C scheme or the different qCPA parameter sets are very similar, with qCPA being slightly better. More importantly both modeling approaches predict the intersecting isobaric heat capacities at approximately 300 bar quite accurately (see figure 7.4b), whereas CPA without association predicts this point around 800 bar. The C_V^{res} predictions in figure 7.4a illustrate clearly that most of the models have difficulties with the C_V^{res} predictions.

Notice that while CPA without association yields the best C_V^{res} prediction it is the poorest in terms of C_P^{res} . However, C_P^{res} depends on C_V^{res} as can be

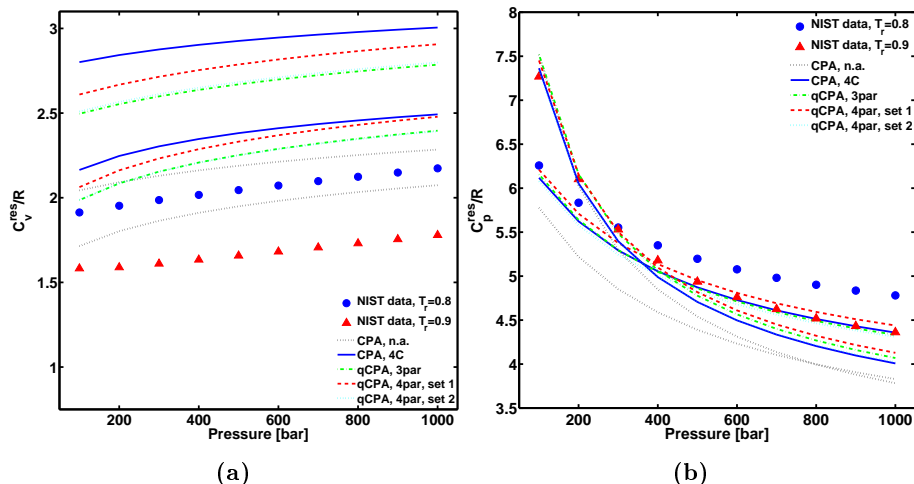


Figure 7.4: Normalized isochoric (a) and isobaric (b) heat capacity predictions for CO₂ with CPA and qCPA in the compressed liquid region and at $T_r = 0.8$ and $T_r = 0.9$. Pseudo-experimental data from the Span and Wagner EoS [15].

seen from equation (7.11) in section 7.1. This suggests that a large part of the improved C_P^{res} predictions with qCPA and CPA with association is due to the over-prediction of C_V^{res} . In this way at least part of the improvement is in fact due to a cancellation of errors between the C_V^{res} and the ratio between $(\partial P/\partial T)_{V,n}^2$ and $(\partial P/\partial V)_{T,n}$.

Figure 7.5 shows that the speed of sound and Joule-Thomson coefficient predictions for CO₂ are slightly improved with qCPA, both of which suggest a slightly more accurate ratio between $(\partial P/\partial T)_{V,n}$ and $(\partial P/\partial V)_{T,n}$.

As the model parameters are correlated to the saturated liquid density it is expected that the density is predicted fairly well, even outside the saturation region. Figure 7.6a compares the predictions of the liquid density of CO₂ at $T_r=0.8$ and $T_r=0.9$ against data from the Span and Wagner EoS [15]. Figure 7.6b shows the predictions against the experimental data from Brewer et al. [176] in the more restricted pressure range of 200-400 bar and at $T_r = 0.9$ and $T_r = 0.93$. Both figures confirm that the predictions are quite satisfactory for all modeling approaches, in particular at moderate pressures.

At elevated pressures it can be seen from especially figure 7.6a that the density predictions for CPA without association are worse than when CO₂ is modeled as an associating or quadrupolar compound. The predictions with qCPA are satisfactory in the whole pressure range. Table 7.6 show the %AAD between model predictions and the density values from [176]. Although slightly smaller for the quadrupolar approaches the deviations are around 1% in all cases.

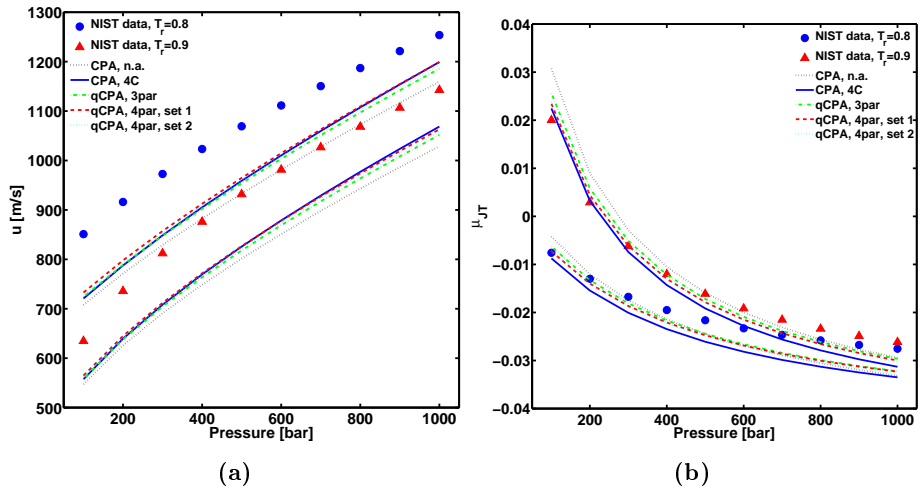


Figure 7.5: Speed of sound (a) and Joule-Thomson coefficient (b) predictions for CO_2 with CPA and qCPA in the compressed liquid region and at $T_r = 0.8$ and $T_r = 0.9$. Pseudo-experimental data from the Span and Wagner EoS [15].

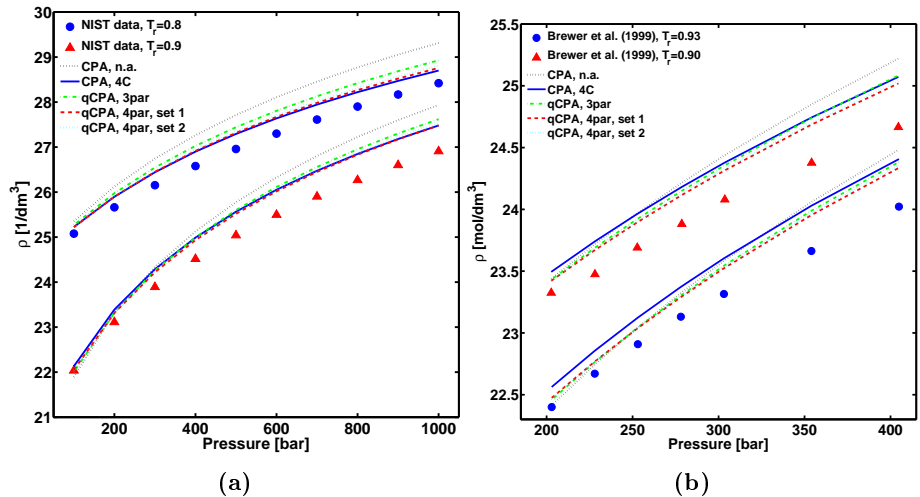


Figure 7.6: Density predictions for CO_2 with CPA and qCPA in the compressed liquid region. At $T_r = 0.8$ and $T_r = 0.9$ (a) compared to pseudo-experimental data from the Span and Wagner EoS [15] and at $T_r = 0.9$ and $T_r = 0.93$ (b) compared to experimental data from Brewer et al. [176].

Table 7.6: %AAD values between the experimental liquid density data from Brewer et al. [176] and the predicted values for CO₂ using CPA n.a., CPA 4C and qCPA with three different parameter sets. The pressure range of the data is 200-400 bar.

Model	CPA n.a.	CPA 4C	qCPA, 3par	qCPA, set 1	qCPA, set 2
$T_r = 0.9$	1.4	1.2	1.1	1	1
$T_r = 0.93$	0.9	1.1	0.8	0.8	0.8

7.3.3 Critical region

The critical region is important due to the observed extrema and inflection points present in the derivative properties, which serves as a valuable test for the partial derivatives of an EoS. Table 7.7 shows the %AAD values for the derivative properties of CO₂ utilizing the different modeling approaches at $T_r = 1.1$ and in a pressure range of 0-250 bar (corresponding to a reduced pressure range of 0-3.4). With the exception of C_V^{res} the prediction of all modeling approaches are quite good as the low %AAD suggests.

Figure 7.7a clearly shows that the maximum in C_V^{res} is not predicted by any of the models. A similar result was obtained by de Villiers et al. [115] for n -alkanes using CPA, SAFT and PC-SAFT. Diamantonis and Economou [6] also found increasing inaccuracies in the predicted residual isochoric heat capacity of CO₂ with SAFT and PC-SAFT. In the vicinity of the critical point the authors found that SAFT and PC-SAFT predicts (as a function of temperature) the opposite trend for C_V^{res} as that seen in the experimental data.

These failures to represent the qualitative form of the residual isochoric heat capacity suggests a fundamental problem with the temperature dependence of both the physical SRK term and the dispersion term in SAFT. On the other hand, using SAFT-VR Mie, Lafitte et al. [173] found that the maximum in C_V could be predicted for 1-hexanol and 1-decanol. The maximum was found to be mainly governed by the association term. It is interesting, however, that no such behaviour was observed when CO₂ was considered an associating compound. As the maximum in C_V for 1-hexanol is also predicted with CPA (see figure 7.8) we suspect, that the reason for the absence of the maximum for CO₂ is primarily due to the relatively small contribution from the association term for CO₂. As seen in figure 7.7b all the model variants evaluated in this work capture the maximum for C_P^{res} with good accuracy.

As the low %AAD in table 7.7 suggests all model approaches predict the inflection point in the density and Joule-Thomson coefficient as well as the minimum in the speed of sound. Especially the density predictions are extremely accurate, as shown in figure 7.9.

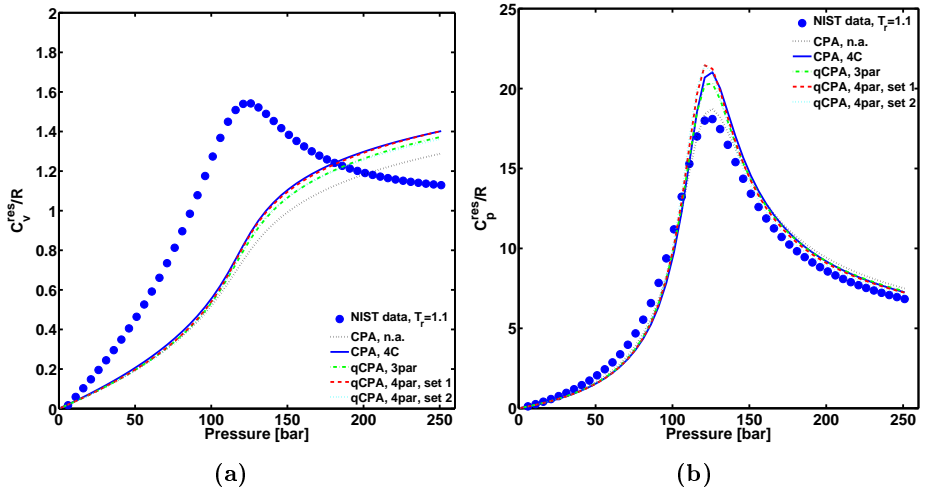


Figure 7.7: Normalized isochoric (a) and isobaric (b) heat capacity predictions of CO₂ with CPA and qCPA in the critical region ($T_r = 1.1$). Pseudo-experimental data from the Span and Wagner EoS [15].

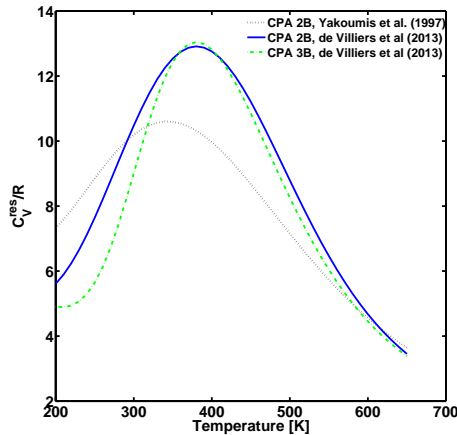


Figure 7.8: C_V^{res} predictions of 1-hexanol using 3 different CPA parameter sets with the 2B [51, 115] and 3B [115] schemes respectively. The parameters from de Villiers et al. [115] have been correlated to C_P^{liq} and ΔH^{vap} in addition to the saturated density and vapor pressure.

Table 7.7: %AAD values for ρ^{liq} , u , C_P^{res} , C_V^{res} , and μ_{JT} in the near critical region at reduced temperature $T_r = 1.1$ using CPA n.a., CPA 4C and qCPA with three different parameter sets. Pseudo-experimental data from the Span and Wagner EoS [15].

Modeling approaches	T_r	P range [bar]	ρ^{liq}	u	% AAD		
					C_P^{res}	C_V^{res}	μ_{JT}
CPA, n.a.			3.2	4.9	3.9	32.5	7.3
CPA, 4C			1.6	3.8	6.3	31.4	4.8
qCPA, 3par	1.1	0-250	2.0	4.2	5.4	32.2	5.1
qCPA, 4par, set 1			1.4	4.0	5.9	32.2	4.3
qCPA, 4par, set 2			1.1	4.1	4.7	32.2	4.2

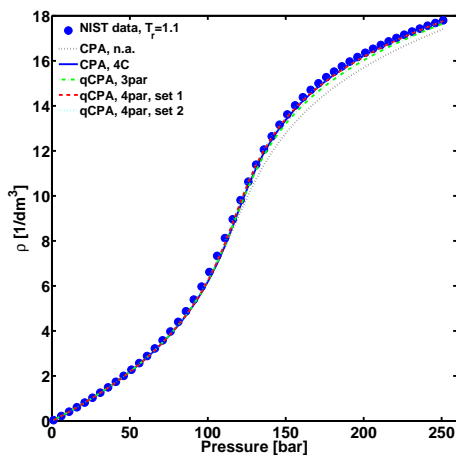


Figure 7.9: Density predictions of CO₂ with CPA and qCPA in the critical region ($T_r = 1.1$). Pseudo-experimental data from the Span and Wagner EoS [15].

7.3.4 Summary of derivative property results

Overall it has been shown that for most predicted properties, in both the saturation-, the compressed liquid- and the critical region, the qualitative performance is not significantly different for the various models (CPA n.a., CPA 4C and qCPA), and all modeling approaches predict the same trends. With the clear exception of C_V^{res} all models generally perform satisfactory considering that the model parameters have not been correlated to any of these properties, rendering the models purely predictive.

In regards to the density and the derivative properties qCPA and CPA with the 4C scheme typically perform slightly better quantitatively than CPA without association (again with C_V^{res} as the exception). This is illustrated in figure 7.10 which shows the overall deviations in the density and the derivative properties,

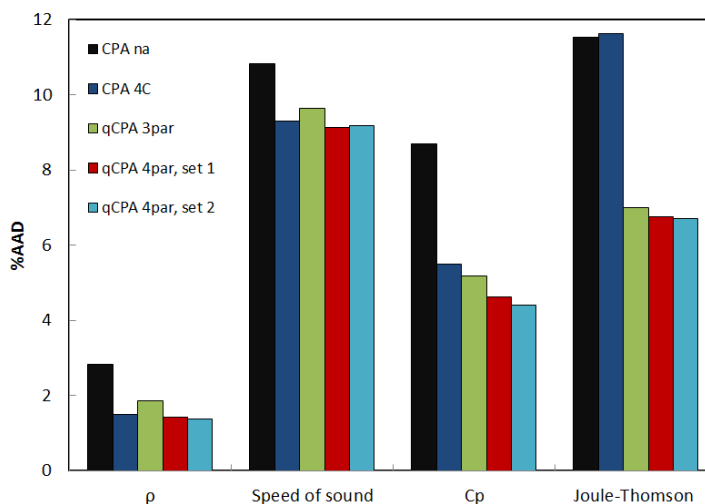


Figure 7.10: Model comparison of the overall %AADs for the density, speed of sound, isobaric heat capacity and the Joule-Thomson coefficient in the liquid or supercritical phase using the five modeling approaches.

with the exception of C_V^{res} , which cannot be represented well by any of the modeling approaches. Figure 7.10 also shows that the predictions are only marginally improved when the four parameter version of qCPA is employed, rather than the three parameter version. In most cases qCPA and CPA gives similar predictions, however, the Joule-Thomson coefficient is, at least in terms of %AAD, predicted significantly better with the various qCPA approaches.

Considering that qCPA should result in a physically more correct model, the improvement, at least for the quadrupolar term, is clearly smaller one might expect. Of course part of the explanation is that most of the pure compound predictions with inert CPA are quite good to begin with, another reason may be that the artificially large attractive energies for e.g. inert CPA may compensate quite well for the added energetic quadrupole term so long as there are not cross interactions.

7.4 Critical Points

The traditional parameters of the SRK EoS are obtained from the critical properties, which ensures that the model reproduces the correct critical point, at the cost of the saturated liquid density. On the other hand, models such as CPA and SAFT, whose parameters are fitted to the saturated liquid density and saturated pressure typically overestimate the critical point. As there are

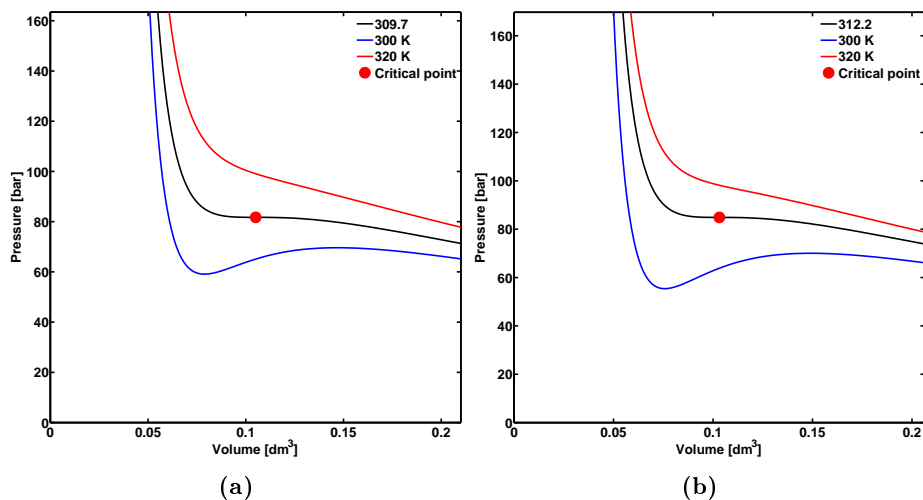


Figure 7.11: PV-diagram with predicted temperature isotherms at 300 K, 320 K and the critical temperature isotherm using CPA n.a. (a), and qCPA with 3 parameters (b) to model CO₂.

several applications of CO₂ near the critical region, it is of interest to calculate its critical temperature and pressure with the different models.

At the critical point only one phase exists, and there is an inflection point in the critical temperature isotherm. That is

$$\left(\frac{\partial P}{\partial V}\right)_T = \left(\frac{\partial^2 P}{\partial V^2}\right)_T = 0 \quad (7.17)$$

To illustrate the calculated critical point for CO₂ with qCPA and inert CPA figure 7.11 shows, in a PV diagram, different temperature isotherms below, above and at the critical point. The critical point, determined as the inflection point in the critical temperature isotherm, is marked with a circle.

The experimental critical temperature, pressure and volume are compared with the calculated critical points with the different CPA modeling approaches in table 7.8. Figure 7.12 also compare, for three of the modeling approaches, the saturated density predictions with pseudo-experimental data from the Span and Wagner EoS [15].

Figure 7.12a shows the complete saturation curve from the triple point to the critical point, while figure 7.12b is a close-up of the part of the curve which the saturated liquid density have not been correlated to. Unfortunately the addition of a quadrupolar term does not improve the prediction of the critical points. Both CPA with the 4C scheme and the three versions of qCPA overestimate the critical pressure by approximately 12 bar and the critical temperature by roughly 9 K. The overall best model is CPA without association, which is

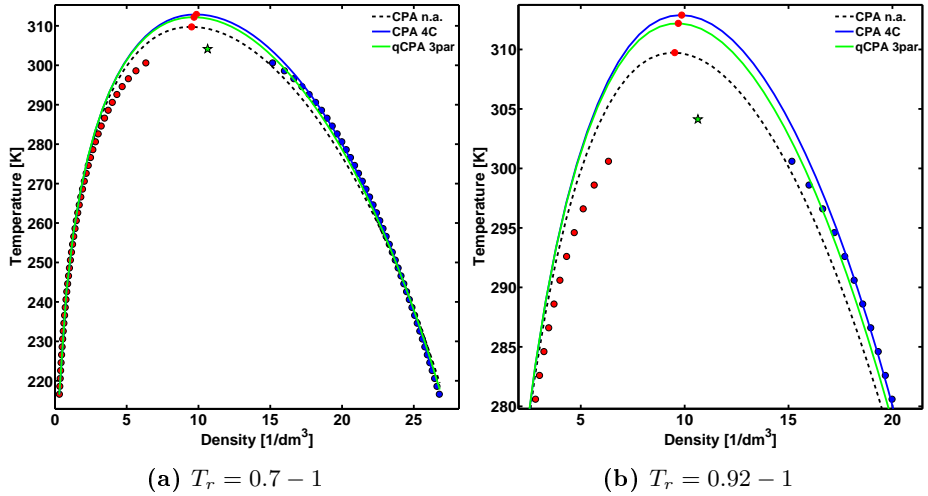


Figure 7.12: Predictions of the saturated density from the triple point to the critical point (a) and in the narrower temperature interval from 280 K to the critical point (b).

essentially equivalent to the SRK with fitted parameters. Comparable critical points were obtained for CO₂ by Diamantonis and Economou [6] using SAFT (309.5 K and 79.2 bar) and PC-SAFT (315.5 K and 90.9 bar) respectively. CO₂ was treated as a non-associating species in both cases.

Table 7.8: Experimental [15] and predicted critical pressure, temperature and volume of CO₂ modeled with inert CPA, CPA with the 4C association scheme and qCPA with three different parameter sets.

Modeling approaches	Exp	CPA n.a. n.a.	CPA 4C 4C	qCPA 3par	qCPA 4par, set 1	qCPA 4par, set 2
T_C [K]	304.13	309.7	312.9	312.2	313.5	313.4
P_C [bar]	73.8	81.7	86.4	84.9	86.3	85.7
V_C [dm ³]	0.094	0.105	0.101	0.103	0.102	0.103

7.5 The Second Virial Coefficient

A limiting low-density test for a thermodynamic model is to evaluate its capabilities in predicting the second virial coefficient, B . It may be calculated from the expression

$$\lim_{\rho \rightarrow 0} \left(\frac{\partial Z}{\partial \rho} \right)_T = B \quad (7.18)$$

The contribution to the second virial coefficient from the SRK term is

$$B^{SRK} = b - \frac{a(T)}{RT} \quad (7.19)$$

The contribution from the association term can be expressed as

$$B^{assoc} = -S \left[\exp\left(\frac{\varepsilon^{AB}}{RT}\right) - 1 \right] b\beta^{AB} \quad (7.20)$$

where the constant S depend on the association scheme. Its value for several different schemes is shown in table 7.9.

Table 7.9: Value of S in equation (7.20) for eight different association schemes. Details for scheme 1A, 2B, and 4C can be found in [177, 178]. Nomenclature follows Huang and Radosz [61].

Scheme	1A	2A	2B	3A	3B	4A	4B	4C
S	0.5	2	1	4.5	2	8	3	4

The quadrupolar term is given solely as a Helmholtz energy model. The compressibility factor is expressed through the Helmholtz energy pressure equation as

$$Z = \rho \frac{\partial F'}{\partial \rho} + 1 \quad (7.21)$$

where F' is the Helmholtz energy pr. mole. From this expression it is straightforward to show, that the contribution to the second virial coefficient from the quadrupole term may be expressed as

$$B^{quad} = \frac{F'_2 - F'_{3,2}}{\rho(1 - F'_{3,2}/F'_2)^2} \quad (7.22)$$

where subscripts have the same meaning as in chapter 5. The expression is similar to that presented by Karakatsani and Economou [31] for the tPC-PSAFT.

The second virial coefficient of CO₂ was predicted with CPA and qCPA using the different modeling approaches from table 7.2. The predictions are visualized at relatively low temperatures in figure 7.13 and the %AADs are shown in table 7.10. All models are in reasonable agreement with the experimental data, although deviations increase for all models at low temperatures where the sharp decrease in the virial coefficient is not fully captured. Figure 7.13 and table 7.10 both show, that the least convincing result is obtained when CO₂ is assumed to be self-associating. This may be due to the fact, that CO₂ is not self-associating and this theoretically unfounded approach may become poor in the low density limit. On the other hand, when qCPA is employed the predictions, are also slightly worse than when regular non associating CPA is employed for CO₂. The differences, however, are rather small.

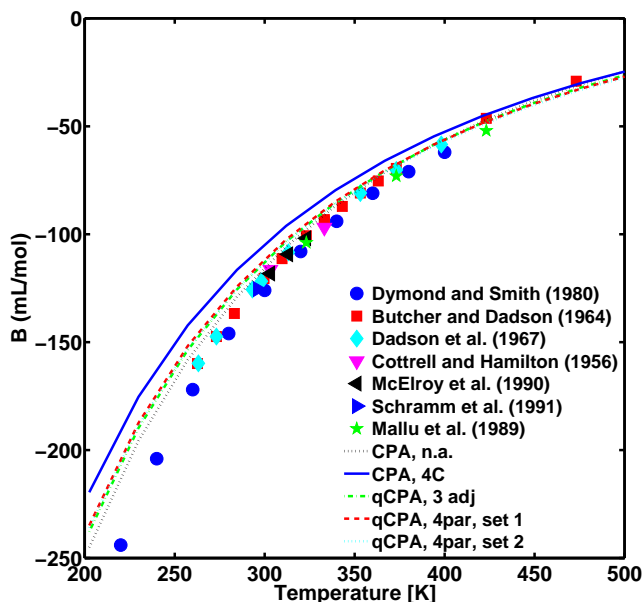


Figure 7.13: Model predictions against experimental data for the second virial coefficient of CO_2 using CPA, n.a., CPA 4C, and the qCPA. Experimental data from [179–185].

Table 7.10: %AADs between experimental and calculated second virial coefficients with the different models. Experimental data from [179–185].

Model	CPA, n.a.	CPA, 4C	qCPA, 3par	qCPA, 4par, set 1	qCPA, 4par, set 2
%AAD	5.5	13.3	7.3	7.9	7.1

7.6 Summary

In this chapter qCPA and CPA were employed to predict pure compound properties of CO_2 . Both the three and four parameter versions of qCPA were evaluated. When CO_2 was modeled with CPA, CO_2 was assumed to be either inert or pseudo self-associating following the 4C association scheme.

It was observed that a systematic improvement in the correlation of the saturated liquid density and vapor pressure was obtained when the same number of adjustable parameters were used for inert CPA and qCPA.

The models were employed to predict various pure compound properties for CO_2 including the second virial coefficient, the critical point and various derivative properties. It is difficult, however, to reach any definite conclusions as to which

model is superior in regards to the predicted pure compound properties as the models generally predict the same trends for all properties.

qCPA and CPA with the 4C association scheme seem to perform slightly better than CPA without association in regards to the derivative properties. On the other hand inert CPA is slightly more accurate in representing the second virial coefficient and the critical point. The main reason for the deviations in the derivative properties seem to be caused by a deficiency in the second order derivatives, particularly the temperature derivatives. This is for example the reason why none of the models can predict the maximum in C_V^{res} in the critical region. Unfortunately the derivatives does not seem to be improved by the addition of an explicit quadrupolar term.

Phase Equilibria of Binary Mixtures Containing CO₂

The primary objective of an equation of state is typically the correlation and prediction of the phase equilibria between mixtures of different compounds. For this reason the CPA and qCPA approaches which were employed for pure compound properties in the previous chapter, are evaluated for their ability to predict and correlate the phase equilibria of several different binary mixtures containing CO₂. Both non-associating, self-associating and quadrupolar compounds are considered in this chapter, although the primary focus is on mixtures containing CO₂ and *n*-alkanes, water, or alcohols. Part of the chapter has been published in Fluid Phase Equilib. (2016), 408, 151-169 [37].

8.1 Pure Compound Parameters

The pure compound parameters for the different modeling approaches for CO₂ were shown in the previous chapter in table 7.2. The pure compound CPA parameters for the compounds which, together with CO₂, form the binary mixtures under investigation, have been estimated using the objective function in Eq. (6.1). It is worth noting that the most pronounced change in the pure compound parameters, compared to the case where CO₂ is considered an inert compound, is that the energetic parameter in the attractive part of the SRK term is reduced, which should lead to more realistic cross-interactions and thus a smaller k_{ij} . The parameters obtained from the literature are shown in table 8.1.

Table 8.1: Pure compound CPA parameters from literature employed in this work.

Compound	Association scheme	b_0 [mL/mol]	Γ [K]	c_1 -	$\beta \cdot 10^3$ -	ε/R [K]	Ref
Methane	n.a.	29.10	959.03	0.45	-	-	[81]
Ethane	n.a.	42.90	1544.55	0.58	-	-	[81]
Propane	n.a.	57.83	1896.45	0.63	-	-	[51]
<i>n</i> -Butane	n.a.	72.08	2193.08	0.71	-	-	[51]
<i>n</i> -Pentane	n.a.	91.01	2405.11	0.80	-	-	[51]
<i>n</i> -Hexane	n.a.	107.89	2640.03	0.83	-	-	[51]
<i>n</i> -Decane	n.a.	178.65	3190.54	1.13	-	-	[51]
<i>n</i> -dodecane	n.a.	216.24	3471.04	1.20	-	-	[186]
<i>n</i> -tetradecane	n.a.	250.53	3678.42	1.29	-	-	[186]
<i>n</i> -pentadecane	n.a.	274.53	3751.99	1.34	-	-	[186]
<i>n</i> -eicosane	n.a.	374.38	4161.40	1.54	-	-	[34]
<i>n</i> -tetracosane	n.a.	454.45	4658.90	1.68	-	-	[34]
<i>n</i> -hexatriacontane	n.a.	717.66	5068.10	1.99	-	-	[34]
Nitrogen	n.a.	26.05	634.07	0.50	-	-	[186]
Benzene	n.a.	74.99	2867.19	0.76	-	-	[51]
Toluene	n.a.	92.14	3051.36	0.80	-	-	[51]
Water	4C	14.52	1017.34	0.67	69.20	2003.25	[52]
Methanol	2B	30.98	1573.71	0.43	16.10	2957.78	[52]
Ethanol	2B	49.11	2123.83	0.74	8.00	2589.85	[187]
1-Propanol	2B	64.11	2234.52	0.92	8.10	2525.86	[187]
1-Octanol	2B	148.80	3367.99	1.15	0.14	3218.55	[187]

Besides CO₂ we employ a few other quadrupolar compounds, namely water, ethane, benzene, toluene, nitrogen and acetylene. We assume, however, that the quadrupolar moment of water is negligible compared to the directional forces of the association term, moreover water is not axially symmetric, which means that its quadrupole moment is a tensor and it is thus difficult to treat with current models. It is also assumed that the small quadrupole moment of ethane can be ignored. For benzene, toluene, acetylene and possibly nitrogen, however, the quadrupole moment cannot be ignored, and the pure compound parameters must be re-estimated. Table 8.2 shows these parameters, for the three parameter version of qCPA. Table 8.2 also presents CPA parameters for 1-nonanol and acetylene, which were not found in the literature.

As previously discussed, the value for the quadrupolar moment of CO₂ is assumed to be $-4.3 \text{ D}\text{\AA}$ [84, 86–91]. Experimental values of the quadrupolar moment of benzene and acetylene, however, may vary considerably depending on the reference. The experimental quadrupole moment of benzene range from $-9.98 \text{ D}\text{\AA}$ [84] to $-3.6 \text{ D}\text{\AA}$ [89], although most of the experimental data is between $-9.98 \text{ D}\text{\AA}$ and $-8.5 \text{ D}\text{\AA}$ [84]. The situation is similar for acetylene which has a large positive quadrupole moment between $3.0 \text{ D}\text{\AA}$ and $8.4 \text{ D}\text{\AA}$ [84]. In this work we assume a fixed quadrupolar moment of $-9 \text{ D}\text{\AA}$ for benzene and $4 \text{ D}\text{\AA}$ for acetylene. For toluene Reynolds et al. [188] calculated an effective quadrupole moment of $7.92 \text{ D}\text{\AA}$. The quadrupole moment of nitrogen is between -1.4 and $-1.5 \text{ D}\text{\AA}$ [84], in this work a value of $-1.5 \text{ D}\text{\AA}$ is employed.

Table 8.2: Correlated CPA and qCPA pure compound parameters and %AAD in the saturated liquid densities and saturated pressures. Experimental data from raw DIPPR data [172]. The experimental quadrupole moments of benzene ($\approx -9 \text{ D}\text{\AA}$), acetylene ($\approx 4 \text{ D}\text{\AA}$) and nitrogen ($\approx -1.5 \text{ D}\text{\AA}$) are employed in the three parameter version of qCPA. Following Reynolds et al. [188] it is assumed that the effective quadrupole moment of toluene is $-7.92 \text{ D}\text{\AA}$.

Compound	Model	Association scheme	T_r (= T/T_c)	b_0 [mL/mol]	Γ [K]	c_1 -	Q (fixed) D \AA	$\beta \cdot 10^3$ -	ε/R [K]	%AAD	
										P^{sat}	ρ^{liq}
Benzene	qCPA	n.a.	0.5-0.9	75.57	2763.73	0.73	-9	-	-	0.46 (0.68) ^a	0.71 (0.84)
Toluene	qCPA	n.a.	0.4-0.9	92.2	3017.2	0.80	-7.92	-	-	0.52 (0.72)	0.73 (0.74)
Nitrogen	qCPA	n.a.	0.5-0.9	26.41	624.90	0.45	-1.5	-	-	0.76 (0.86)	1.65 (1.73)
Acetylene	qCPA	n.a.	0.6-0.9	33.54	1469.45	0.65	4	-	-	0.41 (0.43)	0.52 (0.68)
Acetylene	CPA	n.a.	0.6-0.9	33.28	1576.91	0.70	-	-	-	0.43	0.68
1-Nonanol	CPA	2B	0.45-0.9	163.79	3508	0.956	-	0.25	3570	0.40	0.79

^a Numbers in parenthesis are the %AAD with CPA.

To keep the number of adjustable parameters as low as possible the potential cross-association between CO₂ and self-associating compounds is taken into account either through the CR-1 combining rule (Eqs. (3.14) and (3.15)) or by using the approach suggested by Kleiner and Sadowski [60], see section 8.3 for more details on this. Unless otherwise noted a single temperature independent binary interaction parameter is employed for all correlations.

8.2 CO₂ + *n*-alkanes

As discussed in chapters 1 and 3, binary mixtures of CO₂ and *n*-alkanes behave non-ideally, which is believed to be due to the large quadrupole moment of CO₂. The quadrupole moment of CO₂ is, for instance, believed to be part of the reason for the LLE between CO₂ and heavy hydrocarbons, as well as the low temperature azeotrope formed between mixtures of CO₂ and lighter hydrocarbons. When CO₂ is treated as an inert compound a single binary interaction parameter of around 0.12-0.15 is typically needed to correlate the phase equilibria of mixtures containing CO₂ and an *n*-alkanes [8, 14].

In this regard it is crucial to evaluate mixtures of CO₂ + *n*-alkanes. A successful quadrupolar term should result in improved predictions ($k_{ij} = 0$) for CO₂ + *n*-alkane mixtures since essentially only physical (dispersion) and quadrupolar interactions should be present for these systems. As good predictions are typically obtained for mixtures consisting of two hydrocarbons (where dispersion forces dominate) any inaccuracy can be attributed primarily to model errors in the quadrupolar term or parametrization problems. The binary mixtures of CO₂ + *n*-alkanes are thus valuable systems for isolating the complexity of dealing with multiple interactions, such as polar and hydrogen bonding interactions.

8.2.1 VLE of CO₂ + *n*-alkanes

The VLE of several different CO₂ + *n*-alkane mixtures have been predicted over a range of temperatures using the different CPA-based models. The deviations from experimental data, in terms of %AAD, are presented in table 8.3 both for the predictions ($k_{ij} = 0$) as well as when an interaction parameter has been correlated to the VLE data. Characteristic results for some of these predictions are visualized in figures 8.1-8.4.

Table 8.3: Deviations for CPA and qCPA predictions ($k_{ij} = 0$) and correlations ($k_{ij} \neq 0$) of CO₂ + *n*-alkane VLEs (C₁-C₆ and C₁₀). Including the correlated k_{ij} . Compared to experimental data from Refs. [66, 67, 165, 189–195].

System	T range [K]	Modeling approach	%AAD P ^a	% AAD y_1	%AAD x_1	k_{ij}	% AAD P ^a	% AAD y_1	%AAD x_1
$k_{ij} = 0$									
CO ₂ (1) + methane(2)	230-293	CPA, n.a.	16.4	11.5	10.2	0.089	1.0	4.6	0.4
		CPA, 4C	4.9	9.0	2.0	0.016	2.3	5.2	0.7
		qCPA, 3par	1.3	8.1	0.9	-0.007	1.2	4.7	0.4
		qCPA, 4par, set 1	12.2	7.4	5.6	-0.057	1.3	4.9	0.5
		qCPA, 4par, set 2	6.0	7.6	3.8	-0.032	1.3	4.8	0.4
CO ₂ (1) + ethane(2)	213-270	CPA, n.a.	17.5	>100	>100	0.130	3.0	2.7	4.9
		CPA, 4C	9.3	29.7	71.0	0.067	0.3	2.1	1.9
		qCPA, 3par	6.2	18.4	45.0	0.042 ^b	0.6	2.5	4.4
		qCPA, 4par, set 1	0.7	2.8	4.4	0.000	0.7	2.8	4.4
		qCPA, 4par, set 2	3.1	9.3	22.3	0.017	0.9	3.5	6.2
CO ₂ (1) + propane(2)	230-270	CPA, n.a.	29.1	6.4	104.1	0.129	5.0	1.6	11.6
		CPA, 4C	17.7	2.9	50.4	0.074	3.0	2.2	6.6
		qCPA, 3par	12.9	2.1	34.3	0.035	4.3	1.8	10.0
		qCPA, 4par, set 1	3.7	1.9	8.5	0.000	3.7	1.9	8.5
		qCPA, 4par, set 2	8.2	1.8	20.0	0.021	4.0	1.9	9.1
CO ₂ (1) + butane(2)	250-418	CPA, n.a.	22.6	8.5	59.4	0.124	4.2	11.1	11.5
		CPA, 4C	14.1	6.9	32.7	0.071	2.8	5.3	9.3
		qCPA, 3par	10.3	6.4	24.0	0.040 ^b	3.0	5.4	9.8
		qCPA, 4par, set 1	3.3	5.4	10.3	0.000	3.3	5.4	10.3
		qCPA, 4par, set 2	7.2	5.9	17.5	0.028	3.3	5.3	9.6
CO ₂ (1) + pentane(2)	294-423	CPA, n.a.	19.5	1.9	29.7	0.110	2.1	1.3	2.6
		CPA, 4C	11.8	1.5	16.0	0.065	2.2	1.3	2.7
		qCPA, 3par	7.3	1.4	9.6	0.038	2.1	1.3	2.6
		qCPA, 4par, set 1	2.3	1.3	2.8	0.000	2.3	1.3	2.8
		qCPA, 4par, set 2	4.6	1.3	5.9	0.024	2.3	1.3	2.8
CO ₂ (1) + hexane(2)	273-303	CPA, n.a.	23.68	-	27.55	0.115	1.83	-	2.44
		CPA, 4C	14.32	-	18.68	0.067	1.02	-	1.4
		qCPA, 3par	8.71	-	11.58	0.037	1.45	-	1.98
		qCPA, 4par, set 1	1.38	-	2.04	0.000	1.38	-	2.04
		qCPA, 4par, set 2	5.27	-	7.1	0.021	1.6	-	2.27
CO ₂ (1) + decane(2)	277-584	CPA, n.a.	25.82	0.28	34.65	0.103	5.73	0.26	5.87
		CPA, 4C	15.55	0.28	18.79	0.060	2.46	0.26	2.48
		qCPA, 3par	9.1	0.26	10.25	0.028	3.19	0.26	3.34
		qCPA, 4par, set 1	1.93	0.26	1.87	0.000	1.93	0.26	1.87
		qCPA, 4par, set 2	5.34	0.27	5.69	0.011	2.96	0.26	3.06

^a Liquid phase deviation only.

^b Improved value compared to [37].

As described in chapter 7, some of the CO₂ + *n*-alkane mixtures have been utilized indirectly to obtain the two parameter sets for qCPA when b_0^Q is used as an additional adjustable. Parameter set 1 for qCPA was selected partly based on the VLE of CO₂ + propane, while parameter set 2 has been selected partly based on the CO₂ + *n*-dodecane LLE (see section 8.2.2).

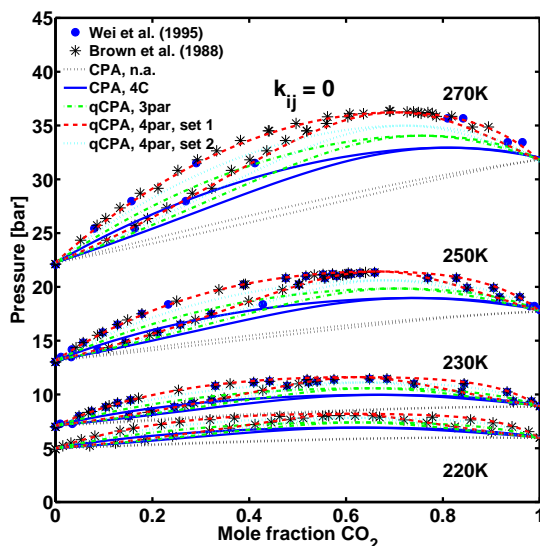


Figure 8.1: Predictions ($k_{ij} = 0$) compared to experimental data for the CO₂ + ethane VLE at four temperatures using CPA where CO₂ is treated either as an inert (n.a.) or self-associating compound (scheme 4C) and qCPA with either three or four parameters. Experimental data from Refs. [66, 67].

Predictions ($k_{ij} = 0$) compared to experimental data for the CO₂ + ethane VLE at four temperatures using CPA where CO₂ is treated either as an inert (n.a.) or self-associating compound (scheme 4C) and qCPA with either three or four parameters. Experimental data from Refs. [66, 67].

The predictions of the CO₂ + ethane VLE using the various modeling approaches is compared to experimental data at four temperatures in figure 8.1. The low temperature azeotrope, observed for this VLE, is predicted very well with qCPA at all temperatures. Particularly when parameter set 1 is employed. Inert CPA fails to predict the phase behavior, clearly indicating the need for an improved model for the phase behavior of CO₂.

These excellent results for qCPA are quite encouraging. Tang and Gross [100] achieved equally good correlations of the CO₂ + ethane VLE using the PCP-SAFT with a similar sized binary interaction parameter ($k_{ij} = 0.038$), as that employed to correlate the mixture with qCPA using three parameters ($k_{ij} = 0.042$). Using a group contribution method with a quadrupole term

for CO₂ NguyenHuynh et al. [108] also presented excellent results for the CO₂ + ethane and CO₂ + propane systems. These results, however, are not directly comparable to the results in this work, as the authors correlated the CO₂ parameters to the CO₂ + propane VLE in addition to the saturated liquid density and vapor pressure. Moreover a non-zero k_{ij} is employed; its value being obtained from another correlation. The predictions and correlations presented by Tsivintzelis et al. [14] for CO₂ + *n*-alkane mixtures with CPA, where CO₂ is treated as either an inert or a self-associating compound, are obviously similar to the CPA results presented in this work for the same approaches, as the pure compound parameters are almost the same.

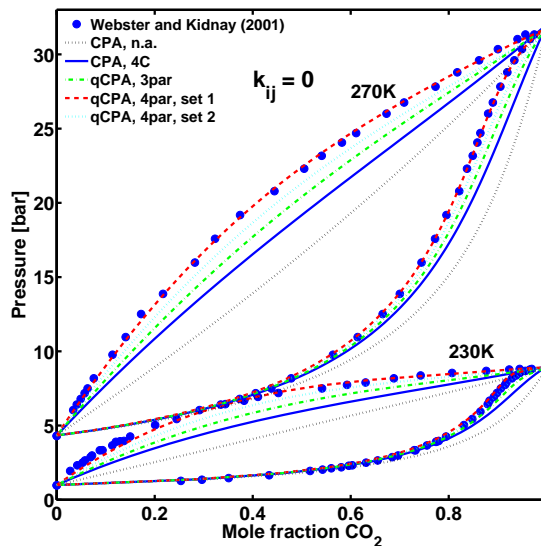


Figure 8.2: Predictions ($k_{ij} = 0$) compared to experimental data for the CO₂ + propane VLE at at 270 K and 230 K using CPA, where CO₂ is treated either as an inert (n.a.) or self-associating compound (scheme 4C), and qCPA with either three or four parameters. Experimental data from Ref. [165].

The CO₂ + propane VLE is shown in figure 8.2 at two temperatures. Not surprisingly qCPA with parameter set 1 results in the best predictions. The two other qCPA parameter sets also perform better than when CO₂ is treated either as an associating or inert compound.

Figures 8.1-8.4 illustrate that the series behavior from C₂-C₁₀ is captured very well with qCPA, and that the predictions with qCPA continues to be excellent, especially for parameter set 1. Unfortunately all models overestimate the critical point (see figure 8.3). As already mentioned this is an unfortunate characteristic of such equations of state. Cross-over approaches exist which may deal with the problem, at the cost of more complex expressions and additional parameters [196, 197].

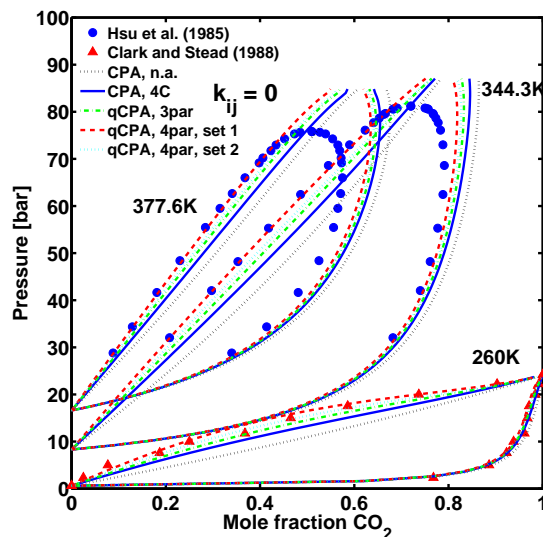


Figure 8.3: Predictions ($k_{ij} = 0$) compared to experimental data for the CO₂ + *n*-butane VLE at three temperatures using CPA, where CO₂ is treated either as an inert (n.a.) or self-associating compound (scheme 4C), and qCPA with either three or four parameters. Experimental data from Refs. [189, 191].

Figure 8.3 shows the CO₂ + *n*-butane VLE prediction. Gross [28] also showed very good results for this system using the PCP-SAFT. Using the same model Tang and Gross [100] presented excellent results for the CO₂ + *n*-pentane VLE. In these cases a k_{ij} of approximately 0.04 was needed to correlate both systems. Using qCPA with parameter set 1, however, the best k_{ij} is approximately zero. A more fair comparison, considering the number of adjustable parameters, may be to compare the optimum k_{ij} for the three parameter version of the qCPA (see table 8.3) with those found for PCP-SAFT. It is comforting to see that the binary interaction parameters are of a similar magnitude despite the different base models, and the fact that the correlation integrals in qCPA are significantly simpler, than the one employed by Gross [28]. Close to the critical point, however, PCP-SAFT seem to perform better.

Generally the qCPA approaches with four parameters appear to yield the best VLE predictions of CO₂ + *n*-alkanes, followed by the three parameter version of qCPA, then CPA where CO₂ is treated as an associating compound, and finally by CPA where CO₂ is treated as an inert. An exception to this trend is the CO₂ + methane system which is shown in figure 8.5. Except in the vicinity of the critical point quite good predictions are obtained when CO₂ is considered an associating species and when qCPA with three adjustable parameters is employed. However, when qCPA is employed with an additional adjustable

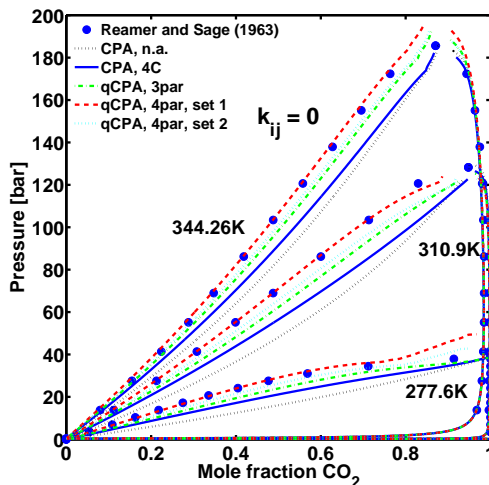


Figure 8.4: Predictions ($k_{ij} = 0$) compared to experimental data for the CO₂ + *n*-decane VLE at three temperatures using CPA, where CO₂ is treated either as an inert (n.a.) or self-associating compound (scheme 4C), and qCPA with either three or four parameters. Experimental data from Ref. [190].

parameter rather poor predictions are obtained. This is in contrast to the results for the whole C₂-C₁₀ series, where the two versions of qCPA with four parameters performed best among all approaches. We suspect that the reason for this may be due to the fact that methane's octopole moment isn't taken into account. In any case, the VLE predictions for the CO₂ + methane system seem to be extremely sensitive to the pure compound CO₂ parameters, which means that even small inaccuracies in the model or the parameters may have a large influence on the results.

8.2.2 LLE of CO₂ + heavy *n*-alkanes

As the LLE between CO₂ and heavy hydrocarbons is believed to be, partly, due to the quadrupole moment of CO₂, a successful quadrupolar term should result in improved LLE predictions or, at least, improve the models ability to correlate the LLEs with a smaller binary interaction parameter. For this reason, the LLE of a number of CO₂ mixtures containing heavy alkanes (C₁₂, C₁₄, C₁₅, C₂₀, C₂₄ and C₃₆) have been predicted and correlated to experimental data using the different modeling approaches. The results in terms of %AADs are presented in table 8.4 ($k_{ij} \neq 0$) and 8.5 ($k_{ij} = 0$).

A characteristic correlation of the phase behavior of the binary CO₂ + C₁₂, C₁₄ and C₁₅ systems are exemplified in figure 8.6a for the CO₂ + *n*-pentadecane

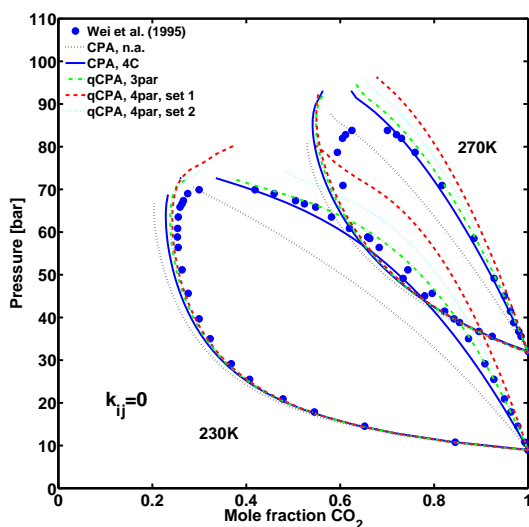


Figure 8.5: Predictions ($k_{ij} = 0$) compared to experimental data for the CO₂ + methane VLE at two temperatures using CPA, where CO₂ is treated either as an inert (n.a.) or self-associating compound (scheme 4C), and qCPA with either three or four parameters. Experimental data from [67].

(C₁₅) LLE. All model approaches can correlate the upper solution temperature LLE of CO₂ and the heavy alkane. A much larger interaction parameter, however, is needed when CO₂ is modeled as an inert or self-associating compound, compared to when CO₂ is modeled as a quadrupolar compound. The correlated interaction parameter and the results, in terms of %AAD, are shown in table 8.4.

As is typically the case for LLE, the phase equilibrium calculations are very sensitive to the binary interaction parameter, and many models does not even predict the presence of a liquid-liquid equilibrium without the use of a binary interaction parameter. As figure 8.6b illustrates, however, the four parameter versions of qCPA can predict ($k_{ij} = 0$) the LLE of this mixture fairly well, especially when parameter set 2 is employed. Recall, however, that this parameter set has been partly based on the CO₂ + *n*-dodecane LLE, and it may not be surprising that the parameter set can predict the LLEs of related mixtures fairly well. The %AAD of the predictions are shown in table 8.5.

Figure 8.7a shows the correlated LLE for the CO₂ + *n*-eicosane (C₂₀) system. The correlations are all fairly similar, except perhaps at the upper critical solution pressure, however there is clearly also some experimental scatter at these conditions. Compared to the results for the CO₂ + C₁₂, C₁₄ or C₁₅ systems, smaller, and even negative, binary interaction parameters are needed for the heavier alkane. Moreover, the shape of the liquid-liquid phase diagram is not

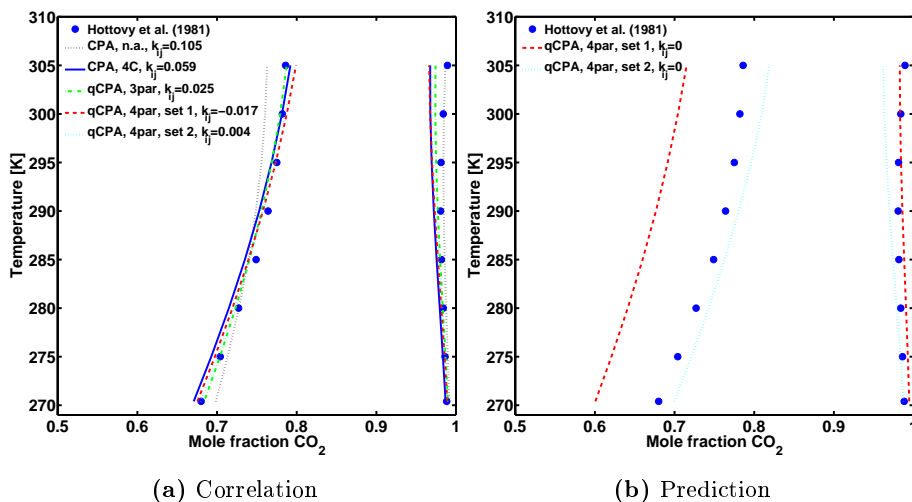


Figure 8.6: Correlations (a) and predictions (b) of the CO₂ + *n*-pentadecane LLE, using CPA, where CO₂ is treated either as an inert (n.a.) or self-associating compound (scheme 4C), and qCPA with either three or four parameters. Experimental data from Ref. [166].

captured quite as well for the CO₂ + C₂₀ mixtures as for the CO₂ + C₁₂, C₁₄ and C₁₅ mixtures. The reason for this may be that the correlation of the binary interaction parameters may give a too high weight to the experimental points near the critical pressure, so that the correct shape of the curve at lower pressures is lost.

Figure 8.7b shows the predictions for the CO₂ + *n*-eicosane system with all five modeling approaches. It can be seen that the four parameter versions of qCPA are capable of predicting the LLE, although the solubility of CO₂ in the heavy alkane is significantly under-predicted with parameter set 1, whereas parameter set 2 results in excellent LLE predictions. The remaining modeling approaches cannot predict the LLE in the whole pressure range, although qCPA with just three parameters results in fairly good predictions at low pressures. As shown in figure 8.7a, a k_{ij} can be employed to better match the phase behavior at higher pressures.

For mixtures of CO₂ + *n*-tetracosane (C₂₄) and CO₂ + *n*-hexatriacontane (C₃₆) meaningful predictions with the three parameter version of qCPA are possible. Deviations for these qCPA predictions are also shown in table 8.5. In fact, increasingly better predictions are obtained with the three parameter version of qCPA as the length of the alkane increases. The LLE of the CO₂ + *n*-Hexatriacontane is, for instance, predicted most accurately with the three parameter version of qCPA (see figure 8.8a).

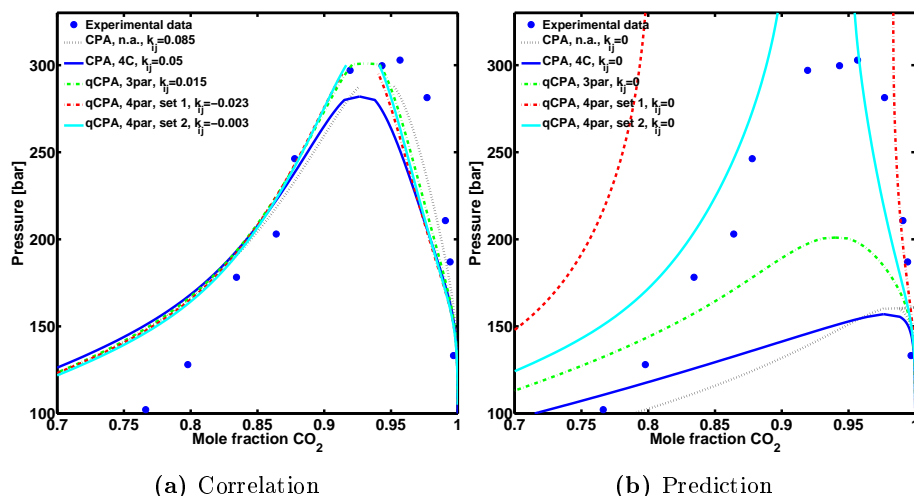


Figure 8.7: Correlations (a) and predictions (b) of the CO₂ + *n*-eicosane LLE at 348 K, using CPA where CO₂ is treated either as an inert (n.a.) or self-associating compound (scheme 4C) and qCPA with either three or four parameters. Experimental data from Ref. [198].

Satisfactory correlations, in terms of %AAD, are generally obtained with all modeling approaches (see table 8.4). There is a tendency for CPA to model the phase behavior of the hydrocarbon rich phase somewhat less accurately when CO₂ is modeled as an inert, rather than a self-associating or quadrupolar species, resulting in slightly higher deviations. This can for instance be observed visually in figure 8.6a. On the other hand, with the exception of the CO₂ + *n*-dodecane LLE the CO₂ rich phase is correlated most accurately when CO₂ is assumed to be inert. Whereas the other approaches tend to over-estimate the solubility of the hydrocarbon in CO₂.

It can be seen from table 8.5 that the CO₂ rich phase is often predicted more accurately with qCPA before a binary interaction parameter is employed to correlate the phase equilibrium data. The hydrocarbon rich phase is not predicted quite as well. To correlate the hydrocarbon rich phase better the k_{ij} is adjusted, which, unfortunately, also results in an increased solubility of hydrocarbon in the CO₂-rich phase. When CO₂ is treated as an inert compound neither phase is predicted very well without a binary interaction parameter, but the binary interaction parameter may improve the correlation of both phases.

This is illustrated in figure 8.8 which shows the predicted and correlated LLE for the CO₂ + *n*-Hexatriacontane system. The figure shows both the whole LLE and a close-up on the CO₂-rich liquid phase. qCPA with four parameters (set 1) predicts the CO₂ rich phase very well, but is somewhat off in regards to the hydrocarbon rich phase (figures 8.8a-8.8b). CPA without association does not model any of the two phases very well. When a binary interaction parameter

is used to correlate the LLE, the hydrocarbon rich phase is accurately correlated with qCPA, but the representation of the CO₂ rich phase is compromised. CPA without association is now the best model for the correlated liquid liquid equilibrium (although a large k_{ij} is needed). Additionally the figure shows that qCPA with three parameters predicts the solubility of CO₂ in the hydrocarbon rich liquid phase very well.

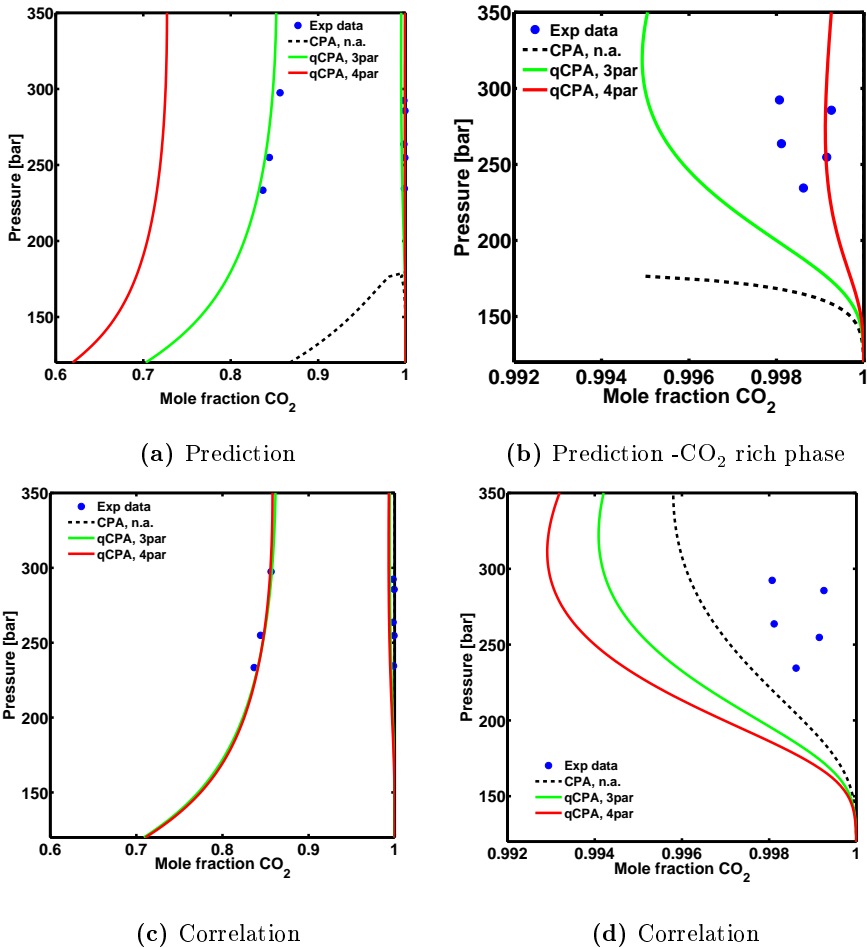


Figure 8.8: Predictions and correlations of the CO₂ + *n*-Hexatriacontane LLE at 349 K. CO₂ is modeled with inert CPA and qCPA with three and four parameters. Only parameter set 1 is shown in the figure for qCPA. The predicted LLE is shown in (a) and (b), (a) shows the whole LLE region and (b) is a close-up of predictions for the CO₂ rich phase. (c) and (d) correspond to the correlated versions of (a) and (b).

Table 8.4: Correlated binary interaction parameters and calculated %AADs for the CO₂ + heavy *n*-alkane LLE systems using the CPA and qCPA. Compared to experimental data from Refs. [166, 198].

System	P range [bar]	T range [K]	Approach	k_{ij}	%AAD	
					HC phase	CO ₂ phase
CO ₂ (1) + <i>n</i> -dodecane(2)	20-29	254-267	CPA n.a.	0.102	4.4	3.3
			CPA 4C	0.054	2.9	1.6
			qCPA, 3par	0.019	3.5	2.6
			qCPA, 4par, set 1	-0.025	3.0	2.2
			qCPA, 4par, set 2	-0.003	3.2	2.4
CO ₂ (1) + <i>n</i> -tetradecane(2)	31-83	269-310	CPA n.a.	0.100	3.2	0.6
			CPA 4C	0.058	3.4	1.1
			qCPA, 3par	0.023	2.1	0.7
			qCPA, 4par, set 1	-0.017	3.4	1.0
			qCPA, 4par, set 2	0.003	2.6	1.0
CO ₂ (1) + <i>n</i> -pentadecane(2)	32-80	270-305	CPA n.a.	0.105	1.9	0.3
			CPA 4C	0.059	1.2	0.9
			qCPA, 3par	0.025	0.5	0.6
			qCPA, 4par, set 1	-0.017	0.9	0.8
			qCPA, 4par, set 2	0.004	0.7	0.7
CO ₂ (1) + <i>n</i> -eicosane(2)	100-300	348	CPA n.a.	0.085	3.8	0.8
			CPA 4C	0.050	4.2	1.7
			qCPA, 3par	0.015	3.8	1.2
			qCPA, 4par, set 1	-0.023	3.7	1.5
			qCPA, 4par, set 2	-0.003	3.5	1.4
CO ₂ (1) + <i>n</i> -tetracosane(2)	172-277	348	CPA n.a.	0.073	1.1	0.7
			CPA 4C	0.033	1.3	1.5
			qCPA, 3par	-0.002	1.1	1.2
			qCPA, 4par, set 1	-0.040	1.4	1.3
			qCPA, 4par, set 2	-0.020	1.0	1.3
CO ₂ (1) + <i>n</i> -hexatriacontane(2)	233-297	349	CPA n.a.	0.070	2.0	0.2
			CPA 4C	0.030	0.4	0.6
			qCPA, 3par	-0.003	0.4	0.4
			qCPA, 4par, set 1	-0.043	0.4	0.5
			qCPA, 4par, set 2	-0.021	0.2	0.4

Table 8.5: %AADs for the predicted ($k_{ij} = 0$) LLEs of CO₂ + heavy *n*-alkane systems using the four parameter version of qCPA. The three parameter version of qCPA is used when possible. Compared to experimental data from Refs. [166, 198].

System	P [bar]	T [K]	Approach	%AAD	
				HC phase	CO ₂ phase
				$k_{ij} = 0$	
CO ₂ (1) + <i>n</i> -dodecane(2)	20-29	254-267	qCPA, set 1	19.2	3.9
			qCPA, set 2	4.5	2.9
CO ₂ (1) + <i>n</i> -tetradecane(2)	31-83	269-310	qCPA, set 1	14.9	0.9
			qCPA, set 2	1.5	0.6
CO ₂ (1) + <i>n</i> -pentadecane(2)	32-80	270-305	qCPA, set 1	11.1	0.5
			qCPA, set 2	2.7	1.1
CO ₂ (1) + <i>n</i> -eicosane(2)	100-300	348	qCPA, set 1	15.1	6.0
			qCPA, set 2	6.9	3.2
CO ₂ (1) + <i>n</i> -tetracosane(2)	172-277	348	qCPA, 3 par	1.8	1.0
			qCPA, set 1	16.7	0.1
			qCPA, set 2	9.2	0.3
CO ₂ (1) + <i>n</i> -hexatriacontane(2)	233-297	349	qCPA, 3 par	0.7	0.3
			qCPA, set 1	14.8	0.1
			qCPA, set 2	8.0	0.1

8.2.3 Correlations for the binary interaction parameter

Sections 8.2.1-8.2.2 show that while it is possible to greatly improve the predicted phase behavior of the CO₂ + *n*-alkane mixtures by taking the quadrupole moment of CO₂ into account, all modeling approaches need a non-zero binary interaction parameter to accurately model both VLE and LLE for CO₂ + *n*-alkane series. A temperature independent interaction parameter is sufficient in all cases.

It is often convenient to have generalized correlations for the binary interaction parameter between a specific compound such as CO₂, H₂S or water and a compound series such as hydrocarbons. For CO₂ + *n*-alkane mixtures, for instance, it is well-known that the k_{ij} decreases with the carbon number (or molecular weight) of the *n*-alkane when SRK is employed [8]. It can be seen from tables 8.3 and 8.4 that the k_{ij} also seems to decrease for most modeling approaches from ethane towards heavier *n*-alkanes. In figure 8.9 the interaction parameters of the binary CO₂ + *n*-alkane pairs are plotted as a function of the molecular weight of the *n*-alkane (from C₂-C₃₆). The vertical dashed line indicates the transition from VLE data (left-hand side) to LLE data (right-hand side). The figure shows the trend in k_{ij} for qCPA with three parameters and for CPA without association. It is clear that there is a tendency for the interaction parameter to decrease as a function of the molecular weight (or carbon number) of the *n*-alkane.

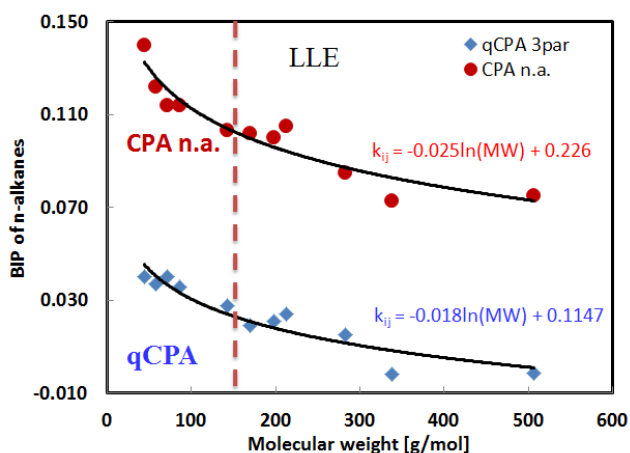


Figure 8.9: Binary interaction parameters with qCPA (using 3 parameters) and CPA without association for CO₂ + *n*-alkane mixtures, as a function of the molecular weight of the *n*-alkane. Points are the correlated values for each subsystem and lines are correlations to the series behavior. The vertical dashed line indicates the transition from VLE to LLE.

Frost [199] recently showed that the binary interaction parameters for the water + hydrocarbon series seem to follow a logarithmically decreasing function of the molecular weight of the hydrocarbon, rather than the linear correlation previously assumed. In this regard it is interesting that although the interaction parameters for the CO₂ + *n*-alkane systems are somewhat scattered, they do appear to decrease as a function of the natural logarithm to the molecular weight. The correlated functions are:

$$\text{qCPA (3 par): } k_{ij} = -0.018 \ln(MW) + 0.115 \quad (8.1)$$

$$\text{CPA n.a.: } k_{ij} = -0.025 \ln(MW) + 0.226 \quad (8.2)$$

It is obvious from the correlation that the interaction parameters for qCPA decrease somewhat slower than those for CPA. The value of the k_{ij} for large *n*-alkanes is close to zero with qCPA. The correlations can be employed either as a good initial guess for correlating the binary interaction parameter of a binary CO₂ + *n*-alkane mixture with qCPA or inert CPA or directly as the k_{ij} , if no binary data is available for the system. When the correlations are employed, however, it should be considered that the experimental data for the heavier *n*-alkanes may be quite uncertain, and even small changes in the interaction parameters for the heavier *n*-alkanes, could mean that a linear correlation is preferable to the proposed logarithmic correlation.

It is no coincidence that figure 8.9 only plots the binary interaction parameters, for the two approaches which employ three adjustable parameters. For the remaining approaches the trends are less clear; for one of the two qCPA approaches with four adjustable parameters, for instance, the binary interaction parameter is essentially zero for all VLE systems, but non-zero for LLE systems.

To illustrate the use of equations (8.1)-(8.2), figure 8.10 shows the VLE and LLE of the mixtures CO₂ + propane and CO₂ + hexatriacontane (C₃₆) respectively, where the correlations have been employed. The correlations gives quite satisfactory results for both models. As is typically the case, the LLE (figure 8.10b) is more sensitive to the k_{ij} and the results with both qCPA and CPA, where CO₂ is treated as an inert, are not quite as good as with an individually fitted k_{ij} , whereas results for the VLE is similar to the individual correlation.

In this work we typically employ the independently correlated k_{ij} 's for each subsystem, rather than the developed correlations.

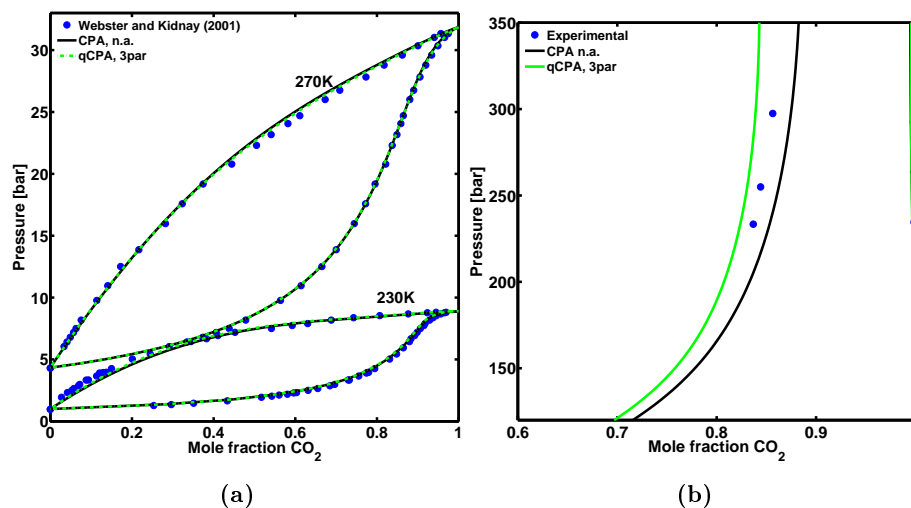


Figure 8.10: VLE of (a) CO₂ + propane and LLE of (b) CO₂ + C₃₆ where the correlations in (8.1)-(8.2) have been employed for qCPA with three parameters and inert CPA. Experimental data from Refs. [165, 198]

8.3 CO₂ + Self-associating Compounds

When mixtures containing CO₂ and a self-associating compound, such as alcohols and water, are considered it raises the important question of whether CO₂ should be modeled only as a quadrupolar molecule or as a quadrupolar *and* a solvating molecule (i.e. a molecule with either electron donor or electron acceptor sites). As discussed in chapter 3 several studies indicate that Lewis acid-Lewis base type interactions play a role for mixtures of CO₂ and associating compounds such as water and alcohols [14, 68–71]. As an engineering approach the Lewis acid-Lewis base interaction can be viewed as an induced cross-association (solvation). This kind of cross-association, where one component self-associates but the other only has electron donor or electron acceptor sites, is difficult to treat since the association parameters, $\varepsilon^{A_i B_i}$ and $\beta^{A_i B_i}$, are available only for the self-associating compound. As a pragmatic solution the cross-association volume, $\beta^{A_i B_j}$ (or β_{crs}), is often fitted to experimental data together with the binary interaction parameter, while the association energy, $\varepsilon^{A_i B_i}$, of the solvating compound is set to zero. The success of this approach, however, may be, at least partially, attributed to a higher model flexibility due to the extra parameter.

A simple alternative to correlating the cross-association volume, $\beta^{A_i B_j}$, for solvating mixtures was proposed by Kleiner and Sadowski [60]. The method assumes that the cross-association volume can be set equal to the association volume of the self-associating compound. In this way equations (3.14)-(3.15) can be directly employed without the need for any adjustable parameters be-

yond a k_{ij} . To reduce the number of binary adjustable parameters this approach is employed for qCPA, when mixtures of CO₂ and associating compounds are considered. Clearly improved correlations can be obtained if both the binary interaction parameter and the cross-association volume are fitted to the experimental data. The increased model flexibility of such an approach would, however, result in a multi-plum of possible solutions making it difficult to critically compare the models.

Another important question is how many solvation sites CO₂ has. Indeed in a recent work NguyenHuynh et al. [111], illustrated, using the GC-PPC-SAFT, that very good results could be obtained for mixtures of CO₂ and alcohols if CO₂ was assumed to have two cross sites. Similarly Figure 8.11 illustrate the predictions ($k_{ij} = 0$) with qCPA for the CO₂ + ethanol mixture and the VLLE of the CO₂-rich phase of the CO₂ + water mixture using zero, one, or two cross-association sites. The cross-association parameters were determined using the approach by Kleiner and Sadowski [60]. When cross-association is not taken into account, or only one cross-association site is considered, the equilibrium pressure in figure 8.11a is significantly overestimated and false liquid-liquid phase splits are predicted. When two cross-association sites are assumed the equilibrium pressure is barely overestimated.¹ Similarly the minimum in the water solubility in the CO₂-rich phase is captured quite accurately when two cross-association sites are assumed, but not when CO₂ has one or zero sites (see figure 8.11b). Therefore, when qCPA is employed CO₂ is assumed to have two solvation sites, and the cross-association parameters are found using the approach suggested by Kleiner and Sadowski [60].

In the case where we consider CO₂ to be a self-associating compound the cross-association between CO₂ and the associating compound is handled by directly applying the CR-1 mixing rule (see eq. (3.14)-(3.15)).

8.3.1 CO₂ + alcohols

In this section we present the calculation of VLE and VLLE for selected CO₂ + alcohol mixtures using the different CPA-based models. CO₂ is assume to have two cross-association sites, and the approach of Kleiner and Sadowski [60] is employed to determine the cross-association volume of CO₂ when qCPA is employed.

In general qCPA performs quite well for many of the alcohol systems, even with no binary interaction parameter, but a non-zero temperature independent interaction parameter is used to better represent the phase equilibria. The results are summarized in terms of %AADs in table 8.6. Characteristic correlations of

¹Note that the minimum and maximum observed in figure 8.11a when CO₂ is treated as having two cross-association sites suggests phase instability and a false liquid-liquid split, as small k_{ij} solves this problem.

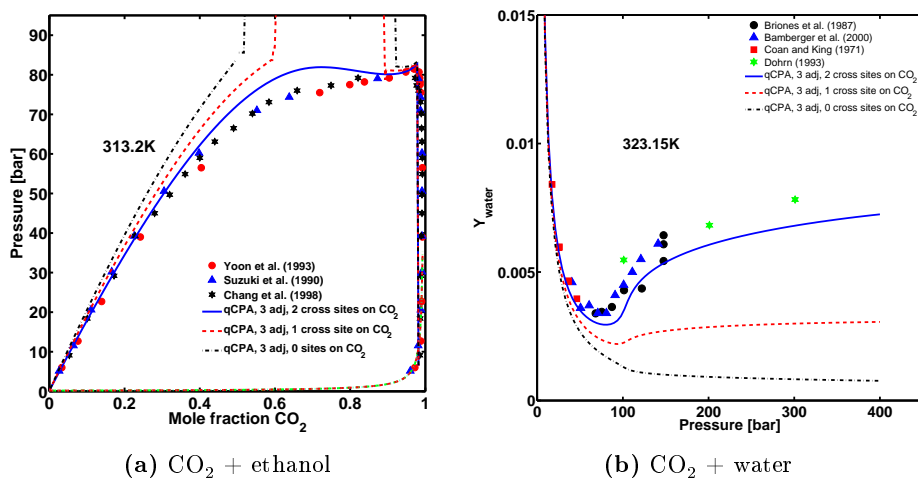


Figure 8.11: Predicted ($k_{ij} = 0$) VLEs of the CO₂ + ethanol system (a) and the CO₂-rich vapor phase of the CO₂ + water system (b) using qCPA with three parameters and assuming zero, one or two solvation sites. It is assumed for both systems that $\beta_{crs} = \beta_{assoc}$. Experimental data from Refs. [75, 200–205].

the VLE between CO₂ + methanol are shown in figure 8.12 at three temperatures. Despite a very large binary interaction parameter the highest deviations are obtained when CO₂ is considered a self-associating molecule following the 4C association scheme. It appears that this approach is not capable of describing the shape of the liquid phase, at least not when the CR-1 combing rule is employed. This is particularly pronounced for the CO₂ + methanol system at higher temperatures (figure 8.12). This is in good agreement with Tsvintzelis et al. [14], who found that poor results are obtained for mixtures of CO₂ and self-associating compounds, when the CR-1 and a single binary parameter is employed. The model which captures the trend of the VLEs most accurately is clearly qCPA. The correlations with the different qCPA parameter sets for CO₂ are similar, although a smaller interaction parameter (in absolute terms) is needed when qCPA with three adjustable parameters is employed. In all cases a small negative interaction parameter is employed, whereas a positive interaction parameter is used when CO₂ is considered either self-associating or inert. Surprisingly good correlations, with a small interaction parameter, are obtained when CO₂ is treated as an inert. The model, however, does not capture the trend of the experimental data quite as well as qCPA, especially at higher temperatures where the pressure is overestimated and a false liquid-liquid split may occur.

Figure 8.13 illustrates that the phase behavior description of the simultaneous VLE and LLE of the CO₂ + nonanol system is satisfactory with all models

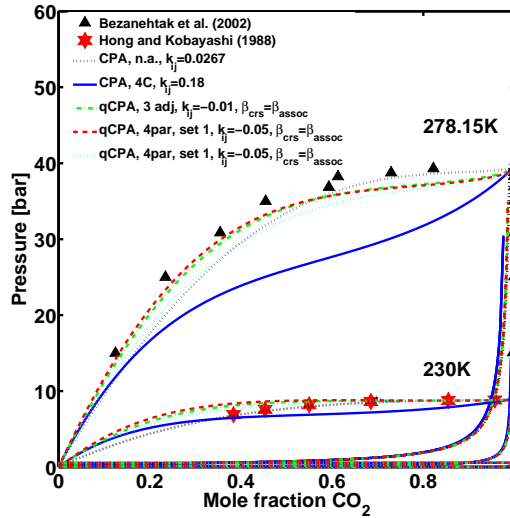


Figure 8.12: Correlation of the CO₂ + methanol VLE, using CPA where CO₂ is treated either as an inert (n.a.) or self-associating compound (scheme 4C) and qCPA with either three or four parameters. Correlated to experimental data from Refs. [206, 207].

using a temperature independent interaction parameter. The same is the case for the CO₂ + octanol system. Note that when qCPA with three parameters is employed for the CO₂ + octanol system the optimum k_{ij} is found to be zero, i.e. the model is predictive for this system. It is noteworthy, that as the chain length of the alcohols increases the binary interaction parameter tend to decrease when CO₂ is treated as a self-associating compound and increase when CO₂ is treated as an inert compound. When CO₂ is treated as a quadrupolar compound, however, the small interaction parameter seem to be almost constant for the various systems.

8.3.2 CO₂ + water

The capabilities of association theories for modeling the important CO₂ + water mixture has been extensively studied in recent literature using both CPA [14, 21, 79, 208] (see chapter 3) and SAFT-based models [21, 79, 209–211]. As discussed in chapter 4 the mixture has also been studied, with mixed success, using some of the multipolar SAFT-based equations of state [100, 103, 104, 110].

Tang and Gross [100] presented correlations at several temperatures for CO₂ + water using the PCP-SAFT with a temperature dependent k_{ij} . No devia-

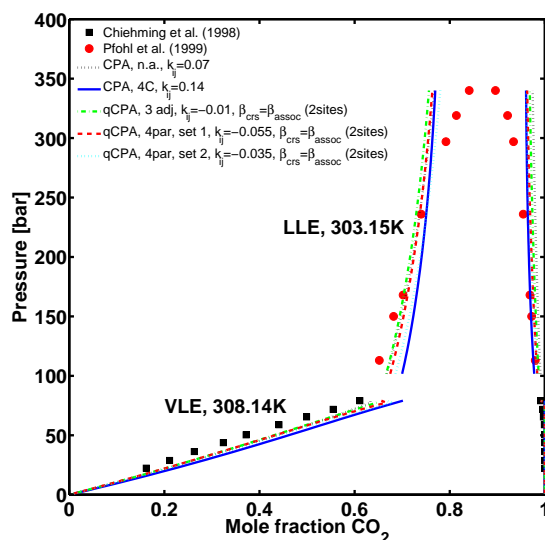


Figure 8.13: Correlation of the CO₂ + nonanol VLE and LLE using CPA where CO₂ is treated either as an inert or self-associating compound, or qCPA with three or four adjustable parameters. Experimental data from Refs. [73, 202].

tions were reported, but it can be seen from their figures that there are significant deviations in the CO₂-rich vapor phase. Diamantonis and Economou [104] recently investigated the performance of various SAFT and tPC-PSAFT approaches for modeling the CO₂ + water system. The best results were obtained with PC-SAFT when solvation was assumed between CO₂ and water. Solvation between CO₂ and water, however, was not considered in either works when CO₂ is treated as a quadrupolar compound. On the other hand assuming solvation between CO₂ and water and using the tPC-PSAFT, Karakatsani et al. [103] obtained excellent results for the CO₂ + water system. In a recent investigation NguyenHuynh et al. [110] modeled CO₂ + water with the pGC-PC-SAFT. The authors treated CO₂ as a quadrupolar molecule and water as a dipolar molecule, moreover CO₂ was assumed to cross-associate with water (two sites). The cross-association volume was assumed equal to that found for H₂S, however the cross-association energy was fitted. This approach yielded qualitatively correct results for the CO₂ + water system

It is clear from most investigations that the best results for CO₂ + water are almost always obtained when CO₂ is considered to be a solvating molecule. This may be due to the strong Lewis acid-Lewis base interactions between CO₂ and water, which may be modeled as an induced solvation. However, the improved correlations may also, partly, be attributed to the additional adjustable parameter which is introduced (the cross-association volume).

Table 8.6: CPA and qCPA deviations and k_{ij} for CO₂ + alcohol VLE and LLE mixtures. Compared to experimental data from Refs. [200–202, 206, 207, 212, 213].

System	T range (K)	Modeling approach	k_{ij}	% AAD in P	% AAD in y_1	%AAD in x_1
CO ₂ (1) + methanol(2)	230-313.2	CPA, n.a.	0.027	7.9	0.4	10.5
		CPA, 4C	0.180	18.7	0.5	48.6
		qCPA, 3par	-0.010	4.7	0.2	8.9
		qCPA, 4par, set 1	-0.050	5.6	0.2	9.7
		qCPA, 4par, set2	-0.050	5.6	0.2	10.1
CO ₂ (1) + ethanol(2)	291.15-313.2	CPA, n.a.	0.050	9.4	0.4	10.1
		CPA, 4C	0.200	6.1	0.2	7.2
		qCPA, 3par	-0.019	3.9	0.4	8.3
		qCPA, 4par, set 1	-0.057	2.7	0.3	6.5
		qCPA, 4par, set2	-0.030	2.9	0.3	6.5
CO ₂ (1) + propanol(2)	313.4	CPA, n.a.	0.058	10.7	0.2	7.4
		CPA, 4C	0.180	6.7	0.1	11.0
		qCPA, 3par	-0.020	4.1	0.2	5.1
		qCPA, 4par, set 1	-0.050	3.4	0.2	3.2
		qCPA, 4par, set2	-0.030	3.0	0.2	3.1
CO ₂ (1) + octanol(2) ^a	308.2-328.2	CPA, n.a.	0.070	12.9	0.4	10.8
		CPA, 4C	0.160	14.8	0.3	10.3
		qCPA, 3par	0.000	11.0	0.3	7.4
		qCPA, 4par, set 1	-0.040	10.4	0.3	6.6
		qCPA, 4par, set2	-0.020	10.8	0.3	7.7
CO ₂ (1) + nonanol(2) ^a	308.1-328.2	CPA, n.a.	0.070	19.6	0.8	9.1
		CPA, 4C	0.140	23.5	0.5	13.7
		qCPA, 3par	0.000	18.5	0.8	6.4
		qCPA, 4par, set 1	-0.045	17.1	0.7	6.4
		qCPA, 4par, set2	-0.025	18.1	0.7	7.6

^a Deviations based on both VLE and LLE data.

As stated previously we assume that CO₂ cross-associates with two solvation sites and that $\beta^{A_i B_j} = \beta_{cross} = \beta_{water}$. Figure 8.14 illustrates the correlation of the CO₂-rich vapor phase and the water-rich liquid phase at 323.15K, using a single k_{ij} . All models correlate the solubility of CO₂ in the water-rich phase quite well (figure 8.14a), although a large interaction parameter is needed when CO₂ is assumed to be a self-associating compound. However, as also demonstrated by Tsivintzelis et al. [14], CPA cannot describe the minimum in the solubility of water in the vapor phase, since the transition to a liquid phase is not captured when CO₂ is modeled as an inert compound, nor is the trend of the experimental data captured if CO₂ is modeled as a self-associating compound (see figure 8.14b). In this case the increased water solubility due to the phase transition is vastly over-estimated. When CO₂ is treated as a quadrupolar compound which cross-associates with water the minimum in the solubility of the CO₂ phase is, at least qualitatively, captured.

Better correlations may be obtained for both qCPA and CPA (where CO₂ is treated as associating) if the cross-association volume is fitted, however, the purpose of this exercise was to reduce the number of adjustable parameters, rather than to make a perfect fit.

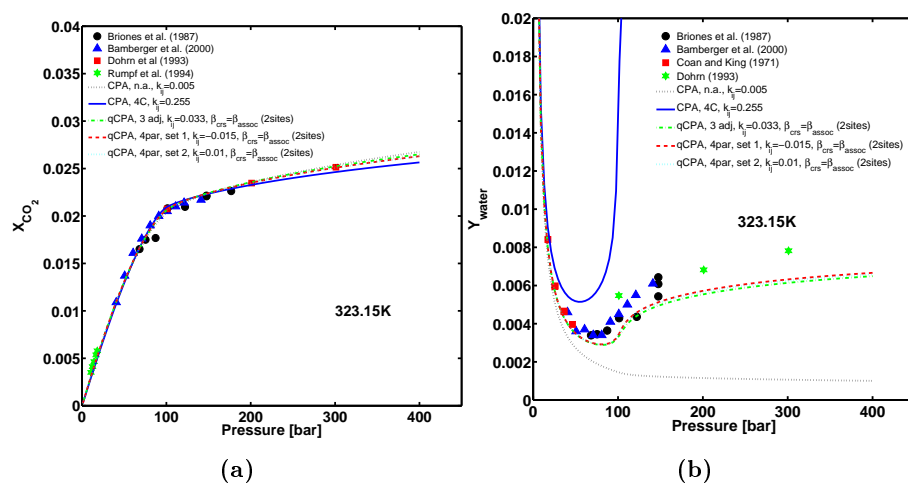


Figure 8.14: Correlation of the CO₂ solubility in the water rich liquid phase (a) and the water solubility in the CO₂ rich vapor phase (b) for the CO₂ + water system. CPA, where CO₂ is treated either as an inert or an associating compound, or qCPA with three or four adjustable parameters is employed. Experimental data from Refs. [75, 203–205, 214].

Instead of treating CO₂ as a purely inert compound with CPA a more fair model comparison may be to also assume CO₂ to cross-associate. To keep the number of adjustables low the same assumptions as we made for qCPA are employed. Figure 8.15 compares the model correlations in the CO₂-rich vapor phase using either CPA or qCPA with three adjustable parameters where CO₂ is assumed

to solvate with water in both cases. It can be seen from the figure that if CO₂ is assumed to be solvating, then the minimum in the water solubility is captured equally well in CPA and qCPA. This suggests that taking cross-association between CO₂ and water into account is in fact the dominant factor, when it comes to modeling the CO₂ + water system. However, when the quadrupolar nature of CO₂ is not explicitly taken into account a relatively high k_{ij} is needed. Table 8.7 summarizes the results in terms of %AAD both with and without an interaction parameter.

Table 8.7: Deviations for CPA and qCPA predictions ($k_{ij} = 0$) and correlations ($k_{ij} \neq 0$) for the CO₂(1) + water(2) mixture at 323.15 K (both VLE and LLE data). Including the correlated k_{ij} . Compared to experimental data from references [75, 203–205, 214].

Modeling approach	% AAD in y_2	%AAD in x_1	k_{ij}	% AAD in y_2	%AAD in x_1
$k_{ij}=0$					
CPA, n.a.	62.5	4.6	0.005	62.9	3.6
CPA with solvation	10.3	>100	0.128	21.5	4.2
CPA, 4C	>100	>100	0.255	>100	4.5
qCPA, 3par	13.7	25.9	0.033	17.1	3.7
qCPA, 4par, set 1	17.0	11.5	-0.015	15.5	3.6
qCPA, 4par, set2	14.7	7.5	0.010	15.8	3.5

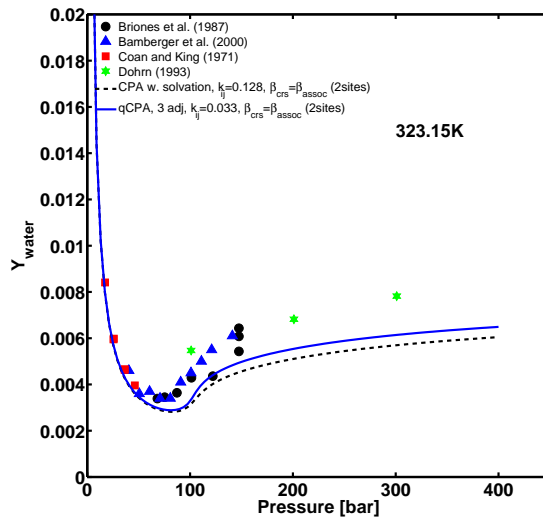


Figure 8.15: Correlation of the water solubility in the CO₂ rich vapor phase for the CO₂ + water system. Comparing the performance of CPA with solvation, and qCPA with solvation. Experimental data from [75, 203–205].

8.3.2.1 On the temperature dependence of the k_{ij}

It is typically necessary to use a temperature dependent k_{ij} to correlate the experimentally observed phase equilibria for the CO₂ + water mixture over an extended temperature range. Tsivintzelis et al. [14] presented temperature dependent binary interaction parameters for several CPA approaches, . The authors suggest a linear temperature dependence (i.e. $c_{kij} = 0$ in Eq. (3.8)). It was found, however, that an inverse temperature proportionality (i.e. $b_{kij} = 0$ in Eq. (3.8)) provided more consistent results, and this temperature dependence is used in the following.

The temperature dependent binary interaction parameter for qCPA was correlated to experimental data in the temperature range 278 – 473 K. The resulting temperature dependent binary interaction parameters were found to be:

$$\text{qCPA 3 par: } k_{\text{CO}_2\text{-H}_2\text{O}}(T) = 0.41 - 124.0/T \quad (8.3)$$

$$\text{qCPA 4 par, s1: } k_{\text{CO}_2\text{-H}_2\text{O}}(T) = 0.39 - 132.7/T \quad (8.4)$$

$$\text{qCPA 4 par, s2: } k_{\text{CO}_2\text{-H}_2\text{O}}(T) = 0.41 - 129.6/T \quad (8.5)$$

Figure 8.16 illustrates the performance of qCPA with three parameters for modeling the phase equilibria of the CO₂ + water mixture at three different temperatures. The temperature dependent binary interaction parameter in Eq. (8.3) was employed. Excellent agreement between the temperature dependent correlations and the experimental data is obtained.

It is apparent from Eqs. (8.3)-(8.5) that the k_{ij} for the various qCPA approaches are highly temperature dependent. A similar temperature dependence is found for CPA when CO₂ is assumed to be self-associating and the CR-1 rule is employed:

$$\text{CPA 4C : } k_{\text{CO}_2\text{-H}_2\text{O}}(T) = 0.71 - 149.3/T \quad (8.6)$$

It is interesting, however, that if the experimental value for the cross-association energy is employed the k_{ij} becomes significantly less temperature dependent. For CPA with the 4C scheme the temperature dependence becomes $k_{\text{CO}_2\text{-H}_2\text{O}} = 0.11 - 24.8/T$. The weaker temperature dependence is probably due to the balance between $\beta^{A_i B_j}$ and $\varepsilon^{A_i B_j}$ in Eq. (3.11). When the experimental value of the association energy is employed, the cross-association volume is almost an order of magnitude smaller, and the cross-association energy about one third larger, than when the CR-1 rule is employed.

8.4 CO₂ + Quadrupolar Compounds

CO₂ has so far been the only quadrupolar compound explicitly considered with qCPA in this thesis. Although both water and ethane have quadrupolar moments, these have been ignored in this work, as previously described. It is

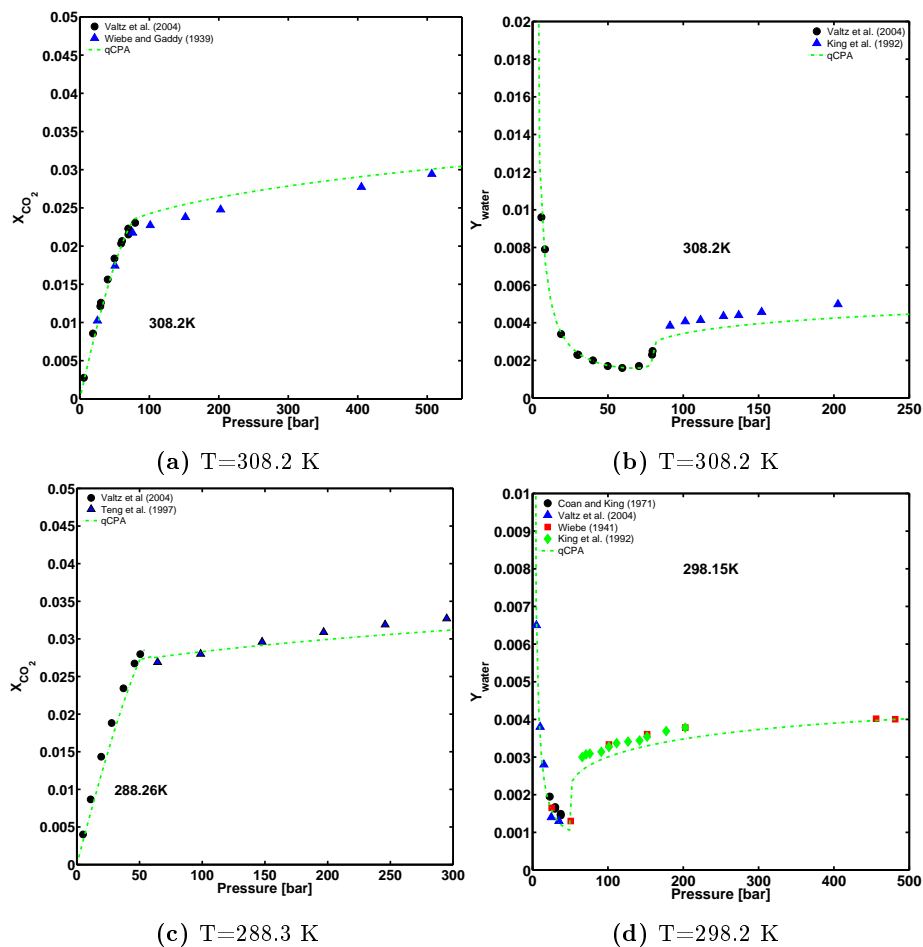


Figure 8.16: Correlated phase equilibria of the binary CO₂ + water mixture at three different temperatures using the three parameter version of qCPA with the temperature dependent k_{ij} shown in Eq. (8.3). (a) Solubility of CO₂ in the water rich liquid phase at 308.2 K. (b) Water solubility in the CO₂-rich vapor and liquid phase. (c) As (a) but at 288.3 K. (d) As (b) but at 298.2 K. Experimental data from Refs. [75–78, 82, 215].

important, however, to evaluate the capabilities of the new model for mixtures of two or more quadrupolar compounds. More specifically such an evaluation may provide an indication as to the adequacy of the proposed cross-quadrupolar interactions, as well the proper magnitude of the quadrupolar term itself. To investigate this qCPA is employed to calculate the phase equilibria of mixtures containing CO₂ and either benzene, toluene, acetylene, or nitrogen.

8.4.1 CO₂ + benzene

When benzene is modeled as a quadrupolar compound, a fixed experimental quadrupole moment of $-9 \text{ D}\text{\AA}$ is employed and the three adjustable pure compound parameters are re-estimated. See table 8.2 for the re-estimated qCPA benzene parameters. In this case no attempt is made to improve the parametrization by fitting the quadrupolar co-volume or quadrupolar moment, as was done for CO₂. The predicted VLE of benzene and CO₂ is compared to experimental values in figure 8.17. All model approaches, except when both CO₂ and benzene are treated as inert compounds, gives similar quite accurate predictions. Interestingly CPA performs very well when CO₂ is assumed to be associating. The results in terms of %AAD are presented in table 8.8. Gross [28] modeled this system using the PCP-SAFT and regular PC-SAFT, however, the results with the former model were worse than with PC-SAFT. To improve the results, Gross had to set the cross-quadrupolar interactions to zero. While such modifications were not necessary in this work, the results are quite sensitive to the value of the quadrupolar moment, and use of a slightly different quadrupolar moment for benzene might alter the conclusions. The experimental values are typically between $-9.98 \text{ D}\text{\AA}$ and $-8.5 \text{ D}\text{\AA}$.

Table 8.8: Deviations from experimental data for CPA and qCPA predictions ($k_{ij} = 0$) and correlations ($k_{ij} \neq 0$) for the CO₂ + benzene mixture in the temperature range 298.2-347.3 K. Including the correlated k_{ij} . Compared to experimental data from Refs. [212, 216].

Modeling approach	% AAD in P	%AAD in x_1	k_{ij}	% AAD in P	%AAD in x_1
	$k_{ij}=0$				
CPA, n.a.	26.8	23.9	0.068	14.3	6.2
CPA, 4C	15.8	9.5	0.020	12.0	3.9
qCPA, 3par	17.8	13.3	0.008	10.5	3.4
qCPA, 4par, set 1	11.9	5.7	-0.038	12.0	3.8
qCPA, 4par, set2	15.8	10.9	-0.014	12.0	3.8

8.4.2 CO₂ + methylbenzene (toluene)

Due to a lack of symmetry the quadrupole moment tensor for toluene and other alkyl benzenes does not reduce to a scalar value and the quadrupole moments cannot readily be used in Eqs. (5.4)-(5.6). As previously discussed, Gubbins

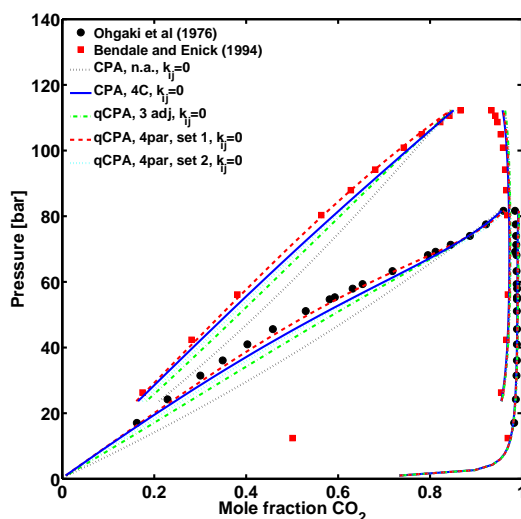


Figure 8.17: Prediction of the CO₂ + benzene VLE at two temperatures (upper: 315.45 K and lower: 347.25 K) using CPA, where CO₂ is treated either as an inert (n.a.) or self-associating compound (scheme 4C), and qCPA with either three or four parameters. Experimental data from Refs. [212, 216].

et al. [85] suggested an approximation, which allows for the use of an 'effective' scalar quadrupole moment.

To the best of the authors knowledge there are no direct experimental data for the quadrupole moment, or effective quadrupole moment, of toluene, although values close to that of benzene might be expected. Reynolds et al. [188] calculated an effective scalar (and absolute) quadrupole moment of toluene of 7.92 DÅ. Such calculations should be treated with care, however, as significant differences are often seen when calculated and experimental values are compared. Reynolds et al. for instance calculated the (absolute) quadrupole moment of CO₂ to be 5.46 DÅ, whereas the experimental values is around -4.3 DÅ. In this section the 'effective' quadrupole moment is first assumed to be -7.92 DÅ (same sign as the quadrupole moment of benzene). See table 8.2 for the re-estimated pure compound parameters of toluene.

Figure 8.18 show the predicted VLE of the CO₂ + toluene mixture at two temperatures. The predictions for the case where CO₂ is modeled as a self-associating compound and toluene is assumed to be inert, are essentially identical to the prediction with qCPA where both CO₂ and toluene are modeled as quadrupolar fluids. Both approaches, improve the predictions compared to the case where both CO₂ and toluene are inert compounds. For qCPA a $k_{ij} = 0.03$ accurately correlates the VLE. A similar sized k_{ij} was employed by Gross [28] to correlate the mixture at 308.2 K.

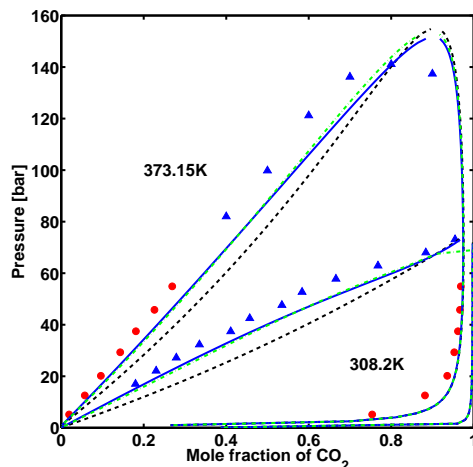


Figure 8.18: Prediction ($k_{ij} = 0$) of the CO₂ + toluene VLE at 373.15 K and 308.2 K where CO₂ is treated either as an inert (black dashed line), a self-associating compound (blue line) or modeled with the three parameter version of qCPA (green dashed line). Experimental data from ▲: [217] and ●: [218].

If, instead of using the effective quadrupole moment from Reynolds et al. [188], the uncertain quadrupole moment is simply set to zero the phase equilibrium calculations become almost predictive as shown in figure 8.19. A small binary interaction parameter of about $k_{ij} = 0.01$ correlates the VLE at both temperatures.

8.4.3 CO₂ + nitrogen

Nitrogen has a relatively weak quadrupole moment of approximately $-1.5 \text{ D}\text{\AA}$. This value is initially employed when nitrogen is modeled as a quadrupolar compound. See table 8.2 for the re-estimated parameters.

The low temperature CO₂ + nitrogen VLE predicted with qCPA (three parameter) and inert CPA is compared to experimental data at 250 K in figure 8.20. The predictions are rather similar in the gas phase. In the liquid phase and close to the critical point, however, the predictions with qCPA becomes worse than when both CO₂ and N₂ are treated as inert compounds. Correlation of a quadrupolar volume in addition to the three other parameters does improve the predictions with qCPA slightly, so that the VLE predictions of the CO₂ + N₂ mixture essentially becomes identical to the predictions with inert CPA.

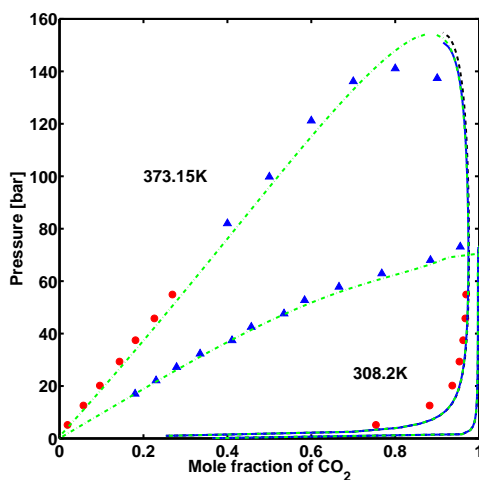


Figure 8.19: Prediction ($k_{ij} = 0$) of the CO₂ + toluene VLE at 373.15 K and 308.2 K where CO₂ is modeled as a quadrupolar fluid, but the quadrupole moment of toluene is ignored. Experimental data from ▲: [217] and ●: [218].

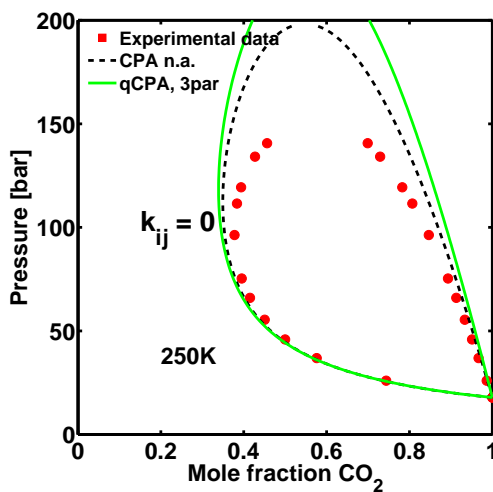


Figure 8.20: Prediction of the CO₂ + N₂ VLE at 250 K using qCPA with three parameters and inert CPA. Experimental data from Ref. [193]

Interestingly, if the quadrupolar moment of nitrogen is correlated to the saturated liquid density and saturated pressure rather than the volume parameter, significantly better predictions are apparently obtained with qCPA for the CO₂ + N₂ VLE as illustrated in figure 8.21. The pure compound parameters for this model approach is shown in table 8.9. The 'effective' quadrupolar moment, however, is doubled compared to the experimental value, which does seem rather high.

It should be emphasised, however, that the correlations for four parameter qCPA, where the quadrupolar moment is the additional adjustable parameter, have been performed as a simple LSQ estimation, without considering uncertainties in the parameters and the propagated errors such as done in chapter 6 for CO₂. It was observed that especially the value of the effective quadrupolar moment and the attractive energetic CPA parameter in the SRK term (Γ) seemed to be highly correlated and sensitive to the experimental data. This indicates that the results should be considered with some reservations. At the very least it should be investigated how the new nitrogen parameter set perform for mixtures without cross-quadrupolar interactions, such as N₂ + hydrocarbon mixtures, as there are considerable uncertainties, as to whether the quadrupolar-quadrupolar interaction are properly handled with the current combining rules. It may be, that the failure of the model to improve the predictions for these systems are due to erroneous combining rules rather than the need for more, and different, adjustable parameters.

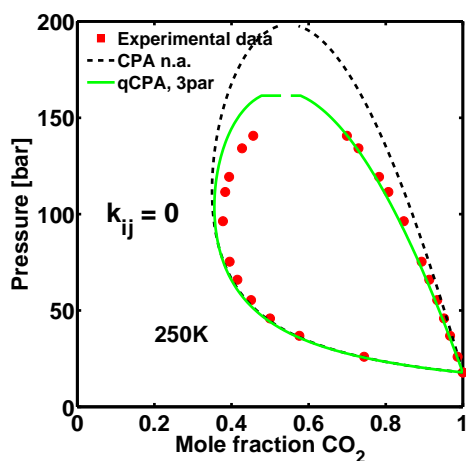


Figure 8.21: Prediction of the CO₂ + N₂ VLE at 250 K using qCPA with four parameters. A fitted quadrupolar moment of 3.0 DÅ is employed. Experimental data from Ref. [193]

To preliminarily investigate the adequacy of the N₂ parameters of qCPA for mixtures of N₂ + hydrocarbons the low temperature vapor liquid equilibria of N₂ + propane and N₂ + *n*-butane were calculated and compared to experimental

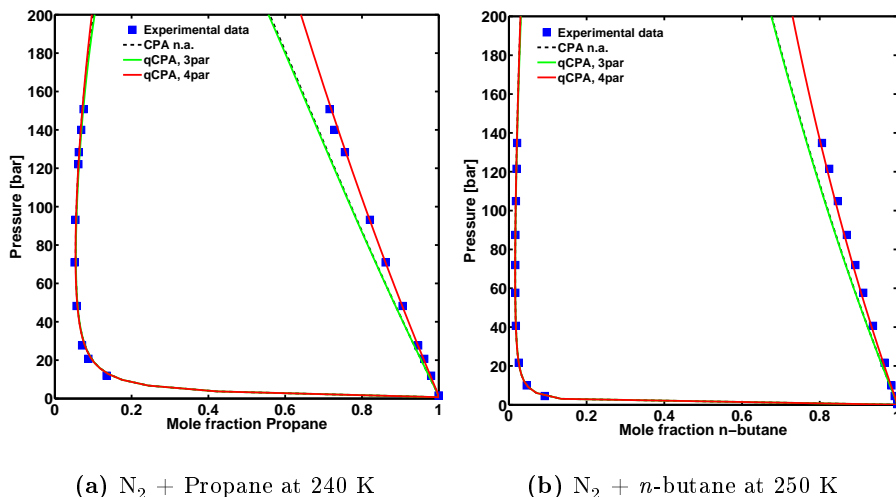


Figure 8.22: Predictions compared to experimental data for the low temperature VLEs of (a) N₂ + propane at 240 K and (b) N₂ + *n*-butane at 250 K using in both cases inert CPA and qCPA with three and four parameters respectively. In the latter case it is the quadrupolar moment which has been fitted as the fourth parameter. Experimental data from Refs. [193, 219].

data in figure 8.22. Both phase diagrams indicate that the solubility of N₂ in the liquid phase is modeled slightly better with the four parameter version of qCPA, where the extra parameter is a fitted quadrupole moment rather than a fitted co-volume (pure compound parameters in table 8.9). Unfortunately the critical region is not well-defined experimentally. All approaches predicts the N₂ rich vapor phase very well.

8.4.4 CO₂ + acetylene

Acetylene has a large positive quadrupole moment. When qCPA is employed acetylene is initially modeled with a fixed quadrupolar moment of 4 DÅ, the re-estimated pure compound parameters for the three parameter version of qCPA can be found in table 8.2.

The VLE between CO₂ and acetylene results in an uncommon negative azeotrope, which is believed to be caused by the opposite sign of their quadrupole moments [220]. Ideally a quadrupolar term would, of course, be able to model this effect, however, figure 8.23 shows, that none of the modeling approaches are able to predict the trends of this system. In fact, the opposite trend (i.e. a positive azeotrope) is predicted by both qCPA and CPA 4C. All models are capable of correlating the azeotrope, which is shown in figure 8.23b. By far the poor-

est predictions are obtained when CO₂ is assumed to be associating, which is probably due to the fact that while the quadrupolar interactions between CO₂ is approximated by self-association no such interactions, or cross-interactions with CO₂, are considered for acetylene, which is considered an inert compound when CPA is employed. When qCPA is employed both molecules are modeled as quadrupolar compounds which seem to, at least partly, cancel out the tendency for the positive azeotrope.

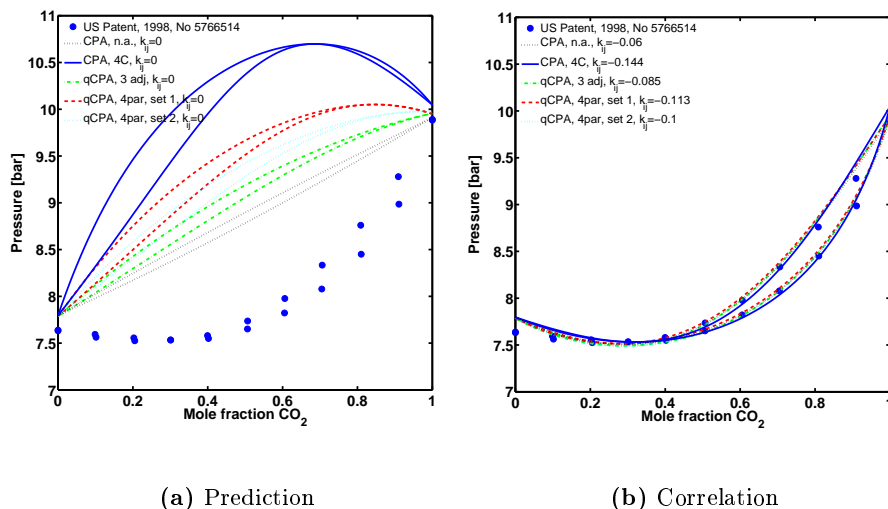


Figure 8.23: Prediction (a) and correlation (b) of the CO₂ + acetylene VLE at 233 K using either CPA without association (n.a.), with the 4C scheme, or qCPA with either three or four adjustable parameters. Experimental data from Ref. [221].

8.4.4.1 On the qCPA and the CO₂ + acetylene predictions

Part of the reason that this quadrupole-quadrupole pair is poorly represented by the quadrupolar model is essentially due to the quadrupoles of opposite sign and the too simple combining rules used in the quadrupole term (Eqs. (5.9) and (5.10)). Due to the employed square roots and cubic roots the combining rules does not allow the use of quadrupole moments of different signs, as this would lead to complex values for the cross-quadrupole moment. To perform the calculations CO₂ and acetylene are in practise modeled as two quadrupolar molecules of the same sign. This, of course, leads to the serious errors in the VLE predictions as the preferred molecular orientation for two quadrupoles of opposite sign is end to end whereas it is perpendicular if they are of the same sign, see figure 4.1 in chapter 4.

If instead the cross-quadrupolar moments in Eqs. (5.4)-(5.6) are replaced by Eqs. (8.7)-(8.9)

$$Q_{ij}^4 = Q_i^2 Q_j^2 \quad (8.7)$$

$$Q_{ij}^6 = Q_i^3 Q_j^3 \quad (8.8)$$

$$Q_{ijk}^6 = Q_i^2 Q_j^2 Q_k^2 \quad (8.9)$$

Quadrupoles of different signs are no longer a (numerical) issue. Eq. (8.8) can even give a negative contribution to equation (5.5). Except for mixtures containing quadrupolar compounds of opposite sign Eqs. (8.7)-(8.9) gives the same results as the original combining rules, Eqs. (5.9) and (5.10), indicating that all other results presented thus far are unchanged by this modification. The expressions in Eqs. (8.7)-(8.9) means that the structure of the quadrupolar second and third-order perturbation terms becomes similar to that of Gubbins and Twu [94, 95]. Although the correlation integrals employed in this work are significantly simpler.

Figure 8.24 shows the VLE prediction with the three parameter version of qCPA for the CO₂ + acetylene system, where the modified combining rules are employed. If these modified combining rules are employed the two opposite quadrupoles seem to 'cancel each other out' as the results are quite close to the results obtained when both CO₂ and acetylene are modeled as inert compounds. On the other hand, no positive azeotrope is predicted, as was the case with the original combining rules.

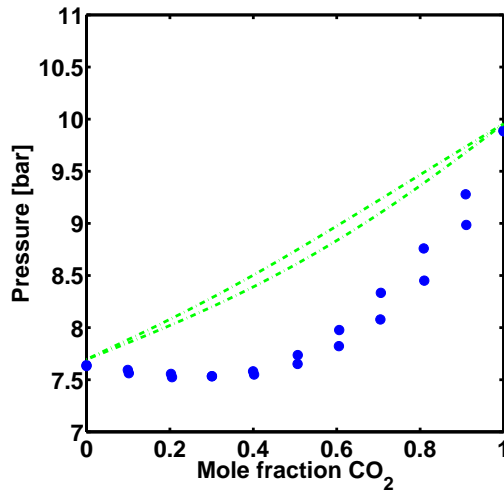


Figure 8.24: Prediction of the CO₂ + acetylene VLE at 233 K using qCPA with three adjustable parameters and the modified combining rules. Experimental data from Ref. [221].

Correlation of the quadrupolar volume of acetylene in addition to the other parameters resulted in similar predictions as those shown in figure 8.24. On the other hand, if the quadrupolar moment of acetylene is correlated to experimental data, similarly to the procedure described for nitrogen in the previous section, very good predictions are obtained for the CO₂ + acetylene VLE as illustrated in figure 8.25. The pure compound parameters for this variation are also shown in table 8.9. The effective (correlated) quadrupole moment of 5.4 D² may seem rather high as a value of 4 D² was assumed previously. However, values between 3 D² and 8.4 D² are found in the literature [84], suggesting that the value is quite reasonable.

Table 8.9: Pure compound parameters and %AAD in the saturated liquid density and saturated pressure for qCPA, where an 'effective' quadrupolar moment is employed as an adjustable parameter rather than the quadrupolar volume. Experimental data from raw DIPPR data [172].

Compound	T_r (= T/T_c)	b_0 [mL/mol]	Γ [K]	c_1 -	Q [D ²]	P^{sat}	%AAD ρ^{liq}
Nitrogen	0.5-0.9	27.18	481.1	0.22	-3.0	1.28(0.86) ^a	0.74(1.73)
Acetylene	0.6-0.9	33.97	1247.5	0.57	5.4	0.44(0.41)	0.29(0.68)

^a Numbers in parenthesis are the %AAD with CPA.

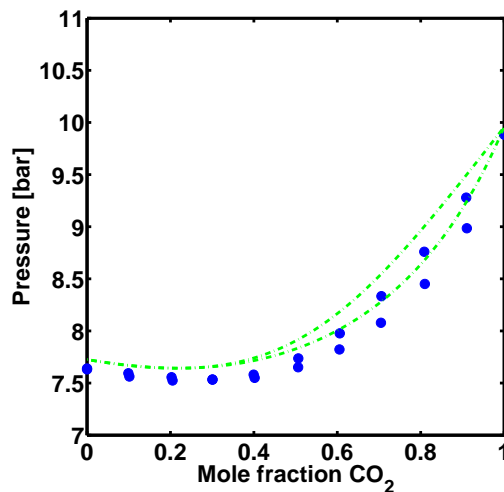


Figure 8.25: Prediction of the CO₂ + acetylene VLE at 233 K using qCPA with four adjustable parameters and the modified combining rules. Contrary to figures 8.23 and 8.24 a fitted quadrupolar moment of 5.4 D² is employed. Experimental data from Ref. [221].

As was the case with nitrogen these correlations have, however, been determined without considering in detail the parameter uncertainties and propagated errors such as demonstrated for CO₂ in chapter 6. Not unlike the observations for nitrogen, the value of the effective quadrupolar moment and Γ seemed to be

sensitive to the experimental data and the temperature interval in which the correlations were performed.

8.5 CO₂ + Polar Molecules

Finally qCPA is preliminarily evaluated for its ability to predict the phase equilibria of mixtures with both a quadrupolar and a strongly polar compound.

8.5.1 CO₂ + acetone

Acetone is, strictly speaking, a polar non self-associating compound. Like CO₂, however, it is often assumed to be (pseudo) self-associating in CPA. As no dipole term has been developed, acetone is assumed to be self-associating in all model approaches using parameters from Ref. [59]. Figure 8.26 illustrates the predictions of the CO₂ + acetone VLE. The predictions and correlations in terms of %AAD are shown in table 8.10. As is clear from the figure, results with qCPA and inert CPA are unsatisfactory. On the other hand very good predictions are obtained when CO₂ is treated as a self-associating molecule. One can only speculate on whether the predictions would improve if a dedicated dipole term were added to qCPA in addition to the quadrupolar term. However, considerable uncertainty remains as to how dipole-quadrupole interactions should be treated.

Table 8.10: Deviations for CPA and qCPA predictions ($k_{ij} = 0$) and correlations ($k_{ij} \neq 0$) for the CO₂ + acetone mixture in the temperature range 291.2-313.1 K. Including the correlated k_{ij} . Compared to experimental data from Refs. [202].

Modeling approach	% AAD in P	%AAD in x_1	k_{ij}	% AAD in P	%AAD in x_1
	$k_{ij}=0$				
CPA, n.a.	33.8	26.1	-0.144	6.6	5.3
CPA, 4C	6.5	5.7	0.037	2.7	2.4
qCPA, 3par	23.6	19.5	-0.110	2.5	2.2
qCPA, 4par, set 1	33.8	27.4	-0.160	2.5	2.1
qCPA, 4par, set2	27.5	22.7	-0.140	2.9	2.3

8.6 Excess Properties

While the main purpose of the equation of state is to correlate and predict the phase equilibria between mixtures, it is also of interest to test how CPA and qCPA predicts other properties such as the excess enthalpy and volume. The

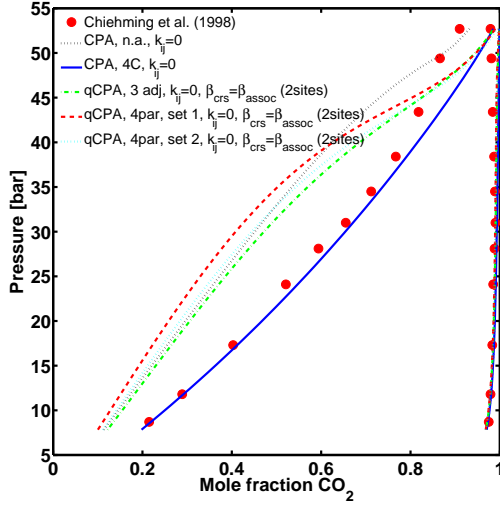


Figure 8.26: Prediction of the CO₂ + acetone VLE at 291.15 K using either CPA without association (n.a.), with the 4C scheme, or qCPA with either three or four adjustable parameters. Acetone is assumed to be self-associating. Experimental data from Ref. [202].

following illustrate how the models predicts the excess enthalpy of the binary mixtures CO₂ + ethane and CO₂ + water.

For a generic property, M , the excess (E) property is defined as the difference between the actual value of the property for a mixture and the value of the property, at the same temperature, pressure and composition, had the mixture formed an ideal solution

$$M^E(T, P, \mathbf{n}) = M(T, P, \mathbf{n}) - M^{is}(T, P, \mathbf{n}) \quad (8.10)$$

The excess enthalpy is determined from the value of the enthalpy of the mixtures subtracted by the value of the property for an ideal mixture as shown in Eq. (8.11)

$$\begin{aligned} H^E(T, P, \mathbf{n}) &= H(T, P, \mathbf{n}) - \sum_i^{nc} n_i H_i(T, P) \\ &= -RT^2 \sum_i^{nc} n_i \left[\left(\frac{\partial \ln \hat{\varphi}_i(T, P, \mathbf{n})}{\partial T} \right)_{P, \mathbf{n}} - \left(\frac{\partial \ln \varphi_i(T, P)}{\partial T} \right)_P \right] \end{aligned} \quad (8.11)$$

where $\hat{\varphi}_i$ is the fugacity coefficient for the i th component in the mixture and φ_i is the fugacity coefficient for the i th pure component.

Figure 8.27a shows the predicted molar excess enthalpy of the CO₂ + ethane mixture at 217 K, saturation pressures and with the binary interaction param-

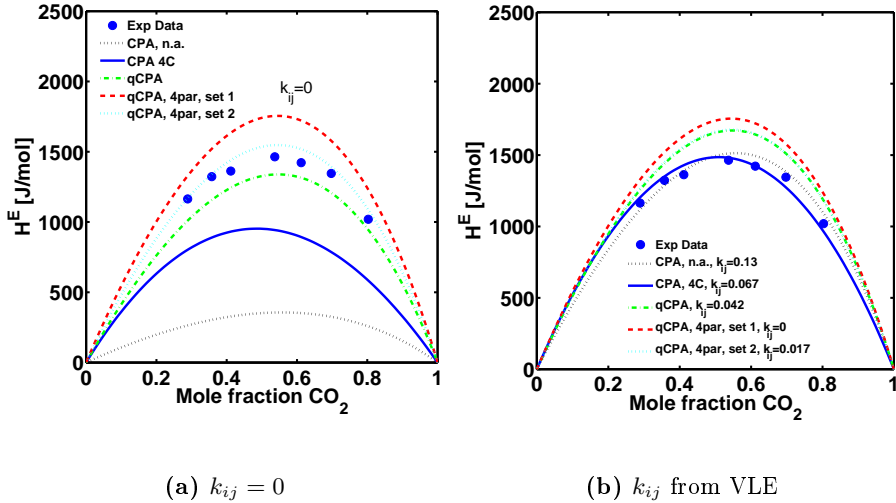


Figure 8.27: Excess enthalpy of the CO_2 + ethane mixtures at 217 K and saturation pressure. The employed modeling approaches are inert CPA, CPA with association, or qCPA with three or four adjustable parameters. (a) shows the predicted excess enthalpy with $k_{ij} = 0$, and (b) shows the predicted excess enthalpy with the k_{ij} correlated from VLE (see table 8.3 and figure 8.1). Experimental data from Ref. [222]

ter set to zero. Figure 8.27b illustrates the excess enthalpy of the mixture using binary interaction parameters correlated to binary VLE data. Both calculations are predictive in the sense that no binary parameters are correlated to the excess enthalpy, although the latter calculation use a binary interaction parameter correlated to VLE. Figure 8.27a shows that all qCPA variants predicts the excess enthalpy quite well and significantly better than when CO_2 is modeled as a self-associating or inert compound. However, when binary interaction parameters correlated to VLE are employed, both CPA variants perform very well and better than qCPA, for which all modeling approaches now over-predict the excess heat.

Figure 8.28 illustrates the excess calculations for the CO_2 + water mixture at 548.2 K and 4.9 MPa, with and without a binary interaction parameter. It can be seen from figure 8.28a that all qCPA variants essentially yields the same predictions and CPA results in the same predictions irrespectively of whether CO_2 is modeled as an associating or inert compound. Figure 8.27b shows that the predictions are relatively insensitive towards the binary interaction parameter, as the same results are essentially obtained except when CO_2 is assumed to be self-associating where a very large binary interaction parameter is employed.

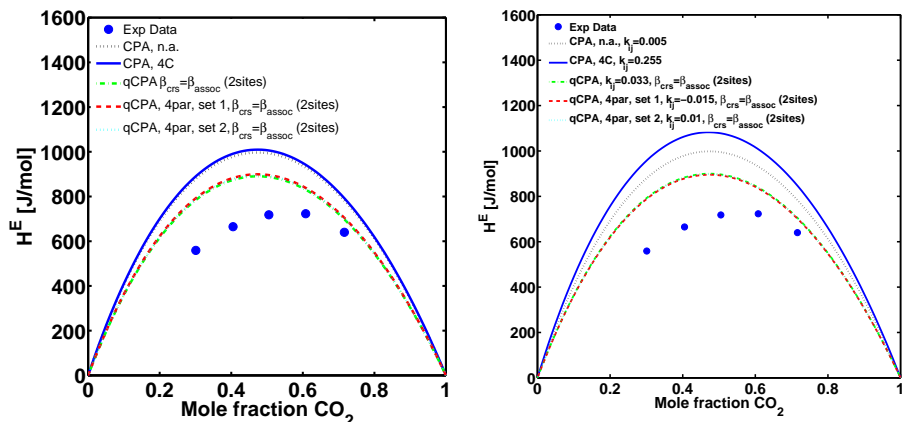
(a) $k_{ij} = 0$ (b) k_{ij} from VLE

Figure 8.28: Excess enthalpy of the CO₂ + water mixture at 548.2 K and 4.9 MPa. The employed modeling approaches are inert CPA, CPA with association, or qCPA with three or four adjustable parameters. (a) shows the predicted excess enthalpy with $k_{ij} = 0$, and (b) shows the predicted excess enthalpy with the k_{ij} correlated from VLE (see table 8.7 and figure 8.14). Experimental data from Ref. [223].

8.7 Summary

The modeling approaches for CO₂ introduced in chapter 7 were employed to predict and correlate the phase behavior of several binary mixtures containing CO₂ and either *n*-alkanes, alcohols, water or different quadrupolar molecules. For correlations a single binary interaction parameter is employed for all modeling approaches.

It was found that qCPA significantly improves the prediction of binary VLE and the correlation of LLE between binary mixtures containing CO₂ and hydrocarbons. In fact one of the parameter sets for qCPA with four adjustable parameters predicts the VLE of these mixtures almost perfectly, while the other parameter set accurately predicts several CO₂ + hydrocarbon LLEs. Overall the four-parameter versions of qCPA perform somewhat better than qCPA with three parameters. Nevertheless the modest improvement relative to the three parameter version of qCPA may not justify the increased model flexibility and uncertainty in the parameter estimation. All CPA models can accurately correlate the experimental data using a non-zero value of the binary interaction parameter, although a significantly smaller interaction parameter is needed with qCPA in all cases.

For binary mixtures containing CO_2 and associating compounds (alcohols and water) excellent correlations were obtained with qCPA when solvation was taken into account with the approach suggested by Kleiner and Sadowski [60] and a single small binary interaction parameter was employed. However, it is clearly more important to account for the solvation between CO_2 and the self-associating compound, than to take the effect of the quadrupole into account. Nevertheless, when the modeling approaches are used to correlate the experimental phase behavior, qCPA seems to consistently result in lower binary interaction parameters, as compared to CPA.

An encouraging feature of qCPA is that excellent predictions for the $\text{CO}_2 + n$ -alkane mixtures are obtained when quadrupolar interactions are included. Simultaneously satisfactory correlations for $\text{CO}_2 +$ self-association mixtures are obtained with the same model when CO_2 is also assumed to be solvating. This is physically much more appealing than to assume CO_2 to be self-associating.

Mixtures containing $\text{CO}_2 +$ another quadrupolar compound turned out to be a quite a challenge for qCPA. While the predictions for some mixtures, such as $\text{CO}_2 +$ benzene, were improved compared to base CPA, other mixtures, such as $\text{CO}_2 + \text{N}_2$, initially gave poorer predictions than base CPA. These results could be improved if the quadrupolar moment was used as a fourth adjustable parameter. In general the performance of qCPA seem to depend on a complex balance between the contributions from the quadrupole moments of each molecule and their cross interaction.

The originally proposed mixing rules for the quadrupolar moment were shown to be insufficient for mixtures containing two opposite quadrupoles such as the $\text{CO}_2 +$ acetylene mixture. Using the expressions suggested in Eqs. (8.7)-(8.9) rather than the old mixing rules seem to resolve this problem. These expressions are identical with the expressions employed by Gubbins and Twu, which arise naturally from the molecular theory developed from their work [224].

Finally the prediction of excess enthalpies were shown for two mixtures, which indicate that qCPA may improve the prediction of excess properties as well, at least when $k_{ij} = 0$.

Overall, explicitly accounting for the quadrupolar forces appears to offer significantly improved predictions, and better (smaller k_{ij}) correlations, for CO_2 containing mixtures compared to when CO_2 is treated as either an inert or a self-associating compound.

CHAPTER 9

Multicomponent Mixtures Containing CO₂

Most studies for mixtures containing CO₂ with advanced equations of state, such as the quadrupolar versions of SAFT, are limited to binary systems, or maybe a few ternary systems [29, 111]. Even for regular CPA or SAFT only few investigations systematically deal with multicomponent mixtures containing CO₂. It may be misleading, however, when conclusions are based only on binary systems, especially when one or more binary parameters are employed to correlate the binary system. A more rigorous test of qCPA involves comparison of its phase equilibrium predictions with those of CPA for both binary and multicomponent systems.

One of the most systematic and extensive investigations for modeling multicomponent systems containing CO₂ has been performed by Kontogeorgis and co-workers [33, 35, 36] during the aforementioned evaluation of different modeling approaches for CO₂ using the CPA (see chapter 3 for more details). The best results were obtained when CO₂ was considered to be either a solvating or a self-associating compound (using the 4C scheme).

In this chapter, as a natural extension of the work on binary mixtures containing CO₂ the quadrupolar CPA is evaluated for multicomponent systems containing CO₂, alkanes, water, and/or alcohols, mostly similar to those studied by Tsvintzelis and Kontogeorgis [35] and Tsvintzelis et al. [33]. Most results in this chapter have been submitted to *Molecular Physics (Thermodynamics 2015, Special Issue)*. The quadrupolar CPA is directly compared with the two CPA approaches that Kontogeorgis and co-workers have found to perform best for CO₂ containing mixtures, as well as the base case where CO₂ is considered to be

an inert compound. In a way this chapter also supplements the work by Kontogeorgis and co-workers, by comparing the best purely CPA based approaches with the quadrupolar CPA.

9.1 Modeling approaches

According to Kontogeorgis and co-workers [14, 33, 35] the best approaches for modeling mixtures containing CO₂, alkanes, water, and/or alcohols is to treat CO₂ as either a self-associating or solvating molecule. In both cases Kontogeorgis and co-workers recommends that the experimental value of the cross-association energy should be employed and two adjustable parameters are employed per binary pair containing CO₂ and water, or alcohols. In this chapter these approaches are compared with two of the qCPA variants evaluated in the two previous chapters. Namely qCPA with three adjustable parameters and qCPA with four adjustable parameters. In the latter case parameter set 1 of the previous two chapters is employed. The approaches are also compared to the base case where CO₂ is treated as an inert compound. That is, five modeling approaches are evaluated in this chapter for multicomponent CO₂-containing mixtures; Three purely CPA based approaches and two approaches where a quadrupolar term has been introduced in the CPA.

More specifically CO₂ will (as in the previous chapters) be considered to be an inert compound i.e. non-associating and non-quadrupolar (case A), a solvating compound with two solvation sites (case B), a self-associating compound following the 4C scheme (case C) and a quadrupolar compound (cases D-E). Notice that cases B and C differs from the previous chapter, as the experimental value of the cross-association energy is employed in this chapter rather than the CR-1 combining rule. For both of these approaches the cross-association volume and the binary interaction parameter was fitted by Tsvintzelis et al. in Ref. [14]. When mixtures of CO₂ and self-associating compounds are considered with qCPA, CO₂ is treated as a quadrupolar *and* solvating compound as described in chapter 8. As the cross-association parameters are determined with the procedure suggested by Kleiner and Sadowski [60] only one adjustable interaction parameter is employed per binary pair for cases D-E, see chapter 8 section 8.3 for more details.

The pure compound parameters for the CO₂ approaches have either been published in the open literature [14, 37] or presented in the previous chapters (table 7.2). Pure compound parameters for the other compounds employed can be found in the Refs. [34, 51, 52, 81, 187] or table 8.1.

Table 9.1: Approaches considered with CPA and qCPA for modeling ternary and quaternary CO₂-mixtures containing alkanes, water, and/or alcohols.

Case	EoS	Association sites in CO ₂	No. pure parameters	k_{ij}	Cross-association parameters ^a for the CO ₂ -associating compound interaction		Reference
A	CPA	0	3	adjustable	ϵ_{cross}	β_{cross}	[14]
B	CPA	2ed-0ea	3	adjustable	-	-	[14]
C	CPA	2ed-2ea	5	adjustable	exp. value	adjustable	[14]
D	qCPA	2ed-0ea	3	adjustable	exp. value	adjustable	[14]
D	qCPA	2ed-0ea	3	adjustable	CR-1	$\beta_{cross} = \beta_{assoc}$	[37]
E	qCPA	2ed-0ea	4	adjustable	CR-1	$\beta_{cross} = \beta_{assoc}$	[37]

^a For the definition of the CR-1 rule see chapter 3 section 3.1.

As is typically the case, the 2B association scheme is employed for alcohols and the 4C scheme is used for water. Details of the five approaches used for modeling CO₂ are shown in table 9.1. The approaches use between three and five pure compound parameters and approaches A, D, and E employ one interaction parameter per binary, whereas approaches B and C employ two. Contrary to the previous chapter a direct comparison between the modeling approaches is, thus not entirely fair in terms of the number of binary adjustable parameters.

All the predicted equilibria for the multicomponent mixtures investigated in this chapter were performed using either interaction parameters correlated from the corresponding binary systems or using no interaction parameters at all. The CR-1 combining rule is employed for all binary pairs consisting of two associating compounds (not including the binary pairs containing CO₂). That is, all calculations for multicomponent mixtures are predictive in the sense that all parameters are based on pure fluid or binary mixture data only.

For the CO₂ containing systems, Tsvintzelis et al. [14] have presented binary parameters for most of the binaries subsystems for cases B and C while binary interaction parameters for cases A, D and E are presented in this thesis (tables 8.3, 8.6 and 8.7) and (for the most part) in Bjørner and Kontogeorgis [37]. In approaches A, D and E the only binary adjustable parameter is the k_{ij} , whereas both the binary interaction parameter and the cross-association volume (β_{cross}) are used as adjustable parameters in cases B and C. Table 9.2 summarizes, for each modeling approach, the binary interaction parameters for the CO₂ containing binary pairs, employed in this chapter. The interaction parameters for the remaining non-CO₂ containing binary pairs are shown in table 9.3. These interaction parameters are obtained from the literature [35, 81, 187, 225–227].

9.2 Vapor Liquid Equilibrium

The VLE of seven ternary systems containing CO₂, *n*-alkanes, water, and/or alcohols were investigated using flash calculations. When possible the centre of the experimental tie lines were employed as the feed composition. With the exception of two mixtures containing CO₂ and two *n*-alkanes, Tsvintzelis et al. [34] and Tsvintzelis and Kontogeorgis [35] have recently evaluated similar mixtures. As the predictions with qCPA are compared to both inert CPA (case A) and the aforementioned best CPA approaches (cases B and C), similar multicomponent results have already been published for these modeling approaches. One difference for case B is that CO₂ is modeled as a solvating molecule with one electron donor site by Tsvintzelis and Kontogeorgis [35] whereas CO₂ is modeled with two electron donor sites in this work.

Table 9.2: Summarized binary interaction parameters for the binary CO₂ + *n*-alkane, alcohol or water systems with CPA and qCPA. Interaction parameters originally presented in Refs. [14, 37].

Binary pair	k_{ij}	ε_{cross}/R [K]	$\beta_{cross} \cdot 1000$
Approach A			
Methanol + CO ₂	0.0267	-	-
Ethanol + CO ₂	0.051	-	-
Propanol + CO ₂	0.005830	-	-
Water + CO ₂	-0.0232	-	-
Methane + CO ₂	0.089	-	-
Ethane + CO ₂	0.130	-	-
Propane + CO ₂	0.129	-	-
Butane + CO ₂	0.124	-	-
Eicosane + CO ₂	0.085	-	-
Approach B			
Methanol + CO ₂	0.0493	Exp: 1489	10.8
Ethanol + CO ₂	0.1076	Exp: 1489	13.4
Propanol + CO ₂	0.0667	Exp: 1489	1.3
Water + CO ₂	0.1252	Exp: 1708	7.9
Methane + CO ₂	0.089	-	-
Ethane + CO ₂	0.130	-	-
Propane + CO ₂	0.129	-	-
Butane + CO ₂	0.124	-	-
Eicosane + CO ₂	0.085	-	-
Approach C			
Methanol + CO ₂	-0.0242	Exp: 1489	4
Ethanol + CO ₂	0.0109	Exp: 1489	2.1
Propanol + CO ₂	-0.0077	Exp: 1489	0.05
Water + CO ₂	0.030	Exp: 1708	3
Methane + CO ₂	0.0292	-	-
Ethane + CO ₂	0.075	-	-
Propane + CO ₂	0.0915	-	-
Butane + CO ₂	0.0599	-	-
Eicosane + CO ₂	0.05	-	-
Approach D			
Methanol + CO ₂	-0.01	CR-1: 1479	$\beta_{methanol}$
Ethanol + CO ₂	-0.019	CR-1: 1295	$\beta_{ethanol}$
Propanol + CO ₂	-0.02	CR-1: 1263	$\beta_{propanol}$
Water + CO ₂	0.033	CR-1: 1002	β_{water}
Methane + CO ₂	-0.007	-	-
Ethane + CO ₂	0.042 ^a	-	-
Propane + CO ₂	0.035	-	-
Butane + CO ₂	0.040 ^a	-	-
Eicosane + CO ₂	0.015	-	-
Approach E			
Methanol + CO ₂	-0.05	CR-1: 1479	$\beta_{methanol}$
Ethanol + CO ₂	-0.057	CR-1: 1295	$\beta_{ethanol}$
Propanol + CO ₂	-0.05	CR-1: 1263	$\beta_{propanol}$
Water + CO ₂	-0.015	CR-1: 1002	β_{water}
Methane + CO ₂	-0.057	-	-
Ethane + CO ₂	0	-	-
Propane + CO ₂	0	-	-
Butane + CO ₂	0	-	-
Eicosane + CO ₂	-0.02	-	-

^a Improved value compared to [37].

Table 9.3: CPA and qCPA binary interaction parameters for non-CO₂ containing binary mixtures. Binary interaction parameters from Refs. [35, 81, 187, 225–227]. binary interaction parameters between two hydrocarbons are assumed to be zero.

Compound	Water	Methanol
	k_{ij}	k_{ij}
Methanol	-0.075	-
Ethanol	-0.041	0
Propanol	-0.038	0
Methane	0.0098	0.01
Ethane	0.0442	0.0204
Propane	0.1135	0.0555
Butane	0.0875	0.0350

9.2.1 Mixtures containing CO₂ and *n*-alkanes

For multicomponent mixtures containing only hydrocarbons the binary interaction parameters are close to zero and satisfactory predictions are typically obtained with CPA (or SRK). In this regard an interesting group of multicomponent systems are those containing CO₂ and multiple *n*-alkanes. For these systems dispersion and quadrupolar forces should essentially be the only interactions and there is no question as to how CO₂ should be modeled with self-associating compounds.

It is obvious from results in the previous chapter that almost quantitative predictions ($k_{ij} = 0$) was obtained for binary mixtures containing CO₂ and hydrocarbons when qCPA was employed with four parameters (case E). The predictions were also quite satisfactory when the model was employed with three parameters (case D). An important question is whether the excellent phase equilibrium results for binary mixtures are extensible to multicomponent mixtures.

To investigate this the VLE of the mixtures CO₂ + methane + ethane and CO₂ + ethane + eicosane are studied with qCPA and CPA. The binary interaction parameters between ethane + methane and ethane + eicosane are both assumed to be zero. Furthermore the mixtures are studied both with and without a k_{ij} between CO₂ and the hydrocarbons. As there are no associating compounds cases A and B becomes identical.

The deviations between model predictions, both with and without interaction parameters, and experimental data are shown in table 9.4. When all k_{ij} 's are set to zero no deviations are presented for case A, as VLEs are not predicted for all data points when the centre of the experimental tie line is used as the feed composition.

The CO₂ + methane + ethane system is a very interesting system, which depends strongly on the pressure. At low pressures the bubble- and dew-point

Table 9.4: CPA and qCPA deviations between model predictions and experimental composition data from Refs. [67, 228, 229] for the VLE of the two ternary systems CO₂(1) + methane(2) + ethane(3) and CO₂(1) + ethane(2) + eicosane(3) using four of the modeling approaches. The pressure and temperature range is 230-250 K and 25-65 bar for the former system and 338.7 K and 104 bar for the latter system. The predictions have been performed both with and without interaction parameters as indicated in the table.

	%AAD in composition					
	x_1	x_2	x_3	y_1	y_2	y_3
CO ₂ (1) + methane(2) + ethane(3)	$k_{ij} = 0$					
Case A	-	-	-	-	-	-
Case C	6.2	70.0	6.9	13.3	31.6	18.2
Case D	4.6	45.5	5.8	10.1	20.3	13.8
Case E	5.3	16.4	2.9	6.6	4.2	7.6
CO ₂ (1) + methane(2) + ethane(3)	$k_{ij} \neq 0$					
Case A	4.6	22.0	4.4	8.6	5.6	10.3
Case C	4.5	23.8	4.5	8.6	6.1	9.9
Case D	4.7	22.9	4.6	8.5	5.8	10.2
Case E	4.8	22.3	4.7	8.4	5.3	9.9
CO ₂ (1) + ethane(2) + eicosane(3)	$k_{ij} = 0$					
Case A	-	-	-	-	-	-
Case C	17.9	4.8	38.3	0.7	1.0	26.9
Case D	10.7	4.1	25.4	1.5	1.4	37.8
Case E	0.5	3.9	7.1	2.7	2.8	60.8
CO ₂ (1) + ethane(2) + eicosane(3)	$k_{ij} \neq 0$					
Case A	9.0	4.3	22.4	1.8	2.1	57.7
Case C	11.0	4.0	25.5	1.5	1.4	55.0
Case D	9.5	4.2	23.2	1.7	1.9	52.8
Case E	4.2	3.8	14.1	2.2	2.3	59.0

curves coincide, while at higher pressures the distance between the curves increases and then decreases again. The predictions were compared to experimental data from Wei et al. [67] at 230 K and 65 bar and Davalos et al. [229] at 250 K and three pressures (21, 25, and 30 bar). It is clear from table 9.4 that case E performs very well without a k_{ij} , as all deviations between model predictions and experimental data are smaller than 10%, with the exception of the composition of the liquid methane phase. The deviations with the different modeling approaches are almost identical when binary interaction parameters are employed (this is also illustrated in figure 9.1b). Interestingly most deviations increase slightly when case E is employed with binary interaction parameters.

Figure 9.1 illustrates, in a ternary diagram, the VLE predictions of the CO₂ + methane + ethane system at 250 K and 30 bar both without k_{ij} 's (figure 9.1a) and with k_{ij} 's (figure 9.1b). While case E clearly gives the best predictions without binary interaction parameters, all models perform well, and almost identically with binary interaction parameters.

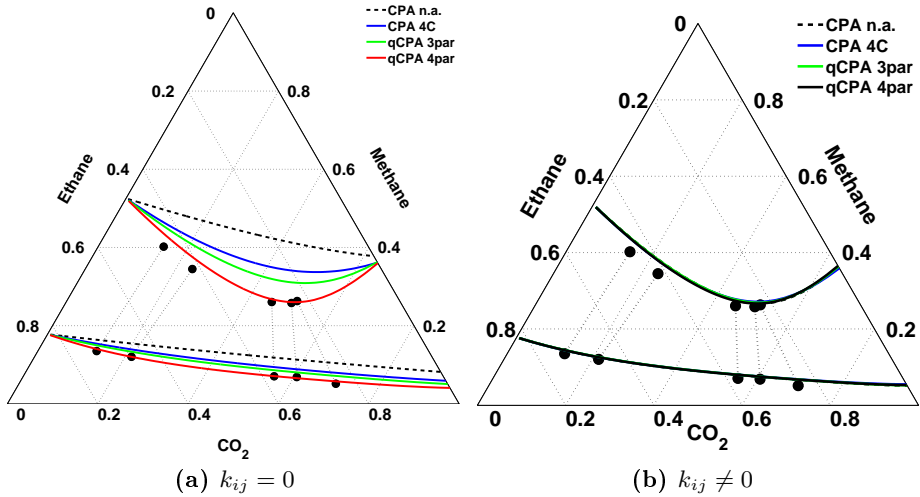


Figure 9.1: Predictions compared to experimental data for the CO_2 + methane + ethane VLE at 250 K and 30 bar. (a) No interaction parameters are employed ($k_{ij} = 0$) and (b) interaction parameters are employed. Circles and dotted lines are experimental data from Ref. [229] and experimental tie lines respectively.

Figure 9.2 compare the predictions of the modeling approaches with experimental data at 250 K and 25 bar (figure 9.2a) and 230 K and 65 bar (figure 9.2b). In both cases all k_{ij} are set to zero. It is clear that case E is fully predictive at low pressures. Close to the critical pressure of the mixture the accuracy of the liquid phase predictions tend to deteriorate for case E. This is undoubtedly caused by the poor representation of the CO_2 + methane binary near the critical point when the binary interaction parameter is ignored for case E. While not quite as good as those of case E the predictions with case D is clearly better than both purely CPA based approaches.

The CO_2 + ethane + eicosane predictions were compared to experimental data from the PhD work of Al-Marri [228] at 338.7 K and 104.4 bar. When the k_{ij} 's are assumed to be zero table 9.4 suggests that very good predictions are obtained for especially the liquid phase with case E, whereas case C actually predicts the vapor phase composition more accurately, especially the small amount of eicosane in the vapor phase.

Figure 9.3a illustrate the predictions. Visually all models predict the vapor phase composition identically, but based on the deviations it seems that case C most accurately predicts the amount of eicosane in the vapor phase. For these large n -alkanes, however, the experimental accuracy may be questionable, especially for the small amount of eicosane in the vapor phase. In the liquid phase both quadrupolar approaches are clearly superior to case C (and case A), despite using fewer pure compound parameters.

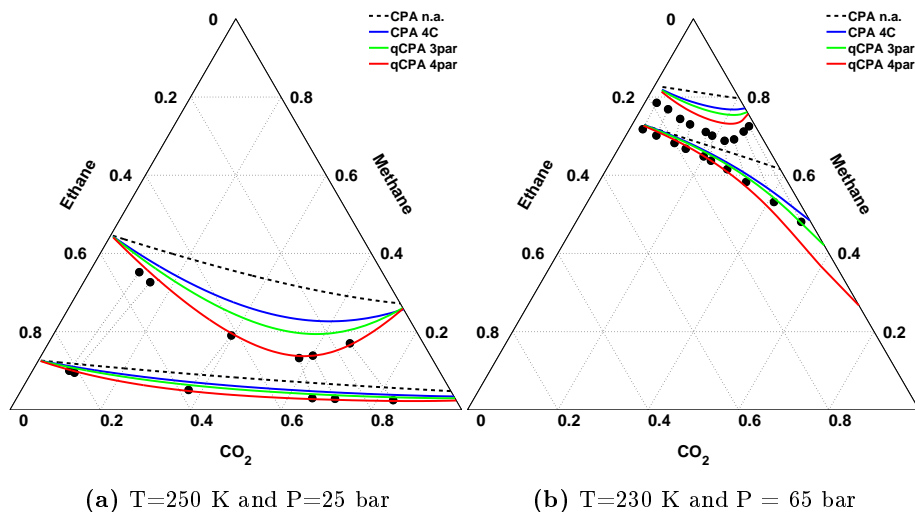


Figure 9.2: Pure predictions compared to experimental data for the CO₂ + methane + ethane VLE at (a) 250 K and 25 bar and (b) 230 K and 65 bar. In either case no interaction parameters are employed ($k_{ij} = 0$). Circles and dotted lines are experimental data from Refs. [67, 229] and experimental tie lines respectively.

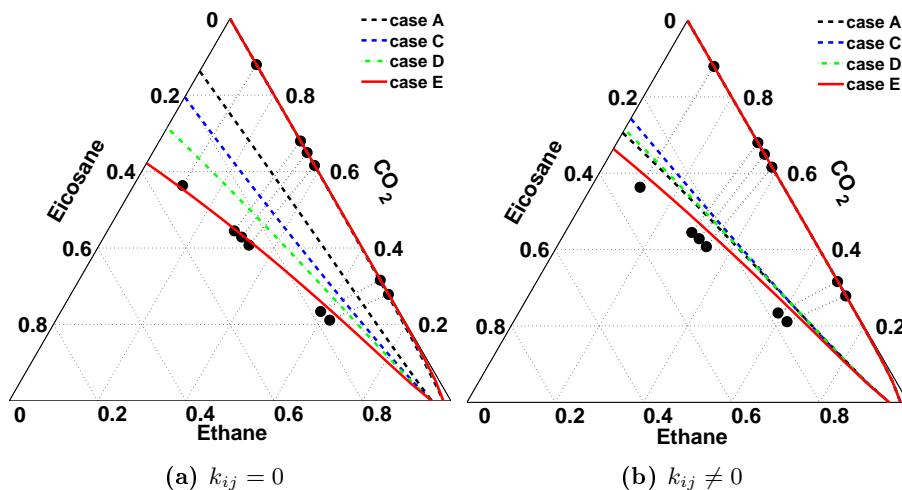


Figure 9.3: Predictions compared to experimental data for the CO₂ + ethane + eicosane VLE at 338.7 K and 104.4 bar. (a) No interaction parameters are employed ($k_{ij} = 0$) and (b) interaction parameters are employed as usual. Circles and dotted lines are experimental data from [228] and experimental tie lines respectively.

As in the case of the CO₂ + methane + ethane system the predictions are very similar when binary interaction parameters are employed. Case E still performs best of the four approaches, although the liquid phase predictions with case E actually becomes slightly poorer, than without binary interaction parameters.

9.2.2 Mixtures containing CO₂ and associating compounds

Next five mixtures containing CO₂ and water and/or alcohols are investigated to evaluate how well qCPA and the best CPA approaches predicts the VLE of mixtures containing CO₂ and associating compounds. binary interaction parameters were employed for all the VLE prediction presented in this section.

The deviations between model predictions and experimental vapor and liquid composition data are summarized in table 9.5 for four of the mixtures. For the final system (CO₂ + water + methane) the composition is only measured for one of the two phases, which means that there are no experimental tie lines. Thus, no deviations are presented for the VLE of this system. The dew point deviations for the CO₂ + water + methane system are also shown in table 9.6.

As would be expected there is an overall tendency for inert CPA (Case A) to result in higher deviations than the other approaches, particularly for the polar species in the gas phase. Nevertheless, table 9.5 shows that the predictions are typically rather similar, irrespective of the modeling approach employed.

Predictions with the five CO₂ approaches for the CO₂ + methanol + propane system were compared to experimental data from Galivel-Solastiouk et al. [230] at two different temperatures (313.1 and 343.1 K) and four pressures (5.1, 12.06, 17.1 and 22.03 bar). At the latter two pressures the calculations are only performed at 343.1 K. The predictions and the resulting deviations with the modeling approaches are almost identical, and satisfactory, for all components in the two phases, although the deviations for the methanol concentration in the gas phase is a little high (see table 9.5). The two quadrupolar cases are the two best approaches but the differences are small and all approaches essentially perform identically.

Figures 9.4a and 9.4b compare the predictions with experimental data at 343.1 K and both 5.1 bar and 22.03 bar respectively. Only case E can be seen in the figure as the predictions are very similar, and the lines lie on top of each other. It is clear from the figures that, at fixed temperature and pressure, the gas phase consists of a small and almost constant amount of methanol, whereas the propane and CO₂ concentration varies depending on the feed. The liquid phase is almost pure methanol. Figure 9.4a illustrates, that the predicted amount of methanol in the equilibrium gas phase is not quite satisfactory at 343 K and low pressures, which is the reason for the higher methanol deviations in the gas phase.

Table 9.5: CPA and qCPA deviations between model predictions and experimental composition data [201, 230–232] for the VLE of four ternary systems containing CO₂ and at least one self-associating compound using the five modeling approaches. The pressure and temperature range is included in the table.

	P [bar]	T [K]	%AAD in composition						
			x_1	x_2	x_3	y_1	y_2	y_3	Average
CO ₂ (1) + methanol(2) + propane(3)									
Case A	5-22	313.15 -	8.9	0.5	5.5	3.5	17.9	3.5	6.6
Case B		343.15	12.2	0.6	5.4	3.4	17.5	3.5	7.1
Case C			10.2	0.5	5.5	3.4	17.4	3.5	6.8
Case D			8.0	0.5	5.4	3.4	17.1	3.3	6.3
Case E			7.6	0.4	5.4	3.4	17.1	3.2	6.2
CO ₂ (1) + methanol(2) + water(3)									
Case A	70-120	313.15	35.8	2.3	4.9	2.0	52.4	57.8	25.9
Case B			48.5	6.2	7.8	0.8	23.2	41.5	21.3
Case C			57.1	10.2	11.3	0.8	20.2	50.0	24.9
Case D			29.9	3.9	4.4	0.4	10.5	40.2	14.9
Case E			28.1	3.7	4.0	0.5	11.5	42.1	15.0
CO ₂ (1) + ethanol(2) + water(3)									
Case A	79-185	313.15 -	41.7	15.9	12.4	6.2	66.5	81.9	37.4
Case B		343.15	35.7	10.2	9.9	4.6	43.1	56.3	26.6
Case C			39.7	8.5	9.1	4.8	50.2	56.7	28.2
Case D			40.8	8.4	9.3	4.8	50.6	54.8	28.1
Case E			39.4	8.2	8.9	4.7	49.0	52.8	27.2
CO ₂ (1) + methanol(2) + ethanol(3)									
Case A	20-80	313.15	6.8	2.8	3.2	0.2	20.3	31.5	10.8
Case B			3.9	1.5	1.9	0.2	17.0	21.6	7.7
Case C			4.3	1.1	1.4	0.2	17.8	27.2	8.7
Case D			4.7	1.2	1.8	0.2	17.5	27.9	8.9
Case E			7.1	1.9	2.6	0.2	17.7	27.2	9.5

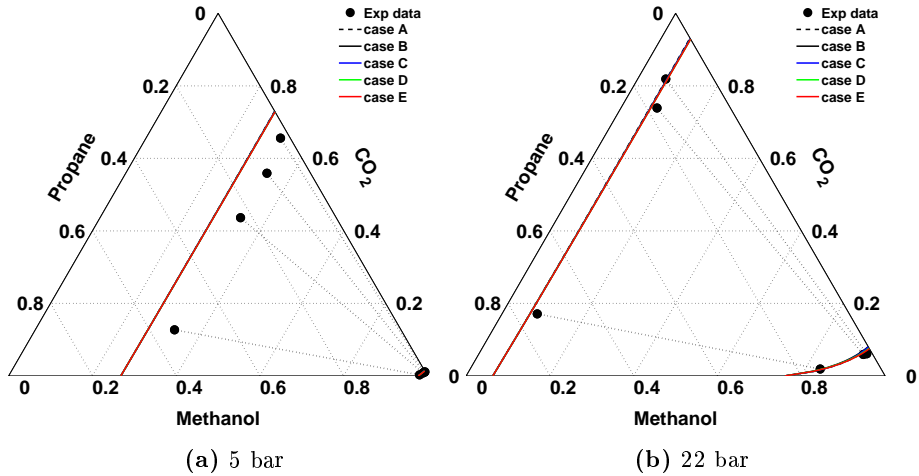


Figure 9.4: Predictions compared to experimental data for the CO₂ + methanol + propane VLE at (a) 343.1 K and 5.1 bar and (b) 343.1 K and 22.03 bar. Full lines are CPA and qCPA predictions. Circles and dashed lines are experimental data from Ref. [230] and experimental tie lines respectively.

Wong and Sandler [233] also investigated the CO₂ + methanol + propane system at 313.1 K and 12.1 bar and 17.1 bar using the Peng-Robinson EoS in conjunction with the Wong-Sandler EoS/ G^E model (using NRTL as the activity coefficient model). Recently NguyenHuynh et al. [111] also presented predictions of the CO₂ + methanol + propanol system at 313.1 K and 5.1 bar using a group contribution polar PC-SAFT. The authors treated CO₂ as a solvating and quadrupolar species just like in this work. No deviations are presented in either investigations, but the results look similar to the results presented here. Utilizing the data sets at 5.1 and 17.1 bar, Tsivintzelis and Kontogeorgis [35] obtained similar deviations as those obtained in this work, for cases A and C.

The pressure range of the available experimental data from Galivel-Solastiouk et al. [230] for the CO₂ + methanol + propane system actually goes up to 32 bar. However, at 313.1 K and from 17.1 bar or higher, all modeling approaches find a three-phase VLLE region (see section 9.4), which is not described by the experimental data. As some of the experimental tie lines enter the predicted three-phase region, deviations cannot be calculated for these data points. Figure 9.5 shows the two predicted VLE regions and the three phase VLLE region at 313.1 K and 17.1 bar. qCPA with three parameters (case D) has been employed in the figure, but all approaches yield similar results. Note that the two experimental tie lines closest to the three-phase region are exactly parallel to the sides of the three-phase region, which connect the vapor phase to the first and second liquid phase. This, along with the rapid change in slope of the tie lines around this region, may suggest that there are, in fact, two VLE regions

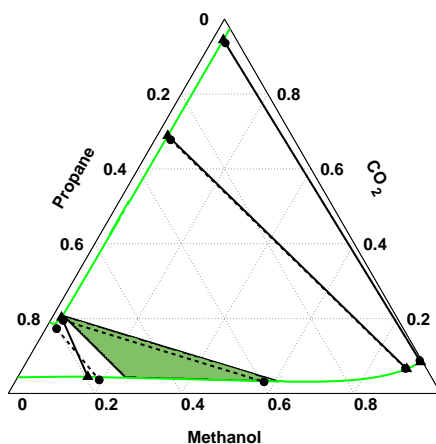


Figure 9.5: Predicted VLE and VLLE for the CO₂ + methanol + propane system at 313 K and 17.1 bar. Green lines are predictions for the whole phase diagram with case D. ▲ Predictions at the experimental conditions, the full black lines are predicted tie lines. ● experimental VLE data from Ref. [230], the dashed black lines are experimental tie lines. The green triangle indicates the predicted three-phase VLLE region at the specified temperature and pressure.

separated by a VLLE region, which has not been detected in the experimental work.

The VLE predictions for the CO₂ + methanol + water system were compared to experimental data from Yoon et al. [232] at 313.2 K and at 70, 100 and 120 bar. It is clear from the results shown in table 9.5 that the best predictions in both the liquid- and vapor phase are obtained when CO₂ is considered to be a quadrupolar *and* solvating compound (cases D and E). Case A performs almost as well as cases D and E in the polar liquid phase. In the CO₂-rich vapor phase, however, case A gives the poorest prediction amongst all approaches, as the water solubility in the CO₂-rich phase is significantly under-predicted. Figure 9.6 shows a characteristic prediction with the five approaches at 313.2 K and 100 bar. It can be seen from the figure that while the predictions with cases A, D and E are very similar in the liquid phase the amount of CO₂ in the vapor phase is over-estimated with case A.

For the CO₂ + ethanol + water system, the VLE predictions were compared to experimental data from Lim and Lee [231] using 11 data sets in a temperature and pressure range of 313.2-343.2 K and 79-185 bar respectively. Deviations are shown in table 9.5, while figure 9.7 shows the predictions at 323.2 K and 118 bar. Treating CO₂ as a solvating compound (case B), results in the overall best

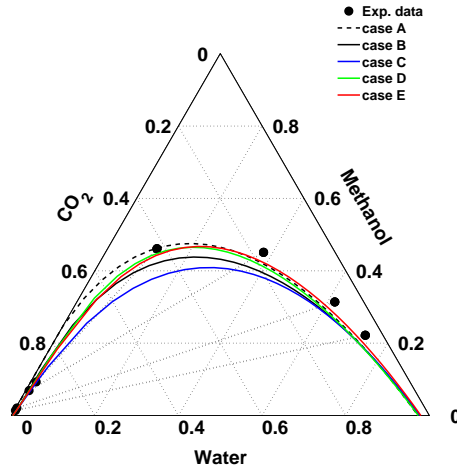


Figure 9.6: Predictions compared to experimental data for the CO_2 + methanol + water VLE at 313.2 K and 100 bar. Full lines are CPA and qCPA predictions. Circles and dashed lines are experimental data from Ref. [232] and experimental tie lines respectively.

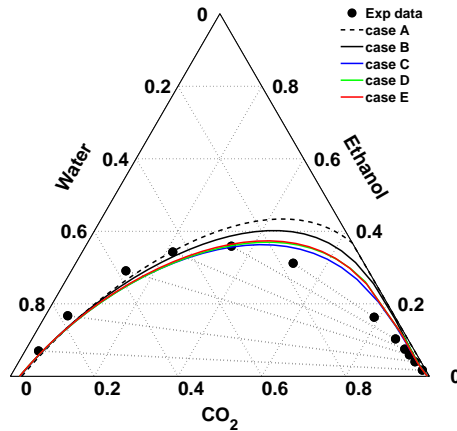


Figure 9.7: Predictions compared to experimental data for the CO_2 + ethanol + water VLE at 323 K and 118 bar. Full lines are CPA and qCPA predictions. Circles and dashed lines are experimental data from Ref. [231] and experimental tie lines respectively.

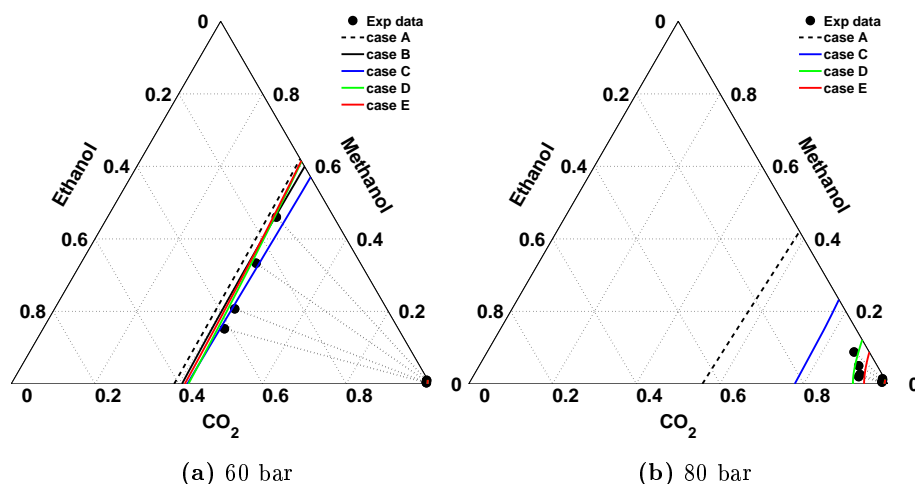


Figure 9.8: Predictions compared to experimental data for the CO₂ + methanol + ethanol VLE at (a) 313 K and 60 bar and (b) 313 K and 80 bar. Full lines are CPA and qCPA predictions. Circles and dashed lines are experimental data from Ref. [201] and experimental tie lines.

predictions, except for the predictions of the composition of ethanol and water in the liquid phase, where cases C, D and E perform better. The differences are quite small, however, and depend on the desired temperature and pressure. As seen from both table 9.5 and figure 9.7, cases C, D and E perform almost identically. Case A results in the poorest predictions for all compositions.

For the CO₂ + methanol + ethanol system the binary interaction parameter between methanol and ethanol was assumed to be zero. The VLE predictions were compared to three experimental data sets from Yoon et al. [201] at 313.2 K and 20, 40 and 60 bar. The deviations (see table 9.5) are quite similar using approaches B-E, although treating CO₂ as a solvating compound (case B) seem to give marginally better results in terms of deviations. A characteristic prediction is shown at 60 bar in figure 9.8a. Besides the experimental data used to calculate the deviations from experimental data, an additional data set is available near critical conditions at 80 bar. Contrary to the other data sets, the predictions begin to differ substantially from each other at these near-critical conditions. Figure 9.8b compares the predicted VLE with four of the different modeling approaches at 80 bar and 313.2 K. Only the two quadrupolar approaches (cases D and E) produce predictions in good agreement with the experimental data, whereas cases A and C severely under-predict the solubility of CO₂ in the polar liquid phase. Only a single (supercritical) phase was detected for case B, which performed marginally better at the other pressures.

Finally the ternary CO₂ + water + methane mixture was investigated using water content data from Song and Kobayashi [234] for a CO₂-rich vapor mixture containing 5.31 mol% methane. This system has recently been studied by Tsvi-

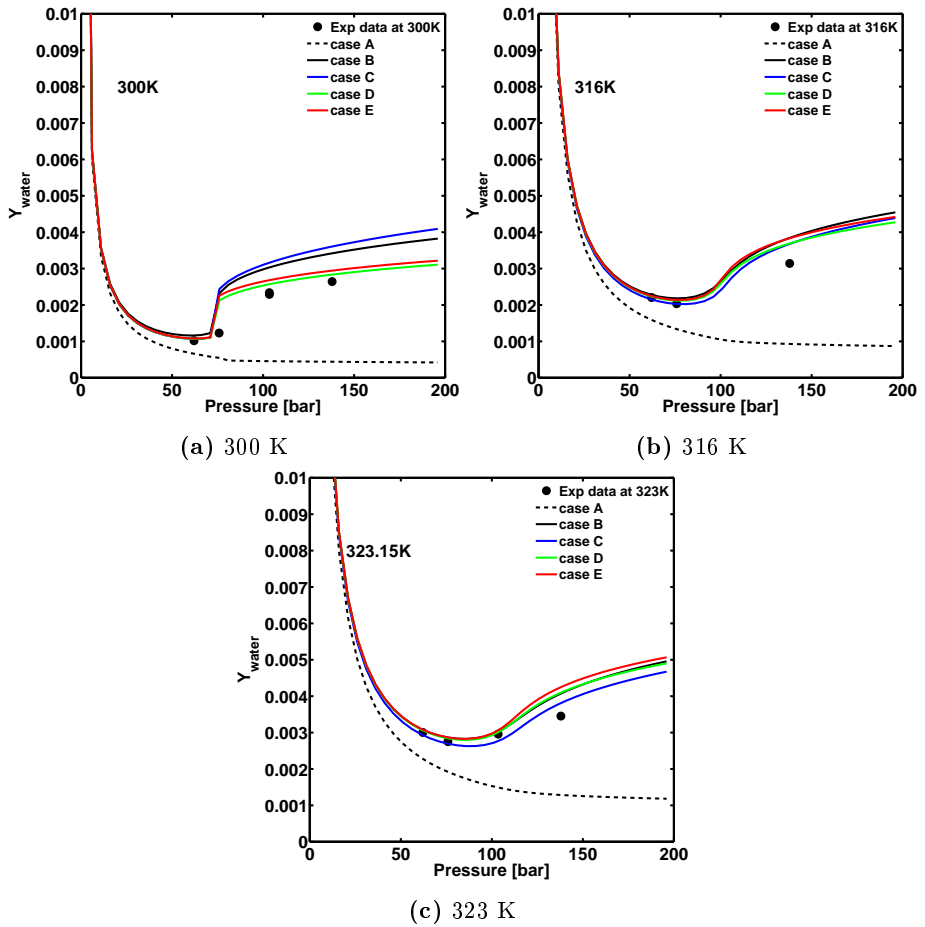


Figure 9.9: Predictions compared to experimental data for the CO_2 -rich phase of the CO_2 + water + methane (5.31mol%) mixture at (a) 300 K (b) 316 K and (c) 323 K. Lines are CPA and qCPA predictions. Circles are experimental data from Ref. [234].

intzels et al. [34] with CPA and Austegard et al. [235] with CPA and SRK/HV. Figure 9.9 shows three predictions of the water content in the vapor phase as a function of pressure. As expected based on the binary CO₂ + water correlation inert CPA fails to predict the minimum in water content of the vapor phase. The predicted behavior is rather similar for the four remaining approaches and they all find, at least qualitatively, the minimum in water content. Cases D and E clearly perform best at 300 K. At higher temperatures case C appears to perform slightly better, but all approaches perform very similarly.

9.3 Dew Point Pressure

The ability of the different approaches for modeling the dew point pressure of two ternary and four quaternary systems was investigated by comparing the predictions with experimental data from Refs. [236–240]. For each system the dew point pressure is calculated for several different compositions in the temperature range 245–290 K. Details of the compositions of these mixtures can be found in Refs. [236–240]. The overall deviations, in terms of %AAD in the dew point pressure, are summarized in table 9.6. With the exception of the CO₂ + methanol + water system, case A (inert CPA) results in overall better dew point predictions than any of the other, more advanced, approaches. The results with cases A–C are almost identical to those obtained by Tsivintzels and Kontogeorgis [35], who arrived at the same conclusion about case A. Cases B–E perform very similarly. It is somewhat surprising, however, that the quadrupolar approaches, cases D and E, perform slightly worse than the other cases except for the CO₂ + water + methane system. The VLE deviations for the CO₂ + water + methane system were shown in table 9.5.

It is not very well understood why inert CPA appears to give more accurate dew point predictions, than the approaches which attempt to account for the interactions between CO₂, and water, and/or alcohols. We may speculate, however, whether the fact, that the concentration of water and methanol in the mixtures is very small may be part of the reason. Another possibility is that the temperature dependence of the binary interaction parameters has been ignored. For instance, if a temperature dependent binary interaction parameter is employed for the binary water + methanol pair the deviations typically decrease by about 2–5% for all approaches. Table 9.7 summarizes the calculated deviations for the dew point pressures when the temperature dependent interaction parameter $k_{\text{H}_2\text{O}-\text{MeOH}} = 0.115 - 60.24/T$ is employed. Note that this linearization has been developed based on equilibrium data in the temperature range 298–473 K, and it is thus assumed that it can be extrapolated to the temperature range of the dew point data. Despite the use of a temperature dependent interaction parameters (and thus an additional binary parameter for the H₂O + methanol subsystem) case A continues to be the overall best approach. It makes little difference for the results if temperature dependent interaction parameters

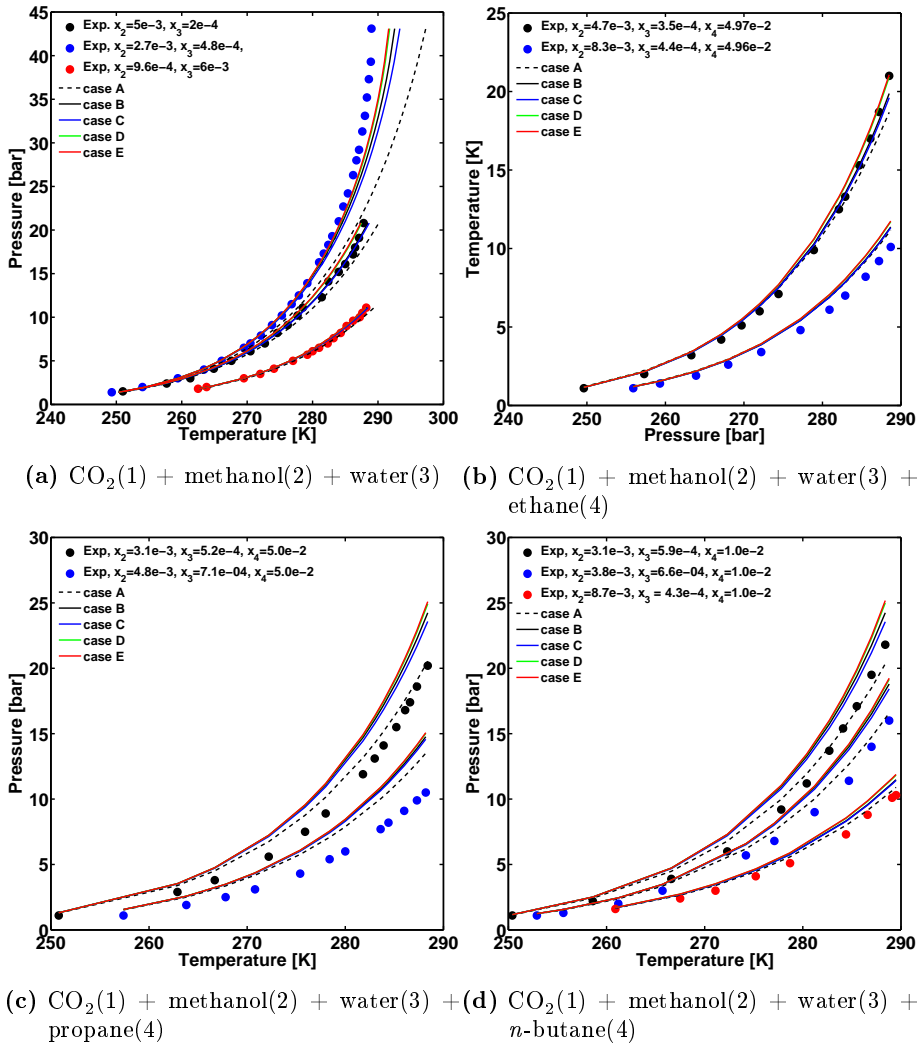


Figure 9.10: Dew point predictions compared to experimental data from Refs. [236, 239, 240] (selected mixtures) for the systems (a) $\text{CO}_2(1) + \text{methanol}(2) + \text{water}(3)$, (b) $\text{CO}_2(1) + \text{methanol}(2) + \text{water}(3) + \text{ethane}(4)$, (c) $\text{CO}_2(1) + \text{methanol}(2) + \text{water}(3) + \text{propane}(4)$, (d) $\text{CO}_2(1) + \text{methanol}(2) + \text{water}(3) + n\text{-butane}(4)$. Symbols are experimental data and the legend indicates the composition of the selected mixtures.

are employed between the other binaries. Typical predictions for four of the mixtures are shown in figure 9.10 for selected compositions of each mixture.

Table 9.6: Deviations between CPA and qCPA predictions and experimental dew point data for the ternary mixtures CO₂ + water + methane, CO₂ + water + methanol and for the quaternary mixtures CO₂ + water + methanol + hydrocarbon (methane, ethane, propane, and *n*-butane). Experimental data from Refs. [236–240]. The temperature range is approximately 245-290 K in all cases.

Mixture	P range [bar]	%AAD in dew point pressure				
		Case A	Case B	Case C	Case D	Case E
CO ₂ + water + methane	1-61	15.5	24.8	22.7	21.5	21.6
CO ₂ + methanol + water	1-44	9.6	7.3	7.2	7.5	7.6
CO ₂ + methanol + water + methane	1-59	22.3	27.6	26.4	27.7	27.9
CO ₂ + methanol + water + ethane	1-22	8.0	11.2	10.6	12.3	12.6
CO ₂ + methanol + water + propane	1-21	22.0	28.8	27.7	31.1	31.6
CO ₂ + methanol + water + <i>n</i> -butane	1-22	14.7	18.9	18.1	19.3	19.5
Average	-	15.4	19.8	18.8	19.9	20.1

Table 9.7: Deviations between CPA and qCPA predictions and experimental dew point data for the ternary mixture CO₂ + water + methanol and for the quaternary mixtures CO₂ + water + methanol + hydrocarbon (methane, ethane, propane, and *n*-butane). Experimental data from Refs. [236, 238–240]. The temperature range is approximately 245-290 K for all systems. A temperature dependent k_{ij} is employed for the binary water + methanol pair ($k_{\text{H}_2\text{O}-\text{MeOH}} = 0.115 - 60.24/T$). Temperature in Kelvin.

Mixture	P range [bar]	%AAD in dew point pressure				
		Case A	Case B	Case C	Case D	Case E
CO ₂ + methanol + water	1-44	10.9	5.7	6.1	5.1	5.2
CO ₂ + methanol + water + methane	1-59	18.2	21.9	20.9	21.8	21.9
CO ₂ + methanol + water + ethane	1-22	7.5	6.5	6.0	7.4	7.5
CO ₂ + methanol + water + propane	1-21	17.6	23.8	22.8	25.5	26.0
CO ₂ + methanol + water + <i>n</i> -butane	1-22	12.0	15.5	14.8	15.8	15.9
Average	-	13.2	14.7	14.1	15.1	15.3

Table 9.8: CPA and qCPA deviations between model predictions and experimental data [241, 242] for the $\text{CO}_2(1) + \text{methanol}(2) + \text{ethane}(3)$ and $\text{CO}_2(1) + \text{water}(2) + 1\text{-propanol}(3)$ VLLE. The temperature and pressure range for the former system is 288-298 K and 38-57 bar and 313.2 K and 83-141 bar for the latter system.

% AAD in	Lower liquid phase			Upper liquid phase			Vapor phase			Average
	x_1	x_2	x_3	x_1	x_2	x_3	y_1	y_2	y_3	
	$\text{CO}_2(1) + \text{methanol}(2) + \text{ethane}(3)$									
Case A	4.9	7.1	8.2	6.8	74.8	8.0	20.4	-	5.0	16.9
Case B	18.2	3.3	4.6	10.2	66.6	6.0	24.2	-	6.1	17.4
Case C	5.4	4.9	5.7	5.9	70.7	7.9	19.0	-	4.7	15.5
Case D	6.1	4.0	5.2	11.5	66.0	5.6	25.4	-	6.5	16.3
Case E	6.0	5.0	5.1	9.7	66.3	6.2	24.2	-	6.0	16.1
	$\text{CO}_2(1) + \text{water}(2) + 1\text{-propanol}(3)$									
Case A	29.2	1.1	34.4	14.2	14.4	9.8	15.5	94.5	89.9	39.3
Case B	11.8	2.3	44.5	10.1	12.9	2.9	14.6	80.8	87.5	29.7
Case C	7.7	2.6	48.0	17.3	11.4	7.7	13.9	76.5	83.8	29.9
Case D	3.3	3.0	48.4	14.9	12.5	1.9	12.9	74.6	75.8	27.5
Case E	3.3	2.6	45.3	8.7	9.4	1.7	14.1	82.2	84.4	28.0

9.4 Vapor Liquid Liquid Equilibrium

As already noted for the $\text{CO}_2 + \text{methanol} + \text{propane}$ equilibria in the previous section, an interesting feature of some ternary mixtures is the formation of a strongly temperature and pressure dependent three-phase vapor-liquid-liquid region. These systems may serve as an even more demanding test of the predictive power of a thermodynamic model than ternary VLEs.

In this section the ability of the modeling approaches for predicting the VLLE of the two ternary mixtures $\text{CO}_2 + \text{methanol} + \text{ethane}$ and $\text{CO}_2 + \text{water} + 1\text{-propanol}$ is investigated using experimental data from Refs [241, 242]. These systems were also studied by Tsivintzelis and Kontogeorgis [35] using, amongst others, approaches A and C of this work. Table 9.8 summarizes, for the two systems, the deviations between predictions and experimental data for the compositions of the three phases in equilibrium.

Overall the predictions for the $\text{CO}_2 + \text{methanol} + \text{ethane}$ system are similar with all five modeling approaches. The model performance is illustrated in figure 9.11 which shows the predicted equilibrium compositions in the three phases at 298 K. The best overall approaches are arguably cases C, D and E. With the exception of the methanol concentration in the upper liquid phase the predictions are generally quite satisfactory. Part of the explanation for the high methanol deviations in the upper liquid phase, however, is the very small methanol concentration which results in high relative errors. There is no experimental data for the amount of methanol in the vapor phase as it was assumed by Hong et al. [241] that the amount of methanol in the vapor phase could be neglected, something which is confirmed by the model predictions.

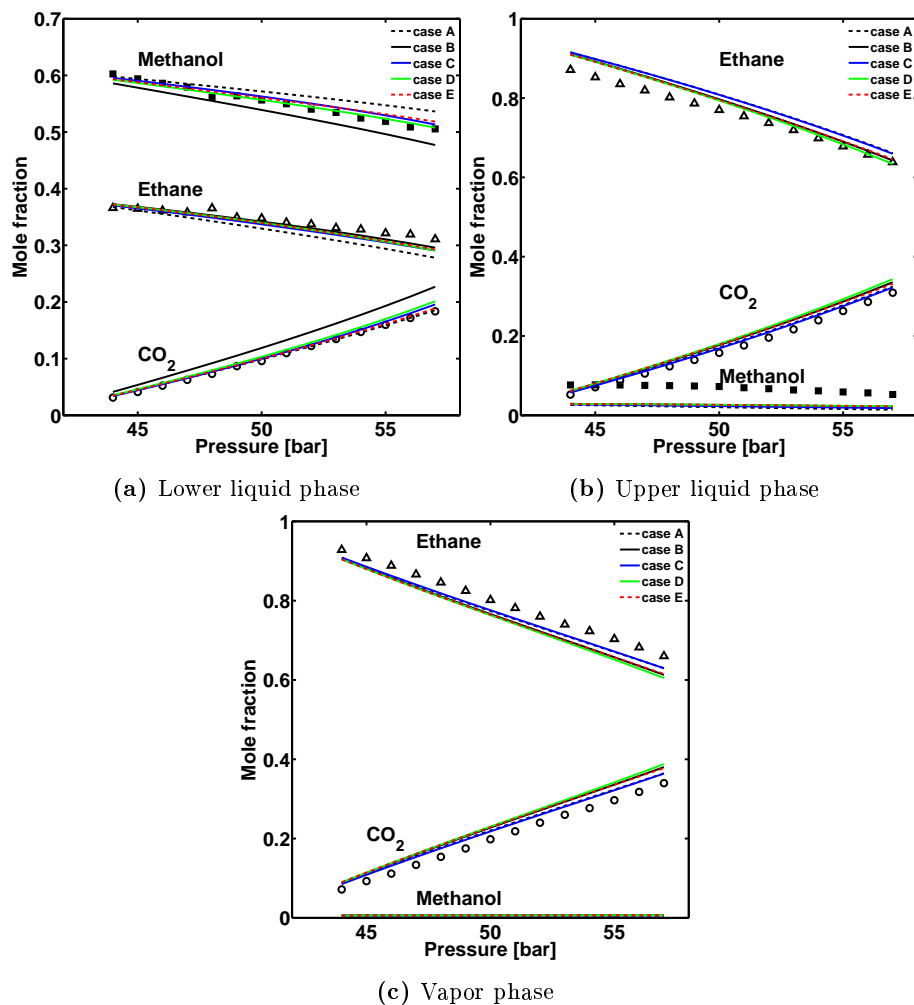


Figure 9.11: VLE predictions compared to experimental data for the CO₂ + methanol + ethane VLE at 298.15 K. Lines are CPA and qCPA predictions. Symbols are experimental data from Ref. [241] ○ CO₂, ■ Methanol, △ Ethane.

If the results for the CO₂ + methanol + ethane system are compared with those obtained by Tsvintzelis and Kontogeorgis [35], it is clear that the predictions in this work are significantly better in the lower liquid phase and similar for the other phases. This is true even for cases A and C, which were employed by Tsvintzelis and Kontogeorgis [35]. The reason for the improvement is that a different value of the interaction parameter is employed for the binary methanol-ethane pair ($k_{\text{MeOH-C}_2} = 0.0204$ rather than $k_{\text{MeOH-C}_2} = 0.05667$ in Ref. [35]).

It is interesting to investigate whether qCPA offers predictive improvements (in the sense that $k_{ij} = 0$) over the CPA approaches for other mixtures than CO₂ + *n*-alkanes. To preliminarily investigate this the VLLE of the CO₂ + methanol + ethane mixture is calculated where all $k_{ij} = 0$. However, without a k_{ij} only qCPA with four parameters (case E) predicts the presence of the VLLE in the whole pressure range. This is of course an improvement in itself, although it makes a direct comparison difficult. As shown in figure 9.12 the predictions with case E are similar to when a binary interaction parameter was employed, except in the lower liquid phase, where the composition of methanol and ethane are captured poorly without a binary interaction parameter. If a methanol-ethane k_{ij} is employed excellent predictions are obtained.

Finally the VLLE of the highly non-ideal CO₂ + water + 1-propanol mixture was investigated. Higher deviations are typically obtained for this system especially for the 1-propanol concentration in the lower liquid phase (around 45%) and for the compositions of water and 1-propanol in the vapor phase (around 80%). In general the two quadrupolar approaches (case D and especially case E) seem to perform slightly better than the CPA approaches, especially for the composition of CO₂ in the various phases.

9.5 Concluding Remarks

This chapter attempted to evaluate and compare the ability of both CPA and the new qCPA for predicting the phase equilibria of multicomponent mixtures containing CO₂, alkanes, water, and/or alcohols. Three approaches were considered for CPA; The base case where CO₂ is modeled as an inert compound (case A), as well as the two approaches recommended by Kontogeorgis and co-workers where CO₂ is modeled either as a solvating compound (case B) or a self-associating compound (case C) [14, 33, 35]. For cases B and C the experimental cross-association energy and two binary parameters (β_{cross} and k_{ij}) are employed for binary pairs of CO₂ and water, or alcohols. qCPA is evaluated with either three or four pure compound parameters for CO₂ (cases D and E) and a single adjustable parameter for each binary system, irrespectively of whether the mixture contains self-associating compounds or not. Cases A, B and C have been employed by Tsvintzelis et al. [35] to several of the mixtures

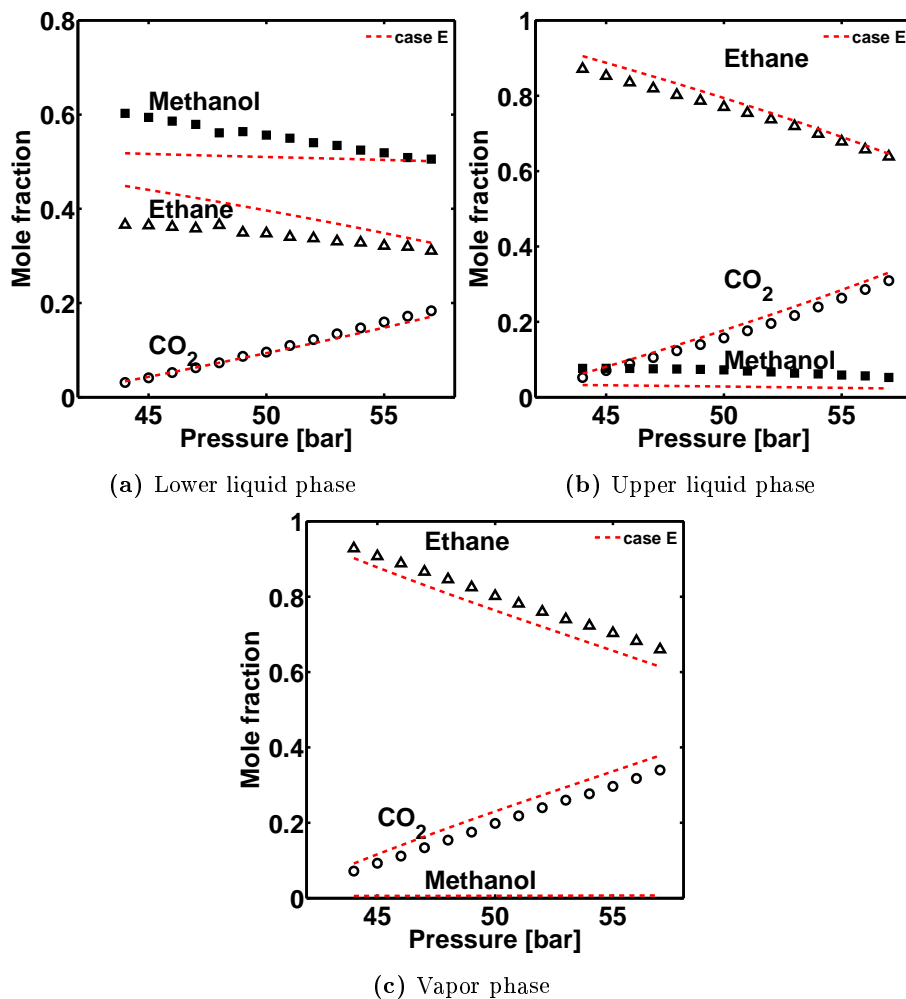


Figure 9.12: VLE predictions with case E, where all $k_{ij} = 0$, compared to experimental data for the CO₂ + methanol + ethane VLE at 298.15 K. Experimental data from Ref. [241] ○ CO₂, ■ Methanol, △ Ethane.

considered in this chapter, although for case B we use two solvation sites for CO₂ rather than one.

The multicomponent CPA and qCPA results are all predictive in the sense that all parameters are based on pure fluid or binary mixture data only. No parameters have been fitted to the ternary or quaternary systems. Systems containing CO₂ and two or more *n*-alkanes were also evaluated without the use of a binary interaction parameter. When interaction parameters are employed the difference between the various model predictions is quite small. This is especially true for cases B-E, for which the predictions rarely differ from each other by more than a few percent.

Somewhat surprisingly case A seems to be the most accurate approach for the dew point predictions. On average case A deviates from the experimental dew point data with about 15% (in terms of %AAD), whereas the other approaches all deviate by around 19-20%. Tsvintzelis and Kontogeorgis [35] came to the same conclusion. It is interesting to note that the deviations can be reduced to about 13% for case A and about 15% for the other approaches if the temperature dependence of the binary water-methanol pair is accounted for. However, this is at the cost of an extra parameter for this binary pair.

VLE and VLLE predictions with case A are typically worse than the other approaches, especially when it comes to predicting the composition of the associating compounds. This is expected, as the approach does not account in any way for the interactions between CO₂ and associating compounds, nor does it take quadrupolar interactions into account. Cases B-E all perform overall satisfactorily, and generally predict the behavior of the multicomponent systems quite well. On a relative scale all models have difficulties predicting the quantitative amount of associating species in the vapor phase. Part of which is due to their typically low concentration in this phase.

qCPA was shown to perform very well for multicomponent mixtures containing CO₂ and *n*-alkanes even without binary interaction parameters, suggesting that the excellent results for binary mixtures obtained in the previous chapter are extensible to multicomponent mixtures. This suggests that qCPA in its four parameter version may be employed for multicomponent mixtures of CO₂ and *n*-alkanes without using any interaction parameters, similar to how SRK or CPA may be employed for multicomponent hydrocarbon mixtures without k_{ij} 's.

While qCPA is definitely among the best approaches for VLE and VLLE the model does, unfortunately, not appear to offer fundamental improvements for the prediction of multicomponent systems compared to CPA approaches B and C, at least not when binary interaction parameters are employed. It is worth noting, however, that qCPA is compared to the, according to Tsvintzelis and Kontogeorgis [35], best CPA approaches, where experimental values of the association energy are employed rather than combining rules and two adjustable parameters are used per CO₂-associating compound pair. When qCPA is em-

ployed the CR-1 mixing rule is used together with a simple approximation for the cross-association volume and with a single binary interaction parameter employed for the binary pairs. Moreover, this interaction parameter is typically significantly smaller, than with the CPA approaches. That is, compared to CPA similar predictions are typically obtained with qCPA, but with fewer adjustable parameters.

For mixtures containing CO₂ and self-associating compounds it essentially seems to be at least as important to account for the induced association between CO₂ and water or alcohols, as to account for the quadrupole moment of CO₂. That is, all successful approaches treat CO₂ as either solvating or self-associating. The effect of the quadrupole is primarily to reduce the value and/or number of interaction parameters.

CHAPTER 10

Conclusion and Future Work

10.1 Conclusion

In this work, in an effort to improve the predictive capabilities of classic thermodynamic models, primarily for mixtures containing CO_2 , the CPA EoS have been extended with an explicit quadrupolar term. The extension is essentially a simplification of a third order perturbation theory for a pure quadrupolar fluid, which have been extended to mixtures. The resulting qCPA can be used with the experimental value of the quadrupole moment and without introducing any additional pure compound parameters. Alternatively a single additional pure compound parameter may be employed. When an additional adjustable parameter is employed it is typically the quadrupolar co-volume, although it is also possible to use the quadrupolar moment itself as an adjustable parameter.

A systematic improvement in the correlation of the saturated liquid density and vapor pressure is observed with qCPA, even when the same number of adjustable parameters are employed in CPA and qCPA. This is particularly true for the strongly quadrupolar CO_2 molecule, but applies to the other investigated quadrupolar compounds as well.

For modeling approaches using more than three adjustable parameters several different parameter sets could be obtained for the same modeling approach. High correlations were observed between the energetic parameters in the quadrupolar model. These observations led to a systematic investigation, which attempted to estimate the uncertainty in the pure compound parameters of CO_2 for several different modeling approaches with CPA and qCPA. The effect of the uncertainties in the pure compound parameters were then quantified

by propagating them to physical properties, VLE, and LLE using Monte Carlo simulations. The analysis indicates that:

- The uncertainty in the pure compound parameters are negligible for modeling approaches which employ three adjustable parameters.
- The uncertainties may be significant for modeling approaches with more than three adjustable parameters.
- The uncertainties are largely due to very high correlations between different parameters, so that a change in one parameter can be compensated by a change in another. For instance the uncertainties in qCPA (four parameters) are largely due to high correlations between the energetic Γ (or a_0) parameter in the SRK term and the volumetric b_0^Q (or effective Q) parameter in the quadrupole term.
- The uncertainties in VLE are much larger when the four parameter version of qCPA is employed than when CPA is employed (even when CO_2 is assumed to be self-associating). On the other hand, the highly temperature dependent properties such as C_V are very uncertain with self-associating CPA. This clearly illustrates that different models are sensitive to different output properties.
- The parametrization of (similar) multi-parameter models are at least as important as the model term itself. It may thus be very difficult to objectively compare two similar models, as the extent to which the predictions from one model is better than the predictions from another may have less to do with an inability of the model to structurally represent the data, and more to do with that particular parameter set.
- Simple parameter estimation procedures based only on pure compound data and least squares estimation may be insufficient for models which incorporate a quadrupole or dipole term.

These conclusions are rigorously only valid for CO_2 and the investigated modeling approaches. However, as other quadrupolar and polar terms are structurally similar to each other, and since SAFT employs the same association term as CPA, one may suspect the conclusion can be extrapolated to other models such as SAFT and its quadrupolar variants.

The new model was extensively evaluated and compared to the non-modified CPA for its ability to predict the thermodynamic properties of pure CO_2 both in the saturation region, the compressed liquid region and in the critical region. The model was subsequently employed to predict and correlate binary VLE and LLE of mixtures containing CO_2 and n -alkanes, water, alcohols, or selected quadrupolar compounds. Finally qCPA have been applied to predict the VLE and VLLE of multicomponent mixtures containing CO_2 and alcohols, water,

and/or n -alkanes. In next to all cases the model is compared to several other CPA approaches.

The predictions of pure compound properties with qCPA are satisfactory but similar to other CPA approaches. For binary mixtures all qCPA approaches appear to offer systematically improved predictions ($k_{ij} = 0$) and correlations (smaller k_{ij}) compared to the cases where quadrupolar interactions are ignored. This improvement is particularly pronounced when mixtures of CO₂ and hydrocarbons are considered, where the four parameter version of the model is almost fully predictive, both for binary and ternary mixtures. However, there are several challenges for mixtures containing CO₂ + another quadrupolar compound. For some of these mixtures qCPA is clearly an improvement, while for other mixtures the performance is down-heartening. It was shown that the originally proposed mixing rules were insufficient for mixtures containing two opposite quadrupoles such as the CO₂ + acetylene mixture, and improvements have been suggested (see chapter 8).

For multicomponent mixtures qCPA were compared to the CPA approaches which Kontogeorgis and co-workers have found to perform best (see discussion in chapters 3 and 9), despite the fact that these approaches typically employ two parameters per binary compound, whereas qCPA only employs one. It was found, that the difference between the various modeling approaches, was very small when binary interaction parameters were employed, even though qCPA uses fewer binary parameters. If binary interaction parameters are ignored for ternary mixtures of CO₂ + n -alkane systems significantly better predictions are obtained with qCPA than with CPA.

Whether qCPA should be investigated further in the future depends very much on the point of view. On the one hand the model certainly improves the phase equilibrium predictions and correlations (smaller or even zero k_{ij}) for several mixtures, both those containing associating compounds but especially those containing hydrocarbons. In the process it typically employs both fewer pure compound parameters and fewer binary parameters. On the other hand, there is little to no improvement in the predicted pure compound properties, the cross-quadrupolar interactions are not well understood and, although the interaction parameters are smaller with qCPA, the quality of the correlations are essentially the same with or without the quadrupolar term. Finally there is little to no improvement in multicomponent predictions at least not when a k_{ij} is employed.

In conclusion, the results certainly indicate, that descriptions of the phase behavior of mixtures containing CO₂ are improved with qCPA compared to CPA. In particular in the sense that the model becomes significantly more predictive. That is, despite a few limitations, the model seem to be a step forward compared to CPA. However, the model does not seem to offer any fundamental improvements that larger binary interaction parameter cannot account for.

10.2 Future Investigations

Despite the overall consistent improvements obtained in almost all cases with qCPA compared to CPA there are several aspects which could be investigated further, to improve both the understanding and the accuracy of the model for phase equilibrium calculations.

10.2.1 Future applications

There are a large number of binary and ternary mixtures, for which the phase behaviour could be studied with qCPA. The general applicability of qCPA for quadrupolar compounds other than CO₂ have only been investigated very sparingly, and almost exclusively for mixtures containing CO₂ + another quadrupolar compound. The performance of qCPA for these mixtures were found to be somewhat erratic. It remains to be seen, however, whether this is due to the complex nature of the quadrupole-quadrupole interaction or a failure of the model for other quadrupolar compounds.

The approximation suggested by Kleiner and Sadowski for the cross-association between CO₂ and a self-associating compound which have been employed in qCPA seem to work fairly well. However, a more fair comparison of CPA and qCPA would probably be to compare the phase equilibrium calculations of qCPA with those of CPA, where CO₂ is modeled as a solvating compound using in both cases the same approximation for the cross-association. This was partly illustrated in figure 8.15 for the CO₂ + water system, indicating that equally good correlations, can be obtained with CPA if this approximation is employed, although with a higher binary interaction parameter.

Alternatively experimental values for the association energy could also be employed in qCPA (as Tsvintzelis et al. [14] suggested for CPA). Unfortunately this results in a plethora of possible combinations for the values of the k_{ij} and β_{cross} which all correlate the phase behavior of CO₂ + alcohol systems very well. On the other hand there are indications (see Ref. [14]) that this approach gives a less temperature dependent k_{ij} for the CO₂ + water system, due to the intricate balance between ϵ_{cross} and β_{cross} in Eq. (3.11).

Of particular interest to the parent FTP project *CO₂-Hydrates - Challenges and Possibilities* are components which may act as promoters for the formation of gas hydrates, such as cyclopentane and tetrahydrofuran. Whereas alcohols, which act as inhibitors, have already been studied. Given the positive results for *n*-alkanes, there is little doubt that qCPA should improve the predictions for CO₂ + cyclic alkanes as well.

Treating both cyclopentane and CO_2 as non-associating compounds with CPA Herslund et al. [243] modeled the VLE between the two compounds. However, the authors found the predictions with CPA to be poor, and that a high binary interaction parameter was needed to correlate the system. To briefly illustrate how accounting for the quadrupolar interactions of CO_2 may improve the capabilities of the CPA for cyclic alkanes, figure 10.1 show the predicted VLE between CO_2 + cyclopentane at a single temperature using qCPA and inert CPA. To correlate the VLE a small k_{ij} of 0.06 and 0.025 is needed for qCPA with three and four parameters respectively, whereas a large k_{ij} of about 0.15 is needed with CPA.

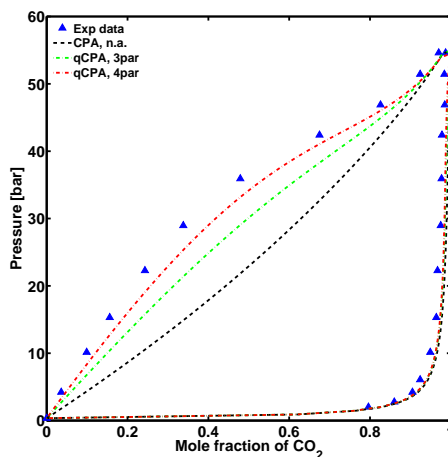


Figure 10.1: Prediction ($k_{ij} = 0$) of the CO_2 + cyclopentane VLE at 293 K using inert CPA and qCPA with three or four adjustable parameters. The predictions are compared with experimental data from Ref. [244].

To evaluate the performance of qCPA for hydrate calculations the model should be incorporated into a van der Waals-Platteeuw hydrate model [245, 246] using for instance Kihara potentials or the Parrish and Prausnitz [247] method to estimate the Langmuir adsorption coefficient in the model. However, as CPA and qCPA perform almost identically for the prediction of multicomponent mixtures when a binary interaction parameter is employed, no appreciable difference between the two models is expected for hydrate calculations, especially considering that the additional hydrate parameters, which are fitted to the pure gas hydrate, may partially compensate for any differences. In a recent PhD thesis Herslund successfully employed the CPA together with the van der Waals-Platteeuw hydrate model [12].

10.2.2 Parameter estimation and uncertainty

In terms of the quadrupolar model the parametrization scheme for the (four parameter) model should be improved as the uncertainties in the parameters are so large, that the differences observed when two similarly structured models are compared may be entirely due to uncertainties in the parameters. Any model improvement may thus be partially obscured by uncertainty in the parameters. If this is not adequately dealt with, it may be almost impossible to evaluate whether a change in the model results in improvements or not. Alternatively the model should only be considered in a three parameter version.

The techniques developed for estimating the pure compound uncertainties and the propagated errors of CO_2 are quite general and applicable to any molecule, however, it may be that the high uncertainties are specific to CO_2 due to its short saturation curve. It would be enlightening to apply the methods to the other quadrupolar molecules for which four parameters have been estimated (either b^Q or Q itself) as well as for a molecule with five parameters such as water, where a substantial number of the many parameter sets suggested in the literature might be explained based on uncertainties in the parameters.

10.2.3 Improvements to qCPA

Following the approximation introduced by Karakatsani et al. [31] the correlation integrals presented in the original quadrupolar terms were truncated in qCPA. However, despite the excellent results obtained in this work, and those by Economou and co-workers for tPC-PSAFT, the approximation may be viewed as rather crude. Moreover the framework of the proposed qCPA is somewhat simplistic, in that it is based on a truncated quadrupolar term derived for a pure hard sphere fluid. It is possible that the base model can be improved if the full polynomial fits to the correlation integrals are employed or if a somewhat more involved quadrupolar term developed directly for mixtures is employed, such as that proposed by Gubbins and Twu [94, 95].

However, to justify the increased complexity caused by the introduction of these terms, the modified and the original models must be compared. Such a comparison, however, may be partially clouded by the identifiability issues observed for the pure compound parameters, and may only be meaningful in the three parameter case. However even in this case the approximate relation between the molecular volume and the co-volume may potentially cloud the conclusions.

Although not directly discussed in the thesis it was found that choosing a proper conversion scheme between the molecular volume and the co-volume is crucial; If the original definition of the co-volume is employed the effect of the quadrupole is negligible, whereas the quadrupole effect is of a much more adequate magnitude when Eq. (5.11) is employed. This may suggest that the approximation for the

co-volume may be improved further if a different conversion scheme is chosen. For instance several authors use a ratio between the hard-core volume and the free volume of 1.5-1.7 [8], whereas this ratio is two in the approximation used. A better value for this parameter may be found by investigating its effect on mixtures containing e.g. hydrocarbons and different quadrupolar compounds.

Dipole and dipole-quadrupole interactions are ignored in the current model, which may be the reason for the poor CO₂ + acetone results. To improve these predictions it may be necessary to explicitly account for such terms in the model. However, accounting for the dipole moment of self-associating molecules may have a detrimental effect on the predictions. In fact several authors choose to ignore the dipole moment of self-associating compounds.

The description of mixtures with more than one quadrupolar component may be problematic in certain cases. This may be due the fact that the cross-interaction between different quadrupolar molecules results in different preferred orientations compared to the pure compound, which may not be adequately modeled by the simple cross-quadrupolar mixing terms. On the other hand, the results may indicate that the description of the cross-quadrupolar interactions may be improved if the quadrupole moment is fitted rather than the quadrupole volume.

This furthermore begs the questions of whether qCPA really can be successfully employed with the experimental quadrupole moment and without an additional adjustable parameter? Certainly this approach seem satisfactory for CO₂ (at least qualitatively), but the predictions for several of the other quadrupolar fluids in mixtures with CO₂ may indicate that an adjustable parameter *is* needed, moreover it may be that this parameter should be related more to the quadrupole moment than the volume parameter. To investigate this more fairly the predictions with the quadrupolar compound should first be evaluated for simple mixtures, e.g. with hydrocarbons.

APPENDIX A

PhD Activities

A.1 List of Publications

Publications, as first or second author, in international peer-reviewed journals:

- M.G. Bjørner, A. Shapiro, G.M. Kontogeorgis., Potential Theory of Adsorption for Associating Mixtures: Possibilities and Limitations., *Industrial & Engineering Chemistry Research* (2013), 52, 2672-2684.
- S. Bartholdy, M.G. Bjørner, E. Solbraa, A. Shapiro, G.M. Kontogeorgis., Capabilities and Limitations of Predictive Engineering Theories for Multicomponent Adsorption., *Industrial & Engineering Chemistry Research* (2013), 52, 11552-11563.
- M.G. Bjørner, G.M. Kontogeorgis., Modeling derivative properties and binary mixtures with CO₂ using the CPA and the quadrupolar CPA equations of state., *Fluid Phase Equilibria* (2016) 408, 151-169.
- M.G. Bjørner, G. Sin, G.M. Kontogeorgis., Uncertainty analysis of the CPA and a quadrupolar CPA equation of state - with emphasis on CO₂., *Fluid Phase Equilibria* (2016) 414, 29-47.
- M.G. Bjørner, G.M. Kontogeorgis., Modelling the phase equilibria of multicomponent mixtures containing CO₂, alkanes, water and/or alcohols using the quadrupolar CPA equation of state., submitted to *Molecular Physics* (December 2015).

The two first publications were written during the PhD but over results from the master's thesis of the author and that of S. Bartholdy and are not part of the material presented in this work.

Publications in popular Danish journals:

- M.G. Bjørner, A. Schlaikjer, G.M. Kontogeorgis., Nye udviklinger i CPA modellen, Dansk Kemi, 10, October, 2015. (English translation of title: New developments in the CPA model)

A.2 Contributions at Conferences

A.2.1 International conferences

- M.G. Bjørner, G.M. Kontogeorgis, An Engineering Equation of State Contribution for Quadrupolar Fluids (**Poster**), Thermodynamics 2013, Manchester, The United Kingdom, Sept. 3-6, 2013.
- M.G. Bjørner, G. Sin, G.M. Kontogeorgis, Uncertainty analysis and derivative properties in advanced equations of state (**Oral, Poster**), SAFT 2014, Tróia, Portugal, April 22-24, 2014.
- M.G. Bjørner, G.M. Kontogeorgis, Utilization of derivative properties for the estimation of pure compound parameters of CO₂ (**Oral**), ESAT 2014, Eindhoven, The Netherlands, July 6-9, 2014.
- M.G. Bjørner, G.M. Kontogeorgis, Evaluation of the quadrupolar CPA EoS for modeling multicomponent CO₂-mixtures (**Oral**), Thermodynamics 2015, Copenhagen, Denmark, Sept. 15-18, 2015.

A.2.2 Internal conferences

- M.G. Bjørner, S. Bartholdy, A.A. Shapiro, G.M. Kontogeorgis, Modeling of Adsorption on Molecular Sieves and Silica Gel using the Potential Adsorption Theory **Poster**, CERE Annual Discussion Meeting, Hillerød, Denmark, June 13-15, 2012.
- M.G. Bjørner, G.M. Kontogeorgis, A. Mohammadi, CO₂ Hydrates - Challenges and Possibilities (**Poster**), CERE Annual Discussion Meeting, Hillerød, Denmark, June 13-15, 2012.
- M.G. Bjørner, G.M. Kontogeorgis, Quadrupolar terms for equations of state (**Oral**), CERE Annual Discussion Meeting, Snekkersten, Denmark, June 19-21, 2013.

- M.G. Bjørner, G.M. Kontogeorgis, Modeling of CO₂ using a Quadrupolar CPA **Oral**, CERE Annual Discussion Meeting, Snekkersten, Denmark, June 25-27, 2014.
- M.G. Bjørner, G.M. Kontogeorgis, Uncertainties in the parameters of advanced equations of state **Poster**, CERE Annual Discussion Meeting, Snekkersten, Denmark, June 17-19, 2015.
- M.G. Bjørner, G.M. Kontogeorgis, Uncertainty analysis and derivative properties for parameter estimation with CPA and qCPA **Poster**, CERE Annual Discussion Meeting, Snekkersten, Denmark, June 25-27, 2014.
- M.G. Bjørner, G.M. Kontogeorgis, Modeling of CO₂ using CPA and quadrupolar CPA: Uncertainties and Phase equilibria **Oral**, CERE Annual Discussion Meeting, Snekkersten, Denmark, June 17-19, 2015.
- M.G. Bjørner, P.L. Fosbøl, K. Thomsen, Evaluation and improvement of wet gas venturi meter correlations **Poster**, CERE Annual Discussion Meeting, Snekkersten, Denmark, June 17-19, 2015.

A.3 Attended Courses

- Thermodynamic Models, Fundamentals and Computational Aspects (2012).
- Statistical Thermodynamics for Chemical Engineering (2012).
- Optimization and Data Fitting (2012).
- Uncertainty and Sensitivity Analysis of Numerical Models (2013).
- Advances in Chemical and Biochemical Engineering (2014).
- Teaching and Learning (2015).

A.4 Teaching and Organization

- Teaching assistant in Introduction to Chemistry and Chemical Engineering (2012, 2013) + development and reporting of solutions to exercises.
- Organizer/Coordinator of PetroChallenge Denmark¹ (2013, 2014).
- Guest Lecturer in Applied Colloid and Surface Chemistry (2013, 2015).

¹PetroChallenge is an international online competition for high school students. The purpose of the competition is to use a simulations tool (OilSim) to find and exploit oil reservoirs. During the event the teachers are instructed in the simulation tool at DTU and the students visit DTU as part of an education day. The event has about 1600 participants.

APPENDIX **B**

Derivatives of the Reduced Residual Helmholtz Energy

All thermodynamic properties from a model may be calculated from the partial derivatives of the (reduced) residual Helmholtz energy (Eq. (B.1)) of the model with respect to the characteristic state variables (T, V, \mathbf{n})

$$F = \frac{A^r(T, V, \mathbf{n})}{RT} = \frac{A^r(T, V, \mathbf{n})}{N_A kT} \quad (\text{B.1})$$

The purpose of this appendix is to illustrate how the partial derivatives of the reduced residual Helmholtz energy of the quadrupolar term may be calculated. The necessary derivatives for the SRK term and the association term can be found in Refs. [54, 62, 63]. To calculate the derivatives we shall follow a modular procedure as recommended in the book by Michelsen and Mollerup (2007) [54]. This procedure is briefly presented in the first section to facilitate the presentation in the following sections of this appendix.

B.1 Partial Derivatives

Let the general form of equation (B.1) be

$$F = F(n, T, V, \mathbf{M}) \quad (\text{B.2})$$

where n is the total number of moles, T the temperature, and V the total volume. \mathbf{M} represents a vector of explicit functions of the temperature, the total volume and the mole numbers \mathbf{n} .

First order derivatives

The derivatives of any function $F(\mathbf{u})$ with respect to y at constant \mathbf{x} can be calculated using the multidimensional chain rule [54]

$$\left(\frac{\partial F}{\partial y}\right)_{\mathbf{x}} = \sum_k \left(\frac{\partial F}{\partial u_k}\right)_{u_m} \left(\frac{\partial u_k}{\partial y}\right)_{\mathbf{x}} = \sum_k F_{u_k} \left(\frac{\partial u_k}{\partial y}\right)_{\mathbf{x}} \quad (\text{B.3})$$

where $u_m \neq u_k$. The vectors \mathbf{u} and \mathbf{x} may have some elements in common. By application of eq. (B.3) it is straightforward to show that the first order derivatives wrt. the mole numbers, temperature and volume are

$$\left(\frac{\partial F}{\partial n_i}\right)_{T,V} = F_n + F_M \mathbf{M}_i \quad (\text{B.4})$$

$$\left(\frac{\partial F}{\partial T}\right)_{V,\mathbf{n}} = F_T + F_M \mathbf{M}_T \quad (\text{B.5})$$

$$\left(\frac{\partial F}{\partial V}\right)_{T,\mathbf{n}} = F_V + F_M \mathbf{M}_V \quad (\text{B.6})$$

where

$$\mathbf{M}_y = \sum_i \left(\frac{\partial F}{\partial M^i}\right)_{u_m} \left(\frac{\partial M^i}{\partial y}\right)_{\mathbf{x}} \quad (\text{B.7})$$

where $M^i \neq u_m$ and M^i denotes the i 'th element in the vector M .

Second order derivatives

The general expression for the second order derivative of F with respect to y and z at constant \mathbf{x} is [54]

$$\begin{aligned} \left(\frac{\partial^2 F}{\partial y \partial z}\right)_{\mathbf{x}} &= \sum_k \sum_l \left(\frac{\partial^2 F}{\partial u_k \partial u_l}\right)_{u_m} \left(\frac{\partial u_k}{\partial y}\right)_{\mathbf{x}} \left(\frac{\partial u_l}{\partial z}\right)_{\mathbf{x}} \\ &+ \sum_k \left(\frac{\partial F}{\partial u_k}\right)_{u_m} \left(\frac{\partial^2 u_k}{\partial y \partial z}\right)_{\mathbf{x}} \\ &= \sum_k \sum_l F_{u_k u_l} \left(\frac{\partial u_k}{\partial y}\right)_{\mathbf{x}} \left(\frac{\partial u_l}{\partial z}\right)_{\mathbf{x}} + \sum_k F_{u_k} \left(\frac{\partial^2 u_k}{\partial y \partial z}\right)_{\mathbf{x}} \end{aligned} \quad (\text{B.8})$$

where again $u_k \neq u_m$ and $u_l \neq u_m$. From eq. (B.8) the second order derivatives may be determined in a similar manner as the first order derivatives.

B.2 Derivatives of the Padé approximation

Almost every multipolar (dipolar and quadrupolar) term suggested in the literature, including the one considered in this work, are set in the form of a Padé approximation of the Helmholtz energy or the reduced residual Helmholtz energy function. It is thus convenient to have general expressions for the first and second order partial derivatives of the Padé approximation, in terms of the two and three body terms and their derivatives.

The generic form of the Padé approximation in terms of the reduced residual Helmholtz energy is

$$F(\mathbf{u}) = \frac{F_2(\mathbf{u})}{1 - F_3(\mathbf{u})/F_2(\mathbf{u})} \quad (\text{B.9})$$

where $\mathbf{u} = (n, T, V, \mathbf{M})$. For brevity we shall write $F_2(\mathbf{u})$ and $F_3(\mathbf{u})$ simply as F_2 and F_3

First order derivatives

Using classical rules of differentiation it is straightforward to show that the partial derivatives of $F(\mathbf{u})$ wrt. to u_k at constant u_m , where $u_k \neq u_m$ is

$$\begin{aligned} \left(\frac{\partial F}{\partial u_k} \right)_{u_m} = F_{u_k} &= \frac{(1 - F_{32}) F_{2u_k} + F_2 F_{32u_k}}{(1 - F_{32})^2} \\ &= \frac{F_2 (F_2 F_{2u_k} - 2F_3 F_{2u_k} + F_2 F_{3u_k})}{(F_2 - F_3)^2} \end{aligned} \quad (\text{B.10})$$

where F_{32} and F_{32u_k} are respectively

$$F_{32} = F_3/F_2 \quad (\text{B.11})$$

$$\left(\frac{\partial (F_3/F_2)}{\partial u_k} \right)_{u_m} = F_{32u_k} = \frac{F_{3u_k} F_2 - F_3 F_{2u_k}}{F_2^2} \quad (\text{B.12})$$

Second order derivatives

Let $g = (1 - F_{32})$, $f = F_{2u_k}$, and $h = F_2 F_{32u_k}$. The second order derivatives wrt. u_k and u_l at constant u_m where $u_m \neq u_l, u_k$, are then given by

$$\begin{aligned} \left(\frac{\partial^2 F}{\partial u_l \partial u_k} \right)_{u_m} &= \left(\frac{\partial}{\partial u_l} \left(\frac{f}{g} - \frac{h}{g^2} \right) \right)_{u_m} \\ &= \frac{g \left(\frac{\partial f}{\partial u_l} \right)_{u_m} - f \left(\frac{\partial g}{\partial u_l} \right)_{u_m}}{g^2} + \frac{g^2 \left(\frac{\partial h}{\partial u_l} \right)_{u_m} - h \left(\frac{\partial g^2}{\partial u_l} \right)_{u_m}}{g^4} \end{aligned} \quad (\text{B.13})$$

where

$$\left(\frac{\partial f}{\partial u_l} \right)_{u_m} = \left(\frac{\partial F_2}{\partial u_k \partial u_l} \right)_{u_m} = F_{2u_k u_l} \quad (\text{B.14})$$

$$\left(\frac{\partial g}{\partial u_l} \right)_{u_m} = - \left(\frac{\partial F_{32}}{\partial u_l} \right)_{u_m} = -F_{32u_l} \quad (\text{B.15})$$

$$\left(\frac{\partial g^2}{\partial u_l} \right)_{u_m} = -2F_{32u_l} g \quad (\text{B.16})$$

$$\left(\frac{\partial h}{\partial u_l} \right)_{u_m} = F_{2u_l} F_{32u_k} + F_2 F_{32u_k u_l} \quad (\text{B.17})$$

and

$$\begin{aligned} \left(\frac{\partial^2 F_{32}}{\partial u_l \partial u_k} \right)_{u_m} &= \left(\frac{\partial}{\partial u_l} \left(\frac{F_{3u_k} F_2 - F_3 F_{2u_k}}{F_2^2} \right) \right)_{u_m} \\ &= \frac{F_2 F_{3u_k u_l} - F_{3u_k} F_{2u_k}}{F_2^2} - \frac{F_2^2 \left(\frac{\partial m}{\partial u_l} \right)_{u_m} - 2m F_2 F_{2u_l}}{F_2^4} \end{aligned} \quad (\text{B.18})$$

where $m = F_3 F_{2u_k}$ and

$$\left(\frac{\partial m}{\partial u_l} \right)_{u_m} = F_{3u_l} F_{2u_l} + F_3 F_{2u_k u_l} \quad (\text{B.19})$$

Which gives all necessary variables in terms of F_2, F_3 and their derivatives.

B.3 Relevant Derivatives of qCPA

The expressions developed in section B.2 are quite general for any multipolar model employing the Padé approximation. To calculate derivatives of the quadrupolar term specific to this work is necessary to calculate the partial

derivatives of the second and third order contributions to the reduced residual Helmholtz energy as required by Eq. (B.10) and Eq. (B.13).

Using the definition of the reduced residual Helmholtz energy in Eq. (B.2) the second and third order contributions to the quadrupolar term as presented in chapter 5 may be written as

$$F_2(T, V, n, \Theta_2) = c_1 \frac{N_A}{V (k_b T)^2} \Theta_2(\mathbf{n}) \quad (\text{B.20})$$

$$F_{3,2}(T, V, n, \Theta_{3,2}) = c_2 \frac{N_A}{V (k_b T)^3} \Theta_{3,2}(\mathbf{n}) \quad (\text{B.21})$$

$$F_{3,3}(T, V, n, \Theta_{3,3}) = c_3 \frac{N_A^2}{V^2 (k_b T)^3} \Theta_{3,3}(\mathbf{n}) \quad (\text{B.22})$$

and

$$F_3(T, V, n, \Theta_{3,2}, \Theta_{3,3}) = F_{3,2}(T, V, n, \Theta_{3,2}) + F_{3,3}(T, V, n, \Theta_{3,3}) \quad (\text{B.23})$$

where the full model is set in a Padé approximation as given by Eq. (B.12), c_1 , c_2 , and c_3 are constants, \mathbf{M} is a vector of explicit functions; $\mathbf{M} = \{\Theta_2, \Theta_{3,2}, \Theta_{3,3}\}$ where Θ_2 , $\Theta_{3,2}$ and $\Theta_{3,3}$ are functions of the mole numbers and are given by:

$$\Theta_2(\mathbf{n}) = \sum_i^{nc} n_i \sum_j^{nc} n_j \frac{Q_{ij}^4}{\sigma_{ij}^7} I_{10}^{HS} \quad (\text{B.24})$$

$$\Theta_{3,2}(\mathbf{n}) = \sum_i^{nc} n_i \sum_j^{nc} n_j \frac{Q_{ij}^6}{\sigma_{ij}^{12}} I_{15}^{HS} \quad (\text{B.25})$$

$$\Theta_{3,3}(\mathbf{n}) = \sum_i^{nc} n_i \sum_j^{nc} n_j \sum_k^{nc} n_k \frac{Q_{ijk}^6}{\sigma_{ij}^3 \sigma_{ik}^3 \sigma_{jk}^3} I_{TQ}^{HS} \quad (\text{B.26})$$

where I_n and I_{TQ} are correlation integrals. In the original work by Larsen et al. [27] these integrals are approximated by density polynomials. In this work, however, the polynomials were truncated at the zeroth order term (see Eqs. (5.8a)-(5.8b)). That is, the correlation functions are essentially three constants.

To calculate the appropriate partial derivatives of the reduced residual Helmholtz energy F_2 , $F_{3,2}$ and $F_{3,3}$ are differentiated with respect to their model variables and the derivatives of the mixture parameters Θ_2 , $\Theta_{3,2}$ and $\Theta_{3,3}$ are evaluated. This results in a set of derivatives independent on the chosen mixing term and a set of mixing derivatives independent on the other terms [54].

The (non-zero) first order partial derivatives of F_2 , $F_{3,2}$ and $F_{3,3}$ are

$$F_{2,V} = -\frac{c_1 N_A}{(V k_b T)^2} \Theta_2 \quad (\text{B.27})$$

$$F_{3,2,V} = -\frac{c_2 N_A}{V^2 (k_b T)^3} \Theta_{3,2} \quad (\text{B.28})$$

$$F_{3,3,V} = -\frac{2c_3 N_A^2}{(V k_b T)^3} \Theta_{3,3} \quad (\text{B.29})$$

$$F_{2,T} = -\frac{2c_1 N_A}{V k_b^2 T^3} \Theta_2 \quad (\text{B.30})$$

$$F_{3,2,T} = -\frac{3c_2 N_A}{V k_b^3 T^4} \Theta_{3,2} \quad (\text{B.31})$$

$$F_{3,3,T} = -\frac{3c_3 N_A^2}{V^2 k_b^3 T^4} \Theta_{3,3} \quad (\text{B.32})$$

$$F_{2,\Theta_2} = \frac{c_1 N_A}{V (k_b T)^2} \quad (\text{B.33})$$

$$F_{3,2,\Theta_{3,2}} = \frac{c_2 N_A}{V (k_b T)^3} \quad (\text{B.34})$$

$$F_{3,3,\Theta_{3,3}} = \frac{c_3 N_A^2}{V^2 (k_b T)^3} \quad (\text{B.35})$$

The (non-zero) second order partial derivatives of F_2 , $F_{3,2}$ and $F_{3,3}$ are

$$F_{2,VV} = \frac{2c_1 N_A}{V^3 (k_b T)^2} \Theta_2 \quad (\text{B.36})$$

$$F_{3,2,VV} = \frac{2c_2 N_A}{(V k_b T)^3} \Theta_{3,2} \quad (\text{B.37})$$

$$F_{3,3,VV} = \frac{6c_3 N_A^2}{V^4 (k_b T)^3} \Theta_{3,3} \quad (\text{B.38})$$

$$F_{2,TT} = \frac{6c_1 N_A}{V k_b^2 T^4} \Theta_2 \quad (\text{B.39})$$

$$F_{3,2,TT} = \frac{12c_2 N_A}{V k_b^3 T^5} \Theta_{3,2} \quad (\text{B.40})$$

$$F_{3,3,TT} = -\frac{12c_3 N_A^2}{V^2 k_b^3 T^5} \Theta_{3,3} \quad (\text{B.41})$$

$$F_{2,TV} = \frac{2c_1 N_A}{(V k_b)^2 T^3} \Theta_2 \quad (\text{B.42})$$

$$F_{3,2,TV} = \frac{3c_2 N_A}{V^2 T^4 k_b^3} \Theta_{3,2} \quad (\text{B.43})$$

$$F_{3,3,TV} = \frac{6c_3 N_A^2}{(V k_b)^3 T^4} \Theta_{3,3} \quad (\text{B.44})$$

$$F_{2,T\Theta_2} = -\frac{2c_1 N_A}{V k_b^2 T^3} \quad (\text{B.45})$$

$$F_{3,2,T\Theta_{3,2}} = -\frac{3c_2 N_A}{V k_b^3 T^4} \quad (\text{B.46})$$

$$F_{3,3,T\Theta_{3,3}} = -\frac{3c_3 N_A^2}{V^2 k_b^3 T^4} \quad (\text{B.47})$$

$$F_{2,V\Theta_2} = -\frac{c_1 N_A}{(V k_b T)^2} \quad (\text{B.48})$$

$$F_{3,2,V\Theta_{3,2}} = -\frac{c_2 N_A}{V^2 (k_b T)^3} \quad (\text{B.49})$$

$$F_{3,3,V\Theta_{3,3}} = -\frac{2c_3 N_A^2}{(V k_b T)^3} \quad (\text{B.50})$$

The (non-zero) partial derivatives of Θ_2 , $\Theta_{3,2}$ and $\Theta_{3,3}$ are

$$\Theta_{2,i} = 2 \sum_j^{nc} n_j \frac{Q_{ij}^4}{\sigma_{ij}^7} I_{10}^{HS} \quad (\text{B.51})$$

$$\Theta_{2,ij} = 2 \frac{Q_{ij}^4}{\sigma_{ij}^7} I_{10}^{HS} \quad (\text{B.52})$$

$$\Theta_{3,2,i} = 2 \sum_j^{nc} n_j \frac{Q_{ij}^6}{\sigma_{ij}^{12}} I_{15}^{HS} \quad (\text{B.53})$$

$$\Theta_{3,2,ij} = 2 \frac{Q_{ij}^6}{\sigma_{ij}^{12}} I_{15}^{HS} \quad (\text{B.54})$$

$$\Theta_{3,3,i} = 3 \sum_j^{nc} n_j \sum_k^{nc} n_k \frac{Q_{ijk}^6}{\sigma_{ij}^3 \sigma_{ik}^3 \sigma_{jk}^3} I_{TQ}^{HS} \quad (\text{B.55})$$

$$\Theta_{3,3,ij} = 6 \sum_k^{nc} n_k \frac{Q_{ijk}^6}{\sigma_{ij}^3 \sigma_{ik}^3 \sigma_{jk}^3} I_{TQ}^{HS} \quad (\text{B.56})$$

The above partial derivatives can be used to calculate the partial derivatives of the full quadrupolar term set in the Padé approximation with respect the model and mixture variables by using Eqs. (B.10) and (B.13). The partial derivatives of the reduced residual Helmholtz energy with respect to the state variables can then be calculated from Eqs. (B.3)-(B.8) as:

$$\left(\frac{\partial F}{\partial V} \right)_{\mathbf{n},T} = F_V \quad (\text{B.57})$$

$$\left(\frac{\partial F}{\partial T} \right)_{\mathbf{n},V} = F_T \quad (\text{B.58})$$

$$\left(\frac{\partial F}{\partial n_i} \right)_{V,T} = F_{\Theta_2} \Theta_{2,i} + F_{\Theta_{3,2}} \Theta_{3,2,i} + F_{\Theta_{3,3}} \Theta_{3,3,i} \quad (\text{B.59})$$

$$\left(\frac{\partial^2 F}{\partial V^2} \right)_{\mathbf{n},T} = F_{VV} \quad (\text{B.60})$$

$$\left(\frac{\partial^2 F}{\partial T^2}\right)_{\mathbf{n},V} = F_{TT} \quad (\text{B.61})$$

$$\left(\frac{\partial^2 F}{\partial T \partial V}\right)_{\mathbf{n}} = F_{TV} \quad (\text{B.62})$$

$$\left(\frac{\partial^2 F}{\partial n_i \partial V}\right)_T = F_{\Theta_2 V} \Theta_{2,i} + F_{\Theta_{3,2} V} \Theta_{3,2,i} + F_{\Theta_{3,3} V} \Theta_{3,3,i} \quad (\text{B.63})$$

$$\begin{aligned} \left(\frac{\partial^2 F}{\partial n_i \partial n_j}\right)_{V,T} &= F_{\Theta_2} \Theta_{2,ij} + F_{\Theta_{3,2,ij}} \Theta_{3,2,ij} + F_{\Theta_{3,3,ij}} \Theta_{3,3,ij} \\ &+ \Theta_{2,i} (F_{\Theta_2 \Theta_2} \Theta_{2,j} + F_{\Theta_2 \Theta_{3,2}} \Theta_{3,2,j} + F_{\Theta_2 \Theta_{3,3}} \Theta_{3,3,j}) \\ &+ \Theta_{3,2,i} (F_{\Theta_{3,2} \Theta_{3,2}} \Theta_{3,2,j} + F_{\Theta_{3,2} \Theta_2} \Theta_{2,j} + F_{\Theta_{3,2} \Theta_{3,3}} \Theta_{3,3,j}) \\ &+ \Theta_{3,3,i} (F_{\Theta_{3,3} \Theta_{3,3}} \Theta_{3,3,j} + F_{\Theta_{3,3} \Theta_{3,2}} \Theta_{3,2,j} + F_{\Theta_{3,3} \Theta_2} \Theta_{2,j}) \end{aligned} \quad (\text{B.64})$$

Which can finally be employed to calculate thermodynamic properties such as fugacity coefficients and their derivatives.

It may seem odd to split the model up in so many terms, especially when the mixture term is relatively simple, but as Michelsen and Mollerup note [54], application of this approach makes it easy to modify the model as changes in one term would not change the overall structure of the model, but only a small subset of derivatives. If, for instance, the non-truncated correlation integrals were to be used in Eqs. (B.24)-(B.26), it would only be necessary to update the equations for these term, their derivatives (including those previously zero), and the equations for the final Helmholtz energy. Similarly, if the changes to the mixture terms suggested in chapter 8 section 8.4.4 were to be implemented it would only require changes in Eqs. (B.24)-(B.26) and (B.51)-(B.56).

APPENDIX C

Numerical Derivatives

It is often convenient to express an equation of state, such as CPA or SAFT, in terms of the (reduced) residual Helmholtz energy ($F(T, V, \mathbf{n})$) since all other residual properties can be obtained as partial derivatives of the state variables T , V and \mathbf{n} . The partial derivatives are typically derived by hand, however, as the models grow in complexity this can become a tedious and error-prone process, and even the most careful efforts does not eliminate the possibility of programming errors. It is thus of utmost importance to numerically check the analytical partial derivatives for errors. This appendix discuss two numerical techniques, which can be used to check the derivatives.

C.1 First Derivative Approximations

Finite difference approximations are a common method for estimating derivatives. These formulas can be derived by truncating a Taylor series expanded about a given point x . A well-known estimate for the first derivative is the forward difference formula

$$f'(x) \approx \frac{f(x+h) - f(x)}{h} \quad (\text{C.1})$$

Where h is the finite difference interval. The truncation error is $O(h)$, and equation (C.1) is thus a first-order approximation. A better estimated may be obtained by using central differences as

$$f'(x) \approx \frac{f(x+h) - f(x-h)}{2h} \quad (\text{C.2})$$

The truncation error is $O(h^2)$ and it is therefore a second-order approximation.

As with any divided-difference approximation one is faced with the dilemma of using a small h to minimize the truncation error, while avoiding the use of such a small h that errors due to subtractive cancellation becomes significant [248, 249].

An alternative method, first investigated by Lyness and Moler [250] and later employed by Squire and Trapp [251], to obtain a very simple expression for estimating the first derivative of a function is to use complex variables to develop estimates of derivatives. Subsequent papers of Martins and co-workers [248, 252, 253] show how the method may be derived from the Cauchy-Riemann equations and illustrate the strength of the method.

If f is an analytic and real function of a real variable, the derivative of f can be approximated by

$$f'(x) \approx \frac{\text{Im}[f(x + ih)]}{h} \quad (\text{C.3})$$

Which is called the complex-step derivative approximation (CSDA). The truncation error is $O(h^2)$, but, more importantly, the estimate does not suffer from subtractive cancellation, which means that it is possible to chose an arbitrary small h without loosing accuracy.¹

C.2 Numerical Examples

C.2.1 Simple equations

To illustrate the power of the CSDA approach consider the same analytical function studied by Squire and Trapp [251] and Martins et al. [248] (equation (C.4)) as well as another simple function (equation (C.5)).

$$f(x) = \frac{e^x}{\sin^3(x) + \cos^3(x)} \quad (\text{C.4})$$

$$f(x) = \ln(x) \sin(3x) \quad (\text{C.5})$$

The exact derivative at $x = 1.5$ was calculated analytically with double precision (exact down to $\approx 2.2 \cdot 10^{-16}$) and then compared with results from the CSDA formula (eq. (C.3)) and the central differences formula (eq. (C.2)) using different values of h from 1 to 10^{-20} . Figure C.1 shows, for both equations, the normalized error in the first derivatives as a function of the step size.

¹Most compilers truncate numbers smaller than 10^{-308} (or thereabout) to zero, which sets a lower limit for h .

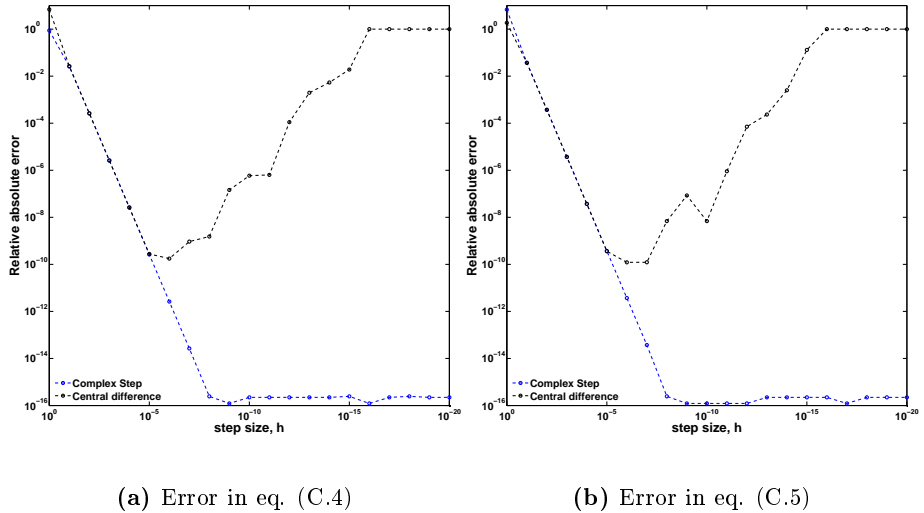


Figure C.1: Relative error in the first derivative estimates in equation (C.4) (a) and (C.5) (b), using either central differences or the complex step approximation. $err = |f'_{num} - f'_{analytic}|/|f'_{analytic}|$

It can be seen from both figure C.1a and figure C.1b that both the central difference estimate and the CSDA estimate initially converges towards the analytical answer, at a quadratic rate, since the truncation error of both methods is $O(h^2)$. However, as the step size is decreased below a value of about 10^{-5} subtractive cancellation errors become an issue for the central difference estimate and the errors begin to increase as the step size is reduced. For values of h smaller than 10^{-16} there is essentially no difference between the outputs and the finite difference estimate becomes zero.

The complex-step estimate, however, is unaffected by the subtraction errors and continues to converge quadratically until a step size of about 10^{-8} . Below this step size the CSDA is accurate to machine precision.

We see that not only is the accuracy of the best derivative approximation with the CSDA almost six orders of magnitude better than the central difference one, below a step size of about 10^{-8} the approximation is also insensitive towards the value of the step size and returns the derivative with machine accuracy. This is a tremendous advantage over the finite difference formulas since we can chose an almost arbitrary small step size without worrying whether it is too small or not. Moreover when analytical derivatives are tested numerically, one no longer have to wonder whether a relative difference of say 10^{-4} is due to an improperly chosen step size or a small mistake in the derivative.

C.2.2 The SRK and the quadrupolar term

Similarly the numerical derivatives of the Helmholtz energy function for e.g. the SRK or quadrupolar term can also be calculated from the finite difference formulas (Eq. (C.1)-(C.2)) or from the CSDA approximation (Eq. (C.3)). The first derivatives are thus estimated by taking a small step, h , in one of the variables, while keeping the other variables constant. To estimate the second derivatives we found it most convenient to ensure that the first derivatives were correct, and then estimate the second derivatives by estimating the numerical derivative of the analytical first derivatives.

The analytical derivatives of the reduced residual Helmholtz energy function, were calculated with double precision and compared to results from Eq. (C.2) and (C.3) using again different values of h . Figures C.2 and C.3 show the relative error in the important first and second order volume derivatives of the reduced residual Helmholtz energy function for the SRK and quadrupolar term at $T=230$ K, $n = 10$ mol and $V = 0.4$ L using parameters for CO_2 , either for inert CPA or qCPA.

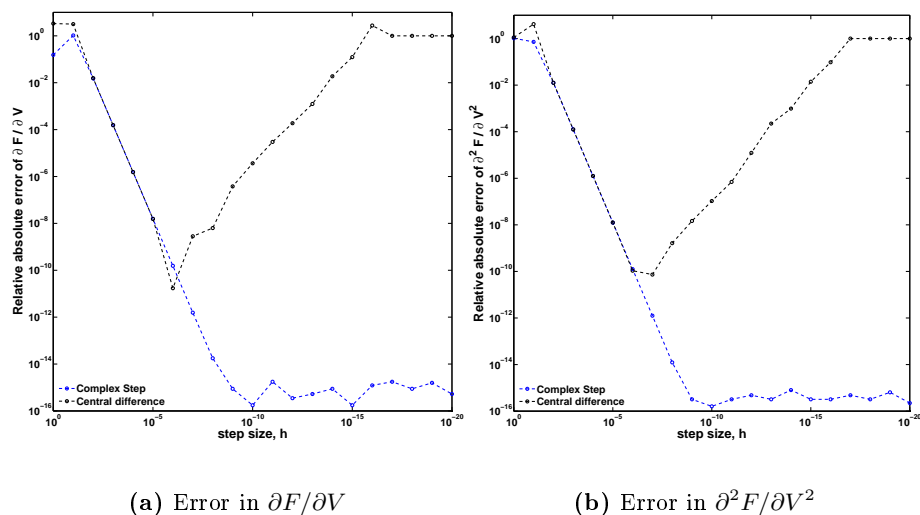


Figure C.2: Relative error in the volume derivatives of the reduced residual Helmholtz energy for the SRK for CO_2 at $T=230$ K, $n = 10$ mol, and $V = 0.4$ L, using either central differences or the complex step approximation. The CO_2 parameters are those employed for inert CO_2 .
 $err = |f'_{num} - f'_{analytic}|/|f'_{analytic}|$

The figures illustrate, that both the SRK and quadrupolar term exhibit the same characteristics as the more simple functions first evaluated. The only difference seem to be, that there is slightly more numerical noise for the first derivative of the SRK term (figure C.2a) at low step sizes. The very low errors returned by the complex step derivative approximation, which are essentially

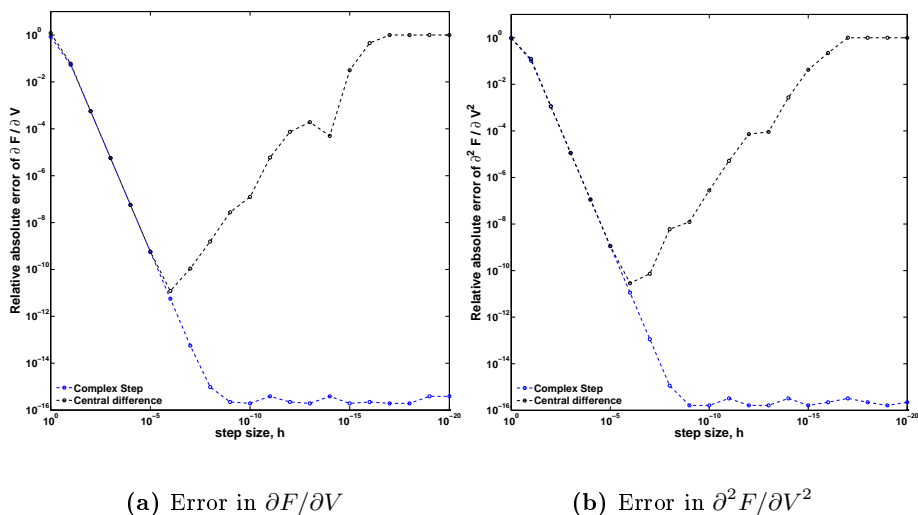


Figure C.3: Relative error in the volume derivatives of the reduced residual Helmholtz energy for the quadrupole term for CO_2 at $T=230$ K, $n = 10$ mol, and $V = 0.4$ L, using either central differences or the complex step approximation. The CO_2 parameters are those employed for qCPA with four parameters for CO_2 . $err = |f'_{num} - f'_{analytic}|/|f'_{analytic}|$

machine accuracy, clearly indicate that the analytical volume derivatives are correct.

Tables C.1 and C.2 show the relative error in all relevant derivatives using either Eq. (C.2) or Eq. (C.3). CO_2 at $T = 230$ K, $n = 10$ mol and $V = 0.4$ L is again used as sample compound and conditions. The step size is $h = 10^{-20}$ for the complex step approximation and $h = \mathbf{x}\epsilon^{1/3}$, for the central differences, where $\mathbf{x} \in \{T, V, \mathbf{n}\}$ and ϵ is machine accuracy.² The tables clearly show that the derivatives of both the SRK term and the quadrupolar term are, essentially, estimated with machine accuracy when Eq. (C.3) is employed. It is also clear that the central difference approximation seem to be quite good (accurate with about 10 digits) when the optimal a priori step size is employed.

²It can be shown that the best estimates of h , in the absence of other information about the function, are $\sqrt{\epsilon}x$ and $(\epsilon)^{1/3}x$ for forward and central difference respectively, where ϵ is machine accuracy ($\approx 2.2 \cdot 10^{-16}$ for floating point double precision) [249].

Table C.1: Relative error in the numerical derivatives of the Helmholtz energy function for the SRK term at $T = 230$ K, $n = 10$ mol and $V = 0.4$ L, using CO_2 as the sample compound. The error is evaluated both for central differences and the CSDA.

Derivative	$\frac{ f'_{\text{centraldiff}} - f'_{\text{analytic}} }{ f'_{\text{analytic}} }$	$\frac{ f'_{\text{complexstep}} - f'_{\text{analytic}} }{ f'_{\text{analytic}} }$
	$\partial F/\partial V$	$1.2 \cdot 10^{-9}$
$\partial F/\partial T$	$7.4 \cdot 10^{-11}$	$2.2 \cdot 10^{-16}$
$\partial F/\partial n_i$	$9.7 \cdot 10^{-11}$	$6.6 \cdot 10^{-16}$
$\partial^2 F/\partial V^2$	$7.6 \cdot 10^{-10}$	$2.2 \cdot 10^{-16}$
$\partial^2 F/\partial T^2$	$9.6 \cdot 10^{-11}$	$2.2 \cdot 10^{-16}$
$\partial^2 F/\partial n_i \partial n_j$	$9.6 \cdot 10^{-10}$	$3.9 \cdot 10^{-16}$
$\partial^2 F/\partial V \partial T$	$7.6 \cdot 10^{-10}$	$2.2 \cdot 10^{-16}$
$\partial^2 F/\partial n_i \partial T$	$2.0 \cdot 10^{-11}$	$2.2 \cdot 10^{-16}$
$\partial^2 F/\partial n_i \partial V$	$2.6 \cdot 10^{-10}$	$2.2 \cdot 10^{-16}$

Table C.2: Relative error in the numerical derivatives of the Helmholtz energy function for the quadrupole term at $T = 230$ K, $n = 10$ mol and $V = 0.4$ L, using CO_2 as the sample compound. The error is evaluated both for central differences and the CSDA.

Derivative	$\frac{ f'_{\text{centraldiff}} - f'_{\text{analytic}} }{ f'_{\text{analytic}} }$	$\frac{ f'_{\text{complexstep}} - f'_{\text{analytic}} }{ f'_{\text{analytic}} }$
	$\partial F/\partial V$	$8.1 \cdot 10^{-11}$
$\partial F/\partial T$	$1.3 \cdot 10^{-10}$	$2.5 \cdot 10^{-16}$
$\partial F/\partial n_i$	$4.2 \cdot 10^{-12}$	$5.9 \cdot 10^{-16}$
$\partial^2 F/\partial V^2$	$8.3 \cdot 10^{-11}$	$2.2 \cdot 10^{-16}$
$\partial^2 F/\partial T^2$	$1.1 \cdot 10^{-10}$	$3.5 \cdot 10^{-16}$
$\partial^2 F/\partial n_i \partial n_j$	$2.1 \cdot 10^{-11}$	$2.2 \cdot 10^{-16}$
$\partial^2 F/\partial V \partial T$	$1.3 \cdot 10^{-10}$	$4.2 \cdot 10^{-16}$
$\partial^2 F/\partial n_i \partial T$	$4.7 \cdot 10^{-12}$	$4.8 \cdot 10^{-16}$
$\partial^2 F/\partial n_i \partial V$	$9.7 \cdot 10^{-13}$	$8.9 \cdot 10^{-16}$

List of Abbreviations

- 2CLJ** two center Lennard-Jones.
- CCS** carbon capture and storage.
- CERE** Center for Energy Resources Engineering.
- CPA** cubic plus association.
- CS** Carnahan-Starling.
- CSDA** complex-step derivative approximation.
- DIPPR** Design Institute for Physical Properties.
- DTU** Technical University of Denmark.
- EoS** Equation of State.
- IEA** International Energy Agency.
- LHS** Latin Hypercube Sampling.
- LLE** liquid liquid equilibrium.
- LSQ** Least Squares.
- mCR-1** modified CR-1.
- MEG** mono-ethylene glycol.
- NIST** National Institute of Standards and Technology.
- PC-PSAFT** Perturbed-Chain Polar-SAFT.

PC-SAFT Perturbed-Chain SAFT.

PCP-SAFT Perturbed-Chain Polar SAFT.

pGC-PC-SAFT polar Group Contribution PC-SAFT.

PR Peng-Robinson.

qCPA quadrupolar CPA.

RDF Radial distribution function.

REFPROP Reference Fluid Thermodynamic and Transport Properties.

SAFT Statistical Association Fluid Theory.

SRK Soave-Redlich-Kwong.

tPC-PSAFT truncated Perturbed-Chain Polar SAFT.

vdW1f van der Waals one-fluid.

VLE vapor liquid equilibrium.

VLLE vapor liquid liquid equilibrium.

List of Symbols

$A^r(T, V, \mathbf{n})$ Residual Helmholtz energy.

A_2^r Second order term in the perturbation expansion for quadrupolar interactions.

A_3^r Third order term in the perturbation expansion for quadrupolar interactions.

A_i^D Coefficient A in the DIPPR correlation for the ideal isobaric heat capacity.

A_i bonding sites on molecule i .

B_i^D Coefficient B in the DIPPR correlation for the ideal isobaric heat capacity.

B Second virial coefficient or expression for co-volume mixing term.

C_P^{ig} Ideal gas isobaric heat capacity.

C_P^{res} The residual isobaric heat capacity.

C_P The isobaric heat capacity.

C_V^{ig} Ideal gas isochoric heat capacity.

C_V^{res} The residual isochoric heat capacity.

C_V The isochoric heat capacity.

C_i^D Coefficient C in the DIPPR correlation for the ideal isobaric heat capacity.

D_i^D Coefficient D in the DIPPR correlation for the ideal isobaric heat capacity.

D Mixing rule for the energetic part of SRK.

E_i^D Coefficient E in the DIPPR correlation for the ideal isobaric heat capacity.

F Reduced residual Helmholtz energy.

- G^E Gibbs Excess.
- H^E Excess enthalpy.
- H^{ig} Ideal gas enthalpy.
- H^{res} Residual enthalpy.
- H Enthalpy.
- I_{TQ} Three-body correlation integral.
- I_n Two-body correlation integral.
- $J_{i,TQ}$ i th Coefficient in the density expansion for I_{TQ} .
- $J_{i,n}$ i th Coefficient in the density expansion for I_n .
- M^E Excess of a generic property.
- M^{is} ideal solution value of a generic property.
- M_W Molecular weight.
- M A generic property.
- N_A Avogadro's constant.
- N number of experiments.
- P_C Critical pressure.
- P Pressure.
- Q Quadrupole moment.
- R The gas constant.
- S Constant in expression for the second virial coefficient of the association term.
- T_C Critical temperature.
- T_r Reduced temperature $T_r = T/T_C$.
- T Temperature.
- V^{mol} Molecular volume.
- V_C Critical volume.
- V Volume.
- X_{A_i} Fraction of sites A on molecule i which do *not* form bonds with other sites (site monomer fraction).
- Z compressibility factor.

- $\Delta^{A_i B_j}$ Association strength between site A on molecule i and site B on molecule j .
- Γ Reduced pure compound energy parameter (a_0/Rb_0).
- α significance level also known as the alpha level.
- $\beta^{A_i B_j}$ cross-association volume between site A on molecule i and site B on molecule j .
- η Reduced density.
- $\hat{\varphi}_i$ Fugacity coefficient for the i th component in a mixture.
- I** Identity matrix.
- Q** Quadrupole moment tensor.
- V** Variance matrix.
- θ vector of adjustable parameters.
- n** Vector of molar composition.
- r_i** Position vector of charge i .
- y** Vector of outputs from a models.
- μ_{JT} The Joule-Thomson coefficient.
- σ Hard-sphere diameter.
- $\varepsilon^{A_i B_j}$ cross-association energy between site A on molecule i and site B on molecule j .
- φ_i Fugacity coefficient for the i th pure component.
- a_0 Pure compound attractive energy parameter in the SRK term.
- a_{ij} Cross energetic parameter in the SRK term.
- a_{kij} zeroth order coefficient in the temperature dependent binary interaction parameter.
- b_0^Q co-volume parameter in the quadrupolar term.
- b^{eff} Effective co-volume.
- b_0 Pure compound co-volume.
- b_{ii} Pure compound co-volume for component i .
- b_{ij} cross-covolume.
- b_{kij} proportionality constant for the linear temperature dependence of the binary interaction parameter.

- c_1 Pure compound parameter in the SRK term.
- c_{kij} proportionality constant for the inverse temperature dependence of the binary interaction parameter.
- f function which represents the equation of state and any auxiliary equations under investigation.
- g Radial distribution function.
- k_b Boltzmann's constant.
- k_{ij} Binary interaction parameter.
- n Total composition.
- p number of estimators (parameters).
- q_i charge i in some molecule.
- s_{ij} Solvation factor.
- s standard deviation.
- $t_{N-p}^{\alpha/2}$ student's t-distribution corresponding to the $\alpha/2$ percentile with $N - p$ degrees of freedom.
- u The speed of sound.
- w weight factor.
- x_p fraction of multipolar segments in a chain molecules.
- x Mole fraction.
- y Output model (equation of state) prediction.
- y An output property.

List of Figures

3.1	Prediction ($k_{ij} = 0$) and correlation ($k_{ij} = 0.13$) of the CO ₂ + ethane VLE at T=270 K using the CPA EoS with CO ₂ modeled as an inert. Experimental data from [66, 67].	15
3.2	Solubility of water in CO ₂ using CPA	17
3.3	Correlation of the VLE and LLE of the CO ₂ + water system . . .	19
4.1	Point-charge schematics of quadrupole interactions	24
5.1	Compressibility factor for a hard-sphere fluid. Comparison of the CS EoS and the repulsive part of the van der Waals EoS as a function of reduced density. Adapted from [116].	35
6.1	Contour plot of the objective function in Eq. (6.1) calculated for CO ₂ treated as an inert compound with CPA at varying Γ and b_0 and with $c_1 = 0.73$ (a) and as a self-associating compound at varying β and ε with $c_1 = 0.73$, $b_0 = 28.4$ L/mol and $\Gamma = 1250$ K using CPA. Blue contours indicate the lowest values and red contours the highest values. The red dot in (a) represents the minimum with the chosen value of c_1 . There is no clear minimum in (b)	39

- 6.2 Predictions of the CO₂ + ethane VLE at 250K using four different parameter sets for qCPA with four adjustable parameters. All parameter sets correlate the saturated liquid density and pressure within experimental error and have been obtained by using different initial guesses for the parameters. 40
- 6.3 Histograms approximating the distribution of each parameter (left y-axis), obtained from 500 re-sampled bootstraps, using modeling approach **E** for CO₂. The full red lines show the estimated probability density function (right y-axis). 49
- 6.4 95% confidence ellipsoids for the bootstrapped parameters of CO₂ when modeling approach **E** is employed. Each dot represents a realized parameter combination and each subfigures represents the dependency (if any) of one parameter on another. 50
- 6.5 Histograms approximating the distribution of each parameter (left y-axis), obtained from 500 re-sampled bootstraps, using modeling approach **F** for CO₂. The full red lines show the estimated probability density function (right y-axis). 51
- 6.6 95% confidence ellipsoids for the bootstrapped parameters of CO₂ when modeling approach **F** is employed. Each dot represents a realized parameter combination and each subfigures represents the dependency (if any) of one parameter on another. 52
- 6.7 Histograms approximating the distribution of each parameter (left y-axis), obtained from 500 re-sampled bootstraps, using modeling approach **D** for CO₂. The full red lines show the estimated probability density function (right y-axis). 53
- 6.8 95% confidence ellipsoids for the bootstrapped parameters of CO₂ when modeling approach **D** is employed. Each dot represents a realized parameter combination and each subfigures represents the dependency (if any) of one parameter on another. 54
- 6.9 Propagated uncertainty in the model predictions for the liquid density at saturation. Approach **A** (a), **D** (b), **E** (c) and **F** (d) is employed. Grey lines represent the simulations, red dashed lines are the 5th and 95th percentile of the simulations and black full lines are the mean of the simulations. As the simulations, and their mean are almost identical the lines are difficult to see. Blue circles are pseudo-experimental data from Span and Wagner [15]. 57

- 6.10 Propagated uncertainty in the model predictions for the residual isochoric heat capacity of CO_2 at saturation, employing approach **A** (a), **D** (b), **E** (c) and **F** (d). Grey lines represent the simulations, red dashed lines are the 5th and 95th percentile of the simulations and black full lines are the mean of the simulations. Pseudo-experimental data from Span and Wagner [15]. 59
- 6.11 Propagated uncertainty in the model predictions for the residual isobaric heat capacity of CO_2 at saturation, employing approach **A** (a), **D** (b), **E** (c) and **F** (d). Grey lines represent the simulations, red dashed lines are the 5th and 95th percentile of the simulations and black full lines are the mean of the simulations. Pseudo-experimental data from Span and Wagner [15]. 60
- 6.12 Propagated uncertainty in the model predictions for the CO_2 + ethane VLE at $T=250$ K. Employing approach **A** (a), **D** (b), **E** (c) and **F** (d). Grey lines represent the simulations, red dashed lines are the 5th and 95th percentile of the simulations and black full lines are the mean of the simulations. Experimental data from [67]. 62
- 6.13 Propagated uncertainty in the model predictions for the CO_2 + propane VLE at $T=230$ K. Employing approach **A** (a), **D** (b), **E** (c) and **F** (d). Grey lines represent the Monte Carlo simulations, red dashed lines are the 5th and 95th percentile of the simulations and black full lines are the mean of the simulations. Experimental data from [165]. 63
- 6.14 Propagated uncertainty in model predictions for the CO_2 + *n*-dodecane LLE using qCPA with 4 adjustable parameters (Approach F). Grey lines represent the Monte Carlo simulations, red dashed lines are the 5th and 95th percentile of the simulations and black full lines are the mean of the simulations. Experimental data from [166]. 64
- 6.15 Histograms approximating the distribution of each parameter (left y-axis), obtained from 500 re-sampled bootstraps, using modeling approach **F** for CO_2 . The parameters have been fitted to ΔH^{vap} in addition to ρ_{sat}^{liq} and P^{sat} . The full red line shows the estimated probability density function (right y-axis). 65
- 6.16 Histograms approximating the distribution of each parameter (left y-axis), obtained from 500 re-sampled bootstraps, using modeling approach **D** for CO_2 . The parameters have been fitted to ΔH^{vap} in addition to ρ_{sat}^{liq} and P^{sat} . The full red line shows the estimated probability density function (right y-axis). 66

6.17	Propagated uncertainty in the model predictions for the CO ₂ + ethane VLE at T=250 K. Approach F (a) and D (b) fitted to ΔH^{vap} in addition to ρ_{sat}^{liq} and P^{sat} . Grey lines represent the simulations, red dashed lines are the 5th and 95th percentile of the simulations and black full lines are the mean of the simulations. Blue circles are experimental data from [67].	67
7.1	Normalized liquid and vapor residual isochoric (a) and isobaric (b) heat capacity predictions of CO ₂ at saturation with CPA and qCPA. Pseudo-experimental data from the Span and Wagner EoS [15].	77
7.2	Liquid and vapor Joule-Thomson coefficient (a) and speed of sound (b) predictions of CO ₂ at saturation with CPA and qCPA. Pseudo-experimental data from the Span and Wagner EoS [15].	78
7.3	Heat of vaporization predictions of CO ₂ at saturation with CPA and qCPA. Pseudo-experimental data from the Span and Wagner EoS [15].	78
7.4	Normalized isochoric (a) and isobaric (b) heat capacity predictions for CO ₂ with CPA and qCPA in the compressed liquid region and at $T_r = 0.8$ and $T_r = 0.9$. Pseudo-experimental data from the Span and Wagner EoS [15].	80
7.5	Speed of sound (a) and Joule-Thomson coefficient (b) predictions for CO ₂ with CPA and qCPA in the compressed liquid region and at $T_r = 0.8$ and $T_r = 0.9$. Pseudo-experimental data from the Span and Wagner EoS [15].	81
7.6	Density predictions for CO ₂ with CPA and qCPA in the compressed liquid region. At $T_r = 0.8$ and $T_r = 0.9$ (a) compared to pseudo-experimental data from the Span and Wagner EoS [15] and at $T_r = 0.9$ and $T_r = 0.93$ (b) compared to experimental data from Brewer et al. [176].	81
7.7	Normalized isochoric (a) and isobaric (b) heat capacity predictions of CO ₂ with CPA and qCPA in the critical region ($T_r = 1.1$). Pseudo-experimental data from the Span and Wagner EoS [15].	83
7.8	C_V^{res} predictions of 1-hexanol using 3 different CPA parameter sets with the 2B [51, 115] and 3B [115] schemes respectively. The parameters from de Villiers et al. [115] have been correlated to C_P^{liq} and ΔH^{vap} in addition to the saturated density and vapor pressure.	83

7.9	Density predictions of CO ₂ with CPA and qCPA in the critical region ($T_r = 1.1$). Pseudo-experimental data from the Span and Wagner EoS [15].	84
7.10	Model comparison of the overall %AADs for the density, speed of sound, isobaric heat capacity and the Joule-Thomson coefficient in the liquid or supercritical phase using the five modeling approaches.	85
7.11	PV-diagram with temperature isotherms and critical points . . .	86
7.12	Predicted saturated density from triple point to critical point . .	87
7.13	Model predictions against experimental data for the second virial coefficient of CO ₂ using CPA, n.a., CPA 4C, and the qCPA. Experimental data from [179–185].	89
8.1	Predictions ($k_{ij} = 0$) compared to experimental data for the CO ₂ + ethane VLE at four temperatures using CPA where CO ₂ is treated either as an inert (n.a.) or self-associating compound (scheme 4C) and qCPA with either three or four parameters. Experimental data from Refs. [66, 67].	96
8.2	Predictions ($k_{ij} = 0$) compared to experimental data for the CO ₂ + propane VLE at at 270 K and 230 K using CPA, where CO ₂ is treated either as an inert (n.a.) or self-associating compound (scheme 4C), and qCPA with either three or four parameters. Experimental data from Ref. [165].	97
8.3	Predictions ($k_{ij} = 0$) compared to experimental data for the CO ₂ + <i>n</i> -butane VLE at three temperatures using CPA, where CO ₂ is treated either as an inert (n.a.) or self-associating compound (scheme 4C), and qCPA with either three or four parameters. Experimental data from Refs. [189, 191].	98
8.4	Predictions ($k_{ij} = 0$) compared to experimental data for the CO ₂ + <i>n</i> -decane VLE at three temperatures using CPA, where CO ₂ is treated either as an inert (n.a.) or self-associating compound (scheme 4C), and qCPA with either three or four parameters. Experimental data from Ref. [190].	99
8.5	Predictions ($k_{ij} = 0$) compared to experimental data for the CO ₂ + methane VLE at two temperatures using CPA, where CO ₂ is treated either as an inert (n.a.) or self-associating compound (scheme 4C), and qCPA with either three or four parameters. Experimental data from [67].	100

- 8.6 Correlations (a) and predictions (b) of the $\text{CO}_2 + n$ -pentadecane LLE, using CPA, where CO_2 is treated either as an inert (n.a.) or self-associating compound (scheme 4C), and qCPA with either three or four parameters. Experimental data from Ref. [166]. 101
- 8.7 Correlations (a) and predictions (b) of the $\text{CO}_2 + n$ -eicosane LLE at 348 K, using CPA where CO_2 is treated either as an inert (n.a.) or self-associating compound (scheme 4C) and qCPA with either three or four parameters. Experimental data from Ref. [198]. 102
- 8.8 Predictions and correlations of the $\text{CO}_2 + n$ -Hexatriacontane LLE at 349 K. CO_2 is modeled with inert CPA and qCPA with three and four parameters. Only parameter set 1 is shown in the figure for qCPA. The predicted LLE is shown in (a) and (b), (a) shows the whole LLE region and (b) is a close-up of predictions for the CO_2 rich phase. (c) and (d) correspond to the correlated versions of (a) and (b). 103
- 8.9 Binary interaction parameters with qCPA (using 3 parameters) and CPA without association for $\text{CO}_2 + n$ -alkane mixtures, as a function of the molecular weight of the n -alkane. Points are the correlated values for each subsystem and lines are correlations to the series behavior. The vertical dashed line indicates the transition from VLE to LLE. 106
- 8.10 VLE of (a) $\text{CO}_2 +$ propane and LLE of (b) $\text{CO}_2 + \text{C}_{36}$ where the correlations in (8.1)-(8.2) have been employed for qCPA with three parameters and inert CPA. Experimental data from Refs. [165, 198] 108
- 8.11 Predicted ($k_{ij} = 0$) VLEs of the $\text{CO}_2 +$ ethanol system (a) and the CO_2 -rich vapor phase of the $\text{CO}_2 +$ water system (b) using qCPA with three parameters and assuming zero, one or two solvation sites. It is assumed for both systems that $\beta_{crs} = \beta_{assoc}$. Experimental data from Refs. [75, 200–205]. 110
- 8.12 Correlation of the $\text{CO}_2 +$ methanol VLE, using CPA where CO_2 is treated either as an inert (n.a.) or self-associating compound (scheme 4C) and qCPA with either three or four parameters. Correlated to experimental data from Refs. [206, 207]. 111
- 8.13 Correlation of the $\text{CO}_2 +$ nonanol VLE and LLE using CPA where CO_2 is treated either as an inert or self-associating compound, or qCPA with three or four adjustable parameters. Experimental data from Refs. [73, 202]. 112

- 8.14 Correlation of the CO_2 solubility in the water rich liquid phase (a) and the water solubility in the CO_2 rich vapor phase (b) for the CO_2 + water system. CPA, where CO_2 is treated either as an inert or an associating compound, or qCPA with three or four adjustable parameters is employed. Experimental data from Refs. [75, 203–205, 214]. 114
- 8.15 Correlation of the water solubility in the CO_2 rich vapor phase for the CO_2 + water system. Comparing the performance of CPA with solvation, and qCPA with solvation. Experimental data from [75, 203–205]. 115
- 8.16 Correlated phase equilibria of the binary CO_2 + water mixture at three different temperatures using the three parameter version of qCPA with the temperature dependent k_{ij} shown in Eq. (8.3). (a) Solubility of CO_2 in the water rich liquid phase at 308.2 K. (b) Water solubility in the CO_2 -rich vapor and liquid phase. (c) As (a) but at 288.3 K. (d) As (b) but at 298.2 K. Experimental data from Refs. [75–78, 82, 215]. 117
- 8.17 Prediction of the CO_2 + benzene VLE at two temperatures (upper: 347.25 K and lower: 315.45 K) using CPA, where CO_2 is treated either as an inert (n.a.) or self-associating compound (scheme 4C), and qCPA with either three or four parameters. Experimental data from Refs. [212, 216]. 119
- 8.18 Prediction of the CO_2 + toluene VLE. 120
- 8.19 Prediction of the CO_2 + toluene VLE with qCPA. The quadrupole moment of toluene is ignored. 121
- 8.20 Prediction of the CO_2 + N_2 VLE at 250 K using qCPA with three parameters and inert CPA. Experimental data from Ref. [193] 121
- 8.21 CO_2 + N_2 VLE at 250 K using a fitted quadrupole moment for N_2 122
- 8.22 VLE predictions of N_2 + Propane and N_2 + Butane 123
- 8.23 Prediction (a) and correlation (b) of the CO_2 + acetylene VLE at 233 K using either CPA without association (n.a.), with the 4C scheme, or qCPA with either three or four adjustable parameters. Experimental data from Ref. [221]. 124
- 8.24 Prediction of the CO_2 + acetylene VLE at 233 K using qCPA with three adjustable parameters and the modified combining rules. Experimental data from Ref. [221]. 125

- 8.25 Prediction of the CO₂ + acetylene VLE at 233 K using qCPA with four adjustable parameters and the modified combining rules. Contrary to figures 8.23 and 8.24 a fitted quadrupolar moment of 5.4 DÅ is employed. Experimental data from Ref. [221]. . . . 126
- 8.26 Prediction of the CO₂ + acetone VLE at 291.15 K using either CPA without association (n.a.), with the 4C scheme, or qCPA with either three or four adjustable parameters. Acetone is assumed to be self-associating. Experimental data from Ref. [202]. 128
- 8.27 Excess enthalpy of the CO₂ + ethane mixtures at 217 K and saturation pressure. The employed modeling approaches are inert CPA, CPA with association, or qCPA with three or four adjustable parameters. (a) shows the predicted excess enthalpy with $k_{ij} = 0$, and (b) shows the predicted excess enthalpy with the k_{ij} correlated from VLE (see table 8.3 and figure 8.1). Experimental data from Ref. [222] 129
- 8.28 Excess enthalpy of the CO₂ + water mixture at 548.2 K and 4.9 MPa. The employed modeling approaches are inert CPA, CPA with association, or qCPA with three or four adjustable parameters. (a) shows the predicted excess enthalpy with $k_{ij} = 0$, and (b) shows the predicted excess enthalpy with the k_{ij} correlated from VLE (see table 8.7 and figure 8.14). Experimental data from Ref. [223]. 130
- 9.1 Predictions compared to experimental data for the CO₂ + methane + ethane VLE at 250 K and 30 bar. (a) No interaction parameters are employed ($k_{ij} = 0$) and (b) interaction parameters are employed. Circles and dotted lines are experimental data from Ref. [229] and experimental tie lines respectively. 139
- 9.2 Pure predictions compared to experimental data for the CO₂ + methane + ethane VLE at (a) 250 K and 25 bar and (b) 230 K and 65 bar. In either case no interaction parameters are employed ($k_{ij} = 0$). Circles and dotted lines are experimental data from Refs. [67, 229] and experimental tie lines respectively. 140
- 9.3 Predictions compared to experimental data for the CO₂ + ethane + eicosane VLE at 338.7 K and 104.4 bar. (a) No interaction parameters are employed ($k_{ij} = 0$) and (b) interaction parameters are employed as usual. Circles and dotted lines are experimental data from [228] and experimental tie lines respectively. 140

- 9.4 Predictions compared to experimental data for the CO₂ + methanol + propane VLE at (a) 343.1 K and 5.1 bar and (b) 343.1 K and 22.03 bar. Full lines are CPA and qCPA predictions. Circles and dashed lines are experimental data from Ref. [230] and experimental tie lines respectively. 143
- 9.5 Predicted VLE and VLLE for the CO₂ + methanol + propane system at 313 K and 17.1 bar. Green lines are predictions for the whole phase diagram with case D. ▲ Predictions at the experimental conditions, the full black lines are predicted tie lines. ● experimental VLE data from Ref. [230], the dashed black lines are experimental tie lines. The green triangle indicates the predicted three-phase VLLE region at the specified temperature and pressure. 144
- 9.6 Predictions compared to experimental data for the CO₂ + methanol + water VLE at 313.2 K and 100 bar. Full lines are CPA and qCPA predictions. Circles and dashed lines are experimental data from Ref. [232] and experimental tie lines respectively. 145
- 9.7 Predictions compared to experimental data for the CO₂ + ethanol + water VLE at 323 K and 118 bar. Full lines are CPA and qCPA predictions. Circles and dashed lines are experimental data from Ref. [231] and experimental tie lines respectively. 145
- 9.8 Predictions compared to experimental data for the CO₂ + methanol + ethanol VLE at (a) 313 K and 60 bar and (b) 313 K and 80 bar. Full lines are CPA and qCPA predictions. Circles and dashed lines are experimental data from Ref. [201] and experimental tie lines. 146
- 9.9 Predictions compared to experimental data for the CO₂-rich phase of the CO₂ + water + methane (5.31mol%) mixture at (a) 300 K (b) 316 K and (c) 323 K. Lines are CPA and qCPA predictions. Circles are experimental data from Ref. [234]. 147
- 9.10 Dew point predictions compared to experimental data from Refs. [236, 239, 240] (selected mixtures) for the systems (a) CO₂(1) + methanol(2) + water(3), (b) CO₂(1) + methanol(2) + water(3) + ethane(4), (c) CO₂(1) + methanol(2) + water(3) + propane(4), (d) CO₂(1) + methanol(2) + water(3) + *n*-butane. Symbols are experimental data and the legend indicates the composition of the selected mixtures. 149

- 9.11 VLLE predictions compared to experimental data for the CO₂ + methanol + ethane VLLE at 298.15 K. Lines are CPA and qCPA predictions. Symbols are experimental data from Ref. [241] ○ CO₂, ■ Methanol, △ Ethane. 152
- 9.12 VLLE predictions with case E, where all $k_{ij} = 0$, compared to experimental data for the CO₂ + methanol + ethane VLLE at 298.15 K. Experimental data from Ref. [241] ○ CO₂, ■ Methanol, △ Ethane. 154
- 10.1 Prediction ($k_{ij} = 0$) of the CO₂ + cyclopentane VLE at 293 K using inert CPA and qCPA with three or four adjustable parameters. The predictions are compared with experimental data from Ref. [244]. 161
- C.1 Relative error in the first derivative estimates in equation (C.4) (a) and (C.5) (b), using either central differences or the complex step approximation. $err = |f'_{num} - f'_{analytic}|/|f'_{analytic}|$ 177
- C.2 Relative error in the volume derivatives of the reduced residual Helmholtz energy for the SRK for CO₂ at T=230 K, n = 10 mol, and V = 0.4 L, using either central differences or the complex step approximation. The CO₂ parameters are those employed for inert CO₂. $err = |f'_{num} - f'_{analytic}|/|f'_{analytic}|$ 178
- C.3 Relative error in the volume derivatives of the reduced residual Helmholtz energy for the quadrupole term for CO₂ at T=230 K, n = 10 mol, and V = 0.4 L, using either central differences or the complex step approximation. The CO₂ parameters are those employed for qCPA with four parameters for CO₂. $err = |f'_{num} - f'_{analytic}|/|f'_{analytic}|$ 179

List of Tables

3.1	Association schemes with Huang and Radosz [61]	13
4.1	Binary mixtures containing CO ₂ + a compound group or compound, to which the SAFT-based quadrupolar equations of state have been employed for phase equilibrium calculations in Refs. [28, 100–106, 108–112]. Similar compounds or compound groups are horizontally aligned.	29
4.2	Ternary mixtures containing CO ₂ + two other components, to which the SAFT-based quadrupolar equations of state have been applied in Refs. [29, 100, 102, 103, 111].	30
4.3	Summary of differences and similarities for SAFT-based equations of state for quadrupolar mixtures. $J_{i,k}$ denotes the two- and three body correlation integrals present in the theories. . . .	31
5.1	Relative error in the numerical derivatives of the Helmholtz energy function for the quadrupole term at T = 250 K, n = 10 mol and V = 1L, using CO ₂ as the sample compound. The numerical derivatives are calculated with the central difference formula. . .	37
6.1	Modeling approaches with CPA, including the number of adjustable pure compound parameters, investigated for CO ₂	43

6.2	Correlated pure compound parameters and %AADs in saturated liquid density and saturated pressure for CO ₂ with the CPA EoS (Approaches A-D) and the qCPA (Approaches E-F). The parameters are correlated in the temperature range $T_r = 0.7 - 0.9$	45
6.3	Estimated CO ₂ parameters, uncertainty as a 95% confidence interval (CI) in percent of the parameter estimate, and parameter correlation matrix when modeling approach E is employed. . . .	46
6.4	Estimated CO ₂ parameters, uncertainty as a 95% confidence interval (CI) in percent of the parameter estimate, and parameter correlation matrix when modeling approach F is employed. . . .	46
6.5	Estimated CO ₂ parameters, uncertainty as a 95% confidence interval (CI) in percent of the parameter estimate, and parameter correlation matrix when modeling approach D is employed. . . .	46
6.6	Estimated CO ₂ parameters, uncertainty as a 95% confidence interval (CI) in percent of the parameter estimate, and parameter correlation matrix when modeling approach B is employed. . . .	47
7.1	DIPPR coefficients for calculation of the isobaric ideal gas heat capacity of CO ₂ using Eq. (7.8).	72
7.2	CPA and qCPA pure compound parameters for CO ₂ together with %AADs between experimental [152–154] and calculated saturated liquid densities and saturated pressures. The quadrupolar moment of CO ₂ is fixed at the (average) experimental value of $-4.3 \text{ D}\text{\AA}^a$ when qCPA is employed. Details on the parameter estimation can be found in chapter 6.	74
7.3	%AAD values for u_{liq}^{sat} , $C_{P,liq}^{res,sat}$, $C_{V,liq}^{res,sat}$, $\mu_{JT,liq}^{sat}$, and ΔH^{vap} of CO ₂ at saturation using CPA n.a., CPA 4C and qCPA with three different parameter sets. The temperature range is $T = 216 - 300 \text{ K}$. Pseudo-experimental data from the Span and Wagner EoS [15]. u represents the speed of sound, μ the Joule-Thomson coefficient and ΔH^{vap} the heat of vaporization.	76
7.4	% AAD values for ρ_{vap}^{sat} , u_{vap}^{sat} , $C_{P,vap}^{res,sat}$, $C_{V,vap}^{res,sat}$ and $\mu_{JT,vap}^{sat}$ of CO ₂ at saturation using CPA n.a., CPA 4C and qCPA with three different parameter sets. The temperature range is $T = 216 - 300 \text{ K}$. Pseudo-experimental data from from the Span and Wagner EoS [15].	76

7.5	%AAD values of ρ^{liq} , u , C_P^{res} , C_V^{res} , and μ_{JT} for CO ₂ at two reduced temperatures in the compressed liquid region using CPA n.a., CPA 4C and qCPA with three different parameter sets. Pseudo-experimental data from the Span and Wagner EoS [15].	79
7.6	%AAD values between the experimental liquid density data from Brewer et al. [176] and the predicted values for CO ₂ using CPA n.a., CPA 4C and qCPA with three different parameter sets. The pressure range of the data is 200-400 bar.	82
7.7	%AAD values for ρ^{liq} , u , C_P^{res} , C_V^{res} , and μ_{JT} in the near critical region at reduced temperature $T_r = 1.1$ using CPA n.a., CPA 4C and qCPA with three different parameter sets. Pseudo-experimental data from the Span and Wagner EoS [15].	84
7.8	Experimental and predicted critical points	87
7.9	Value of S for 8 different association schemes	88
7.10	%AADs between experimental and calculated second virial coefficients	89
8.1	Pure compound CPA parameters from literature employed in this work.	92
8.2	Correlated CPA and qCPA pure compound parameters and %AAD in the saturated liquid densities and saturated pressures. Experimental data from raw DIPPR data [172]. The experimental quadrupole moments of benzene (≈ -9 D \AA), acetylene (≈ 4 D \AA) and nitrogen (≈ -1.5 D \AA) are employed in the three parameter version of qCPA. Following Reynolds et al. [188] it is assumed that the effective quadrupole moment of toluene is -7.92D \AA	93
8.3	Deviations for CPA and qCPA predictions ($k_{ij} = 0$) and correlations ($k_{ij} \neq 0$) of CO ₂ + n -alkane VLEs (C ₁ -C ₆ and C ₁₀). Including the correlated k_{ij} . Compared to experimental data from Refs. [66, 67, 165, 189-195].	95
8.4	Correlated binary interaction parameters and calculated %AADs for the CO ₂ + heavy n -alkane LLE systems using the CPA and qCPA. Compared to experimental data from Refs. [166, 198].	104
8.5	%AADs for the predicted ($k_{ij} = 0$) LLEs of CO ₂ + heavy n -alkane systems using the four parameter version of qCPA. The three parameter version of qCPA is used when possible. Compared to experimental data from Refs. [166, 198].	105

8.6	CPA and qCPA deviations and k_{ij} for CO ₂ + alcohol VLE and LLE mixtures. Compared to experimental data from Refs. [200–202, 206, 207, 212, 213].	113
8.7	Deviations for CPA and qCPA predictions ($k_{ij} = 0$) and correlations ($k_{ij} \neq 0$) for the CO ₂ (1) + water(2) mixture at 323.15 K (both VLE and LLE data). Including the correlated k_{ij} . Compared to experimental data from references [75, 203–205, 214].	115
8.8	Deviations from experimental data for CPA and qCPA predictions ($k_{ij} = 0$) and correlations ($k_{ij} \neq 0$) for the CO ₂ + benzene mixture in the temperature range 298.2–347.3 K. Including the correlated k_{ij} . Compared to experimental data from Refs. [212, 216].	118
8.9	Pure compound parameters and %AAD in the saturated liquid density and saturated pressure for qCPA, where an 'effective' quadrupolar moment is employed as an adjustable parameter rather than the quadrupolar volume. Experimental data from raw DIPPR data [172].	126
8.10	Deviations for CPA and qCPA predictions ($k_{ij} = 0$) and correlations ($k_{ij} \neq 0$) for the CO ₂ + acetone mixture in the temperature range 291.2–313.1 K. Including the correlated k_{ij} . Compared to experimental data from Refs. [202].	127
9.1	Approaches considered with CPA and qCPA for modeling ternary and quaternary CO ₂ -mixtures containing alkanes, water, and/or alcohols.	134
9.2	Summarized binary interaction parameters for the binary CO ₂ + <i>n</i> -alkane, alcohol or water systems with CPA and qCPA. Interaction parameters originally presented in Refs. [14, 37].	136
9.3	CPA and qCPA binary interaction parameters for non-CO ₂ containing binary mixtures. Binary interaction parameters from Refs. [35, 81, 187, 225–227]. binary interaction parameters between two hydrocarbons are assumed to be zero.	137

- 9.4 CPA and qCPA deviations between model predictions and experimental composition data from Refs. [67, 228, 229] for the VLE of the two ternary systems $\text{CO}_2(1) + \text{methane}(2) + \text{ethane}(3)$ and $\text{CO}_2(1) + \text{ethane}(2) + \text{eicosane}(3)$ using four of the modeling approaches. The pressure and temperature range is 230-250 K and 25-65 bar for the former system and 338.7 K and 104 bar for the latter system. The predictions have been performed both with and without interaction parameters as indicated in the table. 138
- 9.5 CPA and qCPA deviations between model predictions and experimental composition data [201, 230–232] for the VLE of four ternary systems containing CO_2 and at least one self-associating compound using the five modeling approaches. The pressure and temperature range is included in the table. 142
- 9.6 Deviations between CPA and qCPA predictions and experimental dew point data for the ternary mixtures $\text{CO}_2 + \text{water} + \text{methane}$, $\text{CO}_2 + \text{water} + \text{methanol}$ and for the quaternary mixtures $\text{CO}_2 + \text{water} + \text{methanol} + \text{hydrocarbon}$ (methane, ethane, propane, and n -butane). Experimental data from Refs. [236–240]. The temperature range is approximately 245-290 K in all cases. . . . 150
- 9.7 Deviations between CPA and qCPA predictions and experimental dew point data for the ternary mixture $\text{CO}_2 + \text{water} + \text{methanol}$ and for the quaternary mixtures $\text{CO}_2 + \text{water} + \text{methanol} + \text{hydrocarbon}$ (methane, ethane, propane, and n -butane). Experimental data from Refs. [236, 238–240]. The temperature range is approximately 245-290 K for all systems. A temperature dependent k_{ij} is employed for the binary water + methanol pair ($k_{\text{H}_2\text{O}-\text{MeOH}} = 0.115 - 60.24/T$). Temperature in Kelvin. . . . 150
- 9.8 CPA and qCPA deviations between model predictions and experimental data [241, 242] for the $\text{CO}_2(1) + \text{methanol}(2) + \text{ethane}(3)$ and $\text{CO}_2(1) + \text{water}(2) + 1\text{-propanol}(3)$ VLLE. The temperature and pressure range for the former system is 288-298 K and 38-57 bar and 313.2 K and 83-141 bar for the latter system. 151
- C.1 Relative error in the numerical derivatives of the Helmholtz energy function for the SRK term at $T = 230$ K, $n = 10$ mol and $V = 0.4$ L, using CO_2 as the sample compound. The error is evaluated both for central differences and the CSDA. 180
- C.2 Relative error in the numerical derivatives of the Helmholtz energy function for the quadrupole term at $T = 230$ K, $n = 10$ mol and $V = 0.4$ L, using CO_2 as the sample compound. The error is evaluated both for central differences and the CSDA. 180

Bibliography

- [1] Pachauri, R. K. and Meyer, L. A. Technical report, IPCC, Geneva, Switzerland, (2014).
- [2] Birol, F. Technical report, International Energy Agency, (2015).
- [3] Tans, P. and Keeling, R. www.esrl.noaa.gov/gmd/ccgg/trends/, Retrieved January 7, 2016.
- [4] Nielsen, O.-K., Plejdrup, M., Winther, M., Nielsen, M., Gyldenkærne, S., Mikkelsen, M., Albrektsen, R., Thomsen, M., Hjelgaard, K., Fauser, P., Bruun, H., Johannsen, V., Nord-Larsen, T., Vesterdal, L., Møller, I., Caspersen, O., Rasmussen, E., Petersen, S., Baunbæk, L., and Hansen, M. Technical report, Aarhus University - DCE – Danish Centre for Environment and Energy, (2015).
- [5] <http://engineeringchallenges.org/cms/challenges.aspx>, Retrieved January 6 (2016).
- [6] Diamantonis, N. I. and Economou, I. G. *Energy Fuels* **25**(7), 3334–3343 (2011).
- [7] Sloan, E. and Koh, C. *Clathrate Hydrates of Natural Gases*. Chemical Industries. CRC Press, Taylor & Francis Group, 3rd edition.
- [8] Kontogeorgis, G. M. and Folas, G. K. *Thermodynamic Models for Industrial Applications: From Classical and Advanced Mixing Rules to Association Theories*. John Wiley & Sons Ltd, (2010).
- [9] Spencer, D. F. December 23 (1997). US Patent 5,700,311.
- [10] Spencer, D. F. August 22 (2000). US Patent 6,106,595.
- [11] Spencer, D. F. and Currier, R. P. March 5 (2002). US Patent 6,352,576.
- [12] Herslund, P. J. *Thermodynamic and Process Modelling of Gas Hydrate Systems in CO₂ Capture Processes*. PhD thesis, Technical University of Denmark, Department of Chemical and Biochemical Engineering, (2013).

- [13] Dhima, A., de Hemptinne, J.-C., and Jose, J. *Ind. Eng. Chem. Res.* **38**(8), 3144–3161 (1999).
- [14] Tsivintzelis, I., Kontogeorgis, G. M., Michelsen, M. L., and Stenby, E. H. *Fluid Phase Equilib.* **306**(1), 38 – 56 (2011).
- [15] Span, R. and Wagner, W. *J. Phys. Chem. Ref. Data* **25**(6), 1509–1596 (1996).
- [16] Soave, G. S. *Chem. Eng. Sci.* **27**(6), 1197 – 1203 (1972).
- [17] Chapman, W. G., Jackson, G., and Gubbins, K. E. *Mol. Phys.* **65**(5), 1057–1079 (1988).
- [18] Chapman, W. G., Gubbins, K. E., Jackson, G., and Radosz, M. *Fluid Phase Equilibria* **52**, 31 – 38 (1989).
- [19] Chapman, W. G., Gubbins, K. E., Jackson, G., and Radosz, M. *Ind. Eng. Chem. Res.* **29**(8), 1709–1721 (1990).
- [20] Kontogeorgis, G. M., Voutsas, E. C., Yakoumis, I. V., and Tassios, D. P. *Ind. Eng. Chem. Res.* **35**, 4310–4318 (1996).
- [21] Perakis, C. A., Voutsas, E. C., Magoulas, K. G., and Tassios, D. P. *Fluid Phase Equilib.* **243**(1-2), 142 – 150 (2006).
- [22] Voutsas, E. C., Perakis, C. A., Pappa, G. D., and Tassios, D. P. *Fluid Phase Equilib.* **261**(1-2), 343 – 350 (2007). Properties and Phase Equilibria for Product and Process Design 11th International Conference on Properties and Phase Equilibria for Product and Process Design.
- [23] Oliveira, M. B., Queimada, A. J., Kontogeorgis, G. M., and Coutinho, J. a. A. *J. Supercrit. Fluids* **55**(3), 876 – 892 (2011).
- [24] Stell, G., Rasaiah, J. C., and Narang, H. *Mol. Phys.* **23**(2), 393–406 (1972).
- [25] Rushbrooke, G. S., Stell, G., and Høye, J. S. *Mol. Phys.* **26**(5), 1199–1215 (1973).
- [26] Stell, G., Rasaiah, J. C., and Narang, H. *Mol. Phys.* **27**(5), 1393–1414 (1974).
- [27] Larsen, B., Rasaiah, J. C., and Stell, G. *Mol. Phys.* **33**(4), 987–1027 (1977).
- [28] Gross, J. *AIChE J.* **51**(9), 2556–2568 (2005).
- [29] Karakatsani, E. K., Spyriouni, T., and Economou, I. G. *AIChE J.* **51**(8), 2328–2342 (2005).
- [30] Karakatsani, E. K., Kontogeorgis, G. M., and Economou, I. G. *Ind. Eng. Chem. Res.* **45**(17), 6063–6074 (2006).

- [31] Karakatsani, E. K. and Economou, I. G. *J. Phys. Chem. B* **110**(18), 9252–9261 (2006).
- [32] NguyenHuynh, D., Passarello, J.-P., Tobaly, P., and de Hemptinne, J.-C. *Fluid Phase Equilib.* **264**(1-2), 62 – 75 (2008).
- [33] Tsivintzelis, I., Ali, S., and Kontogeorgis, G. M. *J. Chem. Eng. Data* **59**(10), 2955 – 2972 (2014).
- [34] Tsivintzelis, I., Ali, S., and Kontogeorgis, G. M. *Fluid Phase Equilib.* **397**, 1 – 17 (2015).
- [35] Tsivintzelis, I. and Kontogeorgis, G. M. *J. Supercrit. Fluids* **104**, 29 – 39 (2015).
- [36] Tsivintzelis, I. and Kontogeorgis, G. M. *J. Chem. Thermodyn.* **93**, 305 – 319 (2016).
- [37] Bjørner, M. G. and Kontogeorgis, G. M. *Fluid Phase Equilib.* **408**, 151 – 169 (2016).
- [38] Bjørner, M. G., Sin, G., and Kontogeorgis, G. M. *Fluid Phase Equilib.* **414**, 29 – 47 (2016).
- [39] Bjørner, M. G. and Kontogeorgis, G. M. *Submitted for publication in Mol. Phys.* (2016).
- [40] Bjørner, M. G. and Kontogeorgis, G. M. *Corrigendum in Fluid Phase Equilib.* (2016).
- [41] Peng, D. Y. and Robinson, D. B. *Industrial & Engineering Chemistry: Fundamentals* **15**(1), 59–64 (1976).
- [42] Tsonopoulos, C. and Heidman, J. L. *Fluid Phase Equilibria* **29**, 391 – 414 (1986).
- [43] Kontogeorgis, G. M. and Folas, G. K. *Thermodynamic Models for Industrial Applications - From classical and advanced mixing rules to association theories*, chapter 9-12 The Cubic Plus Association Equation of State. John Wiley and Sons, 1.st edition (2010).
- [44] Wertheim, M. S. *Journal of Statistical Physics* **35**(1-2), 19–34 (1984).
- [45] Wertheim, M. S. *Journal of Statistical Physics* **35**(1-2), 35–47 (1984).
- [46] Wertheim, M. S. *Journal of Statistical Physics* **42**(3-4), 459–476 FEB (1986).
- [47] Wertheim, M. S. *Journal of Statistical Physics* **42**(3-4), 477–492 FEB (1986).
- [48] Jackson, G., Chapman, W. G., and Gubbins, K. E. *Mol. Phys.* **65**(1), 1–31 (1988).

- [49] Kontogeorgis, G. M., Michelsen, M. L., Folas, G. K., Derawi, S., von Solms, N., and Stenby, E. H. *Ind. Eng. Chem. Res.* **45**(14), 4855–4868 (2006).
- [50] Voutsas, E. C., Kontogeorgis, G. M., Yakoumis, I. V., and Tassios, D. P. *Fluid Phase Equilib.* **132**, 61–75 (1997).
- [51] Yakoumis, I. V., Kontogeorgis, G. M., Voutsas, E. C., and Tassios, D. P. *Fluid Phase Equilib.* **130**(1-2), 31–47 (1997).
- [52] Kontogeorgis, G. M., Yakoumis, I. V., Meijer, H., Hendriks, E. M., and Moorwood, T. *Fluid Phase Equilib.* **158 - 160**(0), 201–209 (1999).
- [53] Kontogeorgis, G. M., Michelsen, M. L., Folas, G. K., Derawi, S., von Solms, N., and Stenby, E. H. *Ind. Eng. Chem. Res.* **45**(14), 4869–4878 (2006).
- [54] Michelsen, M. L. and Mollerup, J. M. *Thermodynamic Models: Fundamentals & Computational aspects*. Tie-Line Publications, 2nd edition, (2007).
- [55] Maribo-Mogensen, B. *Development of an Electrolyte CPA Equation of state for Applications in the Petroleum and Chemical Industries*. PhD thesis, Technical University of Denmark, Department of Chemical and Biochemical Engineering, (2014).
- [56] Coutinho, J. A. P., Kontogeorgis, G. M., and Stenby, E. H. *Fluid Phase Equilib.* **102**(1), 31–60 (1994).
- [57] Derawi, S. O., Kontogeorgis, G. M., Michelsen, M. L., and Stenby, E. H. *Ind. Eng. Chem. Res.* **42**(7), 1470–1477 (2003).
- [58] Voutsas, E. C., Yakoumis, I. V., and Tassios, D. P. *Fluid Phase Equilib.* **158-160**(0), 151–163 (1999).
- [59] Folas, G. K., Kontogeorgis, G. M., Michelsen, M. L., and Stenby, E. H. *Ind. Eng. Chem. Res.* **45**(4), 1516–1526 (2006).
- [60] Kleiner, M. and Sadowski, G. *J. Phys. Chem. C* **111**(43), 15544–15553 (2007).
- [61] Huang, S. H. and Radosz, M. *Ind. Eng. Chem. Res.* **29**(11), 2284–2294 (1990).
- [62] Michelsen, M. L. and Hendriks, E. M. *Fluid Phase Equilib.* **180**, 165–174 (2001).
- [63] Michelsen, M. L. *Ind. Eng. Chem. Res.* **45**(25), 8449–8453 (2006).
- [64] Jog, P. K. and Chapman, W. G. *Mol. Phys.* **97**(3), 307–319 (1999).
- [65] Jog, P. K., Sauer, S. G., Blaesing, J., and Chapman, W. G. *Ind. Eng. Chem. Res.* **40**(21), 4641–4648 (2001).

- [66] Brown, T. S., Kidnay, A. J., and Sloan, E. D. *Fluid Phase Equilib.* **40**(1-2), 169 – 184 (1988).
- [67] Wei, M. S.-W., Brown, T. S., Kidnay, A. J., and Sloan, E. D. *J. Chem. Eng. Data* **40**(4), 726–731 (1995).
- [68] Danten, Y., Tassaing, T., and Besnard, M. *J. Phys. Chem. A* **109**(14), 3250–3256 (2005). PMID: 16833656.
- [69] Reilly, J. T., Bokis, C. P., and Donohue, M. D. *Int. J. Thermophys.* **16**(3), 599–610 (1995).
- [70] Lalanne, P., Tassaing, T., Danten, Y., Cansell, F., Tucker, S. C., and Besnard, M. *J. Phys. Chem. A* **108**(14), 2617–2624 (2004).
- [71] Sadlej, J. and Mazurek, P. *J. Mol. Struct.: THEOCHEM* **337**(2), 129 – 138 (1995).
- [72] Saharayand, M. and Balasubramanian, S. *J. Phys. Chem. B* **110**(8), 3782–3790 (2006).
- [73] Pfohl, O., Pagel, A., and Brunner, G. *Fluid Phase Equilib.* **157**(1), 53 – 79 (1999).
- [74] Kontogeorgis, G. M., Folas, G. K., Muro-Suñe, N., Roca Leon, F., and Michelsen, M. L. *Oil Gas Sci. Technol.* **63**(3), 305–319 (2008).
- [75] King, A. D. and Coan, C. R. *J. Am. Chem. Soc.* **93**(8), 1857–1862 (1971).
- [76] Valtz, A., Chapoy, A., Coquelet, C., Paricaud, P., and Richon, D. *Fluid Phase Equilib.* **226**, 333 – 344 (2004).
- [77] Wiebe, R. *Chemical Reviews* **29**(3), 475–481 (1941).
- [78] King, M. B., Mubarak, A., Kim, J. D., and Bott, T. R. *J. Supercrit. Fluids* **5**(4), 296 – 302 (1992).
- [79] Perakis, C. A., Voutsas, E. C., Magoulas, K. G., and Tassios, D. P. *Ind. Eng. Chem. Res.* **46**(3), 932–938 (2007).
- [80] Pappa, G. D., Perakis, C. M., Tsimpanogiannis, I. N., and Voutsas, E. C. *Fluid Phase Equilibria* **284**(1), 56–63 (2009).
- [81] Tsvintzelis, I., Kontogeorgis, G. M., Michelsen, M. L., and Stenby, E. H. *AIChE J.* **56**(11), 2965 – 2982 (2010).
- [82] Wiebe, R. and Gaddy, V. L. *J. Am. Chem. Soc.* **61**(2), 315–318 (1939).
- [83] Tan, S. P., Adidharma, H., and Radosz, M. *Ind. Eng. Chem. Res.* **47**(21), 8063–8082 (2008).
- [84] Gray, C. G. and Gubbins, K. E. *Theory of Molecular Fluids: I: Fundamentals*. International Series of Monographs on Chemistry. OUP Oxford, (1984).

- [85] Gubbins, K. E., Gray, C. G., and Machado, J. R. S. *Mol. Phys.* **42**(4), 817–841 (1981).
- [86] Buckingham, A. D. *Q. Rev. Chem. Soc.* **13**, 183–214 (1959).
- [87] Buckingham, A. D. and Disch, R. L. *Proc. R. Soc. London, Ser. A* **273**(1353), 275–289 (1963).
- [88] Buckingham, A. D., Disch, R. L., and Dunmur, D. A. *J. Am. Chem. Soc.* **90**(12), 3104–3107 (1968).
- [89] Stogryn, D. E. and Stogryn, A. P. *Mol. Phys.* **11**(4), 371–393 (1966).
- [90] Harries, J. E. *J. Phys. B: At. Mol. Phys.* **3**(12), L150 (1970).
- [91] Graham, C., Pierrus, J., and Raab, R. E. *Mol. Phys.* **67**(4), 939–955 (1989).
- [92] Prausnitz, J., Lichtenthaler, R., and de Azevedo, E. *Molecular thermodynamics of fluid-phase equilibria*. Prentice-Hall international series in the physical and chemical engineering sciences. Prentice-Hall PTR, (1999).
- [93] Flytzani-Stephanopoulos, M., Gubbins, K. E., and Gray, C. G. *Mol. Phys.* **30**(6), 1649–1676 (1975).
- [94] Gubbins, K. E. and Twu, C. H. *Chem. Eng. Sci.* **33**(7), 863 – 878 (1978).
- [95] Twu, C. H. and Gubbins, K. E. *Chem. Eng. Sci.* **33**(7), 879 – 887 (1978).
- [96] Stoll, J., Vrabec, J., Hasse, H., and Fischer, J. *Fluid Phase Equilib.* **179**(1-2), 339 – 362 (2001).
- [97] Gross, J. and Vrabec, J. *AIChE J.* **52**(3), 1194–1204 (2006).
- [98] Kleiner, M. and Gross, J. *AIChE J.* **52**(5), 1951–1961 (2006).
- [99] Vrabec, J. and Gross, J. *J. Phys. Chem. B* **112**(1), 51–60 (2008).
- [100] Tang, X. and Gross, J. *Fluid Phase Equilib.* **293**(1), 11 – 21 (2010).
- [101] Román-Ramírez, L. A., García-Sánchez, F., Ortiz-Estrada, C. H., and Justo-García, D. N. *Ind. Eng. Chem. Res.* **49**(23), 12276–12283 (2010).
- [102] Karakatsani, E. K. and Economou, I. G. *Fluid Phase Equilib.* **261**(1-2), 265 – 271 (2007).
- [103] Karakatsani, E. K., Economou, I. G., Kroon, M. C., Bermejo, M. D., Peters, C. J., and Witkamp, G.-J. *Phys. Chem. Chem. Phys.* **10**, 6160–6168 (2008).
- [104] Diamantonis, N. I. and Economou, I. G. *Mol. Phys.* **110**(11-12), 1205–1212 (2012).
- [105] Kroon, M. C., Karakatsani, E. K., Economou, I. G., Witkamp, G.-J., and Peters, C. J. *J. Phys. Chem. B* **110**(18), 9262–9269 (2006).

- [106] Karakatsani, E. K., Economou, I. G., Kroon, M. C., Peters, C. J., and Witkamp, G.-J. *J. Phys. Chem. C* **111**(43), 15487–15492 (2007).
- [107] Tamouza, S., Passarello, J.-P., Tobaly, P., and de Hemptinne, J.-C. *Fluid Phase Equilib.* **222-223**, 67 – 76 (2004).
- [108] Nguyen-Huynh, D., Passarello, J.-P., Tobaly, P., and de Hemptinne, J.-C. *Ind. Eng. Chem. Res.* **47**(22), 8847–8858 (2008).
- [109] Nguyen-Huynh, D., Tran, T. K. S., Tamouza, S., Passarello, J.-P., Tobaly, P., and de Hemptinne, J.-C. *Ind. Eng. Chem. Res.* **47**(22), 8859–8868 (2008).
- [110] Nguyen-Huynh, D., de Hemptinne, J.-C., Lugo, R., Passarello, J.-P., and Tobaly, P. *Ind. Eng. Chem. Res.* **50**(12), 7467–7483 (2011).
- [111] NguyenHuynh, D., Passarello, J.-P., de Hemptinne, J.-C., Volle, F., and Tobaly, P. *J. Supercrit. Fluids* **95**, 146 – 157 (2014).
- [112] Pereira, C. G., Grandjean, L., Betoulle, S., Ferrando, N., Féjean, C., Lugo, R., de Hemptinne, J.-C., and Mougin, P. *Fluid Phase Equilib.* **382**, 219 – 234 (2014).
- [113] Vega, C. *Mol. Phys.* **75**(2), 427–442 (1992).
- [114] Al-Saifi, N. M. *Prediction and Computation of Phase Equilibria in Polar and Polarizable Mixtures Using Theory-based Equations of State*. PhD thesis, The University of British Columbia, (2011).
- [115] de Villiers, A. J., Schwarz, C. E., Burger, A. J., and Kontogeorgis, G. M. *Fluid Phase Equilib.* **338**(0), 1 – 15 (2013).
- [116] Wong, J. O. and Prausnitz, J. M. *Chem. Eng. Commun.* **37**(1-6), 41–53 (1985).
- [117] van der Waals, J. D. December (1910). Nobel Lecture.
- [118] Kontogeorgis, G. M. *Chem. Eng. Res. Des.* **91**(10), 1840 – 1858 (2013). The 60th Anniversary of the European Federation of Chemical Engineering (EFCE).
- [119] Clark, G. N. I., Haslam, A. J., Galindo, A., and Jackson, G. *Mol. Phys.* **104**(22-24), 3561–3581 (2006).
- [120] Sauer, S. G. and Chapman, W. G. *Ind. Eng. Chem. Res.* **42**(22), 5687–5696 (2003).
- [121] Dominik, A., Chapman, W. G., Kleiner, M., and Sadowski, G. *Ind. Eng. Chem. Res.* **44**(17), 6928–6938 (2005).
- [122] Saager, B. and Fischer, J. *Fluid Phase Equilib.* **72**, 67 – 88 (1992).
- [123] Korden, S., Van Nhu, N., Vrabec, J., Gross, J., and Leonhard, K. *Soft Mater.* **10**(1-3), 81–105 (2012).

- [124] Dohrn, R. and Pfohl, O. *Fluid Phase Equilib.* **194-197**, 15–29 (2002).
- [125] Mah, R. S. H. *Comput. Chem. Eng.* **1**(3), 183 – 189 (1977).
- [126] Nelson, A. R., Olson, J. H., and Sandler, S. I. *Ind. Eng. Chem. Process Des. Dev.* **22**(3), 547–552 (1983).
- [127] Larsen, A. H. *Fluid Phase Equilib.* **29**(0), 47 – 58 (1986).
- [128] Zeck, S. *Fluid Phase Equilib.* **70**, 125–140 (1991).
- [129] Gupta, S. and Olson, J. D. *Ind. Eng. Chem. Res.* **42**, 6359–6374 (2003).
- [130] Hukkerikar, A., Kalakul, S., Sarup, B., Young, D., Sin, G., and Gani, R. *J. Chem. Inf. Model.* **52**(11), 2823–2839 (2012). © 2012 American Chemical Society.
- [131] Reed, M. E. and Whiting, W. B. *Chem. Eng. Commun.* **124**(1), 39–48 (1993).
- [132] Whiting, W. B., Tong, T. M., and Reed, M. E. *Ind. Eng. Chem. Res.* **32**(7), 1367–1371 (1993).
- [133] Whiting, W. B. *J. Chem. Eng. Data* **41**(5), 935–941 (1996).
- [134] Whiting, W. B., Vasquez, V. R., and Meerschaert, M. M. *Fluid Phase Equilib.* **158-160**, 627–641 (1999).
- [135] Vasquez, V. R. and Whiting, W. B. *Ind. Eng. Chem. Res.* **38**(8), 3036–3045 (1999).
- [136] Vasquez, V. R. and Whiting, W. B. *Comput. Chem. Eng.* **23**(11-12), 1825 – 1838 (2000).
- [137] Xin, Y. and Whiting, W. B. *Ind. Eng. Chem. Res.* **39**(8), 2998–3006 (2000).
- [138] Mathias, P. M. and Gilmartin, J. P. *Energy Procedia* **63**, 1171 – 1185 (2014). 12th International Conference on Greenhouse Gas Control Technologies, GHGT-12.
- [139] Mathias, P. M. *J. Chem. Eng. Data* **59**(4), 1006–1015 (2014).
- [140] Mathias, P. M. *Fluid Phase Equilibria* **408**, 265 – 272 (2016).
- [141] Hajipour, S. and Satyro, M. A. *Fluid Phase Equilib.* **307**(1), 78 – 94 (2011).
- [142] Hajipour, S., Satyro, M. A., and Foley, M. W. *Fluid Phase Equilib.* **364**(0), 15 – 30 (2014).
- [143] Hajipour, S., Satyro, M. A., and Foley, M. W. *Energy Fuels* **28**(2), 1569–1578 (2014).

- [144] Wakeham, W. A., Cholakov, G. S., and Stateva, R. P. *Fluid Phase Equilib.* **185**(1 - 2), 1 - 12 (2001). Proceedings of the 14th symposium on thermophysical properties.
- [145] Efron, B. *Ann. Statist.* **7**(1), 1-26 01 (1979).
- [146] Lemmon, E. W., McLinden, M. O., and Huber, M. L. *NIST Standard Reference Database 23: Reference Fluid Thermodynamic and Transport Properties-REFPROP, Version 7*. National Institute of Standards and Technology, Gaithersburg, (2002). Standard Reference Data Program.
- [147] Lemmon, E. W., McLinden, M. O., and Friend, D. G. *NIST Chemistry WebBook, NIST Standard Reference Database Number 69*, chapter Thermophysical Properties of Fluid Systems. National Institute of Standards and Technology, Gaithersburg MD, 20899, <http://webbook.nist.gov> (2014).
- [148] Omlin, M. and Reichert, P. *Ecol. Modell.* **115**(1), 45 - 59 (1999).
- [149] Bayarri, M. J. and Berger, J. O. *Statist. Sci.* **19**(1), 58-80 (2004).
- [150] Seber, G. A. F. and Wild, C. *Nonlinear Regression*. John Wiley & Sons, (1989).
- [151] Sin, G., Meyer, A. S., and Gernaey, K. V. *Comput. Chem. Eng.* **34**(9), 1385 - 1392 (2010). Selected papers from the 7th International Conference on the Foundations of Computer-Aided Process Design (FOCAPD, 2009, Breckenridge, Colorado, USA).
- [152] Duschek, W., Kleinrahm, R., and Wagner, W. *J. Chem. Thermodyn.* **22**(9), 841 - 864 (1990).
- [153] Fernández-Fassnacht, E. and Ríó, F. D. *J. Chem. Thermodyn.* **16**(5), 469 - 474 (1984).
- [154] Roebuck, J. R., Murrell, T. A., and Miller, E. E. *J. Am. Chem. Soc.* **64**(2), 400-411 (1942).
- [155] DiCiccio, T. J. and Efron, B. *Statist. Sci.* **11**(3), 189-228 09 (1996).
- [156] Sin, G., Gernaey, K. V., and Lantz, A. E. *Biotechnol. Prog.* **25**(4) (2009).
- [157] Diwekar, U. M. and Kalagnanam, J. R. *AIChE J.* **43**(2), 440-447 (1997).
- [158] Mckay, M. D., Beckman, R. J., and Conover, W. J. *Technometrics* **21**(2), 239-245 (1979).
- [159] Iman, R. L. and Conover, W. J. *Commun. Stat. Simul. C.* **11**(3), 311-334 (1982).
- [160] Helton, J. C. *Reliab. Eng. Syst. Safe* **42**(2-3), 327 - 367 (1993).
- [161] Metropolis, N. and Ulam, S. *J. Am. Stat. Assoc.* **44**(247), 335-341 (1949).

- [162] Halton, J. H. *SIAM Rev.* **12**(1), 1–63 (1970).
- [163] Helton, J. C. and Davis, F. J. *Reliab. Eng. Syst. Safe* **81**(1), 23 – 69 (2003).
- [164] Deiters, U. K. and Reuck, K. M. D. *Pure & Appl. Chem.* **69**(1), 69 – 81 (1998).
- [165] Webster, L. A. and Kidnay, A. J. *J. Chem. Eng. Data* **46**(3), 759–764 (2001).
- [166] Hottovy, J. D., Luks, K. D., and Kohn, J. P. *J. Chem. Eng. Data* **26**(3), 256–258 (1981).
- [167] Lafitte, T., Bessieres, D., eiro, M. M. P., and Daridon, J.-L. *J. Chem. Phys.* **124**(2), 024509 (2006).
- [168] Kontogeorgis, G. M., Tsvintzelis, I., von Solms, N., Grenner, A., Bøgh, D., Frost, M., Knage-Rasmussen, A., and Economou, I. G. *Fluid Phase Equilib.* **296**(2), 219 – 229 (2010). {VIII} Ibero-American Conference on Phase Equilibria and Fluid Properties for Process Design.
- [169] Tybjerg, P. C., Kontogeorgis, G. M., Michelsen, M. L., and Stenby, E. H. *Fluid Phase Equilib.* **288**(1-2), 128 – 138 (2010).
- [170] Liang, X., Tsvintzelis, I., and Kontogeorgis, G. M. *Ind. Eng. Chem. Res.* **53**(37), 14493–14507 (2014).
- [171] Hendriks, E. M., Kontogeorgis, G. M., Dohrn, R., de Hemptinne, J.-C., Economou, I. G., Žilnik, L. F., and Vesovic, V. *Ind. Eng. Chem. Res.* **49**(22), 11131–11141 (2010).
- [172] (2014).
- [173] Lafitte, T., Piñeiro, M. M., Daridon, J.-L., and Bessières, D. *J. Phys. Chem. B* **111**(13), 3447–3461 (2007). PMID: 17388508.
- [174] Lundstrøm, C., Michelsen, M. L., Kontogeorgis, G. M., Pedersen, K. S., and Sørensen, H. *Fluid Phase Equilib.* **247**(1-2), 149 – 157 (2006).
- [175] Liang, X., Maribo-Mogensen, B., Thomsen, K., Yan, W., and Kontogeorgis, G. M. *Ind. Eng. Chem. Res.* **51**(45), 14903–14914 (2012).
- [176] Brewer, P. G., Friederich, G., Peltzer, E. T., and Orr, F. M. *Science* **284**(5416), 943–945 (1999).
- [177] Zeuthen, J. Masters thesis, The Tehcnical University of Denmark, (2003).
- [178] Breil, M. P., Kontogeorgis, G. M., Behrens, P. K., and Michelsen, M. L. *Ind. Eng. Chem. Res.* **50**(9), 5795–5805 (2011).
- [179] Mallu, B. V., Natarajan, G., and Viswanath, D. S. *J. Chem. Thermodyn.* **21**(9), 989 – 996 (1989).

- [180] Dadson, R. S., Evans, E. J., and King, J. H. *Proc. Phys. Soc.* **92**(4), 1115 (1967).
- [181] Dymond, J. and Smith, E. B. *The virial coefficients of pure gases and mixtures : a critical compilation*. Oxford University Press, (1980).
- [182] Butcher, E. G. and Dadson, R. S. *Proc. R. Soc. London, Ser. A* **277**(1371), 448–467 (1964).
- [183] Cottrell, T. L. and Hamilton, R. A. *Trans. Faraday Soc.* **52**, 156–160 (1956).
- [184] McElroy, P. J., Kee, L. L., and Renner, C. A. *J. Chem. Eng. Data* **35**(3), 314–317 (1990).
- [185] Schramm, B., Elias, E., Kern, L., Natour, G., Schmitt, A., and Weber, C. *Ber. Bunsenges. Physik. Chem.* **95**(5), 615–621 (1991).
- [186] Tsvintzelis, I. and Maribo-Mogensen, B. Technical report, CERE, Center for Energy Resources Engineering Department of Chemical and Biochemical Engineering, Technical University of Denmark, September (2012).
- [187] Folas, G. K. *Modeling of Complex Mixtures Containing Hydrogen Bonding Molecules*. PhD thesis, Technical University of Denmark, (2007).
- [188] Reynolds, L., Gardecki, J. A., Frankland, S. J. V., Horng, M. L., , and Maroncelli, M. *J. Phys. Chem.* **100**(24), 10337–10354 (1996).
- [189] Clark, A. Q. and Stead, K. *J. Chem. Thermodyn.* **20**(4), 413 – 427 (1988).
- [190] Reamer, H. H. and Sage, B. H. *J. Chem. Eng. Data* **8**(4), 508–513 (1963).
- [191] Hsu, J. J. C., Nagarajan, N., and Robinson, R. L. *J. Chem. Eng. Data* **30**(4), 485–491 (1985).
- [192] Pozo de Fernandez, M. E., Zollweg, J. A., and Streett, W. B. *J. Chem. Eng. Data* **34**(3), 324–328 (1989).
- [193] Brown, T. S., Niesen, V. G., Sloan, E. D., and Kidnay, A. J. *Fluid Phase Equilib.* **53**(0), 7 – 14 (1989).
- [194] Cheng, H., Pozo de Fernandez, M. E., Zollweg, J. A., and Streett, W. B. *J. Chem. Eng. Data* **34**(3), 319–323 (1989).
- [195] Kaminishi, G.-I., Yokoyama, C., and Shinji, T. *Fluid Phase Equilib.* **34**(1), 83 – 99 (1987).
- [196] Llovell, F., Pámies, J. C., and Vega, L. F. *J. Phys. Chem.* **121**(21), 10715–10724 (2004).
- [197] Llovell, F., , and Vega, L. F. *J. Phys. Chem. B* **110**(3), 1350–1362 (2006).
- [198] Nieuwoudt, I. and du Rand, M. *The Journal of Supercritical Fluids* **22**(3), 185 – 199 (2002).

- [199] Frost, M. G. *Measurement and Modelling of Phase Equilibrium of Oil - Water - Polar Chemicals*. PhD thesis, Technical University of Denmark, (2014).
- [200] Suzuki, K., Sue, H., Itou, M., Smith, R. L., Inomata, H., Arai, K., and Saito, S. *J. Chem. Eng. Data* **35**(1), 63–66 (1990).
- [201] Yoon, J. H., Lee, H. S., and Lee, H. *J. Chem. Eng. Data* **38**(1), 53–55 (1993).
- [202] Chang, C. J., Chiu, K.-L., and Day, C.-Y. *J. Supercrit. Fluids* **12**(3), 223 – 237 (1998).
- [203] Briones, J. A., Mullins, J. C., Thies, M. C., and Kim, B. U. *Fluid Phase Equilib.* **36**(0), 235 – 246 (1987).
- [204] Bamberger, A., Sieder, G., and Maurer, G. *J. Supercrit. Fluids* **17**(2), 97 – 110 (2000).
- [205] Dohrn, R., Büinz, A. P., Devlieghere, F., and Thelen, D. *Fluid Phase Equilib.* **83**, 149–158 (1993).
- [206] Hong, J. H. and Kobayashi, R. *Fluid Phase Equilib.* **41**(3), 269 – 276 (1988).
- [207] Bezaehtak, K., Combes, G. B., Dehghani, F., Foster, N. R., and Tomasko, D. L. *J. Chem. Eng. Data* **47**(2), 161–168 (2002).
- [208] Kim, S., Kim, Y., Park, B. H., Lee, J. H., and Kang, J. W. *Fluid Phase Equilib.* **328**(0), 9 – 12 (2012).
- [209] Zhang, Z.-Y., Yang, J.-C., and Li, Y.-G. *Fluid Phase Equilib.* **169**(1), 1 – 18 (2000).
- [210] Ji, X., Tan, S. P., Adidharma, H., and Radosz, M. *Ind. Eng. Chem. Res.* **44**(22), 8419–8427 (2005).
- [211] dos Ramos, M. C., Blas, F. J., and Galindo, A. *Fluid Phase Equilib.* **261**(1-2), 359 – 365 (2007). Properties and Phase Equilibria for Product and Process Design 11th International Conference on Properties and Phase Equilibria for Product and Process Design.
- [212] Ohgaki, K. and Katayama, T. *J. Chem. Eng. Data* **21**(1), 53–55 (1976).
- [213] Kodama, D. and Kato, M. *J. Chem. Eng. Data* **50**(1), 16–17 (2005).
- [214] Rumpf, B., Nicolaisen, H., Öcal, C., and Maurer, G. *J. Solution Chem.* **23**(3), 431–448 (1994).
- [215] Teng, H., Yamasaki, A., Chun, M.-K., and Lee, H. *J. Chem. Thermodyn.* **29**(11), 1301 – 1310 (1997).
- [216] Bendale, P. G. and Enick, R. M. *Fluid Phase Equilib.* **94**(0), 227 – 253 (1994).

- [217] Kim, C.-H., Vimalchand, P., and Donohue, M. D. *Fluid Phase Equilib.* **31**(3), 299 – 311 (1986).
- [218] Lay, E. N., Taghikhani, V., and Ghotbi, C. *J. Chem. Eng. Data* **51**(6), 2197–2200 (2006).
- [219] Yucelen, B., , and Kidnay, A. J. *J. Chem. Eng. Data* **44**(5), 926–931 (1999).
- [220] Gray, C. G., Gubbins, K. E., and Joslin, C. G. *Theory of Molecular Fluids Volume 2: Applications*, volume 53. Oxford University Press, (2011).
- [221] Dougill, S., Sajik, W., and Hwang, S. June 16 (1998). US Patent 5,766,514.
- [222] Wallis, K. P., Clancy, P., Zollweg, J. A., and Streett, W. B. *J. Chem. Thermodyn.* **16**(9), 811 – 823 (1984).
- [223] Wormald, C. J. *Eldata. Int. Electron. J.Phys.Chem.Data* **1**, 95–112 (1995).
- [224] Moser, B., Lucas, K., and Gubbins, K. E. *Fluid Phase Equilib.* **7**(2), 153 – 179 (1981).
- [225] Folas, G. K., Derawi, S. O., Michelsen, M. L., Stenby, E. H., and Kontogeorgis, G. M. *Fluid Phase Equilibria* **228-229**(0), 121 – 126 (2005).
- [226] Yan, W., Kontogeorgis, G. M., and Stenby, E. H. *Fluid Phase Equilib.* **276**(1), 75 – 85 (2009).
- [227] Riaz, M., Yussuf, M. A., Kontogeorgis, G. M., Stenby, E. H., Yan, W., and Solbraa, E. *Fluid Phase Equilib.* **337**, 298 – 310 (2013).
- [228] Al-Marri, S. S. *Pvt and phase behaviourpvt and phase behavior and viscosity measurements and modeling of the ternary and binary systems of carbon dioxide + heavy hydrocarbon (n-eicosane) + light gas (ethane or propane)*. PhD thesis, University of Southern California, May (2006).
- [229] Davalos, J., Anderson, W. R., Phelps, R. E., and Kidnay, A. J. *J. Chem. Eng. Data* **21**(1), 81–84 (1976).
- [230] Galivel-Solastiouk, F., Laugier, S., and Richon, D. *Fluid Phase Equilib.* **28**(1), 73 – 85 (1986).
- [231] Lim, J. S., Lee, Y. Y., and Chun, H. S. *J. Supercrit. Fluids* **7**(4), 219 – 230 (1994). Proceedings of the Symposium on Supercritical fluids held at {AIChE} Spring National Meeting.
- [232] Yoon, J. H., Chun, M. K., Hong, W. H., and Lee, H. *Ind. Eng. Chem. Res.* **32**(11), 2881–2887 (1993).
- [233] Wong, D. S. H. and Sandler, S. I. *AIChE J.* **38**(5), 671–680 (1992).
- [234] Song, K. Y. and Kobayashi, R. *J. Chem. Eng. Data* **35**(3), 320–322 (1990).

- [235] Austegard, A., Solbraa, E., Koeijer, G. D., and Mølnvik, M. *Chem. Eng. Res. Des.* **84**(9), 781–794 sep (2006).
- [236] Jarne, C., Blanco, S. T., Artal, M., Rauzy, E., Otin, S., and Velasco, I. *Fluid Phase Equilib.* **216**(1), 85 – 93 (2004).
- [237] Jarne, C., Blanco, S. T., Gallardo, M. A., Rauzy, E., Otin, S., and Velasco, I. *Energy Fuels* **18**(2), 396–404 (2004).
- [238] Jarne, C., Blanco, S. T., Fernandez, J., Rauzy, E., Otin, S., and Velasco, I. *Ind. Eng. Chem. Res.* **43**(2), 662–668 (2004).
- [239] Jarne, C., Blanco, S. T., Avila, S., Berro, C., Otin, S., and Velasco, I. *Can. J. Chem.* **83**(3), 220–226 (2005).
- [240] Gil, L., Avila, S., Garcia-Gimenez, P., Blanco, S. T., Berro, C., Otin, S., and Velasco, I. *Ind. Eng. Chem. Res.* **45**(11), 3974–3980 (2006).
- [241] Hong, S. P., Patton, C. L., and Luks, K. D. *J. Chem. Eng. Data* **39**(1), 90–94 (1994).
- [242] Adrian, T., Oprescu, S., and Maurer, G. *Fluid Phase Equilib.* **132**(1-2), 187 – 203 (1997).
- [243] Herslund, P. J., Thomsen, K., Abildskov, J., and von Solms, N. *Fluid Phase Equilib.* **375**, 89 – 103 (2014).
- [244] Shah, N. N., Zollweg, J. A., and Streett, W. B. *J. Chem. Eng. Data* **36**(2), 188–192 (1991).
- [245] van der Walls, J. H. *Trans. Faraday Soc.* **52**, 184–193 (1956).
- [246] Platteeuw, J. C. and van der Waals, J. H. *Mol. Phys.* **1**(1), 91–96 (1958).
- [247] Parrish, W. R. and Prausnitz, J. M. *Ind. Eng. Chem. Process Des. Dev.* **11**(1), 26–35 (1972).
- [248] Martins, J. R. R. A., Kroo, I. M., and Alonso, J. J. In *AIAA paper 2000-0689, 38th Aerospace Sciences Meetings*, 1–12. American Institute of Aeronautics and Astronautics, January (2000).
- [249] Press, W. H., Teukolsky, S., Vetterling, W., and Flannery, B. *Numerical Recipes - Volume 1 (Fortran 77) The Art of Scientific Computing*. Cambridge University Press, 2.nd edition, (1992).
- [250] Lyness, J. N. and Moler, C. B. *SIAM J. Numer. Anal.* **4**(2), 202–210 (1967).
- [251] Squire, W. and Trapp, G. *SIAM Rev.* **40**(1), 110–112 (1998).
- [252] Martins, J. R. R. A., Sturdza, P., and Alonso, J. J. In *Aerospace Sciences Meetings*, –. American Institute of Aeronautics and Astronautics January (2001).
- [253] Martins, J. R. R. A., Sturdza, P., and Alonso, J. J. *ACM Trans. Math. Softw.* **29**(3), 245–262 September (2003).